A Study on Twin-Screw Rheo-Diecasting of AZ91D Mg-alloy

A thesis submitted to Brunel University

for the

Degree of Doctor of Philosophy

Guojun Liu

Brunel Centre for Advanced Solidification Technology

Brunel University

Uxbridge

UB8 3PH

United Kingdom

May 2006

Supervision : Prof. Zhongyun Fan

Abstract

A newly developed one-step semisolid process by BCAST for semisolid processing of magnesium alloy was studied in this thesis - the Twin-Screw Rheo-Diecasting (RDC) of AZ91D Mg-alloy. The RDC process is an innovative process which combines the dispersive mixing power of the Twin-Screw Slurry Maker (TSSM) for creation of high quality semisolid slurry and the existing cold chamber High-Pressure Die-Casting (HPDC) process for component shaping. Magnesium alloys, due to their low density and superior strength/weight ratio, offer distinct advantages in weight savings, and are gaining increasing interests in applications. The research on the new RDC technology aimed to eliminate the limitations of the conventional HPDC and to meet the requirements from extensive application of Mg-alloys. In this thesis, the major tasks were to optimise of the RDC technology, to evaluate the microstructure and mechanical properties of RDC AZ91D Mg-alloy in both as-cast and heat treated conditions, and to understand the solidification process in the TSSM.

The results of the RDC as-cast state indicated that the microstructure of primary α-Mg particles had a fine size (around 40μm), extremely spherical morphology and uniform distribution throughout the entire castings; the RDC AZ91D samples had extremely low levels of porosity. Due to the unique microstructure and much reduced level of defects, the RDC AZ91D alloy exhibited a substantial improvement in mechanical properties. In addition, a traditional full heat treatment was performed for RDC AZ91D alloy. Compared with HPDC alloy, the RDC AZ91D alloy was found to exhibit an accelerated dissolution of β-$Mg_{17}Al_{12}$ during solution treatment, and a faster age-hardening kinetics of the β-phase during subsequent ageing. The microstructural investigations showed that under intensive forced convection, heterogeneous nucleation occurred continuously throughout the entire volume of the solidifying melt and the nuclei grew spherically. Ostwald ripening took place by dissolution of the smaller particles but at a very slow coarsening rate. Increasing the intensity of forced convection enhanced nucleation and reduced volume fraction of primary phase solidified in the slurry maker. This study has demonstrated that the novel RDC process possesses a number of advantages and it is suitable for production of high integrity Mg-alloy components.

Acknowledgements

I would like to deeply thank Prof. Zhongyun Fan, for providing me the opportunity to do this work and, for his extensive encouragement. My full appreciation is not possible to describe here in words.

This thesis has been made possible by Prof. Fan's help, from the initial organisation and theory creation right through to finishing up. It is certain that without his effort it could not exist! Out of this thesis, he is not only a supervisor or director of BCAST, but also a friend who has taught me beyond the realms of research. The effects of which, extend into my daily life.

Special thanks go to Dr. Yun Wang, for his kind supervision and practical help. He has given great guidance to me in the heat treatment study (Chapter 4.4 and 5.3). In these years, it is a pleasure to share a good working relationship with him.

A number of other people have been of assistance. Dr. S. Ji has provided support in technical and experimental work; it was also benefited from Dr. A. Das's academic knowledge. I would also like to thank Miss K.A. Roberts for her tremendous efforts to correct my writing.

Finally, I want to thank my parents and wife for their love and support during my study.

Publication List

1. Z.Fan, G.Liu: solidification behaviour of AZ91D alloy under intensive forced convection in the RDC process. **Acta Materialia, 53 (2005)** 4345-4357.

2. Z.Fan, G.Liu, Y.Wang: Microstructure and mechanical properties of Rheo-Diecast AZ91D magnesium alloy. **Journal of Materials Science, January 29, 2006.**

3. Y.Wang, G.Liu, Z.Fan: Microstructure evolution of Rheo-Diecast AZ91D magnesium alloy during heat treatment. **Acta Materialia, 54/3(2005)** 689-699.

4. Y.Wang, G.Liu, Z.Fan: A new heat treatment procedure for Rheo-Diecast AZ91D magnesium alloy. **Scripta Maerialia, 54/5(2005)** 903-908.

5. Z.Fan, S.Ji, G.Liu: Development of the Rheo-Diecasting process for Mg-alloys. **Materials Science Forum, 488-489 (2005)** 405-412.

6. Z.Fan, S.Ji, G.Liu, E.Zhang: Development of Rheo-Diecasting process for Mg-alloys and their components. **Proc.8th Inter. Conf. Semisolid metal processing, 2004.**

7. Z.Fan, G.Liu, M.Hitchcock: Solidification behaviour under intensive forced convection. **Materials Science and Engineering A, 413/4(2005)** 229-235.

8. A.Das, G.Liu, Z.Fan: Investigation on the microstructural refinement of a Mg-wt6%Zn alloy. **Materials Science and Engineering A, 419(2005)** 349-356.

Contents

Index of Figures

Index of Tables

Chapter 1. Introduction

1.1 Background

With their low density, magnesium alloys have superior specific strength and stiffness compared to other engineering materials. They also offer a number of attractive properties such as a high damping capacity, electromagnetic shielding, dimensional stability, good machinability and recyclability. As a relatively new structural material, magnesium alloys have demonstrated significant potential for applications in many industries: transportation, power equipment, computer/communication products, and especially in the automotive industry. In recent years, research and application on magnesium has greatly expanded around the world. The increased use of magnesium castings requires the development of special casting technologies to produce castings with fine grain size, no porosity or cracks and further improved metallurgical quality.

Currently, magnesium alloys are mainly manufactured by high-pressure die-casting (HPDC) for structural components in the automobile industry. HPDC is a well-established and efficient process. However, there are still a number of limitations in HPDC process. For example, it requires high cost dies with high levels of maintenance, large castings require large machining and, most importantly, it contains a substantial amount of porosity due to air entrapment during die filling and hot tearing during the solidification in the die cavity. Such porosity deteriorates mechanical properties and limits its applications to non-stress or low-stress components. One of the most promising

technologies capable of producing high integrity magnesium components is semisolid metal (SSM) processing.

SSM processes use a SSM slurry, with substantially increased viscosity, resulting in controlled die filling and close to zero porosity in the final components. Due to these different characteristics, semisolid processing of magnesium alloys is expected to exhibit a number of advantages and it is deemed that magnesium is an ideal material for semisolid processing. In recent years, SSM processes using both the Thixo and Rheo-route for magnesium alloys have been under investigation. The Rheo-route involves preparation of a SSM slurry from liquid alloys by shearing during solidification and transferring directly the slurry to a mould for component shaping; The Thixo-route is basically a two-step process, involving preparation of a feedstock material with thixotropic characteristics, then reheating the feedstock material to semisolid temperature for component shaping.

However, the Thixo-processed microstructure has more rosette shaped primary particles, typical billets in MHD (Magnetohydrodynamic Stirring) stirred continuous castings have some degree of inhomogeneity from both structure and composition. More importantly, the greatest obstacle to the development of the two-step Thixo-route process is the high cost of pre-processed non-dendritic raw materials. In consideration of cost saving, overall energy efficiency in production, and process management, the Rhro-route seems more promising because it integrates slurry making with component shaping in one operation.

The rheology of semisolid slurries suggests that an ideal semisolid slurry for semisolid metal processing should possess a suitable volume fraction of fine and spherical particles

dispersed uniformly in a liquid matrix. Enhancing the effective nucleation and promoting spherical growth during solidification can benefit to obtain this ideal semisolid slurry. Based on this consideration for process creation, an innovative one-step SSM processing technology for metals, especially Mg-alloys, Rheo-Diecasting (RDC), has been developed by BCAST at Brunel University.

The RDC process innovatively adapts the well-established, high shear dispersive mixing action of the twin-screw mechanism to the task of in situ creation of SSM slurry, with fine and spherical solid particles, followed by direct shaping of the SSM slurry into a near-net shape component using the existing cold chamber HPDC process. Although most magnesium alloys can potentially be rheo-diecast, the effort in this study is focused on the AZ91D magnesium die-casting alloy.

The objectives of this study are:

- To optimize the Rheo-Diecasting process for fabrication of AZ91D Mg-alloy castings.

- To study the unique microstructural characteristics and potential mechanical properties of the RDC AZ91D Mg-alloy in the as-cast condition.

- To study the effects of Twin-Screw shearing parameters on the microstructure of RDC AZ91D Mg-alloy samples, and to understand the solidification behaviour of RDC AZ91D Mg-alloy under intensive forced convection in the Twin-Screw Slurry Maker.

- To investigate the microstructural evolution and mechanical response of the RDC AZ91D Mg-alloy under different heat treatment conditions (T4, T5, T6, and T_x).

- To demonstrate the superior castability of the Rheo-Diecasting process for production of high integrity Mg-alloy automobile components.

1.2 Outline of Thesis

After a sincere acknowledgement and an introduction of the study background, the literature is reviewed in Chapter 2 beginning with a brief introduction to the development of semisolid processing of magnesium alloys. Followed by more detailed overview of the semisolid metal slurry, rheology of semisolid slurries, technologies for semisolid metal processing, and alloys for semisolid processing. Finally, the semisolid processing of magnesium alloys are reviewed. Chapter 3 describes the experimental techniques that were used in the production and characterisation of the Rheo-diecast AZ91D Mg-alloy samples and also the methods used to evaluate their properties. In Chapter 4 the results of the RDC process optimisation, microstructure characterisation and mechanical properties, effects of the Twin-Screw shearing on the RDC microstructures, and the responses to heat treatment, are presented. Chapter 5 offers discussions on the solidification behaviour of AZ91D Mg-alloy in the RDC process and the advantages of RDC process. The main conclusions of the study and suggestions for further work are presented in Chapter 6 and Chapter 7, respectively.

Chapter 2. Literature Review

2.1 Introduction

Semisolid metal (SSM) processing is a relatively new method for forming alloys in the semisolid state, to near net shaped products [FAN02a]. It relies on the behaviour of semisolid slurries, in which the solid exists in the form of spherical particles and suspended in a liquid matrix. Such slurries are stiff if left undisturbed and may be handled, but flow like a liquid once sheared. The semisolid alloy slurries may therefore be injected into a die to produce components with good surface finish, fine and uniform microstructures and lower porosity. The semisolid processed components can also be heat treated to give superior mechanical properties.

Initial interest in the mechanical properties and rheology of semisolid slurries, which led to semisolid metal processing can be traced back to the work of Flemings and his co-workers at MIT in the early 1970s [SPE72]. This work was originally directed at the problem of hot tearing in alloy castings, but it was quickly realised that a potential technology for near net shaping of quality components was emerging, initiating the development of semisolid processing [FLE00].

Conventionally, the primary solidified phases are of dendrite morphology in metals. With a limit of vigorous convection and slow cooling during dendritic solidification of metals, grains become non-dendritic or spheroidal. To obtain this particular microstructure, there are a number of preparation techniques investigated and developed, e.g. the earliest method of Mechanical Stirring [FLE91], followed by Magnetohydrodynamic Stirring

[KEN88], Strain Induced Melt Activation process [YOU83], and the Ultrasonic Vibration process [ESK02] to name but a few.

Historically, research on SSM processing has been mainly concentrated on technological development of casting techniques, with very little research on nucleation and growth under forced convection [FLE91][KIR94][FAN02a]. Only a limited understanding of nucleation rate, growth morphology and the mechanisms for the formation of the globular structures has been achieved [BOE00]. The conventional belief [FLE91] is that under forced convection the initial dendrites would fragment through either the bending of dendrite arms followed by liquid penetration of the high angle grain boundaries [DOH84], or through re-melting at the root of dendrite arms due to solute enrichment and thermal-solutal convection [HEL96]. The detached dendrite arms then undergo a coarsening process to provide the observed globular particles. More recently, it is believed that the globular structure is more likely to be a result of spherical growth under forced convection, rather than a consequence of dendrite arm detachment [FAN02a][DAS02][QIN00].

It is known, however, that alloys with a non-dendritic microstructure possess improved rheological properties in the semisolid state, quite different from those of dendritic alloys that behave thixotropically and pseudoplastically [FLE91]. Intensive experimental investigations [FLE91][KIR94][CHE02][LEH85] have confirmed the effects of the particle morphology on the flow behaviour of semisolid slurries. The rheology of semisolid slurries suggests that an ideal semisolid slurry for semisolid metal processing is one in which a suitable volume fraction of fine and spherical particles are dispersed uniformly in a liquid matrix [FAN02a]. Enhancing the effective nucleation and

promoting spherical growth during solidification can obtain such ideal semisolid slurry. The Twin-Screw Slurry Maker (TSSM) is described as providing such enhancements [FAN02b].

Based on the alternative thixotropic and pseudoplastic rheological properties, semisolid alloys can be successfully formed into components by way of thixo-forming or rheo-forming; they are broadly termed ‘ semisolid metal forming processing ’(SSP) [FAN02a][KIR94]. Following from Flemings's work, a number of researchers have investigated and tested both the MIT processes and other newly developed processes [KEN88]. The primary driving force for development of semisolid forming has been the energy efficient automobile and the possible weight savings produced by these techniques [FLE00][CHI00]. Initially, the major commercial semisolid processing activity was in the semisolid forging of a variety of aluminium parts, including military, aerospace and automotive applications [KEN88]. Further, semisolid processing technologies have been demonstrated to be applicable to most engineering alloys, including copper [SOH02], zinc [LEH85], steel [BRA02], titanium [SUN04], and magnesium [AVE99].

Magnesium, with its rich reserves in the earth, is an important engineering material. More importantly, with its low density, magnesium alloys have a higher specific strength and stiffness than most engineering materials, i.e., aluminium, steel and polymer-based composites [KE04]. Magnesium alloys also offer other attractive properties such as a high damping capacity, electromagnetic shielding, dimensional stability, good machinability and recyclability [AGH04]. As relatively new structural materials, magnesium alloys have demonstrated significant potential for applications in many

industries, i.e., transportation, power tool/equipment, and computer/communication products [AGH04] [COL03][SCH03]. In the automobile industry, we have seen an average annual increase of 15% in the usage of Mg over the past few years and it is predicted that this growth trend will continue well into the first decade of the 21st century and beyond [FRI00]. In recent years, research and development on magnesium has greatly expanded around the world, significant progress has been made on its extraction and the casting and forming processes used, as well as in alloy development and product applications. However, magnesium alloys have not yet fully realised their potential, more research in alloy development and processing technologies is still required [SCH05][FRI01].

Currently, semisolid processing of magnesium has become its own industrial field [FLE91][POL95][AGU04][IVA04]. Based on the consideration for process creation, an innovative one-step SSM processing technology for metals and especially Mg-alloys, Rheo-Diecasting, has been developed at Brunel University [FAN99].

In the 35 years since the original work, a great deal of effort and scientific research has been applied to semisolid processing, with eight international conferences since 1990 devoted to the topic. The significance of Mg-alloys to extensive applications is clear and semisolid processing is a developing technique to assist this.

2.2 Semisolid metal slurry

2.2.1 Dendritic growth during solidification of metals

Solidification phenomena play an important role in many of the liquid metal forming processes, and even more so in semisolid metal processing as its basis is solidification control.

There are essentially two basic growth morphologies during alloy solidification: dendritic and eutectic morphologies [KUR86]. Generally, a mixture of both morphologies will be present. In this section, only the first stage of equilibrium solidification (the temperature reduction from liquidus to solidus) for a binary alloy will be summarised, it can be further applied to other alloys.

Shown in **Figure 2.1** is a principle binary alloy phase diagram [POR92]. The liquidus line and solidus line of the phase diagram are illustrated in Figure 2.1, where the chemical composition of the considered alloy is 'X_0'. During cooling of metal alloys, there are a number of processes that take place within the semisolid region. When the temperature of the melt is just below T_1, the alloy X_0 begins to solidify with the formation of a small amount of solid phase. As the temperature is lowered more, e.g., T_2, solid forms with a composition of Xs, and the relative amounts of solid and liquid at the temperature T_2 in equilibrium can be calculated by employing the lever rule [FLE74]:

$$f_s = (X_L - X_0) / (X_L - X_S) \qquad \textbf{Equation 2.2.1}$$

Meanwhile, the liquid is solute concentrated with a composition of X_L.

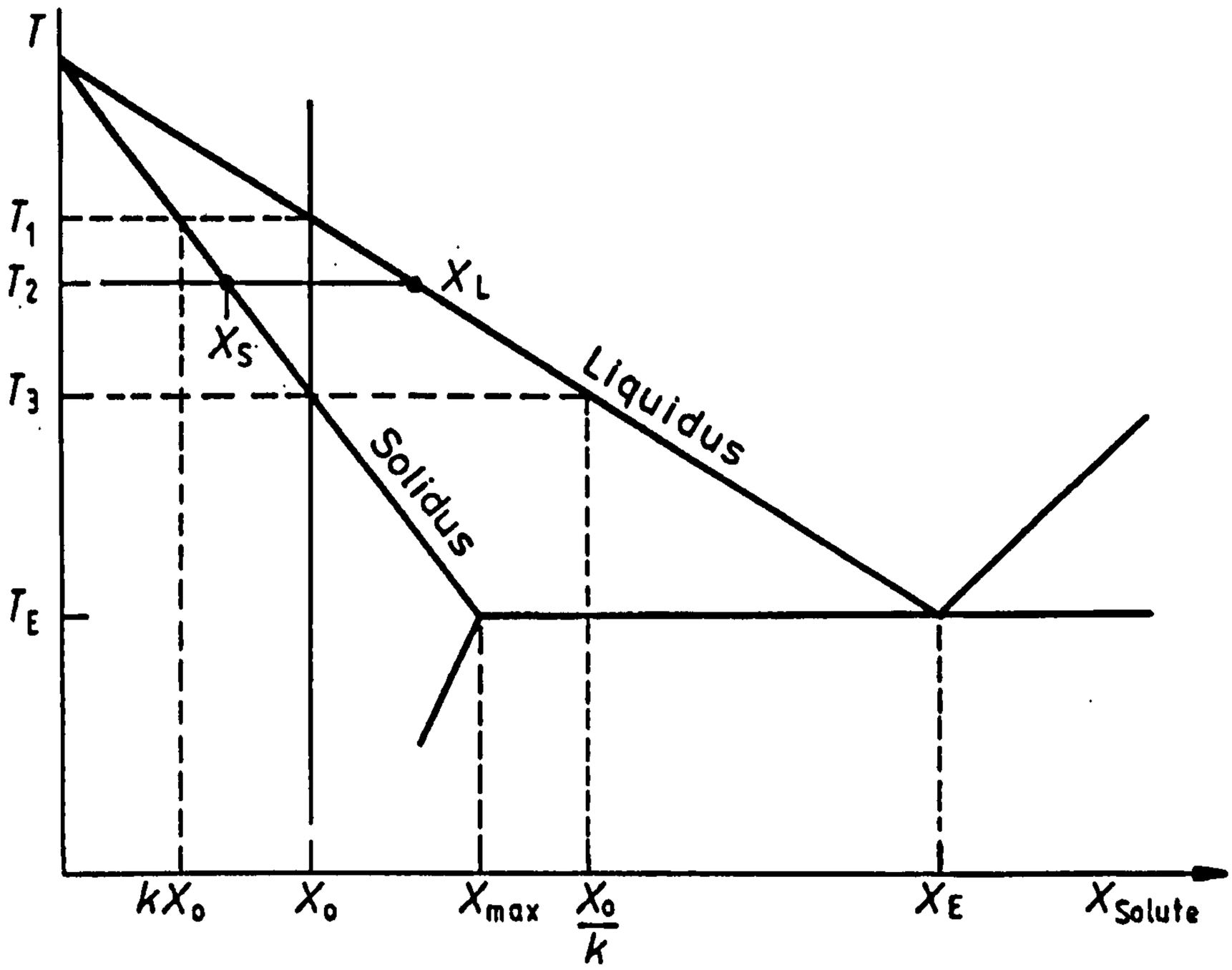

Figure 2.1 A principle binary alloy phase diagram, $K=X_S/X_L$ is constant [POR92].

As the solidification process continues, the alloy is supercooled either by thermal supercooling or compositional (constitutional) surpercooling [POR92]. **Figure 2.2,** the compositional supercooling, the redistribution of solute in an alloy liquid, results in a varying solute concentration ahead of the solidification front (from X_0/k to X_0), the solute distribution in liquid is shown in Figure 2.2 as X_L. Therefore, the corresponding liquidus temperature of the alloy increases with distance from the interface, as shown schematically in Fig 2.2, given by the line T_e. If the actual temperature gradient is less than a critical value, e.g. T_L, the liquid is supercooled in front of the solidification.

From nucleus formation, the growth front of the solidification is considered planar, and eventually, the supercooling in front of the solid area drives the growth. If a supercooling exists ahead of an initially planar solid/liquid interface a protrusion forms. The formation of the first protrusion causes solute to be rejected laterally and pile up at the root of the

protrusion. This also lowers the equilibrium solidification temperature causing recesses, which in turn triggers the formation of other secondary protrusions or arms. At sufficiently low temperature gradients primary, secondary and even tertiary arms develop [POR92].

Therefore, the solidification morphologies of the solid phase in alloys are generally dendritic in profile [KUR86]. With an external forced convection applied, the solidification phenomenon can be controlled to create other morphologies.

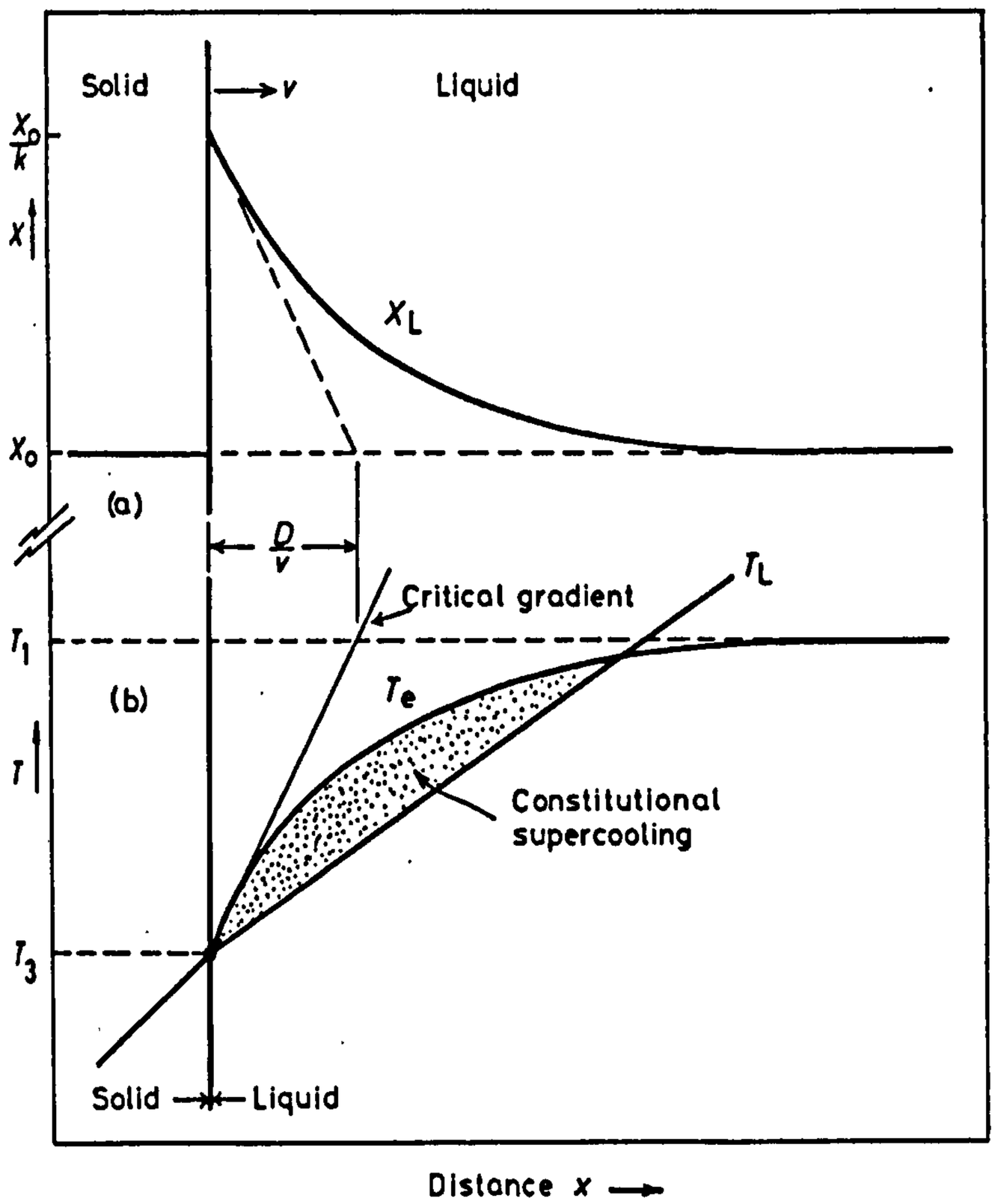

Figure 2.2 *The origin of constitutional supercooling ahead of a planar solidification front [POR92].*

2.2.2 Technologies for producing semisolid slurries

As discussed, in conventional solidification, nearly all alloys of commercial importance solidify dendritically, with either a columnar or an equiaxed dendritic structure [POR92]. Whereas, the solidification under melt stirring or a forced external field generates special solidification phenomena and produces non-dendritic structures [BAR95], i.e., the SemiSolid Metal slurry. The semisolid alloy is characterized as a two-phase mixture in which the spherical primary phase is uniformly distributed in a liquid matrix. All semisolid metal processing are based on such a unique microstructural material [FAN02a]. There are various production techniques for semisolid metal slurries, which are at different stages of research and development.

Mechanical stirring

The technologies for producing non-dendritic slurries originating at MIT were based on mechanical stirring [FLE91]. Melt agitation is commonly generated by means of impellers or multi-paddle agitators mounted on a central rotating shaft. For example, a simple 'batch rheocaster' or the developed 'continuous rheocaster' (**Figure 2.3a,b**) [FLE91], in which superheated liquid flows down into an annulus, between the stirring rod and an outer cylinder, where it is simultaneously stirred and cooled. During mechanical stirring, shear rate can be roughly estimated by the ratio of the velocity of the impeller extremity, to the clearance between the impeller tip and the mould wall [FAN02a]. The shear offered by the stirrer during solidification promotes the formation of non-dendritic structure. The limitations of the mechanical stirring is the contamination of the slurry, low productivity, and the difficulty in process control.

Magnetohydrodynamic (MHD) stirring

MHD process was developed by MIT in the USA and first employed at Alumax Inc [KEN88]. In this technique, local shear is generated by rotating electromagnetic fields within the continuous casting mould, and continuous billets of solidified semisolid alloy can be produced, as sketch illustrated in **Figure 2.3c.** [ZHA03]. Electromagnetic stirring can be achieved through three different modes: vertical flow, horizontal flow, and helical flow [NIE98]. The helical mode is ultimately a combination of the vertical and horizontal modes. In the horizontal flow mode, the motion of the solid particles takes place in a quasi-isothermal plane so that mechanical shearing is probably the dominant mechanism for spheroidisation [FAN02a]. In the vertical flow mode, the dendrites located near the solidification front are re-circulated to the hotter zone of the stirring chamber and partially re-melted, and therefore, thermal processing is dominant over mechanical stirring. As the stirring is deep in the sump of the liquid, contamination is virtually eliminated. Since then the birth of the MHD technology for thixotropic feedstock production, it has been subject to intensive research [BLA96][JUN01][VIV93].

Strain Induced Melt Activation (SIMA) process

The SIMA process was originally developed by Young et al. [YOU83]. An alloy billet or bar is cold worked a critical amount, so that a sufficient strain is induced. On reheating the bar into the semisolid zone, the desired fine and spheroidal structure is obtained. This process is based on the scientific understanding that high angle grain boundaries induced by plastic deformation and recrystallisation grain will be wetted by liquid metal at the semisolid temperature. However, the SIMA process requires plastic deformation and recrystallisation, that are energy and processing intensive, making it cost approximately

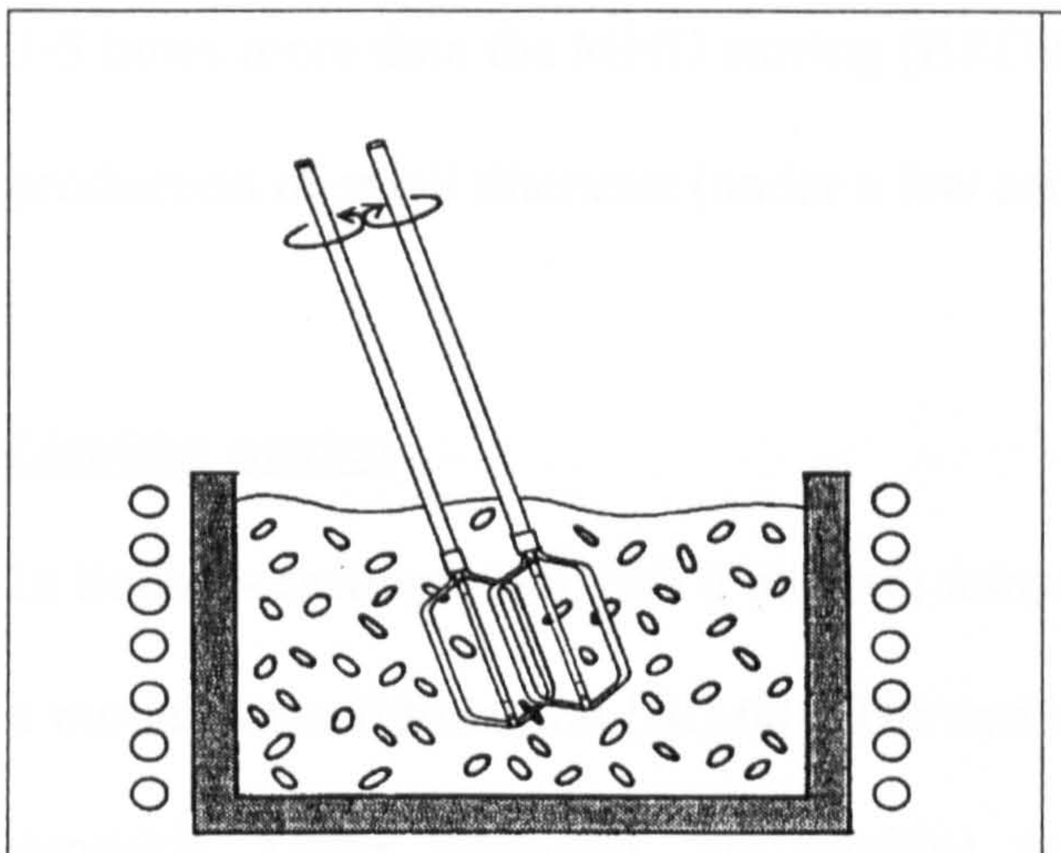

(a)

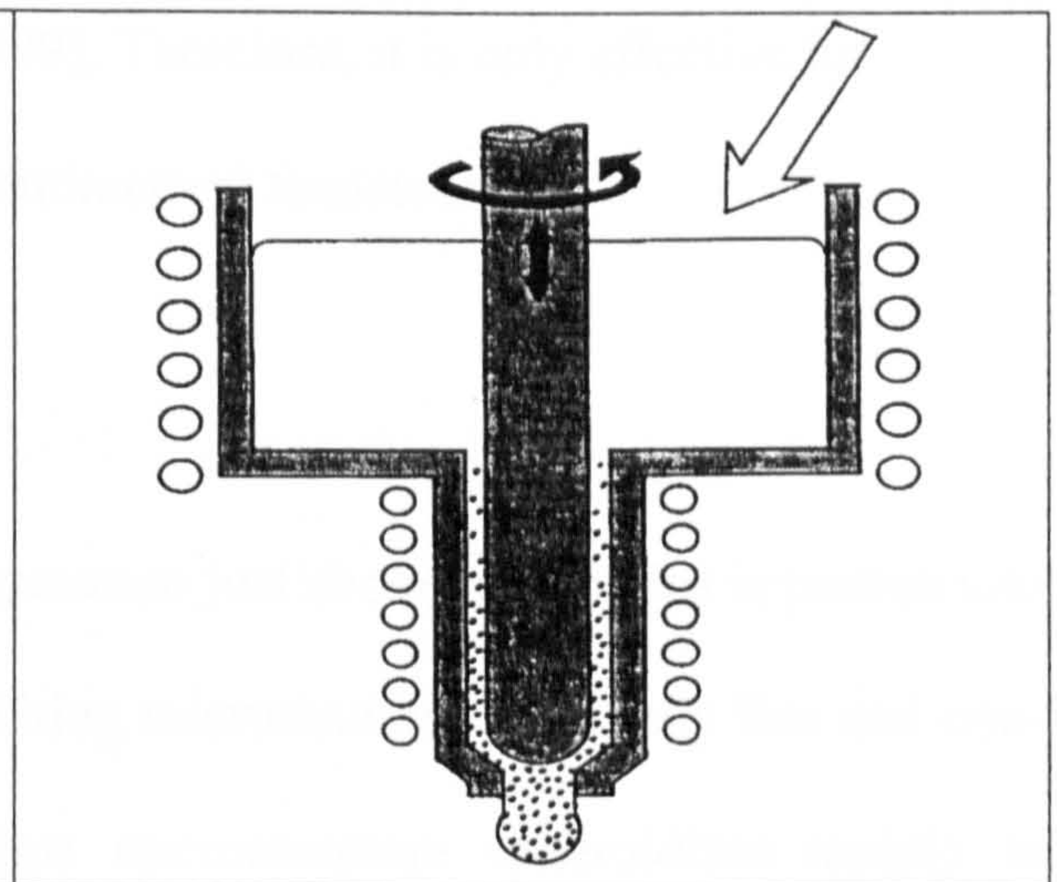

(b)

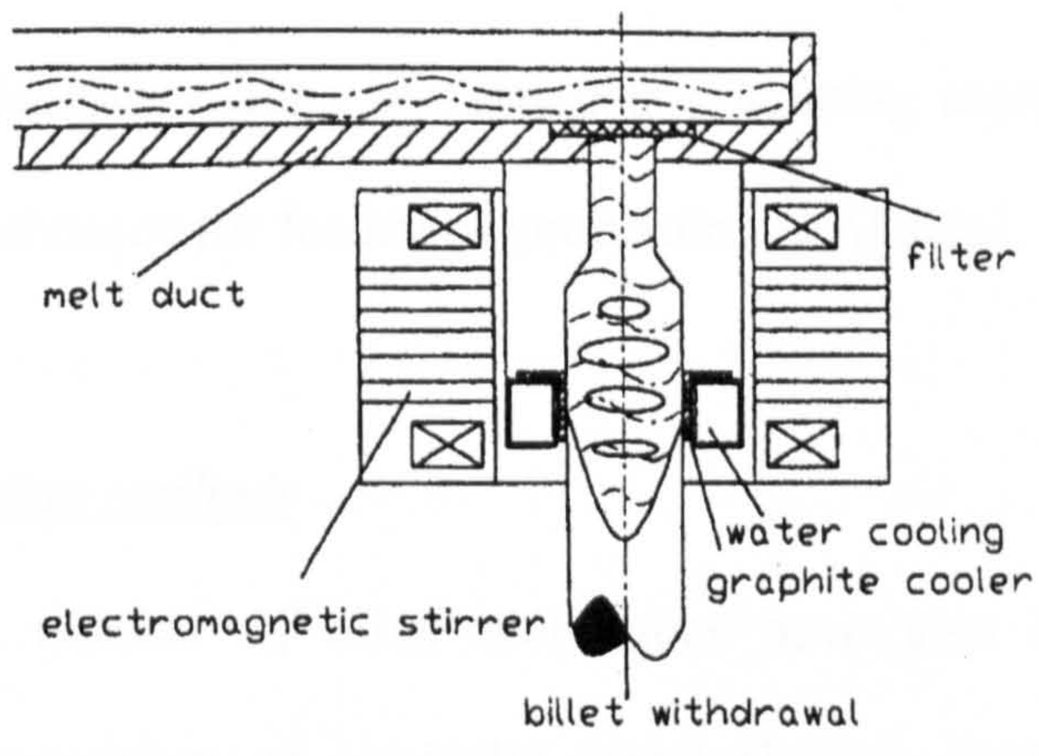

(c)

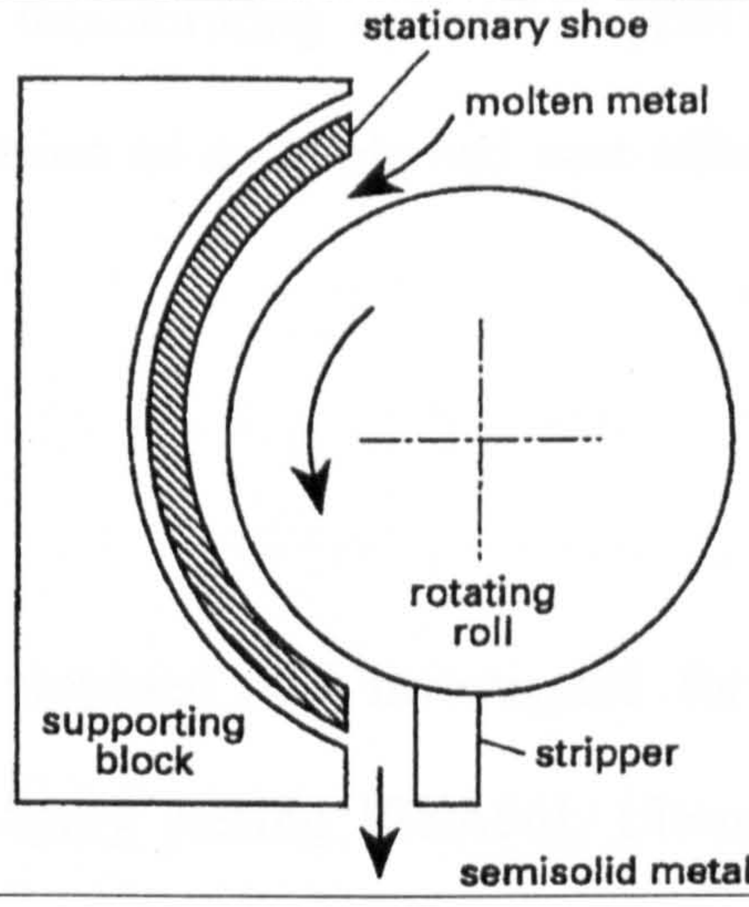

(d)

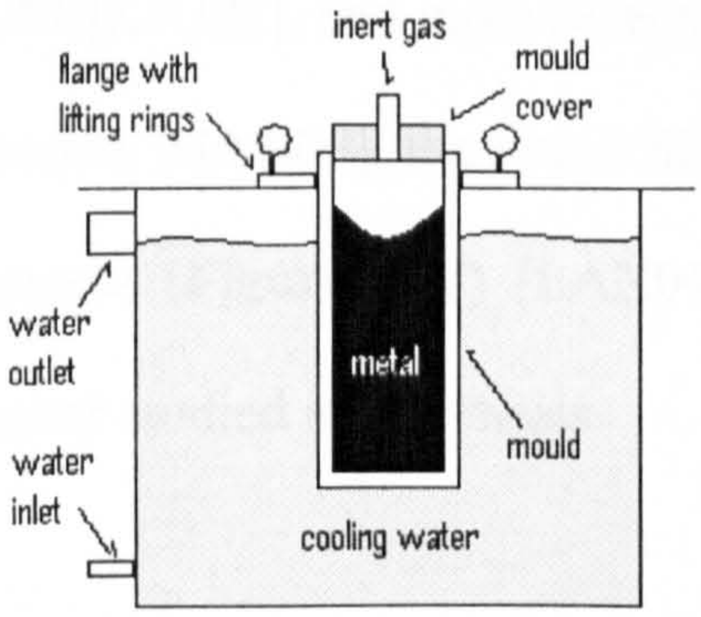

(e)

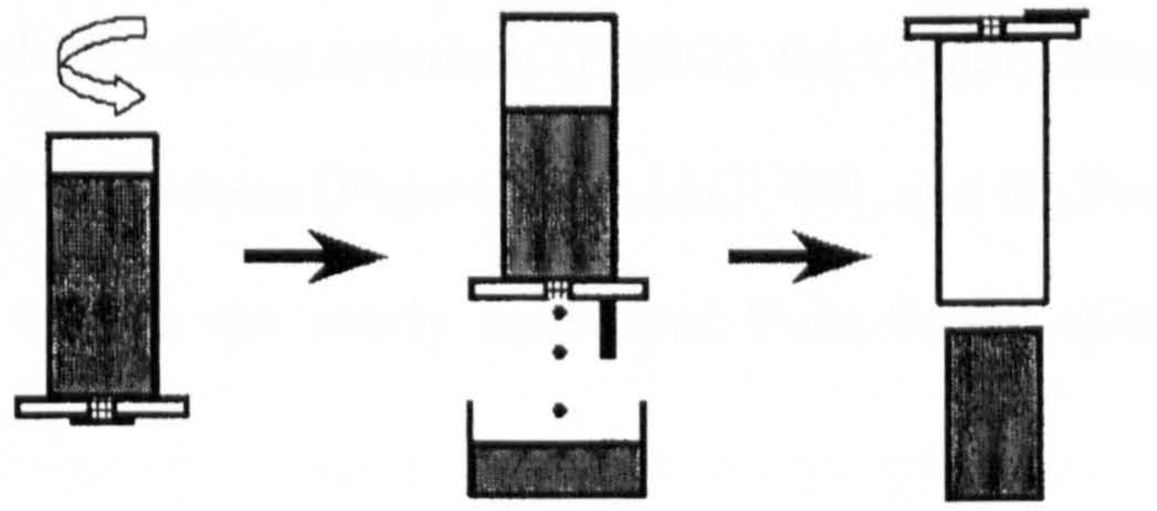

(f)

Figure 2.3 *Preparation techniques for semisolid metal slurries. (a) and (b) Mechanical Stirring process [FLE91], (c) Continuous casting with Magnetohydrodynamic Stirring [ZHA03], (d) Cooling Roll process [KIU92], (e) Rapid Slug Cooling process [AGU04] and (f) Seed process [LAN04].*

3-5 times more than the MHD stirring [BRO99], Therefore, it is only effective for production of small diameter (under a few centimetres) feedstock.

Liquidus casting

In liquidus casting, melt with a uniform temperature just above its liquidus is poured into a mould for solidification [BIL68]. The resulting microstructure is usually fine and non-dendritic. Upon reheating, the liquidus cast microstructure spheroidises rapidly to produce non-dendritic microstructure suitable for thixoforming operations [TAU98]. Liquidus casting in particular is gaining more attention as a simple and cost effective technique for feedstock production [FAN02a].

Other methods

A number of other techniques have also been proposed and investigated for the preparation of semisolid metal slurries. Such as Spray casting [BLA96], Ultrasonic treatment [LIU98], Chemical grain refinement [BRU00], Cooling Roll process (**Figure 2.3d**)[KIU92], and more recently, the Melt Mixing approach [FIN02], the Cooling Slope process [HAG00], the Rapid Slug Cooling process (**Figure 2.3e**) [AGU04], and the Seed process (**Figure 2.3f**) [LAN04], as well as the newly developed Twin-Screw slurry maker studied in this thesis.

2.2.3 Microstructure evolution during melt shearing

The primary goal of slurry preparation is to create an ideal Semisolid microstructure to ensure the favourable rheological characteristics (as described in next section 2-3) to facilitate the subsequent component forming process [FAN02a]. Therefore, the

understanding of microstructural evolution during slurry preparation is very important and hence subjected to a number of investigations.

Microstructure evolution during continuous cooling and shearing

For Al-Cu alloys, Vogel et al [VOG79] observed that with applied shear the primary particles grow as rosettes until a certain limit, beyond which further growth does not occur, but subsequent solidification takes place by formation of new particles. Smith et al. [SMI91] studied the microstructural evolution during solidification of a stirred Al-19wt%Si alloy. They found that with increasing shear rate the average particle diameter decreases, while the particle density increases. Zhang et al. [ZHA03] investigated the structural evolution under the condition of continuous casting with electromagnetic stirring. They concluded that, longer stirring time and lower cooling rate produce a microstructure with a higher degree of sphericity at the billet centre. When the shearing intensity is large enough, the particle size of the primary α phase is mainly dependent on the cooling rate during solidification. The higher the cooling rate, the finer the particle size. Ji and Fan [JI00] studied the effect of turbulent flow on the solidification morphology of Sn-15Pb alloy using a laboratory scale twin-screw rheomoulding (TSRM) machine, developed recently. They found that under intensive turbulent flow, the solidification morphology is spherical even at the very early stage of solidification.

Microstructural evolution during isothermal shearing

The early work by Spencer et al. [SPE72] on the Sn-Pb system using rotational rheometers observed that, with prolonged stirring time, particles change to almost spherical morphology containing entrapped liquid, by a ripening process. Increasing the shear rate accelerates this morphological transition and reduces the amount of entrapped

liquid inside the solid particles. Ryoo and Kim [RYO94] in their isothermal shearing experiments for Mg-Al-Zn-Si alloys found that the particle size and shape factor of the solid particles are almost constant with increasing isothermal shearing time. Ji et al. [JI02a] found for Sn-15wt%Pb alloy that in the low shear rate region: increasing shear rate increases particle density and decreases particle size, while in the high shear rate region both particle size and density reach a plateau. Flemings [KLE91] has concluded earlier that the more vigorous the stirring and the longer the time spent in the semisolid state, the greater the tendency to form equiaxed dendrites, rosettes, and eventually, by a coarsening process, dense spheroids. The microstructure evolution of the primary particles is later related to the rheological behaviour of SSM slurries.

2.2.4 Mechanisms for formation of non-dendritic structure

During dendritic solidification of castings, a number of processes take place within the semisolid region. These include crystallisation, interdendritic fluid flow, solute diffusion and solid growth resulting in a dendritic microstructure [FLE74]. To explain the observed non-dendritic morphology of solid particles under forced convection, several mechanisms have been proposed. These include: dendrite arm fragmentation, dendrite arm root remelting, and growth controlled mechanisms.

Kirkwood [KIR94] suspected that fragmentation mechanisms are likely responsible for the formation of the spheroidal grains in stirred slurries. The early growth of the initial dendritic fragment continues dendritically. With continuing shear and time during solidification, the dendrite morphology becomes that of a 'rosette' as a result of shear and collision and abrasion with other grains. Ripening proceeds during further cooling. Vogel

et al. [VOG79] have proposed a dendrite arm fragmentation mechanism to account for grain multiplication, as schematically illustrated in **Figure 2.4** [DOH84]. They suggested that dendrite arms bend plastically under the shear force created by melt stirring. The plastic strain is accommodated by dislocation generation. At the melting temperature, the dislocations can climb and coalesce to form high angle grain boundaries through recrystallisation. Any grain boundary with an energy greater than twice the solid/liquid interfacial energy is then wetted (penetrated) by liquid metal, resulting in the detachment of dendrite arms.

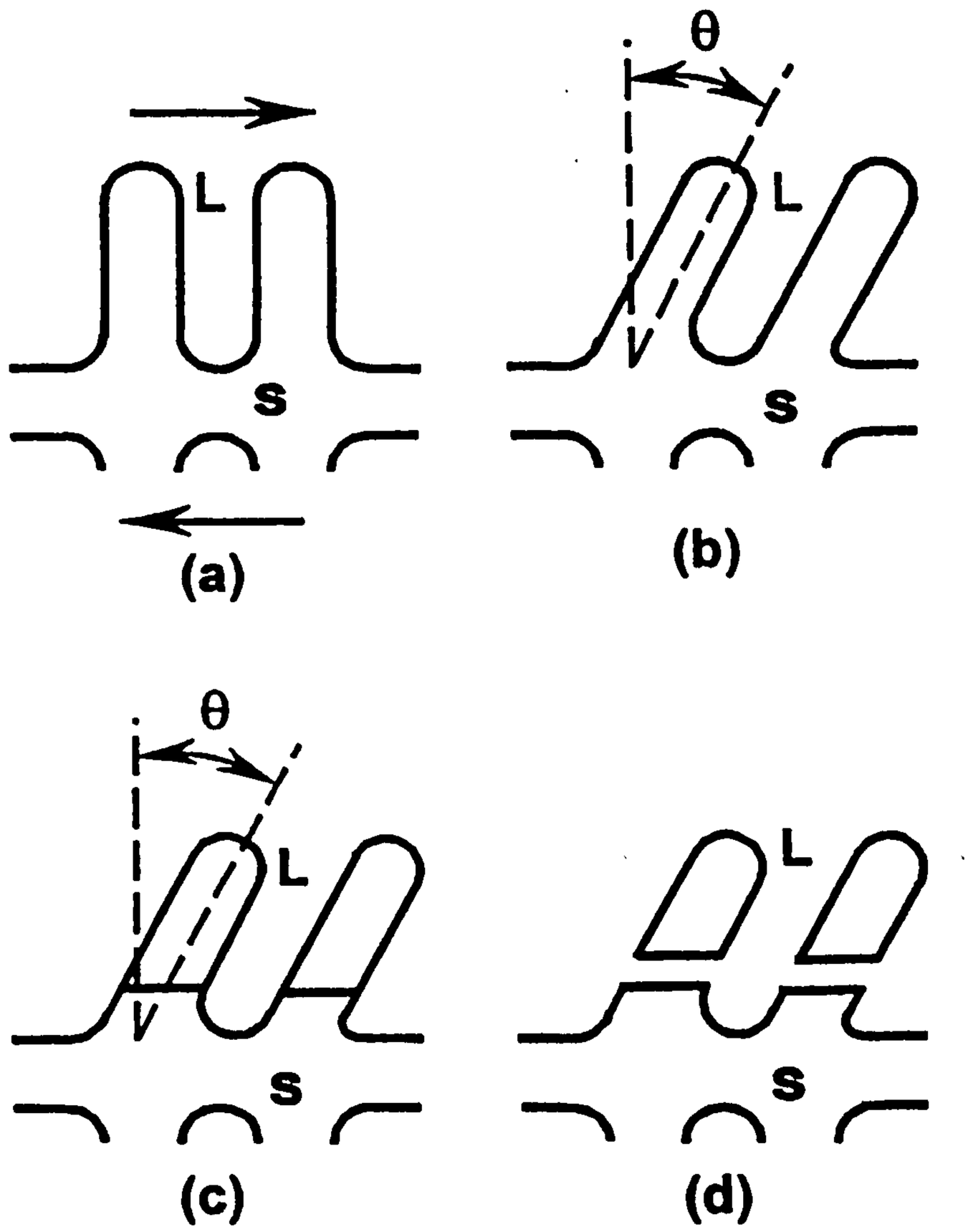

Figure 2.4 Schematic illustration of dendrite arm fragmentation mechanism [DOH84]

However, a question remaining to be answered is whether melt shearing can impose such a high bending moment on small dendrite arms to fracture them [FAN02a]. Flemings [FLE91] earlier suggested that it was possible to melt off or break off dendrite arms at their roots due to shear forces. Following the early proposal by Flemings, Hellawell [HEL96] suggested that secondary dendrite arms could detach at their roots because of remelting due to solute enrichment and thermal-solutal convection.

In recent years, to explain the crystal multiplication in semisolid processing, there has been an increasing belief that the evolution of particle morphology under forced convection is a growth phenomenon, rather than a consequence of dendrite arm detachment [FAN02a][QIN00][ZHA03].

Molenaar et al. [MOL86] in their work proposed that the growth is cellular, based on their experimental observations, they found the thermal boundary layer is hardly affected by stirring, while the hydrodynamic boundary layer is significantly reduced and mass transport is dominated by convection. Ji and Fan [JI02a] experimentally investigated the effect of turbulent flow on growth morphology and concluded that the globular structure is a direct result of spherical growth under intensive forced convection, and no dendrite or dendrite fragments were ever observed. Based on their experimental results, they proposed that the growth morphology changes from dendrite to sphere via rosette with the increasing shear rate and degree of turbulence. This is in good agreement with the theoretical analysis by Qin and Fan [QIN00] using stability analysis and a boundary element method. More recently, Das and Fan [DAS02] have developed a Monte Carlo technique to simulate the microstructural evolution under forced convection. They found that the morphological development of the solid would depend on the geometry of the

diffusion zone around the growing particles. The Monte Carlo simulation shows further that isolated particles rotating in a laminar flow grow with rosette type morphology. At a higher shear rate, where the nature of fluid flow is expected to be turbulent, it stabilises the solid/liquid interface and explains why spherical particles are normally observed when the melt is sheared at a very high intensity.

However, despite uncertainties on structure formation mechanisms, a well known phenomenon is that alloys with the non-dendritic microstructure possess their own special rheological properties in the semisolid state, that are quite deferent from those of dendritic alloys.

2.3 Rheology of semisolid slurries

2.3.1 Rheological behaviour of semisolid slurries

Semisolid metal slurries with a solid fraction less than 0.6 and a globular solid morphology usually exhibit two unique rheological properties: thixotropy and pseudoplasticity [FAN02a]. Thixotropy describes the time dependence of transient state viscosity at a given shear rate, while pseudoplasticity refers to the shear rate dependence of steady state viscosity. All the SSM processing techniques rely on either or both of those properties in the same process. Therefore, it is important to have a good understanding of the rheological behaviour of semisolid slurries.

The first investigation of the rheology of SSM slurries was conducted on the Sn-Pb system by Spencer et al at MIT [SPE72]. They showed that the stirred SSM slurry with a solid fraction higher than 0.2 behaves like a non-Newtonian fluid with an apparent viscosity an order of magnitude less than that of a unstirred dendritic slurry. This observation initiated numerous rheological studies on stirred SSM slurries.

Rheological behaviour during continuous cooling and shearing

During the early investigation into the hot tearing of alloys in 1972, Spencer et al [SPE72] measured the viscosity of Sn-15wt%Pb as a function of solid fraction while continuously shearing the alloy. These results were quite unexpected in that whereas unstirred melts began to stiffen when the solid fraction reached about 0.2, the stirred alloy continued to behave like a liquid beyond 0.4. **Figure 2.5** shows an example of results obtained from the continuous cooling experiments on Sn-15wt%Pb alloy carried

out by Joly and Mehrabian [JOL76]. Following this work, similar studies were carried out on other alloy systems [LEH85][NAN90][KAT91]. The results showed that the viscosity of a semisolid metal slurry is found to be a strong function of cooling rate and shear rate during continuous cooling, low cooling rates and high shear rates decreases the viscosity for a given solid fraction.

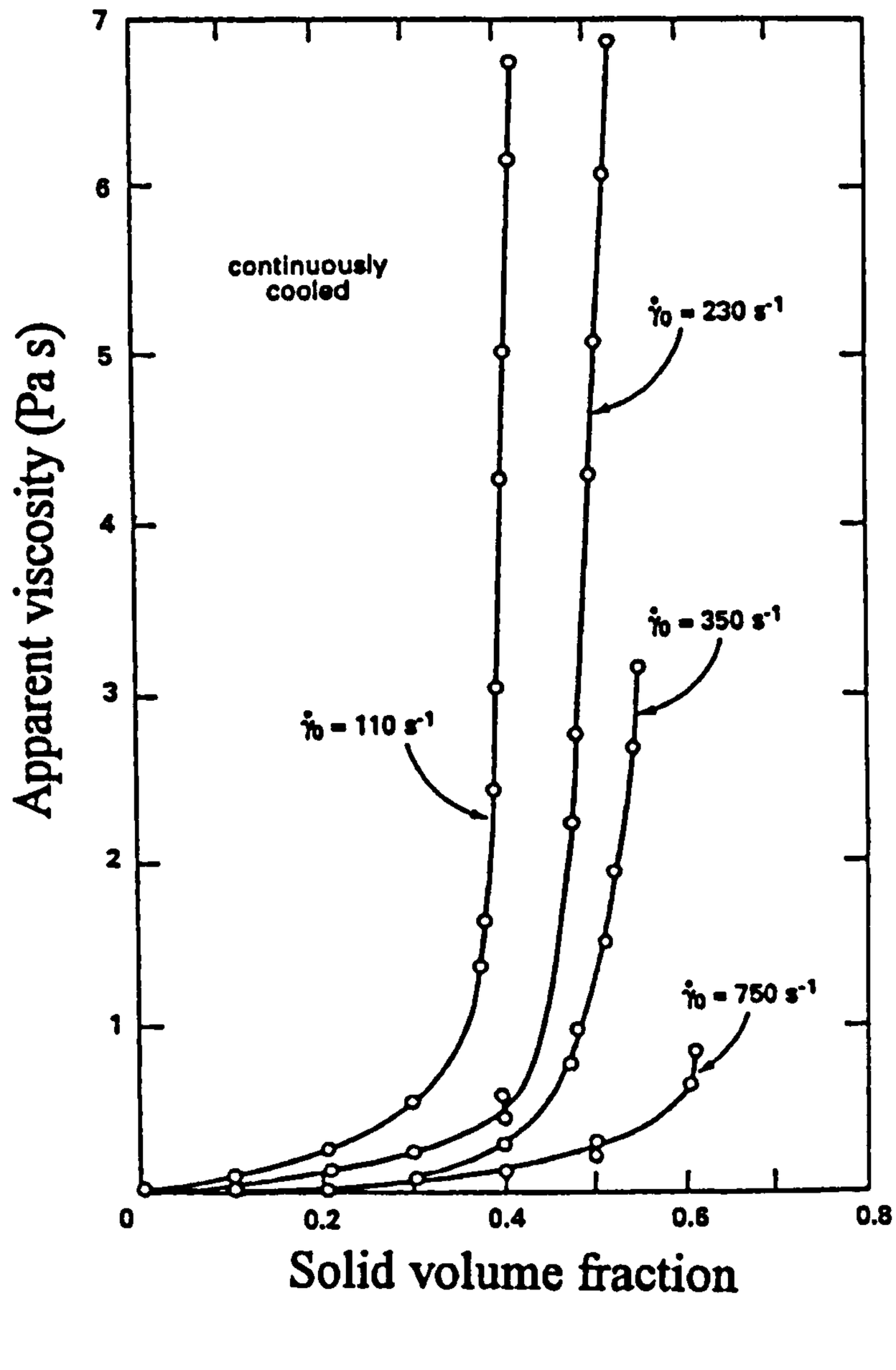

Figure 2.5 *Apparent viscosity versus solid fraction of Sn-15wt%Pb alloy sheared continuously and cooled at 0.33k/min at different shear rates γ_0 [JOL76].*

Koren et.al [KOR02] examined the viscosity of both AZ91 and AM50 magnesium alloys, using a stirring unit with a cooling rate of 1°C/min, stirrer rotation of 100rpm and crucible rotation of 30rpm. In the AZ91 alloy it was observed that there is a tendency toward a moderate rise in viscosity with decreasing temperature in the range of 595°C-575°C. A sharp acceleration in the viscosity rise was observed below that range. In the AM50 alloy it was observed that the range of the moderate rise in viscosity was limited to 620°C-614°C and a similar acceleration in the viscosity rise was exhibited. Therefore, they believed that the appropriate semisolid casting temperature was in the range of 595°C-575°C for AZ91 alloy and 620°C-614°C for AM50 alloy.

Generally, for a given cooling rate and shear rate, the measured apparent viscosity increases with increasing solid fraction, slowly at a low solid fraction and sharply at a high solid fraction. At a given solid fraction, the apparent viscosity decreases with increasing shear rate and decreasing cooling rate. This is because [FAN02a] both increasing shear rate and decreasing cooling rate promote a more spherical particle, which move more easily past one another, i.e., the more spherical and finer the particles, the easier the fluid flow.

Rheological behaviour during isothermal shearing

The isothermal experiments were defined as cooling the alloy at a given rate during stirring, to a predetermined solid fraction and then continuing to shear isothermally. As such, the isothermal shearing leads to a decrease in viscosity until an effectively steady state condition is achieved. The steady state viscosity is a function of solid fraction and shear rate for a given alloy system [FAN02a]. Where, the steady state is defined as a state at which the viscosity of a SSM slurry with a fixed solid fraction and shear rate does not vary with prolonged shearing time.

Turng and Wang [TUR91] showed on a Sn-15wt%Pb alloy that the behaviour is shear thinning (**Figure 2.6**), i.e., for a SSM slurry with a fixed solid fraction, the steady state viscosity decreases with increasing shear rate, approaching an asymptotic value when the shear rate becomes infinite. Such 'pseudoplastic' behaviour has also been confirmed in many other systems [LEH85][FLE92]. It is now generally accepted that the steady state viscosity at a given shear rate depends on the degree of agglomeration between solid particles.

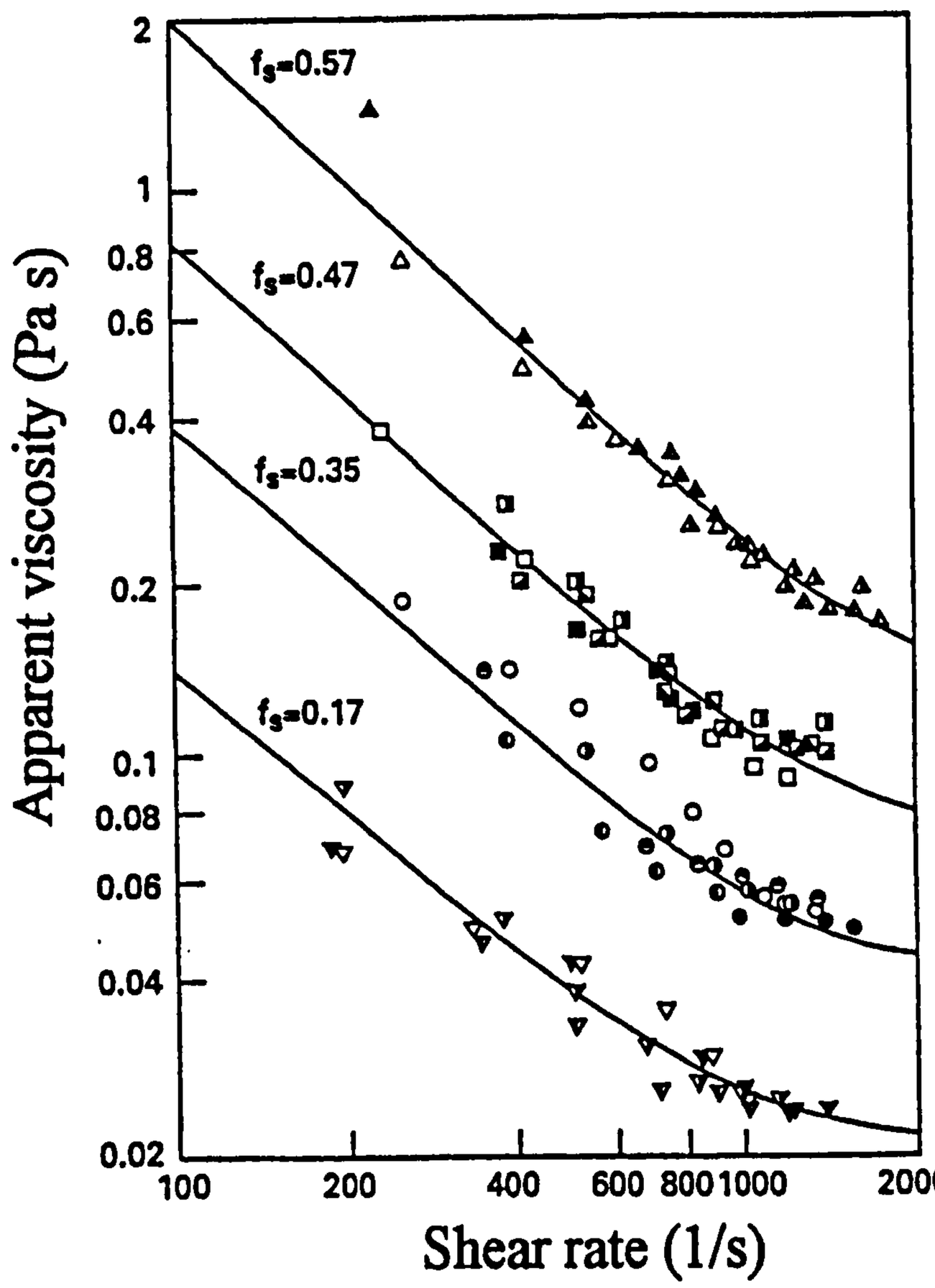

***Figure 2.6** Steady state apparent viscosity versus shear rate in Sn-15wt%Pb alloy for various solid fractions f_s [TUR91].*

Joly and Mehrabian [JOL76] were the first to measure the extent of the 'thixotropy' by the area of the hysteresis loops during a cyclic shear test (**Figure 2.7**). The initial alloy slurry was in a 'steady state' before being isothermally sheared at a solid fraction of 0.4 under a shear rate of $115s^{-1}$ and sheared isothermally for a total time of 5400 seconds, shearing was then stopped. After a rest time t_r, shear rate was increased back to maximum over a time t_u, and then decreased to zero. From Figure 2.7a, the hysteresis loops showed that only a very short shearing time (2 seconds) requires for structural breakdown to reach the 'steady state', for longer than 5 seconds, the thixotropy effect becomes negligible. From Figure 2.7b, the thixotropy continues to increase with increasing rest time (up to 120 seconds). Compared with breakdown process, the structural build-up requires apparently over quite long times. Recently, Fan and Chen [CHE02] have developed a model to study the transient state behaviour of SSM slurries under various shearing conditions. One of the results is a theoretical prediction of the hysteresis loops, which reveals that the physical origin of thixotropy lies in the fact that the deagglomeration kinetics is much faster than the agglomeration kinetics, with the former being a few seconds and the latter a few hundred seconds.

A further study of the steady state viscosity was carried out by Moon (**Figure 2.8**) [FLE91] on Al-6.5wt%Si alloy at $\gamma = 900s^{-1}$ and $fs = 0.4$. The samples were at the steady state viscosity of 0.006 Pa.s at $\gamma = 900s^{-1}$, shearing was then stopped and restarted at the same shear rate after resting time. The instantaneous viscosity is much higher at the start of shear, reflecting the agglomeration that builds up during the rest. With time, viscosity decreases to the steady state value as the structure breaks down. They found that, only quite short times are required for this breakdown, whereas the structure build-up requires much longer times.

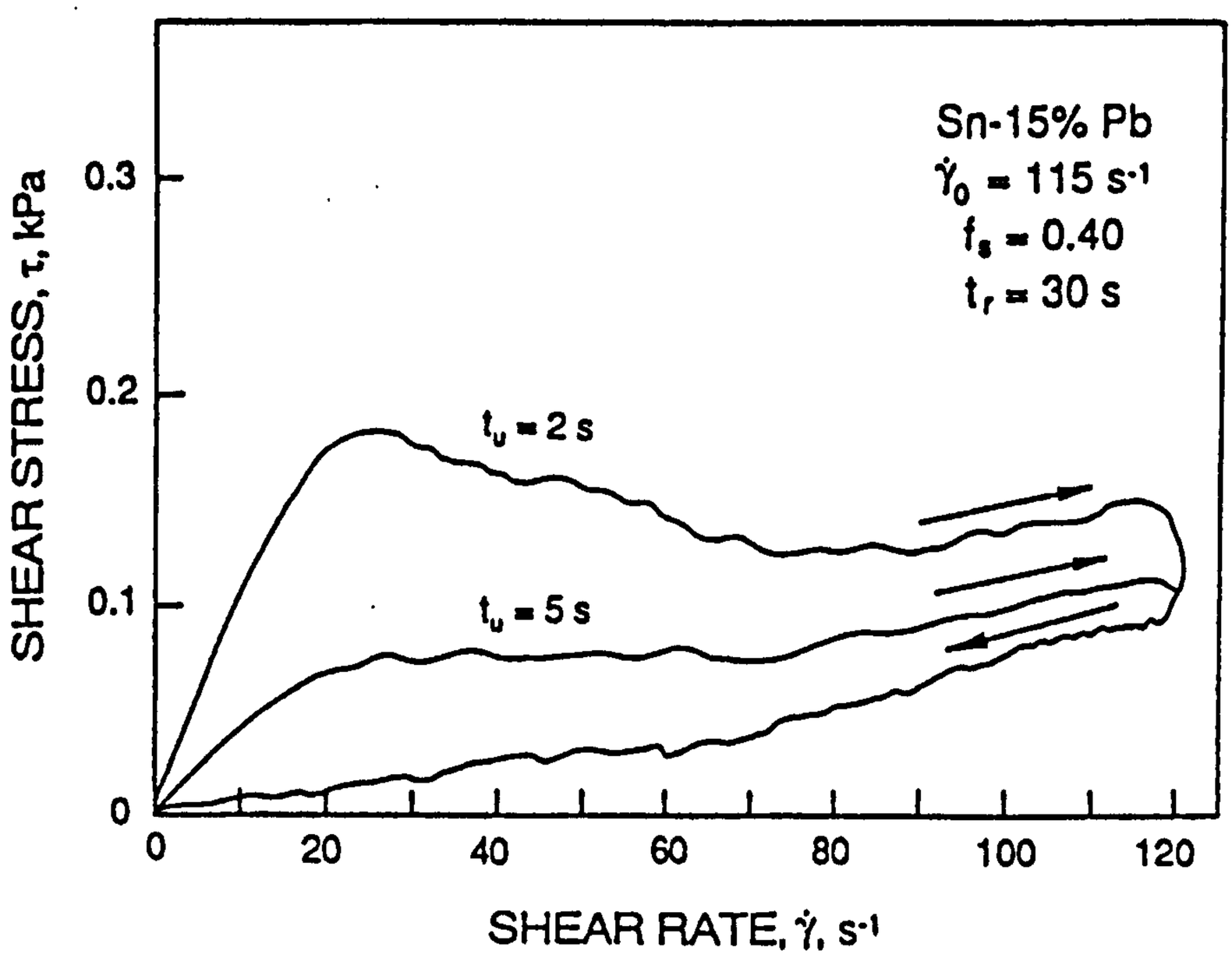

(*a*)

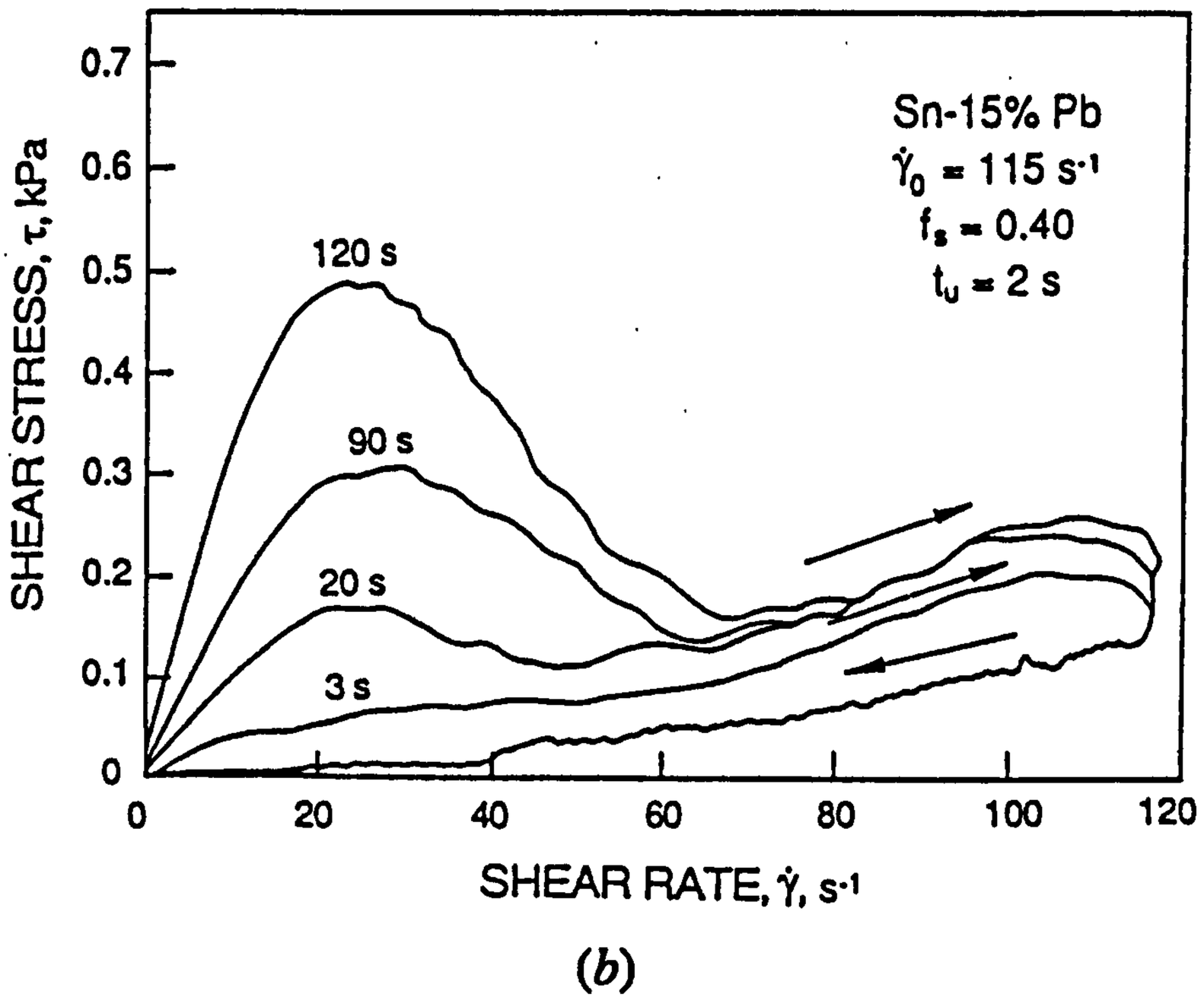

(*b*)

Figure 2.7 *Thixotropy in Sn-15wt%Pb alloy. Area enclosed by each curve is a measure of the thixotropy. (a) Effect of time to reach maximum shear rate for the 'up' portion of the cycle, t_u, and (b) effect of rest time, t_r. [JOL76]*

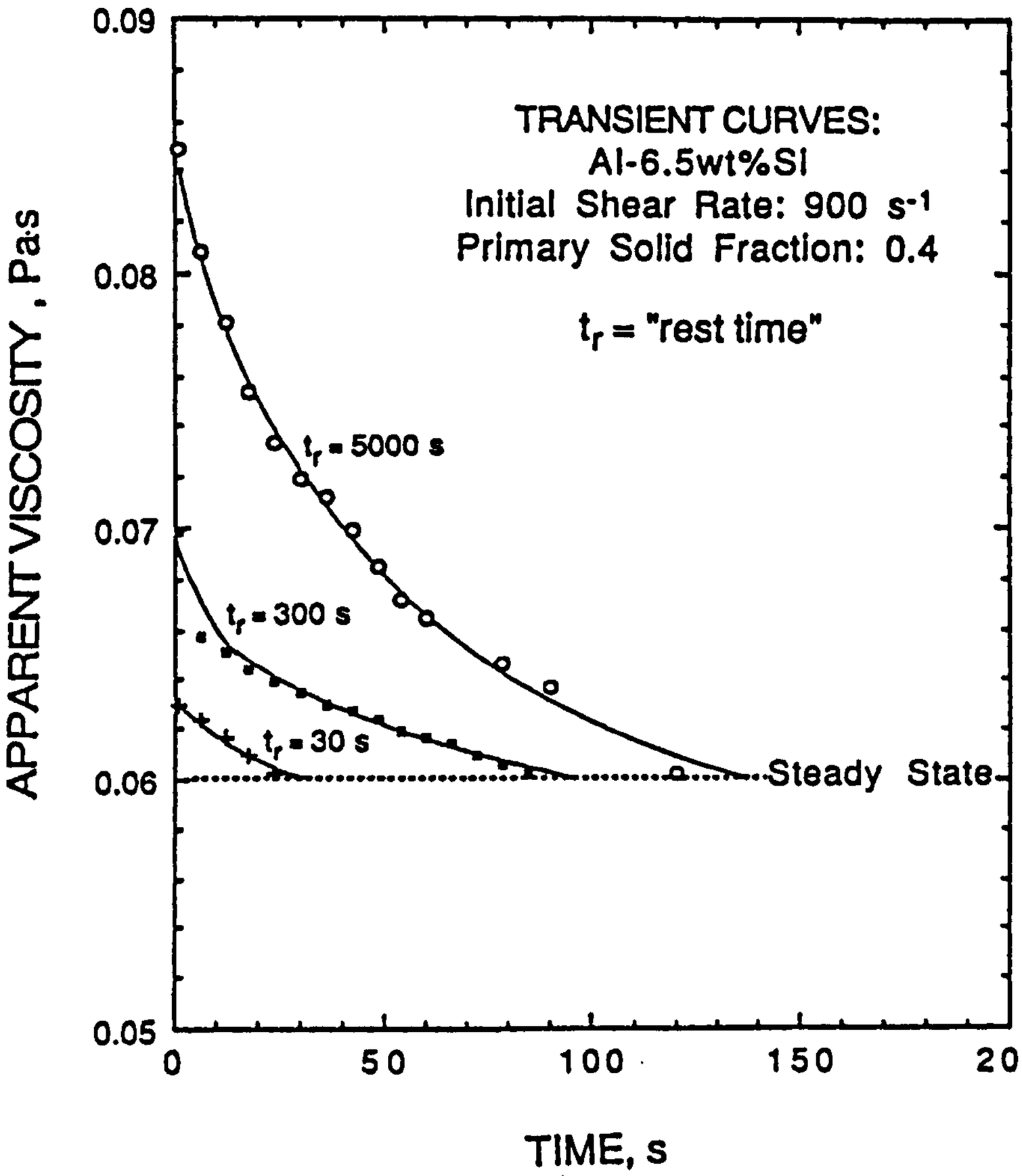

***Figure 2.8** Viscosity of Al-6.5wt%Si alloy at $\gamma = 900\ s^{-1}$ vs time after a "rest time t_r ". All samples were at the steady-state viscosity of 0.06 Pa.s at $\gamma = 900\ s^{-1}$; shearing was then stopped and restarted at the same shear rate after a time t_r [FLE91].*

Another steady state behaviour with a given solid fraction is the presence of yield stress, as has been discussed by Modigell et al [MOD00] for Sn-15wt%Pb SSM slurries. Sannes et al [SAN94] reported that the yield stress for magnesium based SSM slurries is in the range of 10^2-10^4 Pa for solid fractions ranging from 0.3 to 0.6. The yield phenomenon is generally inherent to the thixotropy.

For magnesium alloys, Ghosh and Schilt [GHO94] have experimentally established the thixotropic characteristics of AZ91D and AM50 alloys; their studies confirm that

magnesium alloys exhibit pseudoplastic rheological behaviour comparable to that of the tin-lead system.

2.3.2 Rheological modelling of semisolid slurries

As mentioned above, plenty of experimental work has demonstrated a strong coupling between the slurry structure and the flow behaviour under various external flow conditions, and it has been well established that the semisolid metal slurries exhibit 'pseudoplasticity' and 'thixotropy'. The modelling of thixotropy is quite complex and also subjected to a number of simulations [MAD96][CHE02]. In this section, considering mainly the rheo-route processes, we contemplate the modelling of pseudoplasticity.

In rheological terms, these semisolid slurries are deemed to exhibit 'pseudoplasticity'. Empirical equations developed to describe the full range of viscosity of pseudoplastic metals require at least four parameters [FAN02a]. Following Brown [BRO90], the constitutive relations for semisolid alloys might be written:

$$\eta = \eta(\gamma, f_s, m, s) \qquad \textbf{Equation 2.3.1}$$

Where η is viscosity, γ is shear rate, f_s is solid fraction, m is a measure of particle morphology and s is a measure of degree of particle agglomeration. However, a simple and widely used relation that is often useful over wide ranges of shear rate is the well-known 'power-law' model [JOL76]:

$$\eta = K \gamma^{n-1} \qquad \textbf{Equation 2.3.2}$$

Where n is called the 'power-law' index, and K is the 'consistency'. Both n and K are solid fraction dependent factors. The smaller the power-law index, the greater the

pseudoplasticity. We may use this simple model to understand the effects of process variables on viscosity of semisolid slurries.

Recently, Chen and Fan [CHE02] developed a microstructural model that describes the flow behaviour of liquid-like SSM slurries under simple shearing. In this model, a liquid-like SSM slurry is considered as a suspension in which interacting spherical solid particles of low cohesion are dispersed in a liquid matrix. In a simple shear flow field, the dynamic interactions between solid particles result in the formation of agglomerates. Under the influence of viscous forces, collisions between agglomerates lead to new agglomerates of a larger size and, at the same time, larger agglomerates also break up giving rise to agglomerates of a smaller size. At a particular time, the state of agglomeration is described by a structure parameter n, which is defined as the average particle number in agglomerates. Based on such considerations, both viscosity η and shear stress τ can be expressed through effective solid fraction (Φ_{eff}, defined as the sum of the actual solid fraction and the entrapped liquid fraction) as a function of the structure parameter n:

$$\eta = \eta_0 (1 - \Phi_{eff})^{-5/2} \qquad \textbf{Equation 2.3.3}$$

$$\Phi_{eff} = \left(1 + \frac{n-1}{n} A \right) f_s \qquad \textbf{Equation 2.3.4}$$

$$\tau = \eta (n, \gamma) \gamma \qquad \textbf{Equation 2.3.5}$$

Where η_0 is the viscosity of the liquid matrix, A is another model parameter related to the packing mode. Equation 2.3.4 indicates that the viscosity of a semisolid slurry is a direct function of the viscosity of the liquid matrix and the effective solid fraction. The flow conditions affect viscosity only indirectly through changing the effective solid fraction.

2.3.3 Deformation behaviour of semisolid slurries

Semisolid metal slurry can be roughly divided into two broad categories [FAN02a]: a 'liquid-like' slurry contains dispersed solid particles and behaves like a fluid under external forces, while a 'solid-like' slurry contains an interconnected solid phase and behaves like a solid, exhibiting a well defined yield strength. The deformation mechanisms for these two types of slurry are fundamentally different.

The semisolid slurry with lower solid fraction (<40%) will be allowed to flow under a stress like a suspension in the two-phase region [CHE02]. Semisolid slurries with high solid fractions (40-60%) are usually treated as two phase systems in which a solid skeleton is saturated with a near-Newtonian liquid phase [GEB00]. Such a slurry behaves thixotropically and viscosity can be varied over a wide range, from about 10^{-1} to 10^{6} Pa.s, depending on the shear rate [FLE91]. In magnesium alloys, during the solidification process, the particles are interconnected by solid thin necks or light coalition in a 3D network, which will remain with low melting temperature liquid after the consequent heating to the semisolid state. The particle boundaries in these solid necks are not associated with any preferred orientation relationship [SAN94]. When stress is applied to a semisolid fluid, the fluid shows a solid-like behaviour as long as the applied stress is below the material yield stress (as discussed previously). If the applied stress exceeds the material yield stress, the fluid will flow and display a liquid-like behaviour.

2.4 Technologies for semisolid metal processing

The fluid like behaviour of semisolid metal slurry under a high stress has prompted several new technologies for semisolid metals forming processing. Generally, the technologies for forming the partially melted non-dendritic alloy slurries into a near net component can be divided into two basic routes [FLE00][FAN02a]: rheo-route and thixo-route. The rheo-route involves preparation of a SSM slurry from liquid alloys by shearing during solidification and transferring the prepared SSM slurry directly to a die or mould for component shaping e.g., Rheo-Moulding process [FAN00][JI02b], Rheo-Mixing process [FAN01], and New Rheocasting process [POT00] etc. The thixo-route is basically a two-step process, involving preparation of a feedstock material with appropriate non-dendritic structure, reheating the thixotropic material to a semisolid temperature and subsequently shaping within a die, e.g., Thixomoulding process [POL95], Thixocasting process [SAH98], Thixoforging process [KOP98] etc. The deformation and flow of the semisolid alloy within the die is different from that of pure liquid or pure solid in either process.

Thixocasting

In principle, a variety of reheating methods for raw semisolid materials were used, for instance, radiation and convective heat transfer within an electric resistance furnace [ZHA03]. However, induction heating by the uniform heating performance is generally the preferred approach [HIR98]. When the alloy is known to be in the correct softened condition, the partially melted SSM alloy may be transferred to the die or shot chamber by robot handling, it is then forged (Thixoforging) or injected into the die (Thixocasting), as in **Figure 2.9a** [FAN02a]. In Thixocasting, a reheated billet is transferred to the shot

chamber, under the pressure of the moving shot piston; the viscosity of the metal is reduced prior to die filling due to the high shear rate at the gate. Thixocasting is now a firmly established processing technology for aluminium; trials have shown that the method also works for magnesium alloys [NAD98]. Due to its high productivity and superior mechanical properties, Thixocasting process covers most applications, including automobile wheels, brake cylinders, valve bodies, and various covers and housings, etc. [KEN88][GIO00].

Thixomoulding

Thixomoulding was developed by Dow Chemicals and is currently marketed by Thixomat [PAS92]. It is based on using magnesium alloy granules as thixotropic feedstock in a casting machine, which shows many similarities to a plastic injection-moulding machine. In the Thixomoulding process, shown in **Figure 2.9b** [POL95], the magnesium alloy granules are fed into an electrically heated chamber where they are reheated before transfer by a single reciprocating screw. Finally, the slurry is injected into a die by rapid movement of the screw. Thixomolding combines die casting with injection moulding and has been increasingly used for making near-net-shape Mg-alloy components [CZE01]

Rheo-Moulding

Similar to the Thixomoulding process, Rheo-moulding is a technology adopted from the polymer-processing field using screw mechanism. In last few years, the single screw Rheo-moulding process has been extended from vertical injection to a horizontal injection for moulding magnesium alloy parts [FAN02a]. Recently, Fan [FAN00] has developed a Twin-Screw Rheo-moulding process for use with low melting point alloys or

magnesium alloys. More recently, the TSRM system has been extended to the Rheo-mixing [FAN01] and Rheo-diecasting [FAN05b] processes.

New Rheocasting (NRC)

The NRC process (**Figure 2.9c**) [POT00] starts with a conventional light metal alloys and transforms the melt into the rheocasting billet in a steel permanent mould, by controlled cooling, where the desired globular microstructure is produced. During investigation, the NRC process has reported an overall cost reduction of approximately 20% over the classical Thixocasting process [HAL00].

Furthermore, other SSM technologies including the SSR process developed by MIT [YUR02], the Cooling slope plus Twin-Roll Caster process (**Figure 2.9d**) developed by Osaka Institute of Technology [HAG04], and the Rheo-Container Process (RCP) developed by RWTH [AGU04], are under investigation.

Currently, SSM processing is dominated by Thixocasting using the feedstock produced by MHD continuous casting, which is a two-step process, and the industrial acceptance has been very slow after 30 years of research and development [FAN02a]. As time has progressed, the disadvantages of the Thixocasting route are becoming apparent [FLE00]. However, in consideration of cost saving, overall energy efficiency in production, and process management, it appears that the integration of slurry making and component shaping operation into one single process seems more promising [FLE00][YUR02][GIO02].

(a)

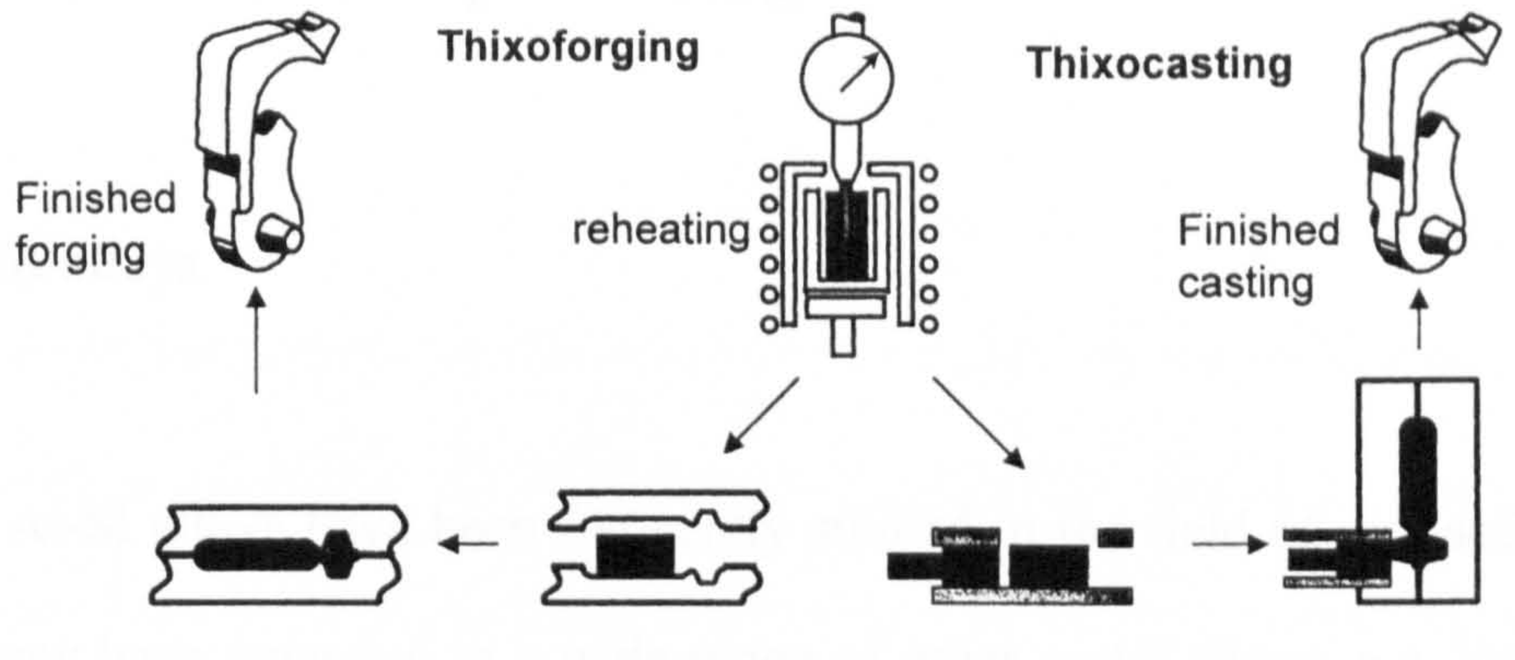

(b)

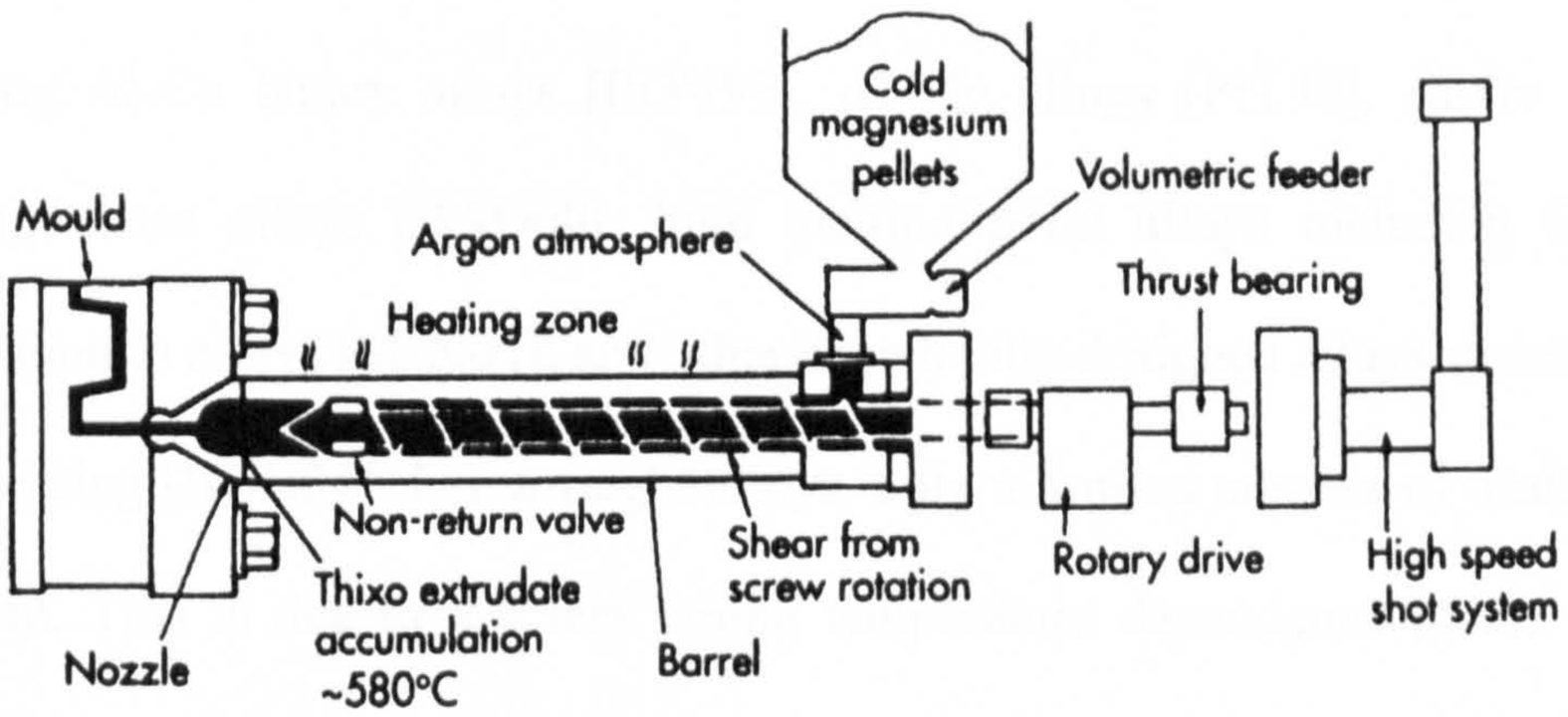

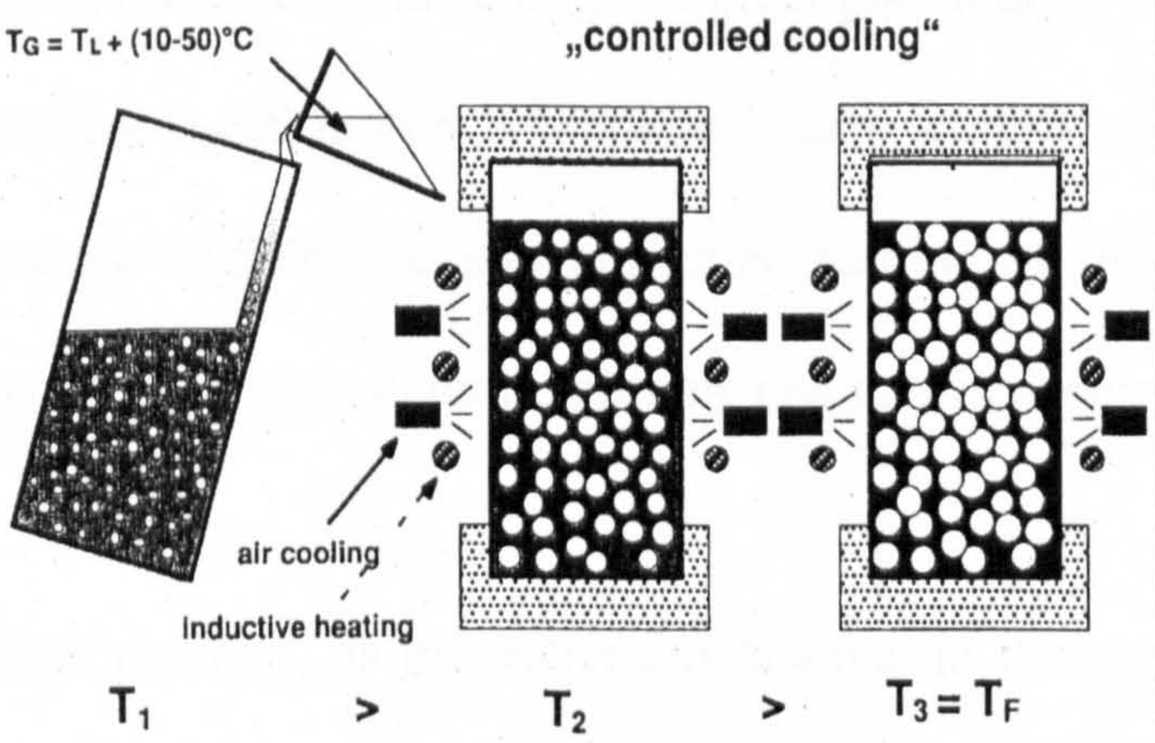

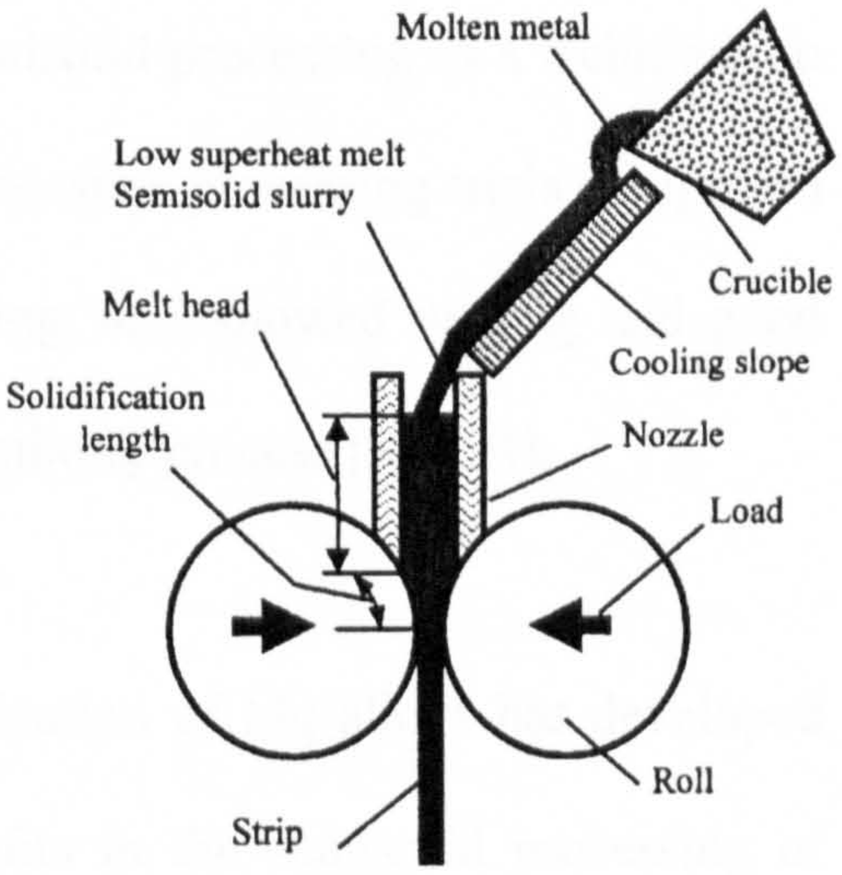

(c) (d)

Figure 2.9 *Technologies for semisolid metals forming. (a) Thixoforging/Thixocasting [FAN02a], (b) Thixomolding [POL95], (c) New Rheocasting [POT00] and (d) Cooling slope plus Twin-Roll caster [HAG04].*

2.5 Alloys for semisolid processing

2.5.1 The SSM alloys

Traditionally Al-Si alloys have been frequently studied in the field of semisolid metals, but this has now been extended to a wide range of other metal alloys, e.g. low melting point alloys, such as Sn-Pb binary alloys; Zn-Al alloys [LEH85]; aluminium based alloys, including Al-Cu binary alloys [ROV99], Al-Mg alloys [PIT98], Al-Ge alloys [ANT96]; copper-base alloys [BAU00]; high melting point alloys including ferrous [KIM98] and titanium alloys [SUN04]; and other specifically designed alloys systems for semisolid processing [BUH04]. For wrought alloys, only a limited number of trials have been carried out. This is due to the very strong temperature dependence of the liquid volume fraction [FAN02a], i.e., a small variation in temperature induces a large change in solid fraction, resulting in a microstructure not favourable to semisolid processing. However it is worth noting the great potential of semisolid processing as a technique to produce metal matrix composites. Early work in composites processing trials recognised that the higher viscosity prevented settling or floating, and allowed wetting and good bonding between ceramic particle and matrix during mixing process [KIR94].

More recently, as the increasing interest in the application of Mg-alloys has developed encouraging investigation of these alloys, the benefits in the semisolid processing of Magnesium alloys have been recognised.

2.5.2 Magnesium alloy selections for semisolid processing

The growing use of magnesium alloys requires the selections of Mg-alloys that can take advantage of SSM processing. In this area, computational thermodynamics is a useful tool for the alloy development for SSM processing [LIU02]. Based on thermodynamic calculations, the effects of alloy composition variation on the factors that influence SSM processability and mechanical properties of the final components can be analysed. These factors include SSM processing temperature, the limitation on temperature sensitivity of solid fraction $\left|df_s / dT\right|$, restriction on solidification range ΔT_{S-L}, potential for age hardening, limitation on proportion of different phases during solidification processing and the stability to composition tolerance. The alloys that offer potential improvement to both processability and mechanical properties can be selected.

Liu and Fan [LIU02] carried out thermodynamic calculations using Thermo-Calc System in combination with the MG-DATA database to evaluate Mg-alloy selections for semisolid processing. They found that for commercial magnesium alloys with a given composition, several Mg-alloys satisfy $\left|df_s / dT\right| \leq 0.015$ for good processability in the Rheo-route ($f_s < 0.6$) (**Figure 2.10**); for SSM alloy selections in the Mg-Al-Zn and Mg-Al-Mn systems, projections of these calculated equilibrium compositions that satisfy $\left|df_s / dT\right| \leq 0.015$ at $f_s = 0.3$ in the Mg-rich corner of both systems as shown in **Figure 2.11**. Currently, alloy design for semisolid processing is gaining more attention.

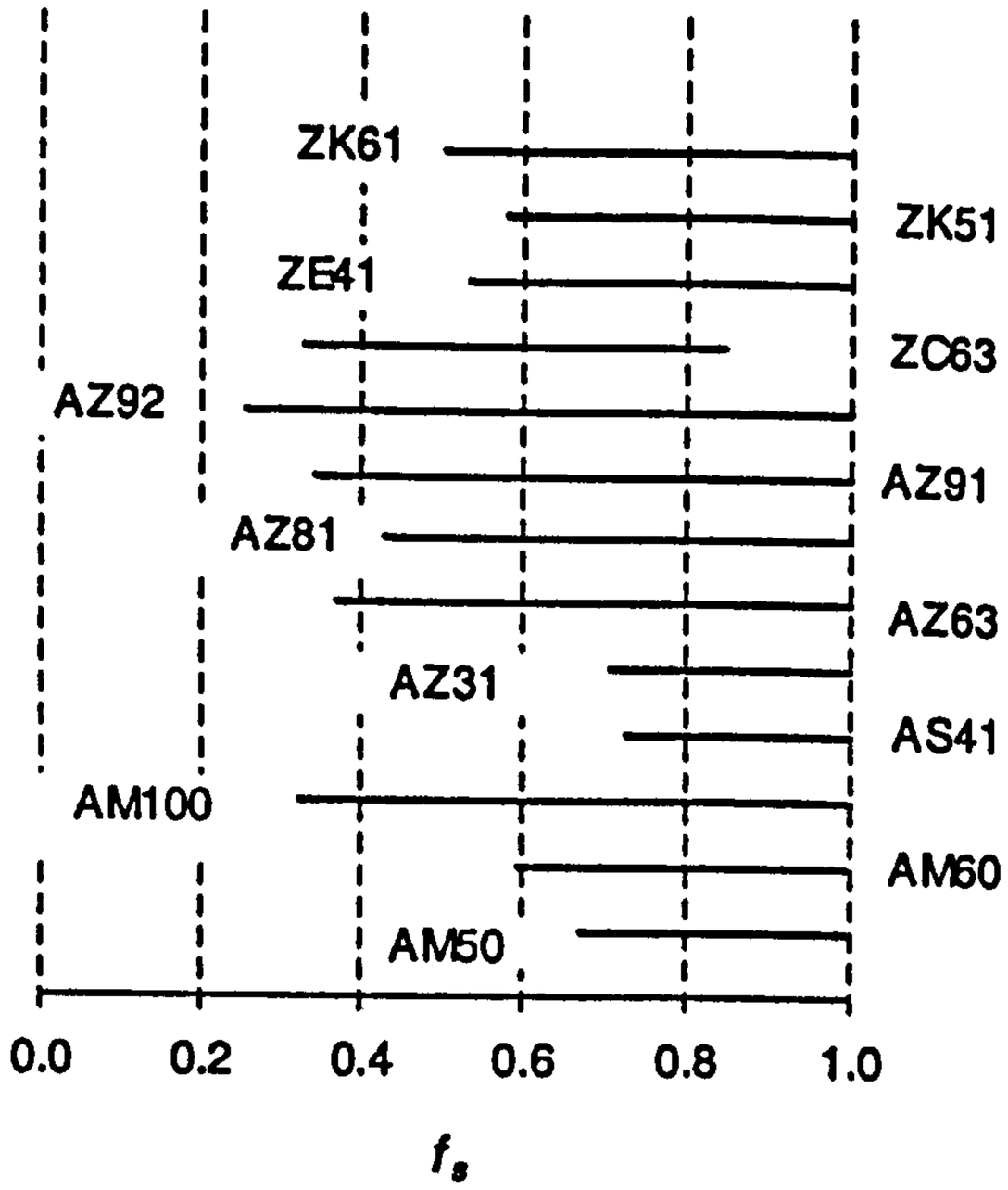

Figure 2.10 *Calculated equilibrium solid fraction range that satisfies* $\left|df_s / dT\right| \leq 0.015$ *for some of the commercial magnesium alloys [LIU02].*

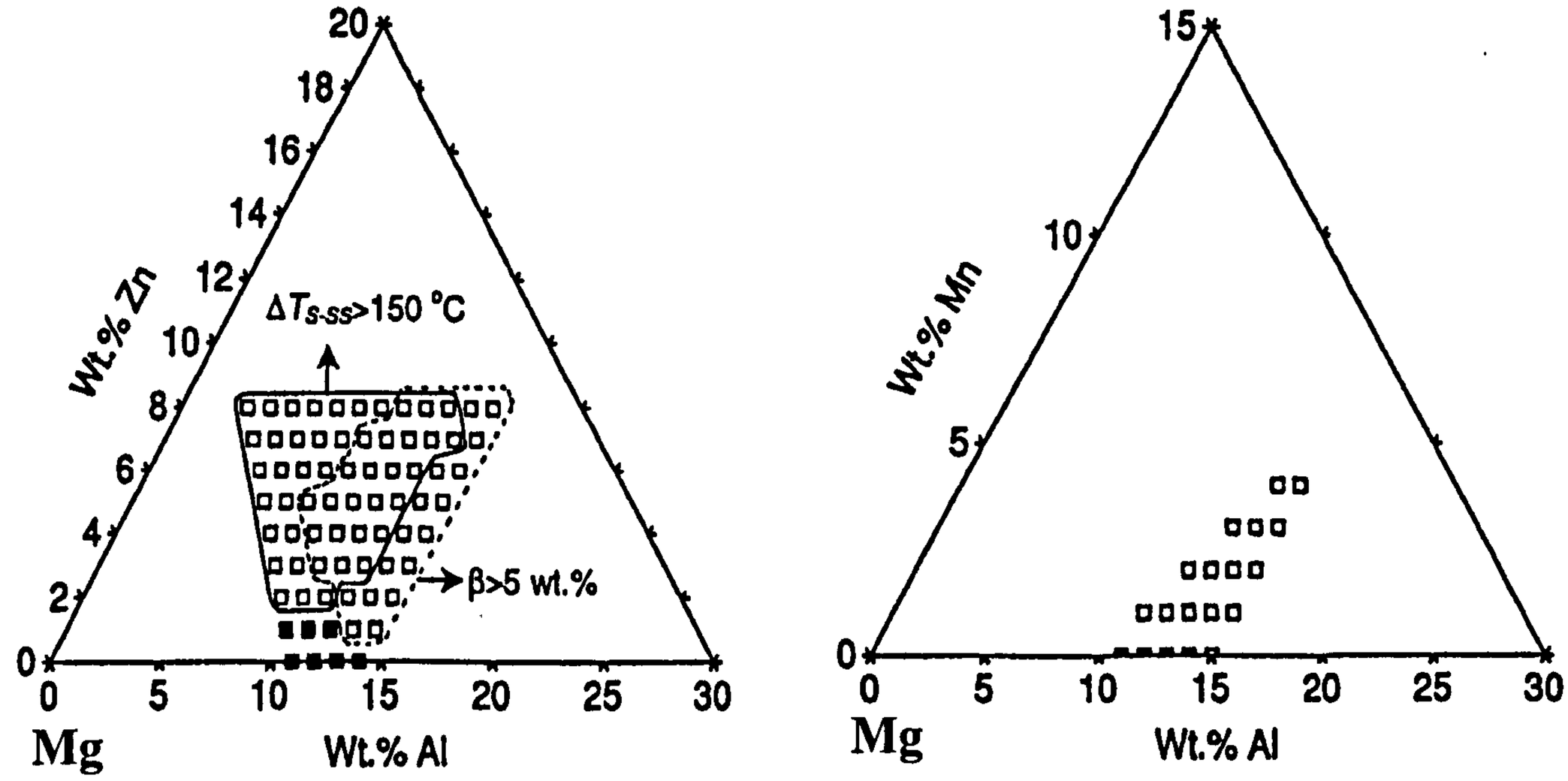

Figure 2.11 *Projections of calculated equilibrium compositions that satisfy* $\left|df_s / dT\right| \leq 0.015$ *at* $f_s = 0.3$ *in the Mg-rich corner of the Mg-Al-Zn (a) and Mg-Al-Mn (b) system [LIU02].*

2.6 Semisolid processing of magnesium alloys

2.6.1 Magnesium and magnesium alloys

Magnesium has a hexagonal close-packed (hcp) crystal structure, with lattice parameters of a=0.3202nm and c=0.5199nm [AGH04]. This structure is essentially different to other commercial metals, for instance, Al (fcc), Cu (fcc) and Fe (bcc) [ROB92]. At temperatures below 498K, plastic deformation of Mg crystal occurs mainly by slip on the basal planes in the close-packed <1 1 $\bar{2}$ 0> directions and by twinning on the pyramidal {1 0 $\bar{1}$ 2} planes. Thus, the magnesium crystal has only 3 geometrical and 2 independent slip systems, much less than in aluminium crystal (**Figure 2-12**)[POL95]. At temperatures above about 498K, additional pyramidal {1 0 $\bar{1}$ 1} slip planes become operative so that deformation becomes much easier and twinning is less important. For this reason, magnesium alloys show limited cold formability but are readily hot worked in various ways. Contrarily, magnesium has excellent castability [AGH04], it allows casting of parts with very complicated shapes.

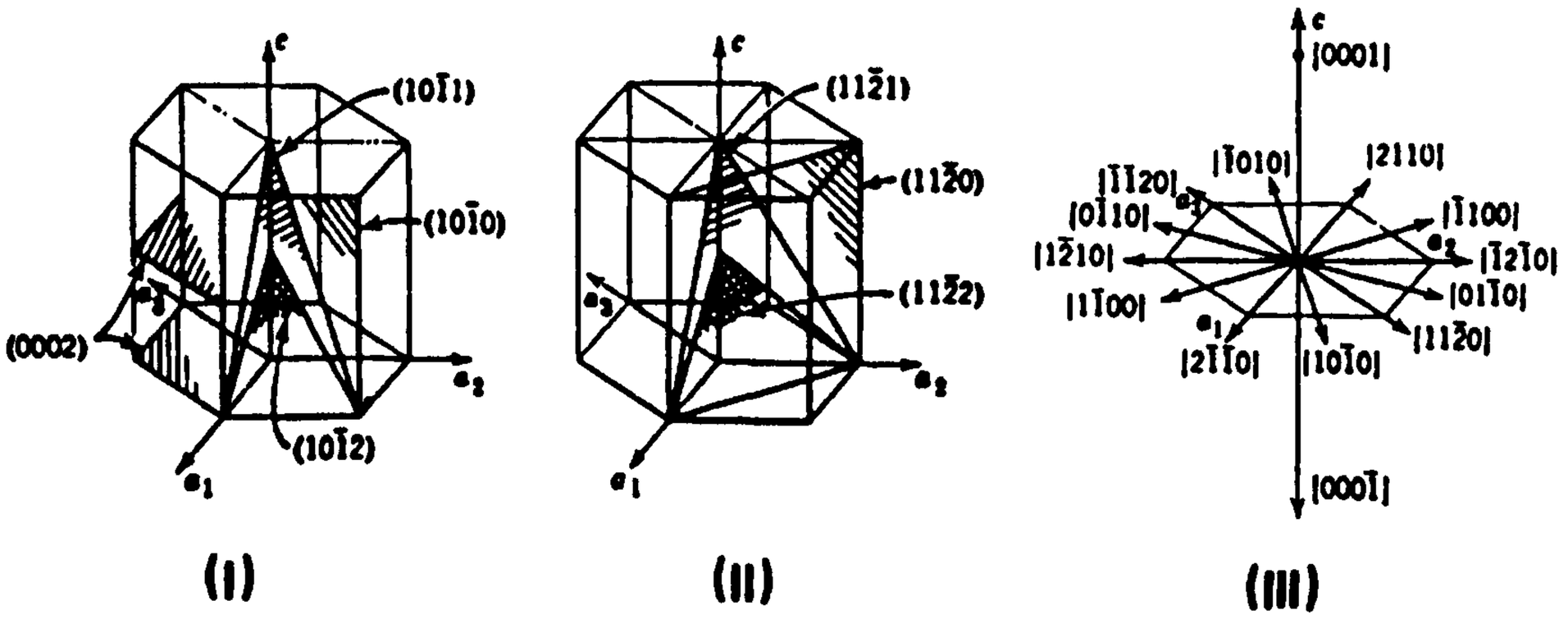

Figure 2.12 Principle planes and directions in the magnesium hexagonal unit cell [POL95].

However, pure magnesium is rarely used for engineering applications and it is commonly alloyed with other metals to improve the alloy properties significantly [GRE72]. Conventional Mg alloys are strengthened by solid solution hardening and/or by precipitation hardening. Extensive solid solutions form if the atomic radii of the solute and the solvent do not differ by more than about 15% [CAH96]. Additional factors governing extensive solid solution include: type of crystal structure, equivalent valencies, and electrochemical factors. Several practically important elements such as Al, Zn, Mn, Y, etc. have relatively high solid solubility in magnesium and the solubility always decreases with increasing temperature [LYO96]. So far, most magnesium alloys can be classified into Mg-Al system, Mg-Mn system, Mg-Zn system, Mg-RE system and Mg-Th system [POL95].

The Mg-Al system has been the basis of the most widely used magnesium casting alloys [AVE99]. Most alloys contain 3%-9% aluminium with small amounts of zinc, which gives some increase in tensile properties, and manganese, which improves corrosion resistance. The AM series of Mg-alloys with reduced aluminium content, have improved properties because of a reduction in the amount of $Mg_{17}Al_{12}$ around grain boundaries. Conversely, the high zinc Mg-alloys also have been investigated recently for die-castings and shown that they also have sufficient fluidity and attractive die-casting characteristics [POL94]. In 1937, Sauerwald, in Germany, discovered that zirconium had an intense grain-refining effect on magnesium [POL95]. Since then, the Mg-Zr alloys (no Al) have become of significant interest. Furthermore, efforts to improve the creep strength of magnesium die-casting alloys at temperatures exceeding 120°C have resulted in the introduction of alloys containing silicon or rare earth metals [BUC04]. These alloying elements form intermetallic constituents that stabilise the grain boundaries. However,

other newly designed alloys for high temperature properties and grain refinement [NIS00], or for semisolid processing [LIU04] are in application and still developing.

2.6.2 Processing of magnesium alloys

Melt processing of magnesium alloys

Unlike aluminium and its alloys, the presence of an oxide film on molten magnesium does not protect it and magnesium alloys tend to oxidise or burn in air rapidly [AVE99]. Due to the strong oxidation nature, suitable fluxes or atmospheres must be used during melting for Mg-alloys. Suitable fluxes include those containing $MgCl_2$, KCl, $BaCl_2$, CaF_2 and MgO [RIC03]. Protecting the melt in this way, results in retention of the flux in the melt, which can further decrease the corrosion resistance of the Mg-alloys. The fluxless method has proved to be more acceptable [AVE99], this comprises either of a single gas (e.g. SO_2 or Ar) or a mixture of a diluting gas (e.g. CO2, N_2 or air) and an active gas, e.g. SF_6 is currently considered the most efficient [CAH96]. However, in order to eliminate the greenhouse gas emissions, several attempts were reported to replace the use of SF_6 [RIC03][GAL03].

Processing of magnesium alloys

Magnesium alloy products can be produced by nearly all of the conventional casting methods, namely, sand, investment, permanent mould, pressure die-casting and other hot working processes [AVE99]. The choice of a casting method for a particular part depends upon factors such as the application, the properties required or the total number of castings required [BAK92].

Magnesium alloy sand castings generally weigh from a few grams to as much as 1400kg[KEN88]. Successful production of sand castings becomes possible only when the metal-mould reactions are prevented from occurring. However, sand cast components do not provide high complexity. Also [AGH04], it is not capable of producing castings that satisfy the level of dimensional accuracy currently being demanded for many Mg-alloy applications.

The main technology for the casting of magnesium alloys is die-casting [FRI00]. The die casting process is an economical method and ideally suited to high-volume production of cast magnesium components, with weight ranging from a few grams to more than 15 kilograms [NAD98]. During the die-casting processing, the mould, which is clamped together by hydraulic force, is filled rapidly (5 to 100m/s) by forcing the molten metal through a narrow gate. The metal solidifies under high-pressure with a high cooling rate (100 to 1000°C/s), resulting in a fine structure material [GRE72]. The pressure die-casting process divided into two types of process, i.e., hot chamber die-casting and cold chamber die-casting (**Figure 2.13**) [NAD98]. In hot-chamber machines, the supplying container is immersed in the bath of a molten alloy, which is forced into the die by a piston or compressed air, thereby keeping it supplied at a stated pouring temperature, whereas, in cold-chamber machines, neither the metal chamber nor the plunger are heated. Normally, the cold-chamber machines are used to make large castings because of the higher injection pressure and faster piston movement. A large, growing application for magnesium die-castings is in the automotive industry [BAK92].

Table 2.1 summarises the mechanical properties of AZ91 Mg-alloys under various conditions from references [POL95][AST81a][AST81b]. Among all of the Mg-alloy

processes, Mg-alloy sand castings are of normally uniform quality, while die-castings have improved structure soundness. Nevertheless, there are still a number of limitations existing in HPDC process [BAL01][AGU04], e.g., air entrapment or porosities, poor yield, high die costs and die maintenance work, large castings require large amounts of machining. A further development of mechanical properties for Mg-alloys depends on the advancement of processing technologies [FRI01].

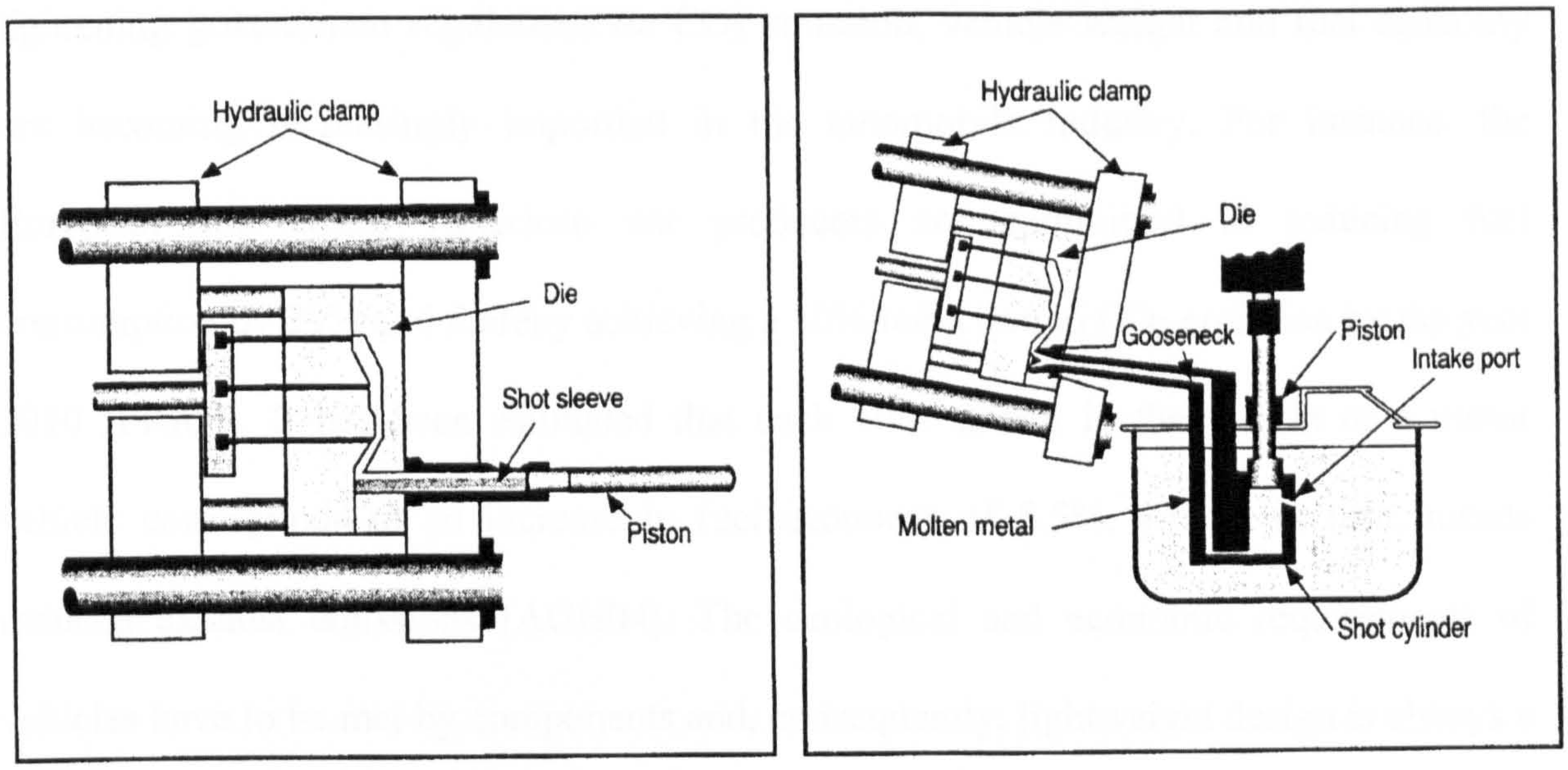

Figure 2.13 *(a) Cold chamber, and (b) Hot chamber die-casting machines [NAD98].*

Table 2.1 *Typical room temperature mechanical properties of AZ91 Mg-alloy processed by different processing techniques.*

Processing condition	UTS (MPa)	Yield stress (MPa)	Elongation (%)	Reference
As-sand cast	135	95	2	[POL95]
As-chill cast	170	100	2	
As-permanent mould cast	160	76		[AST81a]
Permanent mould with T4	230	76	7	
Permanent mould with T5	160	83	2	
Permanent mould with T6	230	110	3	
As Die-cast	230	150	3	[AVE99]

2.6.3 Applications of magnesium alloys

After almost three decades, magnesium alloys have reappeared as a structural material [AGH04]. The main driving forces for this are summarised as the following:

(a) Environment and fuel economy. Due to increasing environmental concerns and tightening government regulations on CO_2 emission, vehicle weight and fuel economy are becoming increasingly important in the automobile industry. For instance, the European and North American car producers are committed to reducing fuel consumption by 25% and thereby achieving a 30% reduction in CO_2 emission by the year 2010 [FRI00]. It has been estimated that each 10% saving in the weight of a motor vehicle corresponds to an increase in fuel economy of 5.5%, which, in turn, means reduced exhaust emissions [AGH04]. The ecological and economic requirements of vehicles have to be met by components and, consequently, lightweight design is always a significant requirement.

(b) Material costs. In recent years (from 1993), the price of magnesium has been decreasing as the price of aluminium has risen, i.e., the Mg/Al price ratio has at times ranged from 2.5/1 to just below 1.5/1[POL95]. In the automotive industry it is estimated that if the price ratio between magnesium and aluminium is less than 1.7/1, then magnesium components will replace the aluminium ones on a one-to-one basis. If the ratio falls below 1.4/1, then magnesium usage will increase exponentially.

(c) Mechanical Properties. Magnesium is the lightest of all structural metals [POL95], and as such has superior strength/weight ratios, low inertia and low density, this

combined with cost savings and reduced energy requirements makes magnesium alloys an appropriate choice in various structural parts. Excellent electromagnetic shielding and damping capabilities, very good castability, and recycling ability, make magnesium a very attractive structural material compared with not only metal alloys, but also plastics and composites [LAN00].

(d) Advanced technological research and development, is encouraging the growth of the magnesium industry as a new metal industry in many countries such as China, Israel, Canada and Australia, more applications are being developed around the globe [KE04]. The constructional uses of Mg-alloys are successfully practiced in a wide variety of applications.

In earlier years, magnesium was employed extensively in aircraft engines, airframes, and landing wheels [EML66][GRE72]. Currently magnesium is used in aircrafts as both castings and wrought products [AGH04]. Major structural pieces include transmission cases, undercarriage legs, and passenger seats, whilst wrought components include overhead compartments, folding tables, tubular frames and flooring. Other small magnesium pieces are also found in many accessories.

Magnesium alloys have been used for many years in motor vehicles beginning in the 50's and 60's with Volkswagen's Beetle [EML66]. Current usage is growing continuously and more components of the vehicle structure are utilising magnesium, for example engine applications, interior applications (steering wheel, instrument panels, seats) and body applications (upper door frame, cross-car beam) [KEN88][POL95][SCH04]. In the past few years we have seen a 15% average annual increase in Mg usage in the

automobile industry [FRI01] and it is deemed that this is the major area for the application of magnesium alloys in the future [SCH04]. In October 2002, a project team comprising of General Motors, Ford, Daimler Chrysler and forty-one North American companies and organisations successfully took a substantial step towards the use of magnesium alloys in automotive power trains [POW04]. The team selected an existing aluminium production engine and successfully redesigned that engine with several Mg-components, AJ52X, AS21X, AS31 and other magnesium alloys were cast and tested using HPDC process.

The low-density characteristic of magnesium alloys is such that they are of interest in the manufacture of many portable pieces of equipment. Such as hand-operated power tools, office machinery and handling equipment [GRE72]. Another promising area in the use of magnesium die-castings are computer housings and mobile phone cases, where lightness and provision of electromagnetic shielding are special advantages [AVE99].

The expanded use of magnesium castings requires the development of special casting technologies to make castings of fine grain size, free of porosity or cracks and further improved metallurgical quality. For this to be achieved, extensive research efforts on effective alloying or new processing of magnesium alloys are still required [FRI01][SCH04], in the long term, the unlimited quantities of magnesium available from the sea will ensure the steady growth in the utilisation of the metal.

2.6.4 Semisolid processing of magnesium alloys

Currently, magnesium alloys are used mainly in high-pressure die-casting (HPDC) form for functional components in the automobile industry [AGU04]. HPDC is a well-established and efficient process. However, the conventional HPDC components contain a substantial amount of porosity due to gas entrapment during die filling and hot tearing during the solidification in the die cavity [BAL01][AGU04]. Such porosity deteriorates mechanical properties and limits its applications to non-stress or low-stress components. One of the promising technologies by far capable of producing high integrity magnesium components is semisolid processing [FLE91][KIR94][FAN02b].

In conventional die casting processes the liquid metal is usually forced into a mould cavity at such a high speed that the flow becomes turbulent or even atomised, leading to high porosity in the final components. In contrast, SSM processing uses a SSM slurry with substantially increased viscosity, resulting in a controlled die filling and close to zero porosity in the final components. Due to the substantial differences to conventional processes, semisolid processing of magnesium alloys is expected to exhibit a number of advantages [FLE91][KIR94] and it is deemed that magnesium is an ideal material for semisolid processing [AGU04]. In recent years, both the thixo and rheo-route for magnesium alloys have been investigated.

Thixocasting of magnesium alloys has had success to some extent. CANMET [SHE02] did experimental work on the thixoforming of AZ91D alloy. They experimentally produced a thixocasting of a box-like component, and thixoforging of a disk-like component, weighing approximately one kilogram each. The thixotropic feedstock was

prepared using a MTL casting simulator with electromagnetic stirring, where slugs of feedstock material having a rosette structure and the slugs were inductively heated to a semisolid state to obtain a globular structure. The need for specially prepared magnesium alloy bars in the thixoforming process has prevented its commercial application to date.

There is a modification of the thixocasting route, which has become of commercial significance for semisolid forming of magnesium alloys: Thixomoulding. A large number of Thixomoulding machines are now in operation for producing magnesium castings, particularly for electronic components and thin-wall hardware components [FLE00], where stiffness, electrical conductivity, heat dissipation and absorption of vibration are of importance. In addition, Thixomoulding has proved its capability for tight dimensional control of moulded features, e.g., the 22mm 'Zero Draft' bearing bore was moulded consistently enough to eliminate the need for machining before pressing in the main bearing [MID04].

Ivanchev and Govender [IVA04] use a modified CSIRO rheocasting system to successfully process both AZ91D and AM60B Mg-alloys. The SSM temperature was found to have a more significant impact on the flow behaviour of AM60B compared to that of AZ91D, but the microstructure of the casting biscuit showed a combination of round and rosette shaped primary grains.

Aguilar et al. [AGU04] uses a meander sample to evaluate the flow properties of magnesium alloys between Thixocasting, Thixomoulding and RCP process. They found that the measured values are smaller with the RCP technology than in Thixocasting.

According to results they concluded that all three processes are very suitable for processing magnesium alloys in the semisolid state.

The mechanical property data for SSM processed magnesium alloys is scarce compared with aluminium alloys. Some mechanical behaviour of semisolid processed magnesium alloys has been reported to exhibit improvements over die-cast counterparts, as cited in **Table 2.2**. In particular, they found that both the tensile strength and ductility of thixomoulded AZ91D alloy decreases with increasing solid fraction. Furthermore, they found the elongation exhibits a stronger dependence on the fraction of primary solid phase than that observed for tensile strength [CZE01]. A study on corrosion behaviour of semisolid cast AZ91D alloy has shown that the semisolid cast alloy possesses a corrosion rate at least 35% below that of the die cast alloy [MAT02]. Koren et al. [KOR02] conducted mechanical testing on semisolid casting of AZ91 and AM50 magnesium alloys. It was shown that there was no significant difference of mechanical properties between thixocast and rheocast magnesium components.

***Table 2.2** Mechanical properties of semisolid processed magnesium alloys.*

Processing condition	Mg-alloy	UTS (MPa)	Yield stress (MPa)	Elongation (%)	Reference
Thixocasting	AZ91D	240	140	3.6	[AGU04]
Thixomolding	AM50	269	140	20	[AVE99]
	AM60	278	150	18.8	[AVE99]
	AZ91D	230	160	6	[MID04]
NRC	AZ91D	230		5.5	[KAU00]
RCP	AZ91D	230	155	2.5	[AGU04]

Up until now, the only commercially available SSM process for magnesium is still the Thixomoulding process [IVA04]. The greatest obstacle for the further development of this two-step SSM process is the high cost of pre-processed non-dendritic raw materials. To overcome the technical and economical difficulties faced by the thixo-processing route, the rheo-route of SSM processing has become popular for research and development [FAN02a].

More recently, a Rheo-Diecasting (RDC) process has been developed by BCAST at Brunel University [FAN02b]. The RDC process is an innovative one-step SSM processing technique for manufacturing near-net shape components of high integrity directly from liquid Mg-alloys. The process innovatively adapts the well-established high shear dispersive mixing action of the twin-screw mechanism to the task of in situ creation of SSM slurry, with fine and spherical solid particles, followed by direct shaping of the SSM slurry into a near-net shape component using the existing cold chamber HPDC process. Although there are many magnesium alloys, which can potentially be rheo-diecast [FAN05c][JI05][DAS06], the effort in this research is focused mainly on the AZ91D Mg-alloy.

Chapter 3. Experimental Procedure

3.1 Material processing

3.1.1 AZ91D alloy and its melting

The magnesium alloy investigated in the present study was AZ91D provided by MEL (Magnesium Elektron, Manchester, UK). The chemical composition of the material as received is shown in **Table 3.1**, it is compared with the Standard Specification of AZ91D Mg-alloy. **Table 3.2** offers some selected physical properties of the AZ91D Mg-alloy [AVE99], the liquidus and solidus temperature of the AZ91D alloy are 598°C and 468°C, respectively.

***Table 3.1** Chemical compositions and the Standard Specification of AZ91D Mg-alloy (wt%)*

	Zn	Al	Si	Cu	Mn	Fe	Ni	Be	Others Each
As received	0.67	8.8	0.03	<0.001	0.22	0.002	0.0005	0.0011	<0.01
Specification [AVE99]	0.45-0.9	8.5-9.5	0.05	0.015	0.17 min	0.004	0.001		0.01

***Table 3.2** Selected physical properties of AZ91D Mg-alloy [AVE99]*

Density g/cm^3	Liquidus Temp. °C	Solidus Temp. °C	Incipient-melt Temp. °C	Casting Temp. °C	Specific heat At 20°C. kJ/kg.K
1.81	598	468	420	640-675	0.8

The AZ91D alloy was melted in a Carbolite resistance furnace at a temperature of 675°C. To avoid oxidation of the molten Mg-alloy, a protective gas mixture of N_2 containing 0.4 vol% SF_6 was used in both the melting furnace and the Twin-Screw Slurry Maker.

3.1.2 The Rheo-Diecasting experiment and process

The core of this study is the Twin-Screw Rheo-Diecasting (RDC) process. The RDC process is a newly developed SSM processing technology founded at Brunel University in 1999 for semisolid processing of Mg and Al alloys [FAN99]. **Figure 3.1** schematically illustrates the Rheo-Diecasting process for manufacturing Mg-alloys components. The RDC equipment consists of two basic functional units: a Twin-Screw Slurry Maker and a standard cold chamber HPDC machine.

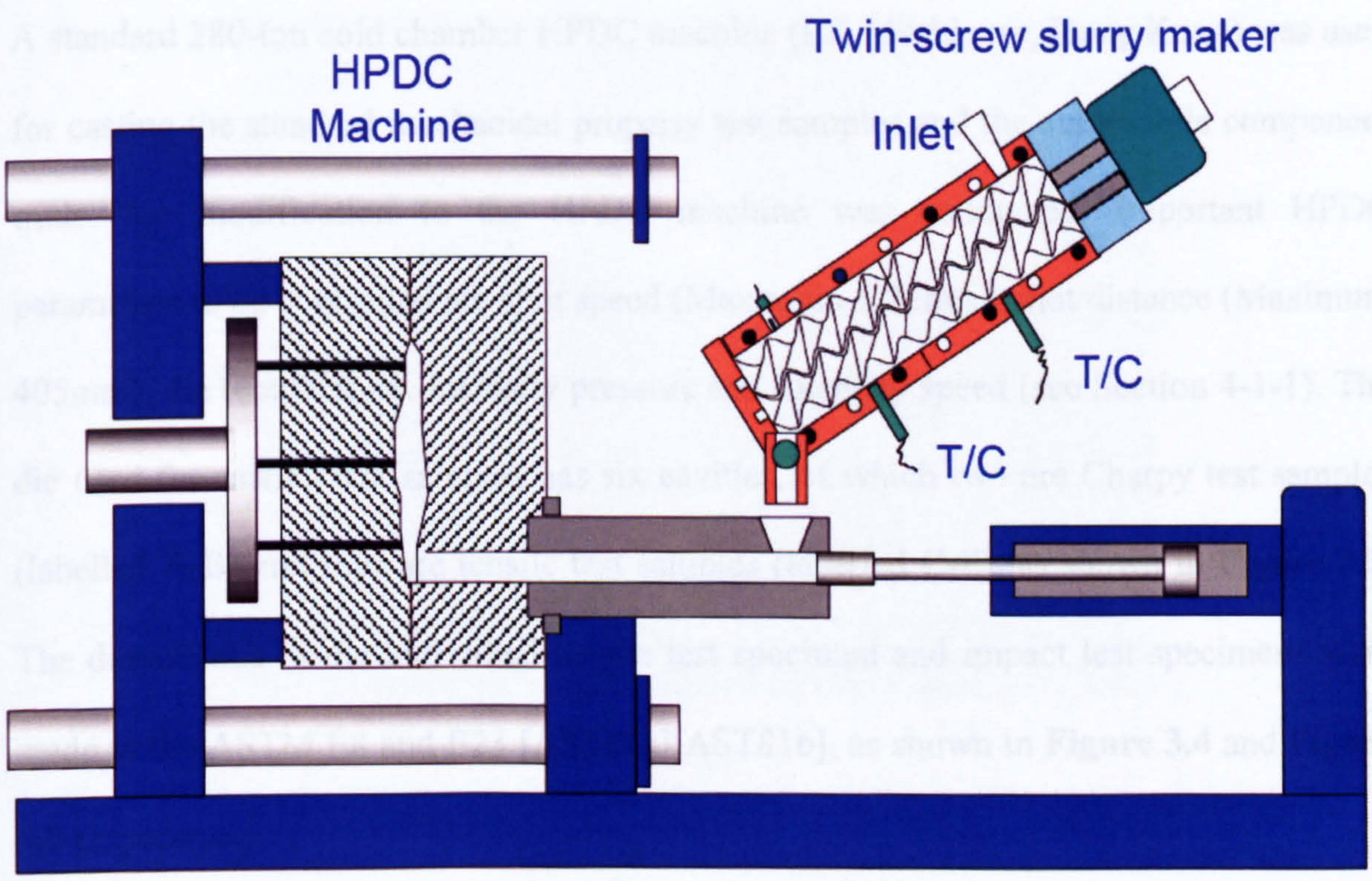

Figure 3.1 *Schematic illustration of the Rheo-Diecasting (RDC) process*

A unique feature of the RDC process is the utilisation of a specially designed Twin-Screw Slurry Maker (TSSM) for semisolid slurry production under high shear rate and high intensity of turbulence. **Figure 3.2a** shows the Twin-Screw Slurry Maker (TSSM) for magnesium alloys, the protective gas is supplied from a valve and a hopper. The detailed central control panel is shown in **Figure 3.2b**. In the TSSM, two closely intermeshing, self-wiping and co-rotating screws (ϕ36mm) rotate inside a steel barrel. Heating and cooling elements are dispersed along the axis of the barrel, to form 5 heating and cooling zones with temperature control accuracy of ± 1°C. At the other end of the barrel, a pneumatic valve is adapted to control the semisolid slurry feeding. The basic function of twin-screw slurry maker is to convert the liquid Mg-alloy into high quality semisolid slurry through solidification of the liquid alloy under intensive shearing. It works in a batch manner, providing magnesium slurry every 30 seconds.

A standard 280-ton cold chamber HPDC machine (LK Machinery, Hong Kong) was used for casting the standard mechanical property test samples and the automobile component trials. No modification to the HPDC machine was conducted. Important HPDC parameters to be controlled are shot speed (Maximum 6.22m/s), shot distance (Maximum 405mm), die temperature, intensity pressure and intensity speed (see Section 4-1-1). The die used for casting test samples has six cavities, of which two are Charpy test samples (labelled A-B) and four are tensile test samples (labelled C-F), as shown in **Figure 3.3**. The dimensions of the individual tensile test specimen and impact test specimens were made to the ASTM E8 and E23 [AST81a][AST81b], as shown in **Figure 3.4** and **Figure 3.5** respectively.

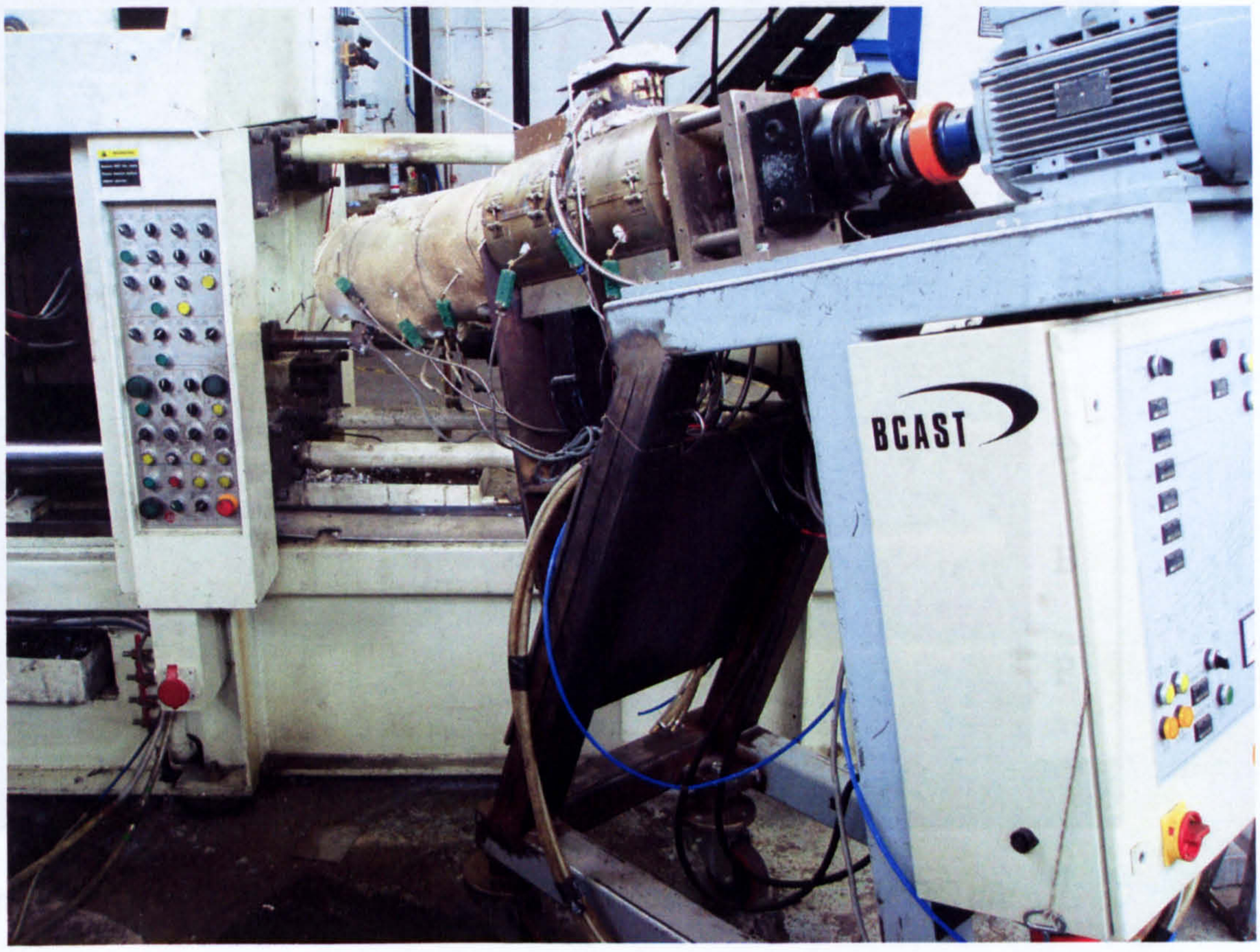

(a)

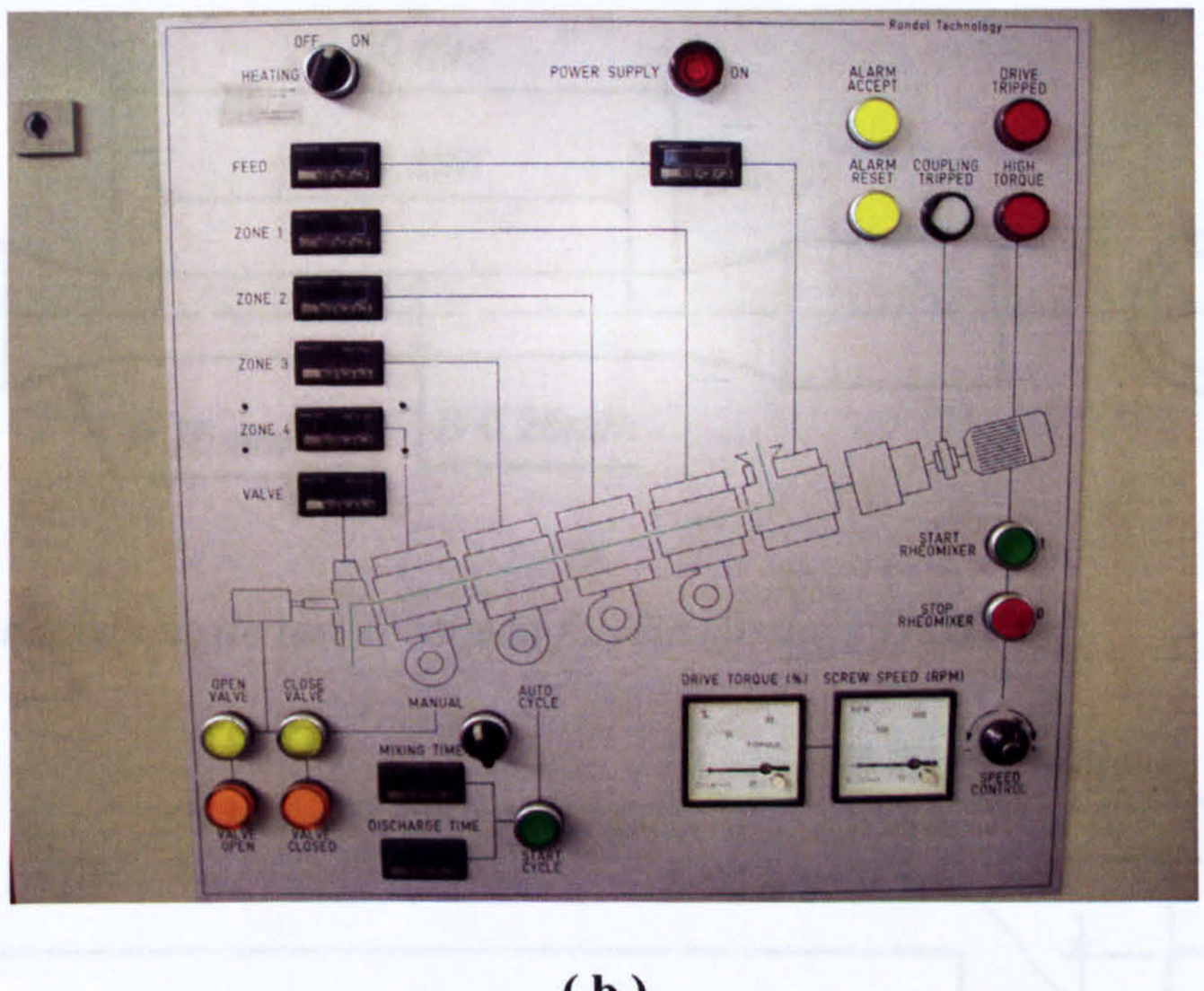

(b)

Figure 3.2 *(a) The Twin-Screw Slurry Maker for Mg-alloys and (b) The layout of central control unit.*

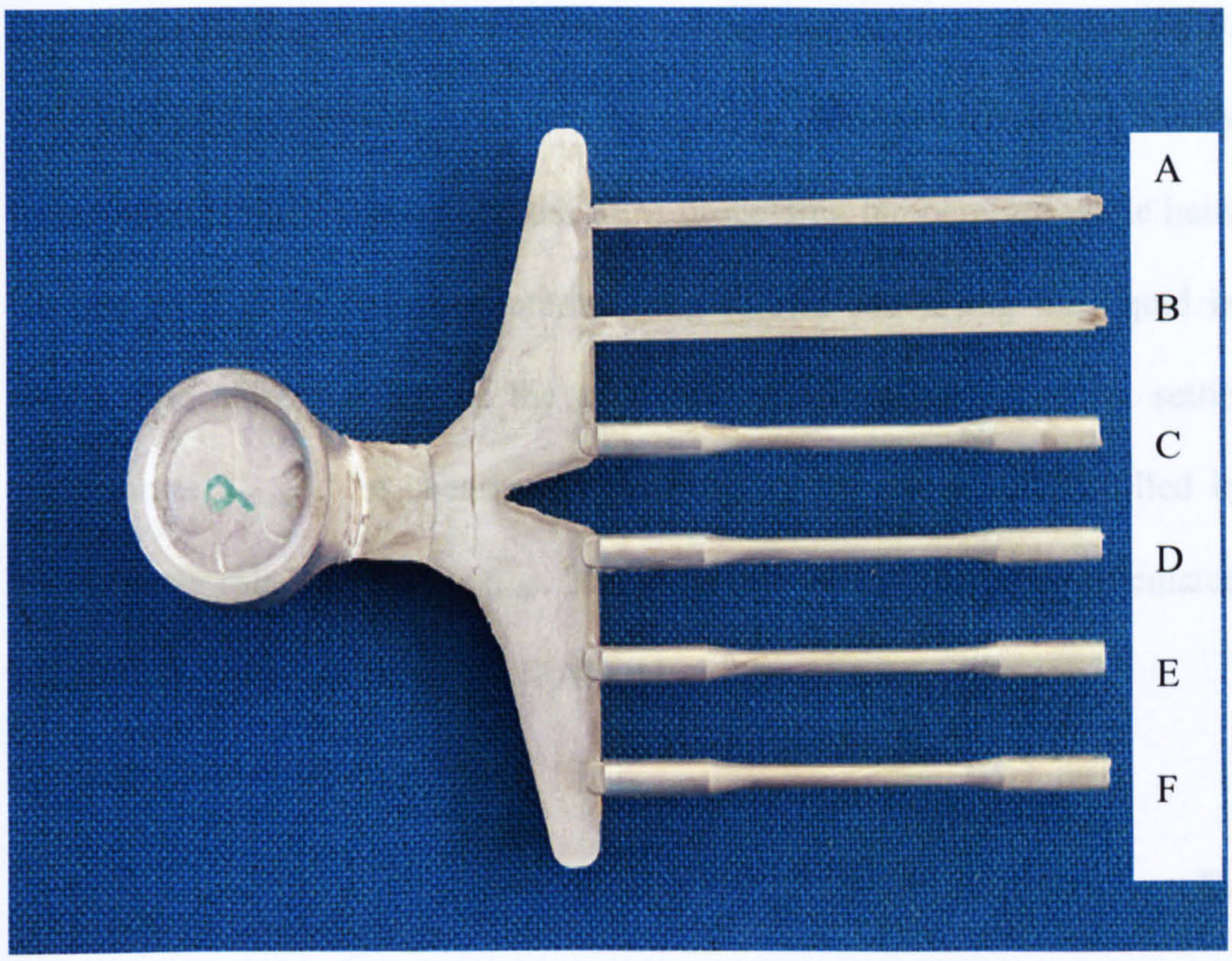

Figure 3.3 *A tensile test casting shows the geometry of the HPDC die*

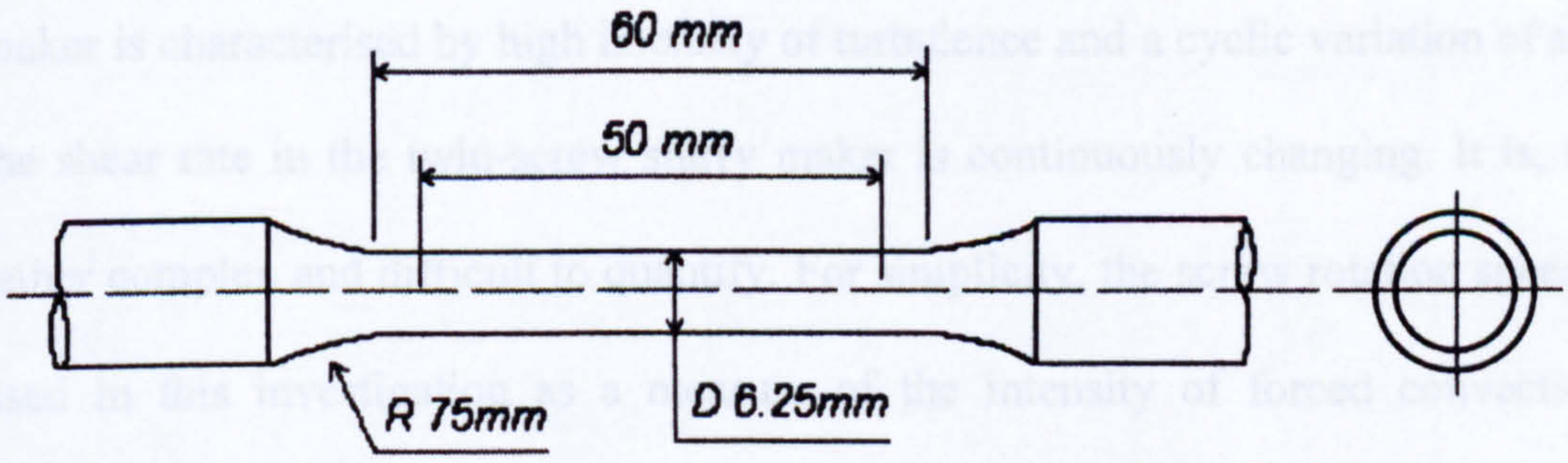

Figure 3.4 *Standard tensile test specimen for die castings [AST81a]*

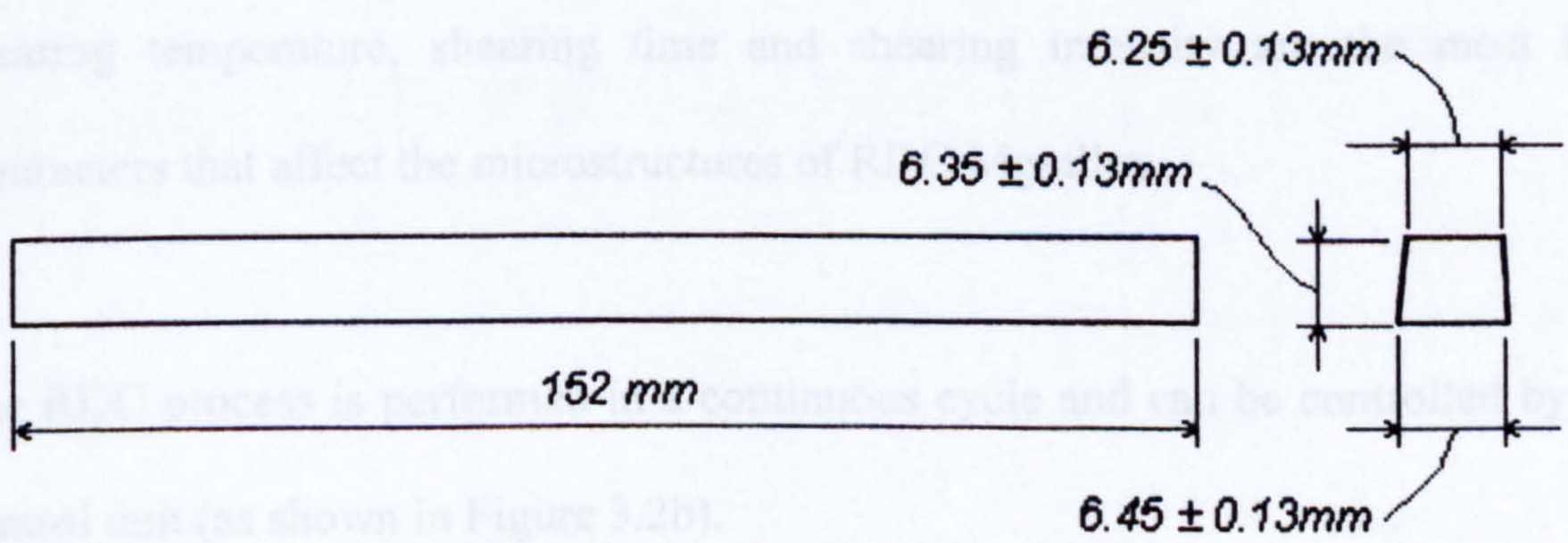

Figure 3.5 *Simple beam impact test bar for die casting alloys [AST81b]*

During the Rheo-Diecasting process, a predetermined dose of liquid AZ91D Mg-alloy from the melting furnace is fed into the steadily rotating Twin-Screw Slurry Maker. The liquid alloy is rapidly cooled to the SSM processing temperature while being intensively sheared by a pair of closely intermeshing screws converting the liquid into semisolid slurry. The solid fraction of the semisolid slurry is controlled by setting the barrel temperature T_{shear}. The shearing intensity upon the slurry is controlled by setting the Twin Screw rotating speed ϖ_{shear}. The shear rate γ can be roughly calculated by a simple equation described in reference [FAN01]:

$$\gamma = \varpi\pi\left(\frac{D}{\delta} - 2\right) \qquad \textbf{Equation 3.1.1}$$

Where D is the screw diameter, ϖ is the screw rotation speed and δ is the gap between the tip of a screw flight and the barrel surface. However, the fluid flow inside the slurry maker is characterised by high intensity of turbulence and a cyclic variation of shear rate, the shear rate in the twin-screw slurry maker is continuously changing. It is, therefore, rather complex and difficult to quantify. For simplicity, the screw rotation speed ϖ_{shear} is used in this investigation as a measure of the intensity of forced convection. After shearing for predetermined period of time, t_{shear}, the semisolid slurry is then transferred to the shot chamber of the HPDC machine for component shaping. Accordingly, the shearing temperature, shearing time and shearing intensity are the most important parameters that affect the microstructures of RDC Mg-alloy.

The RDC process is performed in a continuous cycle and can be controlled by a central control unit (as shown in Figure 3.2b).

3.1.3 Processing conditions

In this study, the investigated RDC processing parameters including High Pressure Die-Casting (HPDC) parameters and Twin-Screw Slurry Maker (TSSM) parameters are listed **Table 3.3** and **Table 3.4**. The varied parameters of Table 3.3 are given in Section 4.1 for process optimisation and those in Table 3.4 are given in Section 4.3 for solidification investigations. For general microstructure investigation (in Section 4.2.2) and heat treatment (in Section 4.4), the processing parameters are shown in **Table 3.5**.

***Table 3.3** The investigated High Pressure Die-Casting (HPDC) parameters*

Mould Temperature (^{o}C)	220	230	235	240	250	260			
Shot Distance (mm)	140	170	180	230	270				
Shot Speed (%)	30	50	60	65	70	75	80	85	90
Intensitying Pressure (bar)	70	80	90	100	105	120			
Intensitying Speed (%)	45	55	65	75	85	100			

Table 3.4 The investigated Twin-Screw Slurry Maker (TSSM) parameters

Shearing Time (second)	3	10	13	16	20	35	70	150	200
Shearing Speed (rpm)	100	300	500	800	900				
Shearing Temperature (°C)	585	589	593	597	600				

Table 3.5 Parameters used for microstructure investigation and heat treatment

Shearing Temperature	Shearing Speed	Shearing Time	Mould Temperature	Shot Distance	Shot Speed	Intensitying Pressure	Intensitying Speed
585-593°C	500rpm	35s	235°C	180mm	65%	90bar	65%

3.2 Heat treatment

The resulting AZ91D Mg alloy tensile test samples, produced by both HPDC and RDC processes, were subjected to two series of heat treatments.

A traditional heat treatment was carried out according to the ASM Speciality Handbook [AVE99]. The microstructure and hardness response of solution treatment and subsequent ageing for RDC AZ91D alloy were then investigated. The solution treatment was carried out in air with protection of carbon powder on the surface of the samples at 413°C for up to 24 hours, the different length of solution times (hour) are listed in **Table 3.6** (A*). After different lengths of solution time, the samples were then quenched in water. The samples that had been subjected to solution treatment at 413°C for 24 hours were then aged at 216°C for different lengths of time up to 144 hours, the different length of ageing times (hour) are listed in Table 3.6 (B*).

***Table 3.6** The traditional heat treatment conditions for RDC AZ91D Mg-alloy*

A*	1	2	3	4	5	6	7	8	9	10	16	20	24					
B*	0.5	1	1.5	2	2.5	3.5	4	5	5.5	6	8.5	11	16	22	48	72	120	144

A*: different length of solution time (hour) at 413°C.
B*: different length of ageing time (hour) at 216°C.

A T5 heat treatment was carried out at 216°C for 5 hours for the AZ91D Mg-alloy. Additionally, a T4 and T6 optimised heat treatment (solution at 413°C for 5 hours, T4, and then aging at 216°C for 5.5 hours, T6), was carried out for evaluation of the mechanical properties for heat-treated RDC AZ91D alloy. Based on microstructure evolution investigations, a new heat treatment, Tx, specially developed for RDC AZ91D Mg-alloy was performed at 365°C for 2 hours [WAN05a].

3.3 Microstructure characterisation

3.3.1 Metallographic sample preparation

For microstructure investigations, the metallographic samples were cut through the middle sections from bars labelled 'E' (see Figure 3.3), produced in different batches. For distribution investigations, the samples were cut from various locations in the final castings.

The specimens for OM (Optical Microscope) and SEM (Scanning Electron Microscope) were prepared by the standard technique: mounting in a hot setting resin, grinding with SiC abrasive paper and polishing with an Al_2O_3 suspension solution, followed by etching in the relevant etchant. A solution of 5vol% HNO_3 in ethanol was used to etch the as-cast AZ91D Mg-alloy, and an aqueous solution of 60vol% ethylene glycol, 20vol% acetic acid, 1vol% concentrated HNO_3 for the heat-treated AZ91D Mg-alloy.

3.3.2 Microscopic observation and analysis

A Zeiss Optical Microscope (OM) was utilised for the OM observations and the quantitative metallography. The images were taken with an AxioCam MRC digital camera and then downloaded onto a PC, shown in **Figure 3.6.**

Quantitative characterisation of the microstructure was performed using an AxioVision image analysis system. Volume fraction, particle size, particle density and the shape factor of primary particles were quantitatively analysed.

The density of particles (ρ) was calculated by $\rho=N/A$, where N is number of particles in a frame and A is the frame area. The shape factor (F) was calculated using $F=4\pi A/P^2$, where A and P are the total area and the peripheral length of the primary particles, respectively. Therefore, higher values of the shape factor, F, indicate more spherical particles i.e., F is 1 for perfectly spherical particles.

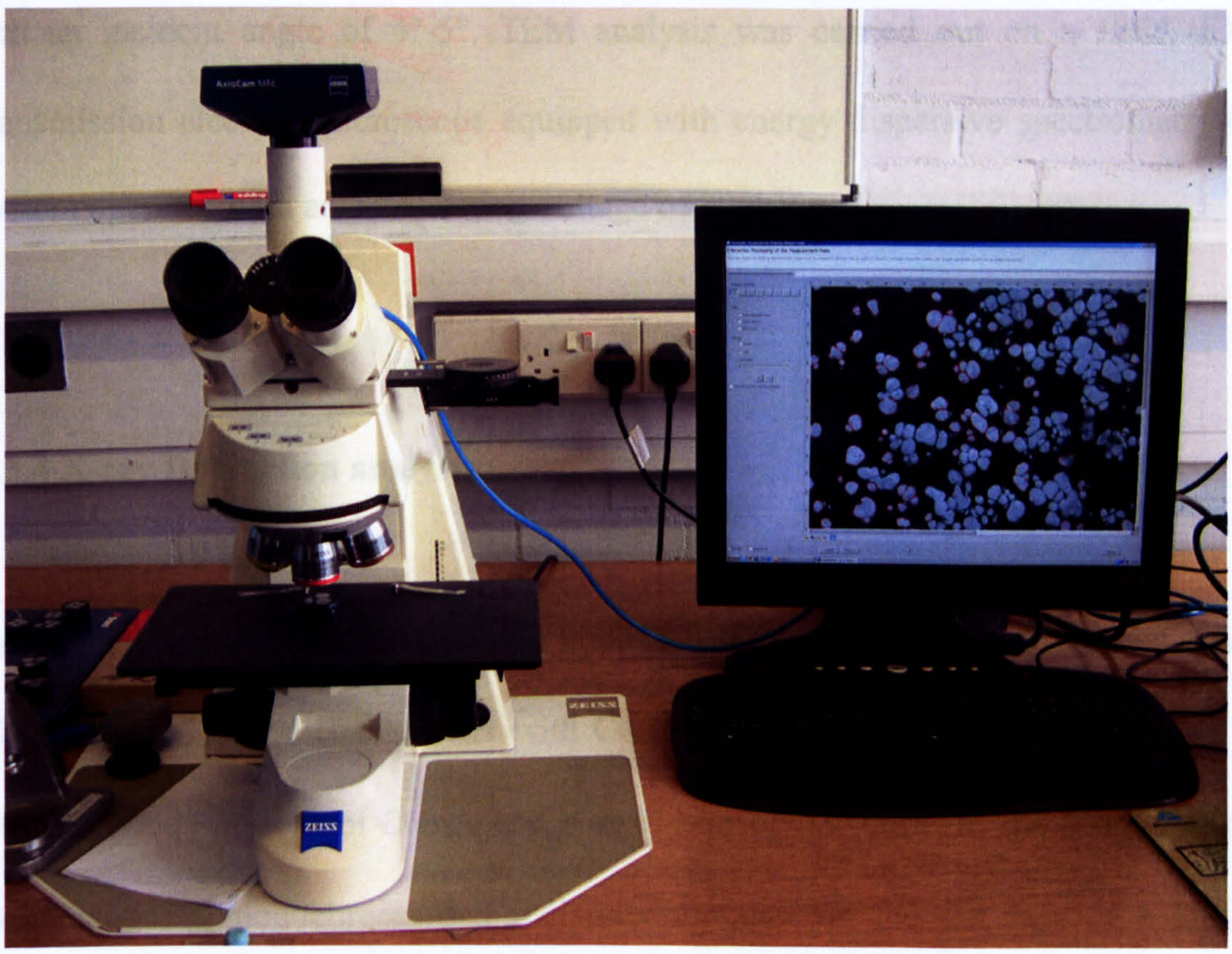

Figure 3.6 *The Zeiss Optical Microscope with an AxioCam MRC digital camera*

3.3.3 SEM and TEM examination

A Jeol JXA-840A scanning electron microscope, equipped with an energy dispersive spectroscopy (EDS) facility, was used to perform the SEM examinations. To obtain a better contrast between the granular α-Mg and β-$Mg_{17}Al_{12}$ phase, some of the SEM

samples were deep etched. The images of backscattered electrons (with an accelerating voltage of 20kV) and secondary electrons were taken.

TEM thin foils were prepared as follows. The transverse slices of the ϕ6mm tensile samples were mechanically ground and cut into 3mm discs which were then hand polished down to 80-90 μm thick. Final preparation of the TEM specimens utilised ion beam thinning on a Gatan precision ion polishing system under the conditions of 5.0kV and an incident angle of 4°-5°. TEM analysis was carried out on a JEOL FX2000 transmission electron microscope equipped with energy dispersive spectrometry (EDS) system operated with an accelerating voltage of 200kV.

3.3.4 X-ray Diffraction analysis

In order to identify the phases present in the alloys, XRD analysis was conducted using a Philips 1700 X-ray diffractometer with CuKα radiation operated at a voltage of 36kV, with an anode current of 26mA and a scan rate of 0.2°/min. In the X-ray diffraction examination, a monochromatised radiation impinges on the flat face of a 10×10mm square specimen. This specimen is rotated at precisely one-half of the angular speed of the receiving slit so that a constant angle between the incident and reflected beams is maintained. Meanwhile, the diffracted intensity at the various angles is recorded. It is further analysed to determine the phases present in the specimens.

3.3.5 Composition analysis

Composition distribution measurements of the RDC component, and the analysis of the prepared material were obtained with a 'Worldwide Analytical Systems AG, Foundry Master', shown in **Figure 3.7**. The 'WAS Foundry Master' is an 'Arc-spark Optical Emission Spectrometer' for routine analysis of metal alloys. The system comprises of a solid-state spark source, a vacuum system, an optical system, and an output system (PC).

A sample of minimum surface size $100mm^2$ was taken from the castings or ingots, surface ground using a SiC 1200 paper to produce a flat surface and washed with methanol, then being blow dried. The sample was then placed on the spark stand for composition testing.

***Figure 3.7** The Worldwide Analytical Systems AG Foundry Master*

3.4 Mechanical properties testing

3.4.1 Tensile testing

The mechanical properties of the alloy under as-cast and heat treated states were characterised with tensile tests using standard tensile samples, carried out at room temperature on a Lloyd Instrument EZ50 tensile test machine (see **Figure 3.8**), with a crosshead tension speed of 1mm/min.

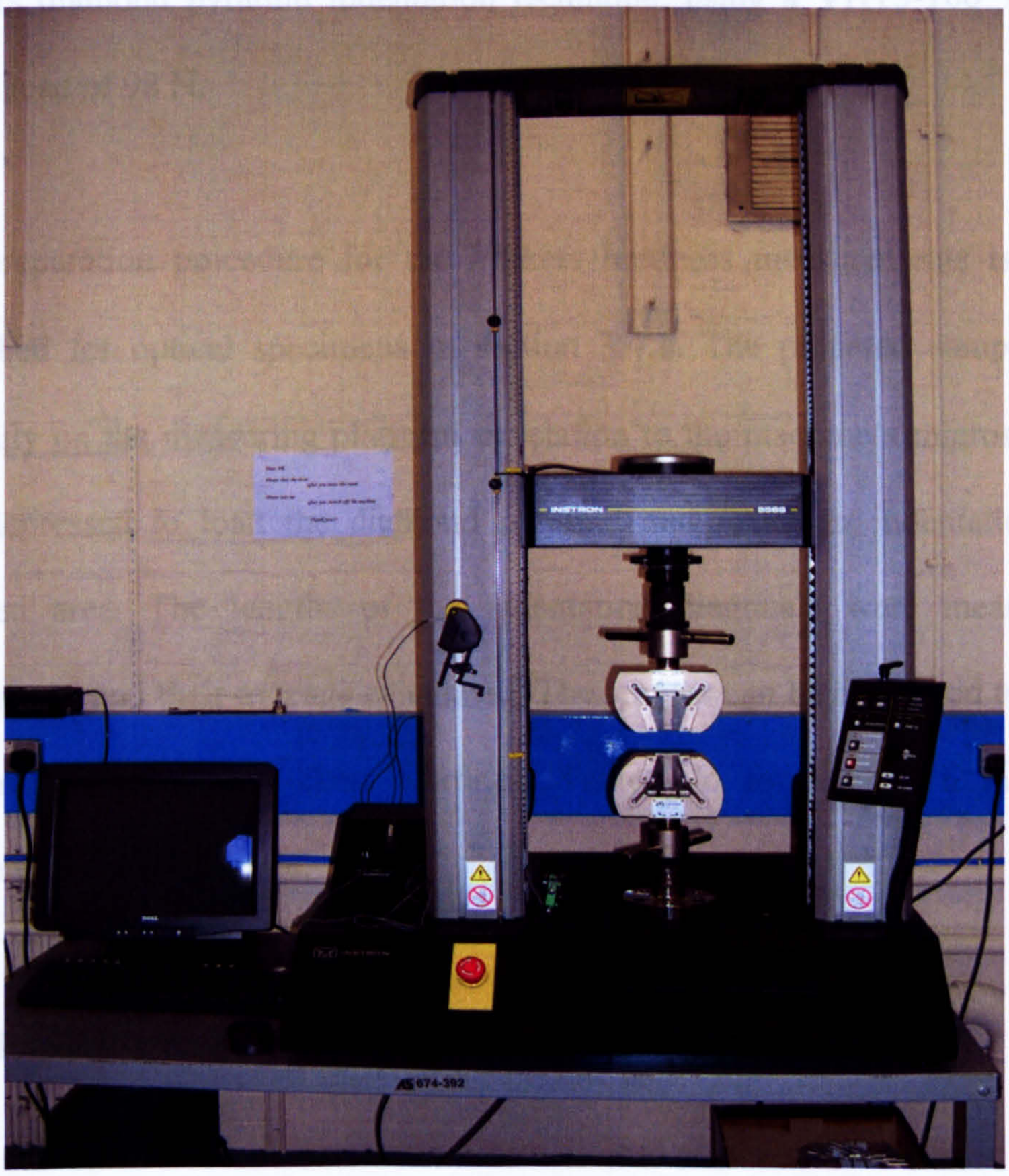

Figure 3.8 *The Lloyd Instrument EZ50 tensile test machine*

Before tensile testing, the rough casting edges of the samples were cleaned thoroughly and polished giving smooth surfaces. The tensile test samples were then clamped at both ends and measured with an Epsilon extensometer, with gauge length of 50mm. During tensile testing, the Stress-Strain Curve is plotted for observation, on a PC screen, until fracture occurs and the curve is finalised.

3.4.2 Vickers hardness measurements

The solution and age-hardening response of the AZ91D alloy was determined by the Vickers diamond pyramid indentation technique, using a VHT5-100 Vickers machine with a load of 98 N.

The preparation procedure for the Vickers hardness measurements is similar to that described for optical specimens in section 3.4.1. The prepared samples were placed carefully on the measuring platform in relation to the machine's microscope. The pedal was depressed to load the diamond pyramid and make an indentation point, in the selected area. The lengths of the indentation diagonals were measured using the microscope and their average calculated. The lengths can be converted to a measurement of hardness using a Vickers Hardness Table. No fewer than 6 indentations were measured for each sample.

3.4.3 Impact testing

As described in section 3.1.2, the RDC Charpy specimens were made to ASTM E23 for impact three point bend testing. A CEAST Torino 6546/000 impact machine with a

support interval of 40mm and a 15J standard pendulum were used to fracture the specimen. The measurement of absorbed fracture energy is indicated on the panel of the machine.

Chapter 4. Results

4.1 Optimisation of the Rheo-Diecasting process

4.1.1 The basic function and injection parameters in the RDC process

As described in the Rheo-Diecasting experiment and process, the RDC process is a combination of the innovatively established twin-screw slurry maker and a conventional high-pressure die-casting machine. Therefore, the quality of RDC castings is related, to a certain degree, with the performance of the injection system. The hydraulic cylinder and shot cylinder in this injection system is sketch illustrated in **Figure 4.1.1**. During die-casting, pressure is applied to '*side 1*', which causes the piston to move the Mg-alloy slurry through the shot sleeve and make the casting. Pressure on '*side 2*' is avoided by the opening of a valve. When pressure is applied to the side 2, the piston returns to the original position.

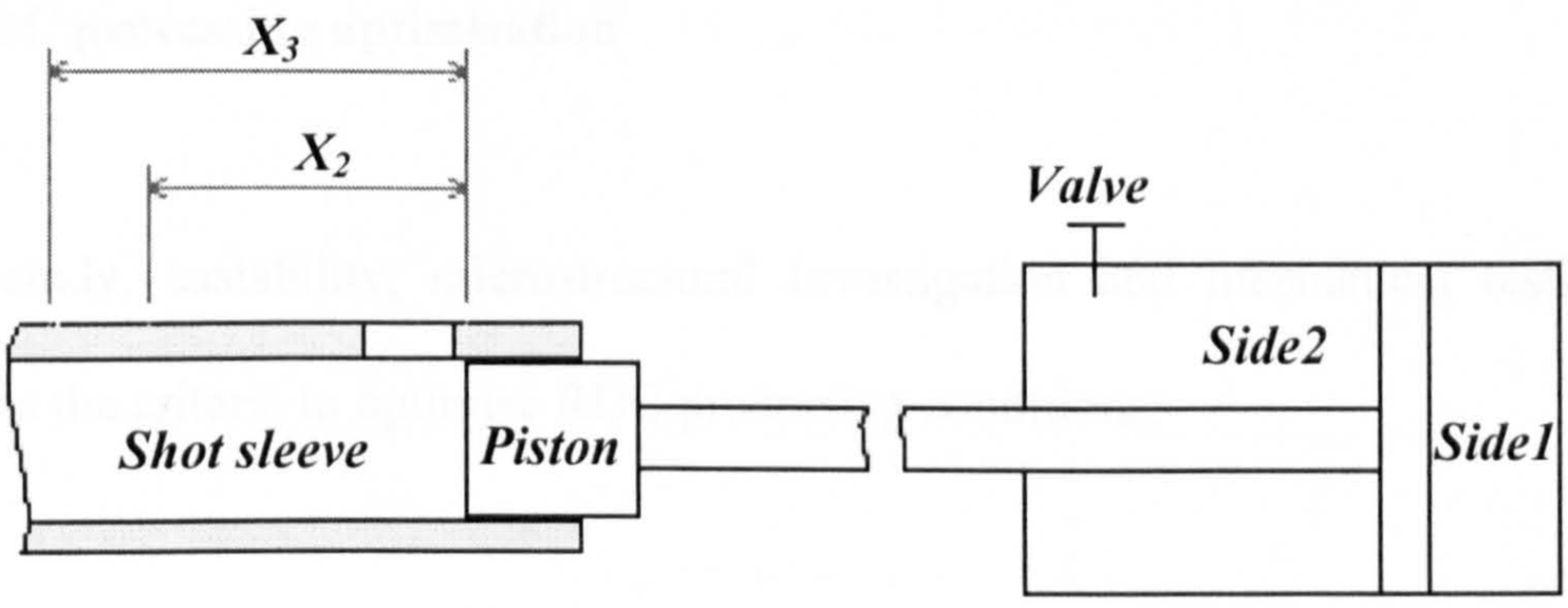

Figure 4.1.1 *Sketch of the injection system and the injection stages.*

In this experiment, the movement of the piston during injection has three stages of performance, the changeover points being controlled by a displacement transducer. The first stage of injection is a slow approach. The second stage starts at the piston displacement X_2 (shot distance), and the velocity of second stage (shot speed, V_2) can be controlled by flow of the valves in the hydraulic system. Therefore, the measure of shot speed V_2, is described by a valve opening percentage, a higher value of valve opening percentage resulting a higher injection speed (maximum is 6.22 m/s), for example, the shot speed from 30% to 90% was investigated in this study.

The third, 'intensification stage', is applied when the piston moves just past a pre-assigned point (intensify distance X_3). The intensification can be obtained with control over the intensifying speed, V_3, and intensifying pressure, P_3.

During process optimisation of the RDC Mg-alloys, the parameters of mould temperature T_m, shot distance X_2, shot speed V_2, intensifying pressure P_3, and the intensifying speed V_3 were investigated (see Table 3.3).

4.1.2 RDC processing optimisation

In this study, castability, microstructural investigation and mechanical testing were utilised as the criteria to optimise RDC processing conditions.

Mould temperature

Temperature of the mould is a noteworthy factor in conventional HPDC process, therefore, it was the first parameter considered for process optimisation. The effects of

mould temperature on the mechanical properties of RDC process are presented in **Figure 4.1.2**. The RDC processing was performed with a shearing temperature of 589°C, shot distance of 200mm, shot speed of 70%, intensifying speed of 55%, and the intensifying pressure of 90bar. The mould temperature, T_m, was varied between 220°C and 260°C; the results show that T_m has only a minor effect on the tensile properties of RDC AZ91D alloy, with the yield stress only fluctuating between 145MPa and 147MPa. Higher die temperatures do, however, improve surface finish of the castings.

From experimental results, a moderate die temperature of between 230-235°C was selected for the RDC process. For RDC AZ91D alloy, this is 15-20°C lower than the suggested temperature range in HPDC process [AVE99].

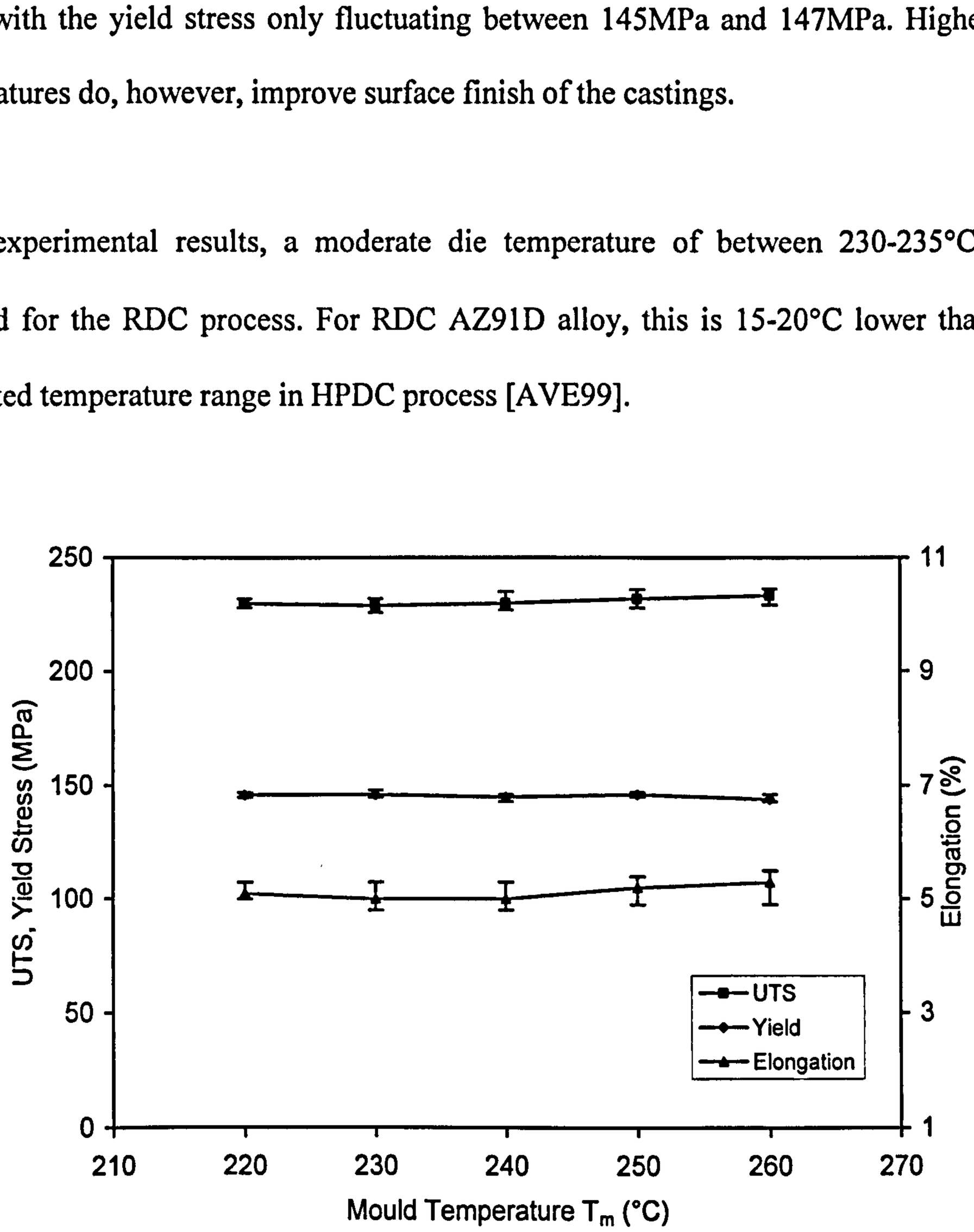

***Figure 4.1.2** The effect of mould temperature on the tensile properties of RDC AZ91D alloy.*

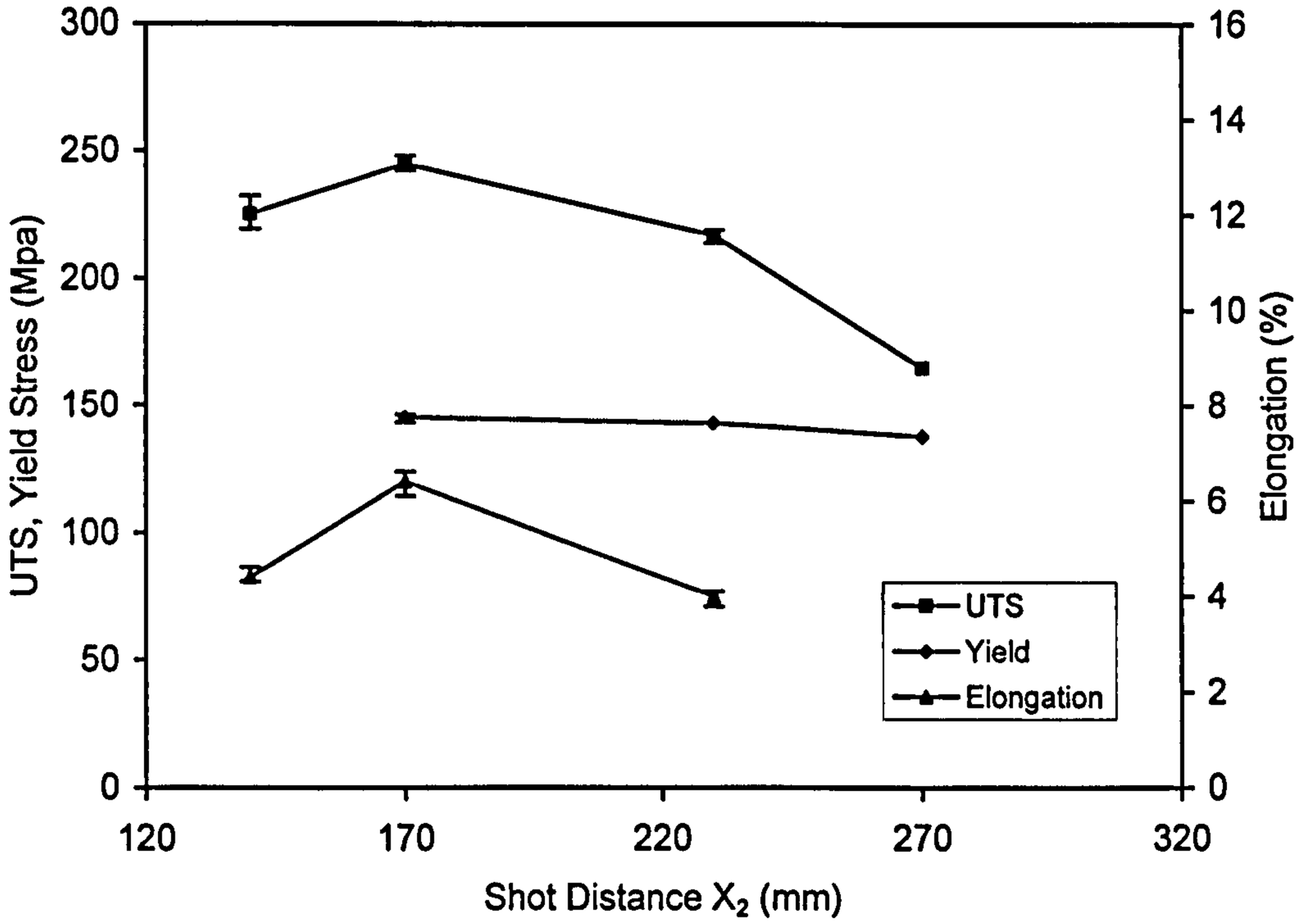

Figure 4.1.3 The effect of shot distance on the tensile properties of RDC AZ91D alloy.

Shot distance

In this experiment, the injection adopts a three-stage shot profile, it uses injection piston position to control the shot speed. **Figure 4.1.3** shows the effect of shot distance on the mechanical properties of RDC AZ91D alloy. The RDC process used a shearing temperature of 589 °C, a mould temperature of 230 °C, a shot speed of 70%, an intensifying speed of 55%, and an intensifying pressure of 80bar. It can be seen from Figure 4.1.3 that, a peak value occurs at the shot distance of 170mm.

According to conventional die casting process, the short distance corresponds to the filling ratio of cavity before shot. Normally, the filling ratio should be kept in the range of 40-50% or more. The filling ratio will decide the content of gas that can possibly be

trapped into the slurry during the die-casting process. The higher the filling ratio is, the lower the porosity is. However, the feeding mechanism of semisolid slurries in RDC is different to that of conventional HPDC, the filling ratio has less importance for semisolid slurries. As illustrated in **Figure 4.1.4**, Due to the relatively high viscosity of the semisolid slurry, the slurry at the shot sleeve does not spread evenly over the sleeve surface. Furthermore, the mould filling of the piled high viscous slurry is characterised to be more stable and, as such, the gas or splash can be much reduced. On the other hand, length of the shot distance will increase residence time of slurry in the shot sleeve which in turn increases the amount of solidification in the shot sleeve, reducing the formability of RDC castings, see **Table 4.1.1**.

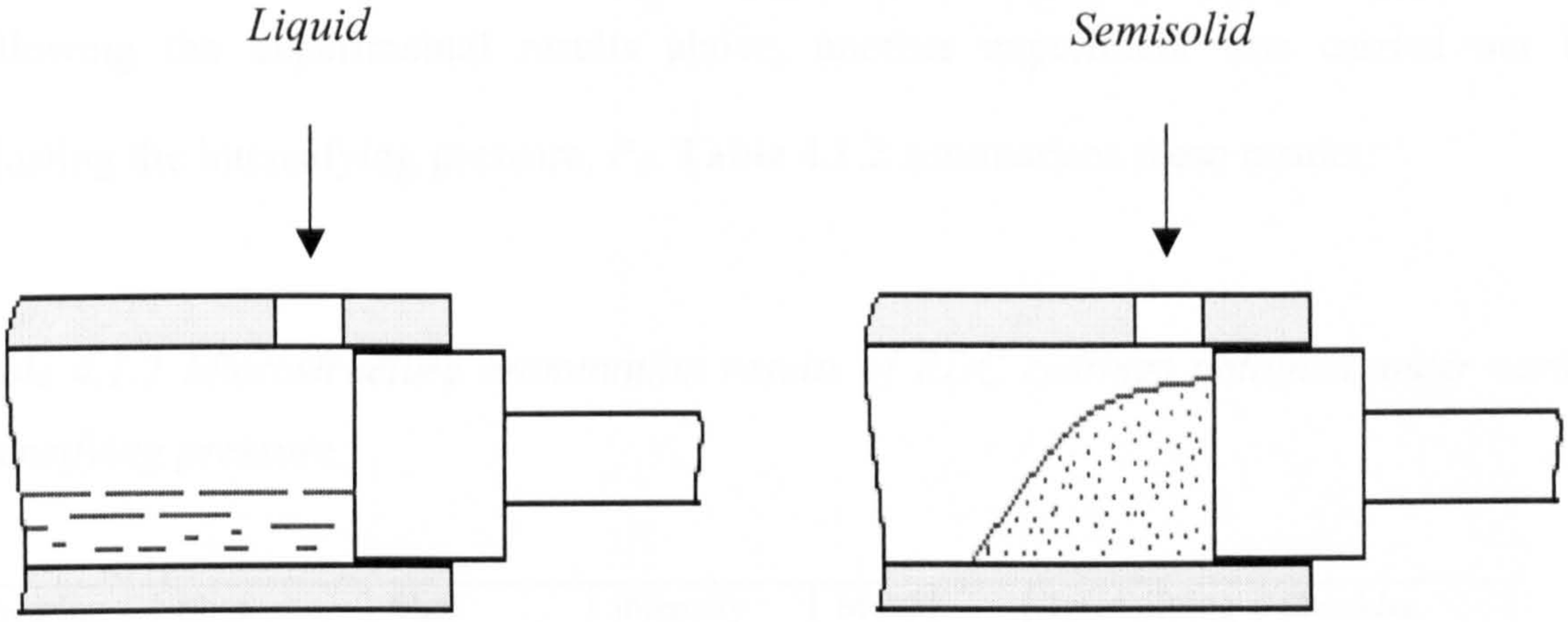

Figure 4.1.4 *The liquid and semisolid alloy feeding in the shot sleeve.*

Table 4.1.1 Microstructure and castability examination results of RDC castings under various shot parameters.

Parameters / Structure		Castability (optical examination)	Microstructure (metallography examination)
Shot Speed (%)	Shot Distance (mm)		
30	140	Normal	Segregation
50		Good	Segregation
70		Good	Uniform
80		Good	Uniform
90		Good	Uniform
70	140	Good	Uniform
	220	Good	Uniform
	300	Normal	Uniform

Intensifying Pressure

Following the experimental results above, another experiment was carried out by adjusting the intensifying pressure, P_3. **Table 4.1.2** summarises these results.

Table 4.1.2 Microstructure examination results of RDC castings obtained under varied intensifying pressure

Shearing Temp. (°C)	Shot Speed (%)	Shot Distance (mm)	Intensify Distance (mm)	Mould Temp. (°C)	Intensifying Pressure (Bar)	Shoulder Crack
593	80	140	200	220-240	70	No
				250	70	No
					80	No
					90	No
					100	Yes
					120	Yes
	65	180	180	220	90	No
					100	Yes
					105	Yes

The parameter of intensifying pressure P_3 was varied from 70bar to 120bar. One noticeable defect termed 'shoulder crack' appeared and disappeared regularly at the 'near gate shoulder' area, the position and morphology of the defect is shown in **Figure 4.1.5**. Further microstructure observations revealed that the 'crack' was 'welded' with a low melting point liquid and it only appeared when the intensifying pressure is above 100bar (Table 4.1.2), no such crack was found at the opposite shoulder. Therefore, an intensifying pressure of 80-90bar was optimised in RDC processing of Mg-alloys.

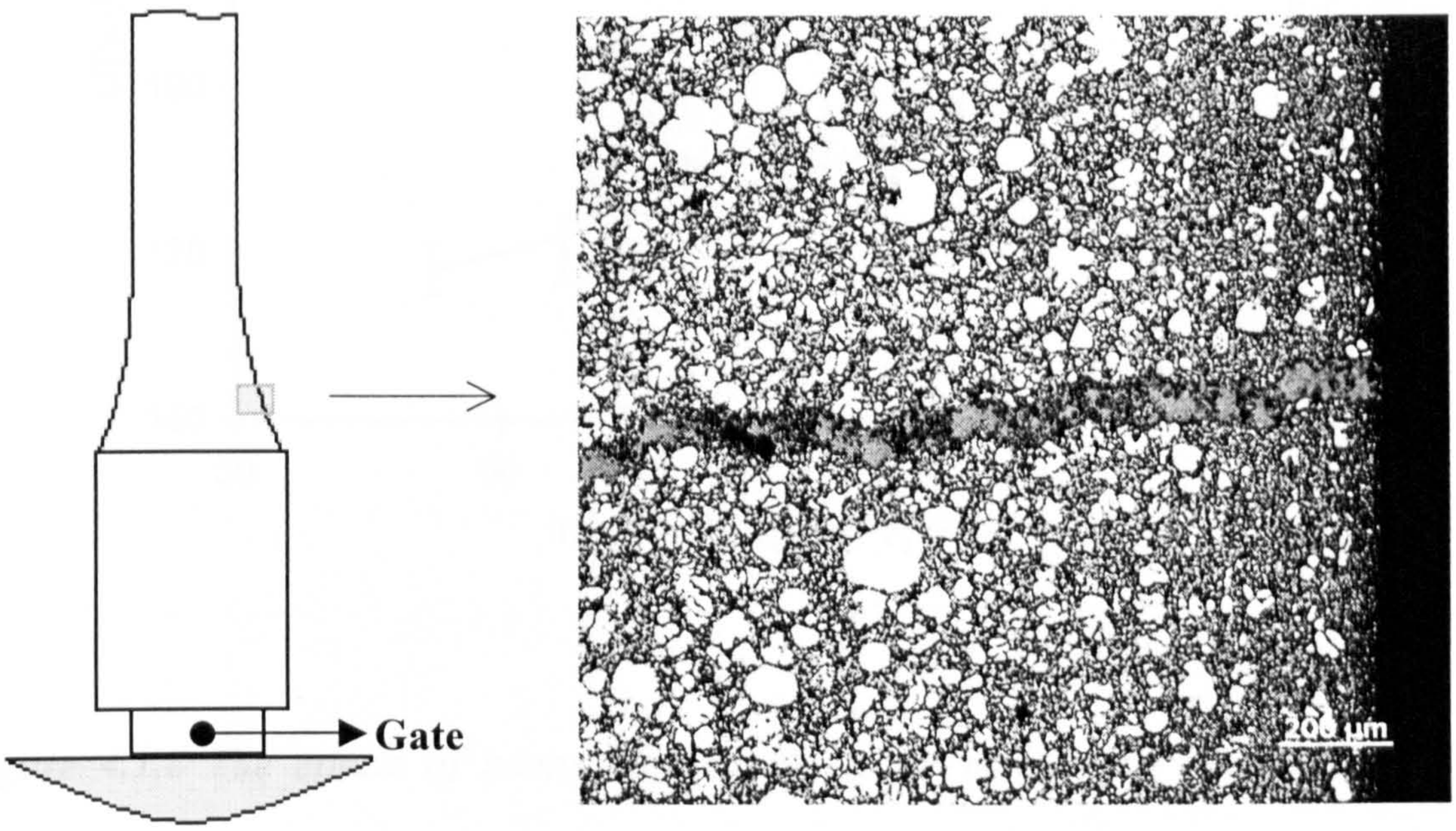

Figure 4.1.5 *A shoulder crack observed during processing optimisation.*

Intensifying Speed

Figure 4.1.6 shows the effects of intensifying speed V_3 on the mechanical properties of RDC AZ91D alloy. The RDC process was performed with a shearing temperature of

593°C, mould temperature of 235°C, shot distance of 170mm, shot speed of 60%, and the intensifying pressure of 80bar. It can be seen from Figure 4.1.6 that, faster intensifying speed improves tensile properties.

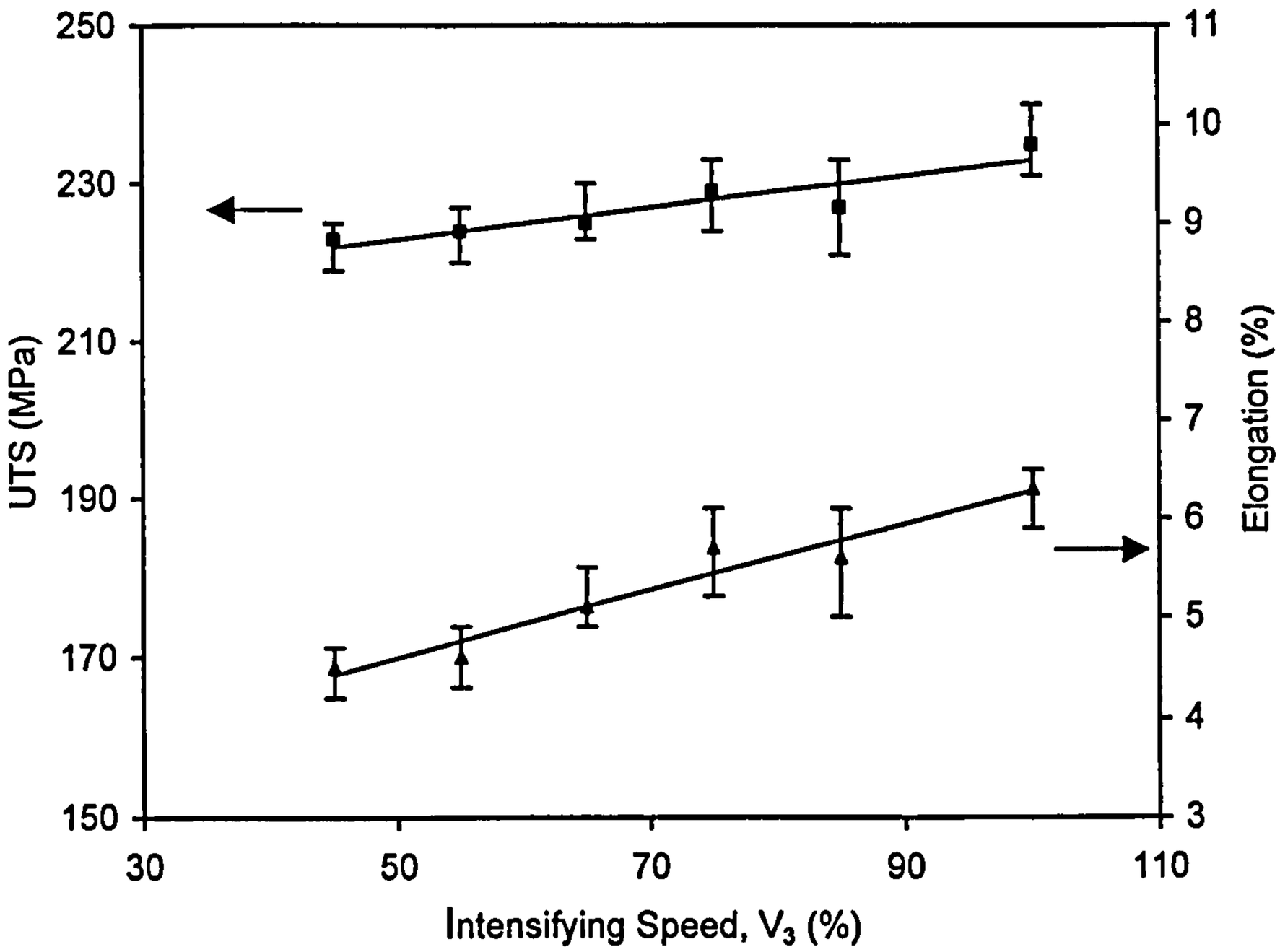

Figure 4.1.6 *The effects of intensifying speed on the mechanical properties of RDC AZ91D alloy.*

Shot speed

During the Rheo-Diecasting process optimisation, it was found that one of the most important factors that affect the microstructure and mechanical properties is the shot speed (V_2). At a very low shot speed of 30%, significant particle segregation was observed, as shown in **Figure 4.1.7a**. With increasing shot speed, the microstructure

segregation was much reduced but could still be observed at a shot speed of 50% (**Figure 4.1.7b**). The microstructure investigations further revealed that the segregation was fully eliminated when shot speed increased above 60% during the RDC process. A perfect structure distribution was produced when processed at a shot speed of 70% is shown in **Figure 4.1.7c**. **Figure 4.1.8** shows the effect of shot speed on the mechanical properties of RDC AZ91D alloy. The graphs in figure 4.1.8 have three different series of data; Series 1 was under the conditions of shearing temperature of 589 °C, mould temperature of 230°C, shot distance of 170mm, intensifying speed of 65%, and the intensifying pressure of 90bar; Series 2 was under the conditions of shearing temperature of 585 °C, mould temperature of 230°C, shot distance of 140mm, intensifying speed of 65%, and the intensifying pressure of 90bar respectively. Table 4.1.1 lists the microstructural analysis results obtained from series 2. At very low shot speed (e.g., 30%), die filling of magnesium slurry may be incomplete as a result of premature freezing. On the other hand, due to the very low heat content, the required die filling time is very short for magnesium alloys [NAD98], especially in the semisolid state. Therefore, the shot speed should be relatively higher for RDC Mg-alloys.

In addition, it is well known that the die design will affect metal flow conditions to a certain extent. By American magnesium alloy die casting experience [EML66], gates should be thin, not normally exceeding 2mm, but wide, aiming to quick filling of the die whilst permitting evacuation of air through the vent holes. Contrarily, in semisolid Mg-alloy die-casting cases, the mode of slurry filling of the die may tends to be reversed to that of liquid filling, i.e. from the back towards the gates. To encourage this reversed filling pattern in the RDC process, the gates should be larger.

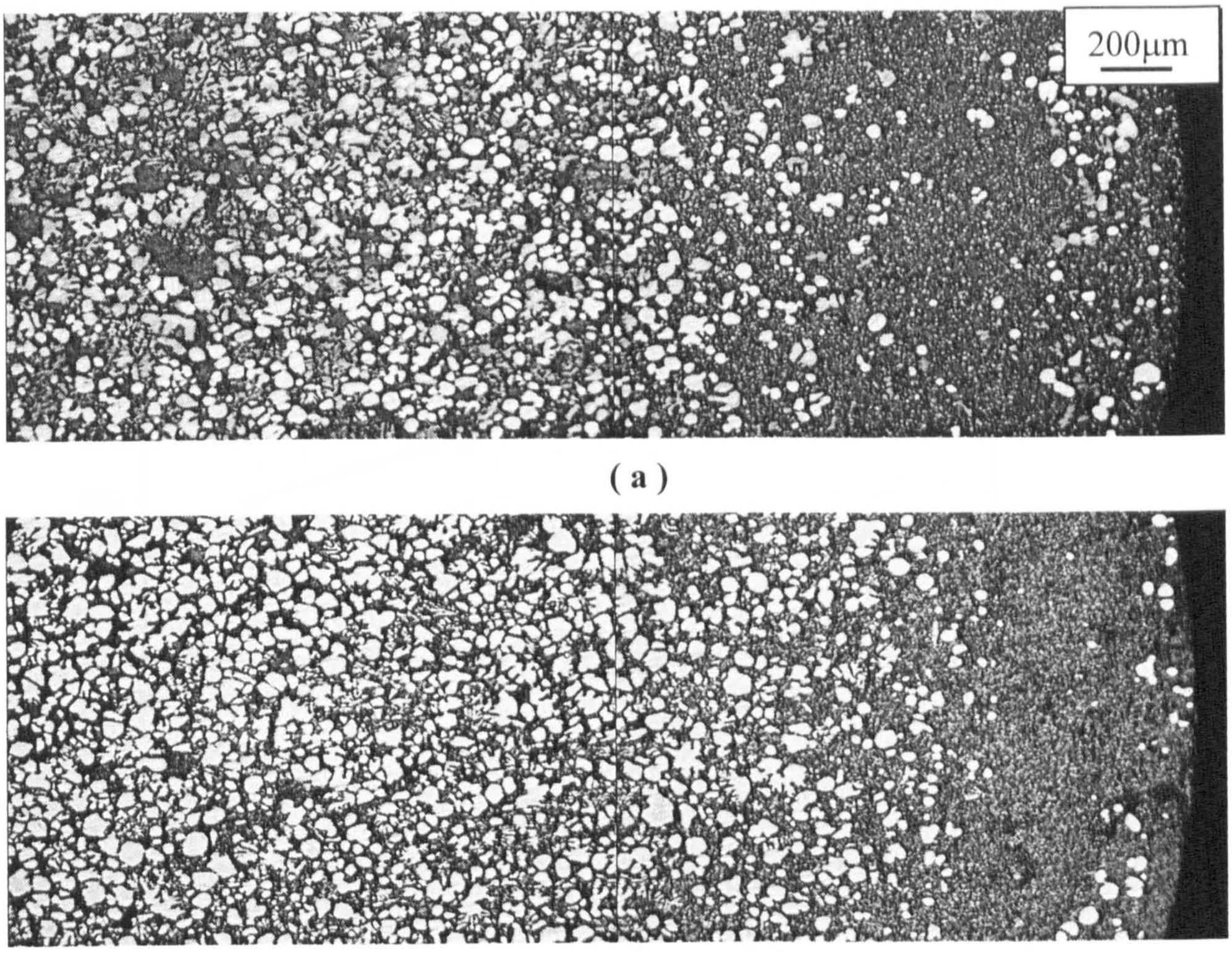

Figure 4.1.7 *The effect of shot speed on the microstructure of RDC AZ91D alloy.*
(a) Shot speed 30%, (b) shot speed 50% and (c) shot speed 70%.

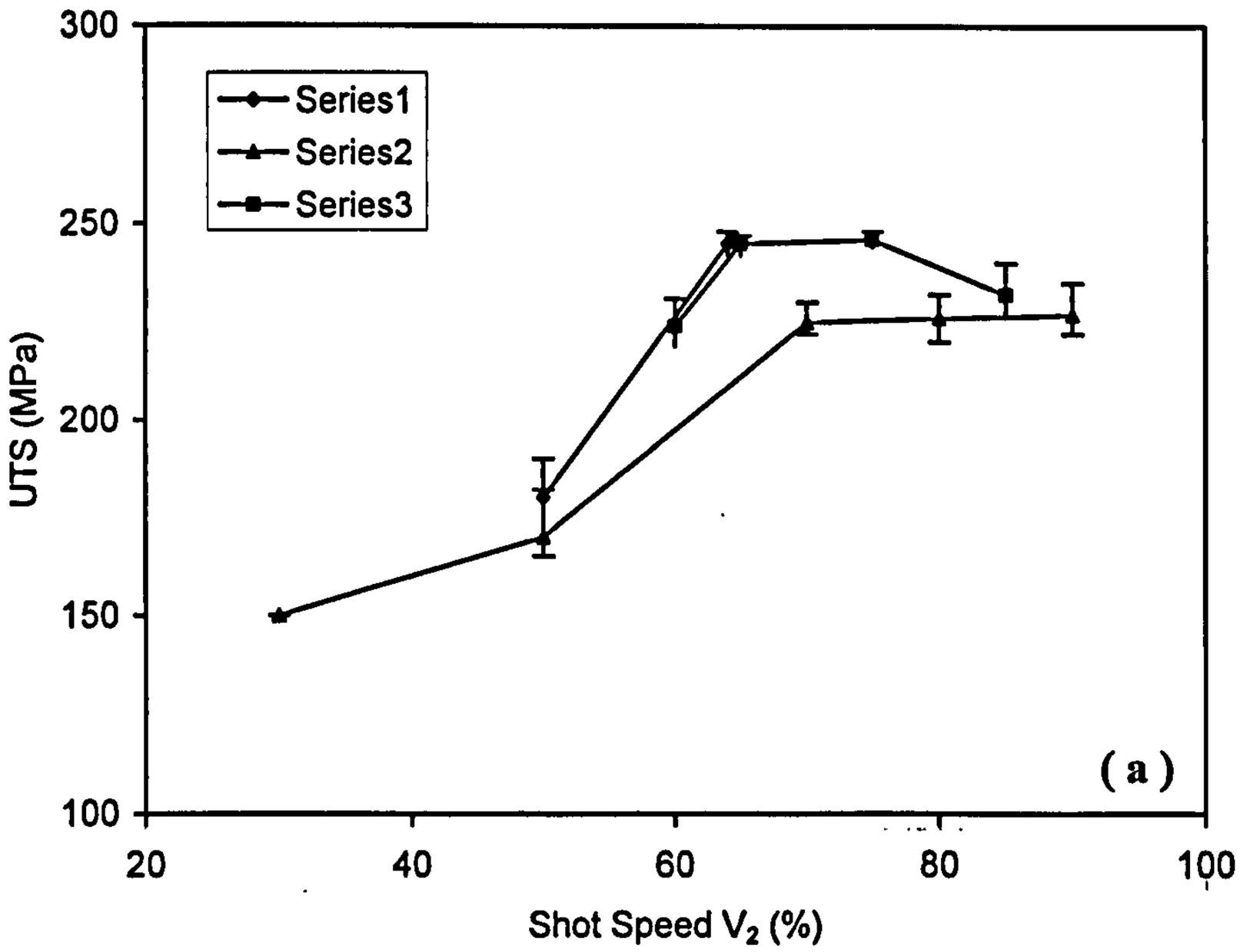

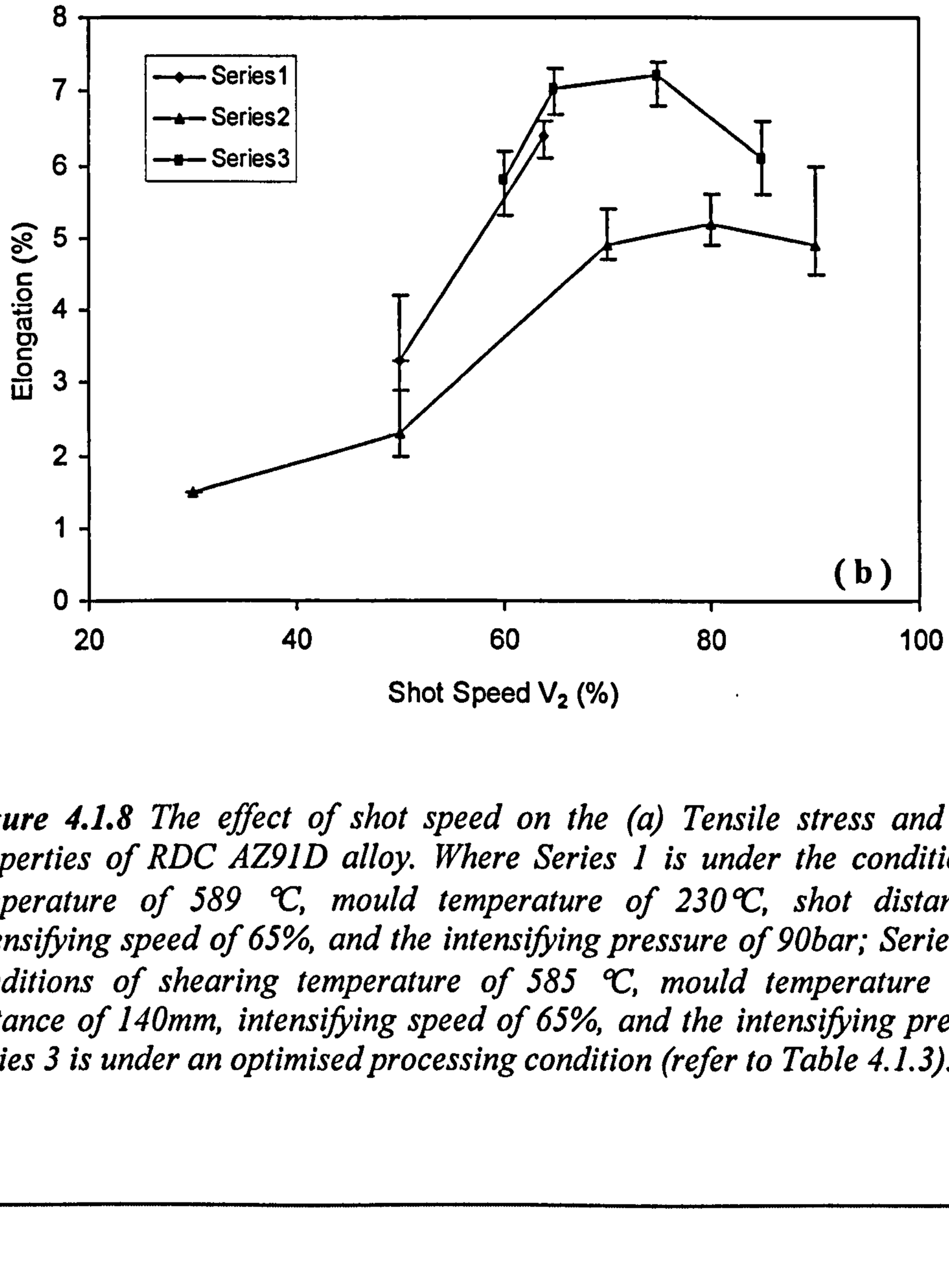

Figure 4.1.8 *The effect of shot speed on the (a) Tensile stress and (b) Elongation properties of RDC AZ91D alloy. Where Series 1 is under the conditions of shearing temperature of 589 ℃, mould temperature of 230℃, shot distance of 170mm, intensifying speed of 65%, and the intensifying pressure of 90bar; Series 2 is under the conditions of shearing temperature of 585 ℃, mould temperature of 230℃, shot distance of 140mm, intensifying speed of 65%, and the intensifying pressure of 90bar; Series 3 is under an optimised processing condition (refer to Table 4.1.3).*

4.1.3 The selected processing parameters

Based on the above understanding and conclusions, an optimised processing condition can be obtained for Rheo-Diecasting of AZ91D Mg-alloy, as summarised in **Table 4.1.3.**

Table 4.1.3 *The optimised processing parameter for Rheo-Diecasting of AZ91D Mg-alloy*

Die Temperature	Shot Distance	Shot Speed	Intensifying Speed	Intensifying Pressure
235°C	180 mm	75%	75%	90 bar

In Rheo-Diecasting, one of the most important mechanisms to get a good microstructure is to achieve laminar die filling. To check this the die cavity was deliberately filled half way so the conditions at the flow front could be examined. The photograph of the half filled sample produced under the selected processing parameter, and the microstructure at the flow front are presented in **Figure 4.1.9**. Figure 4.1.9 revealed that the flow front during the mould filling was parabolic and smooth, indicating that the mould filling was a viscous laminar flow and the body structure was an uniform fine and spherical under the optimised processing conditions. In addition the sample surface was sharp and tidy indicating a very good surface finish produced by the RDC process.

Afterwards, The optimised processing parameters were selected with a mould modification for Rheo-Diecasting of AZ91D Mg-alloy. Series 3 in Figure 4.1.8 was obtained under the selected processing condition (in Table 4.1.3) with four different shot speeds and shows that under these conditions, the optimised tensile strength is 246 MPa, and the elongation is up to 7.4 %.

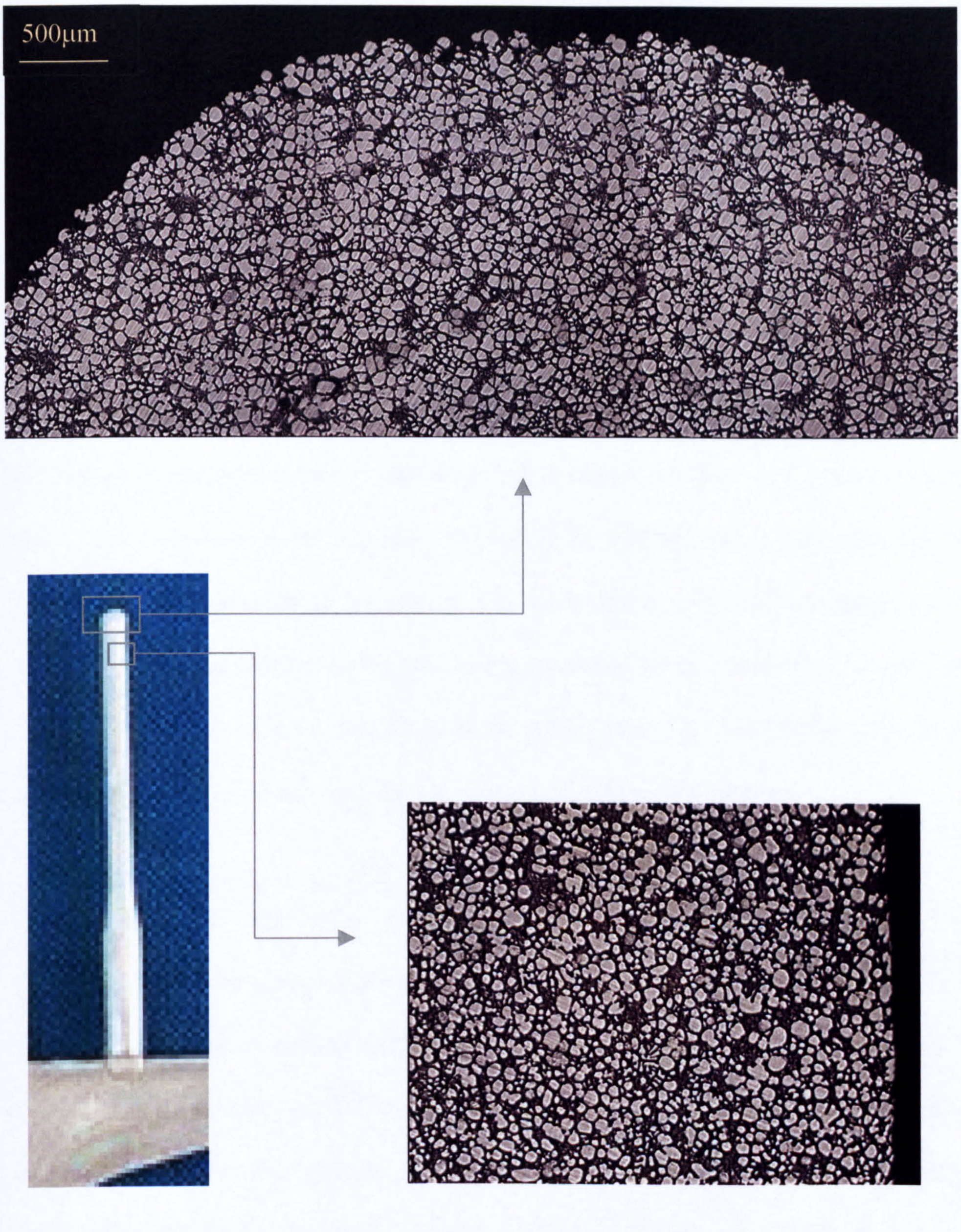

Figure 4.1.9 *Micrographs taken from the relevant positions on a deliberately produced RDC bar showing that the semisolid flow front during the mould filling was parabolic and smooth.*

4.2 Microstructure and mechanical properties of Rheo-Diecast AZ91D Mg-alloy

4.2.1 Characteristics of AZ91D Mg-alloy

AZ91D alloy is the most widely used die-cast Mg-alloy. It contains around 9wt% Al, less than 1wt% Zn and other minor alloying elements such as Mn, Si and Be. Al increases fluidity and therefore increases castability, but decreases ductility and creep resistance due to the formation of the $Mg_{17}Al_{12}$ (β-phase); Zn addition assists strengthening but increases the susceptibility to hot tearing. The composition of AZ91D maintains a good balance between castability and a reasonable combination of mechanical strength and ductility in the as-cast condition. In addition, AZ91D alloy is heat treatable due to the precipitation of the β-phase from the supersaturated α-Mg solid solution.

Thermo-Calc and MG-DATA (a Mg-database developed by Thermo-Tech Ltd, Guildford, UK) were used to assess the thermodynamic properties of the AZ91D alloy. **Figure 4.2.1** shows a vertical section of the ternary Mg-Al-Zn system at constant Zn content (0.67wt%). This vertical section resembles a binary eutectic alloy, as the 3-phase region (L+ α + β) is very narrow. The calculated liquidus and solidus for AZ91D alloy are 602°C and 468°C, respectively. Under equilibrium conditions, AZ91D alloy should solidify as a single-phase α-Mg solid solution, and further cooling should lead to the solid-state precipitation of the $Mg_{17}Al_{12}$ β-phase. However, the solidification structure of Mg-Al alloys in the as cast condition differs significantly from this prediction. Non-equilibrium eutectic is always present in the as-cast microstructure in Mg-Al alloy

containing more than about 2wt% Al [POL95]. The maximum equilibrium solubility of Al and Zn in Mg are 11.7wt% and 0.67wt% at 428°C, respectively. The predicted solid fractions in the liquid-solid region are presented in **Figure 4.2.2** as a function of temperature. Both Figure 4.2.1 and Figure 4.2.2 will be used to guide the selection of processing parameters and heat treatment conditions in this work.

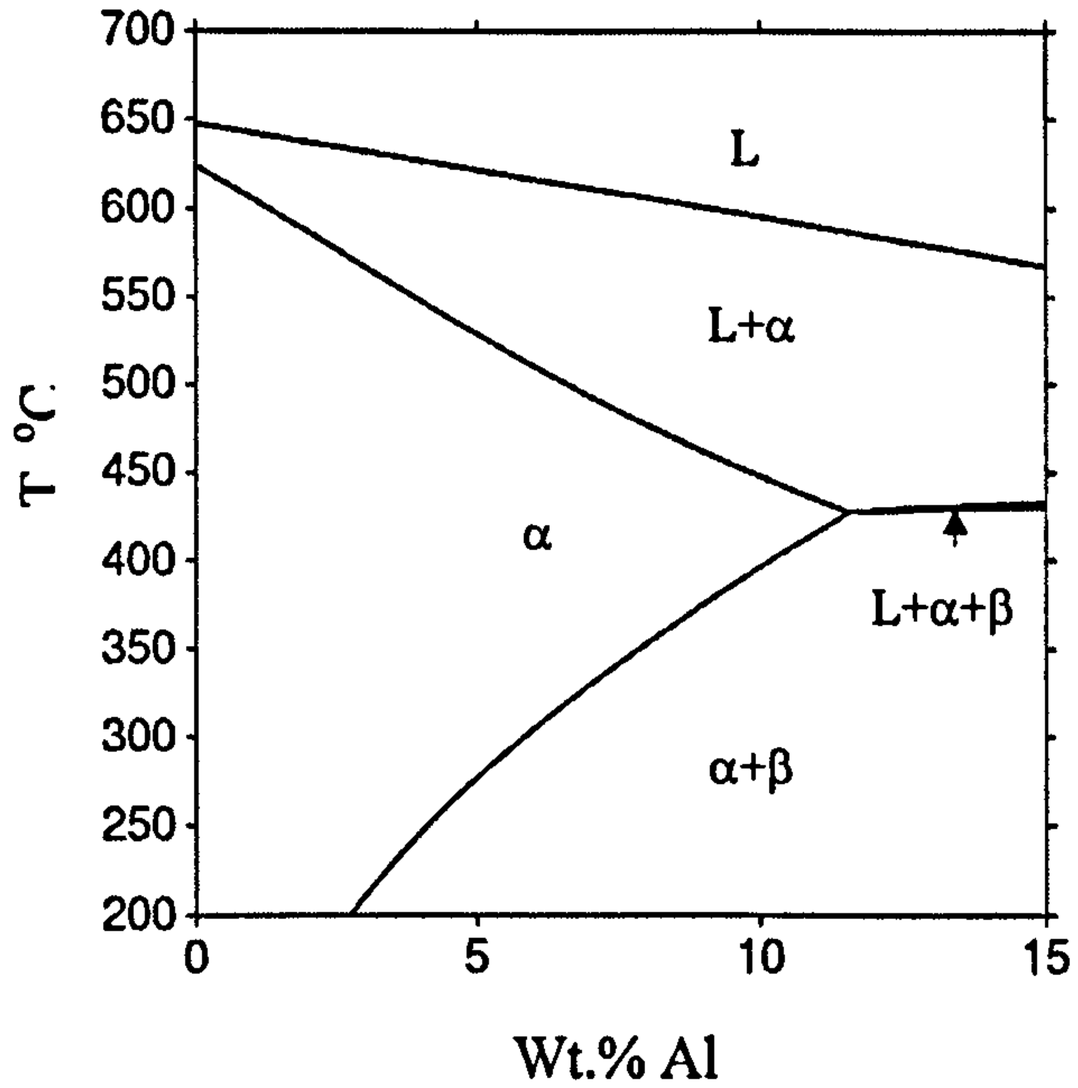

Figure 4.2.1 *Vertical section of the ternary Mg-Al-Zn system phase diagram. The Zn content is fixed at 0.67wt%.*

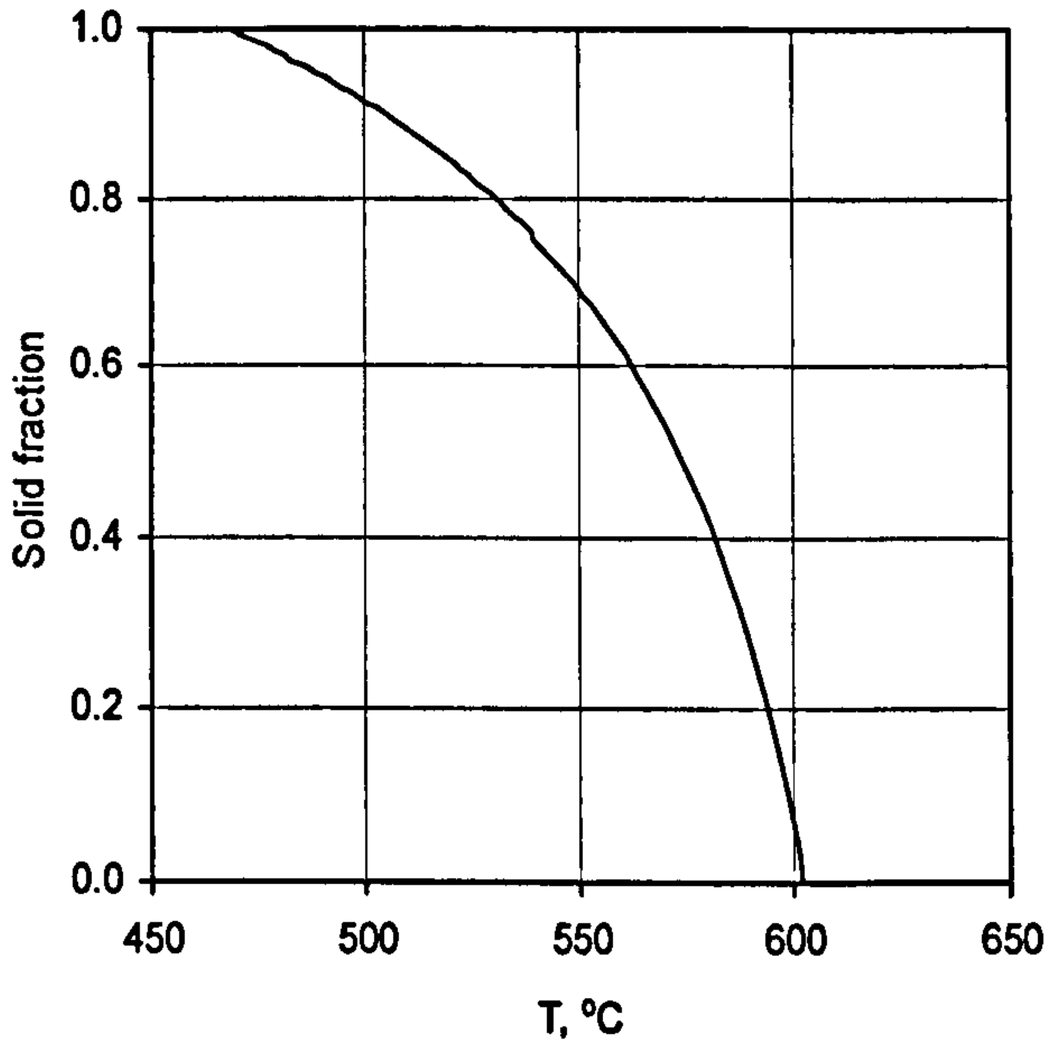

Figure 4.2.2 *Calculated solid fraction of the AZ91D Mg-alloy as a function of temperature*

4.2.2 Microstructures of RDC AZ91D Mg-alloy

General microstructures of RDC AZ91D Mg-alloy

The general microstructure of RDC AZ91D Mg-alloy is dominated by the primary solidification in the Twin-Screw slurry maker. In order to understand the microstructural characteristics of the RDC process, and for comparison purposes, a microstructure of AZ91D alloy produced by conventional HPDC process is introduced first.

Figure 4.2.3 represents the typical microstructure of HPDC AZ91D alloy through a cross section of a ϕ6mm bar. There is a chilled zone near the sample surface, which has a fine structure and is enriched with Al compared with the rest of the sample. This chilled zone, sometimes referred as the surface layer in the literature, is believed to have a strong influence on the mechanical properties of die cast samples [SEQ96]. The sample centre is densely populated with dendrite fregments, as shown in **Figure 4.2.4a** taken from sample centre under higher magnification. The porosity is concentrated in the centre of the sample and consists of both entrapped gas bubbles and cracks caused by hot tearing. In addition, there is a dark circular region observed on the cross section, as arrow marked in Figure 4.2.3. Detailed microstructure analysis indicates that this region was concentrated with hot cracks and enriched with the β -phase. This 'defect band' is a typical feature of HPDC Mg-alloy castings, as has been investigated in detail by Bowles et al. [BOW01]. In addition, the formation of large dendritic primary α-phase was an important feature of HPDC AZ91D alloy, as shown in **Figure 4.2.4b**. It is believed that such dendritic particles were formed in the shot sleeve prior to mould filling. The large shear rate the melt experienced at the gate (estimated to be as high as $10^5 s^{-1}$ by Sequeira et al [SEQ96]), fragmented the dendrites resulting in the morphology of the primary phase observed in

Figure 4.2.3 and 4.2.4. It is also evident from Figure 4.2.3 that some of the dendrites formed in the shot sleeve had survived after the high shear at the gate and were present in the final solidified microstructure.

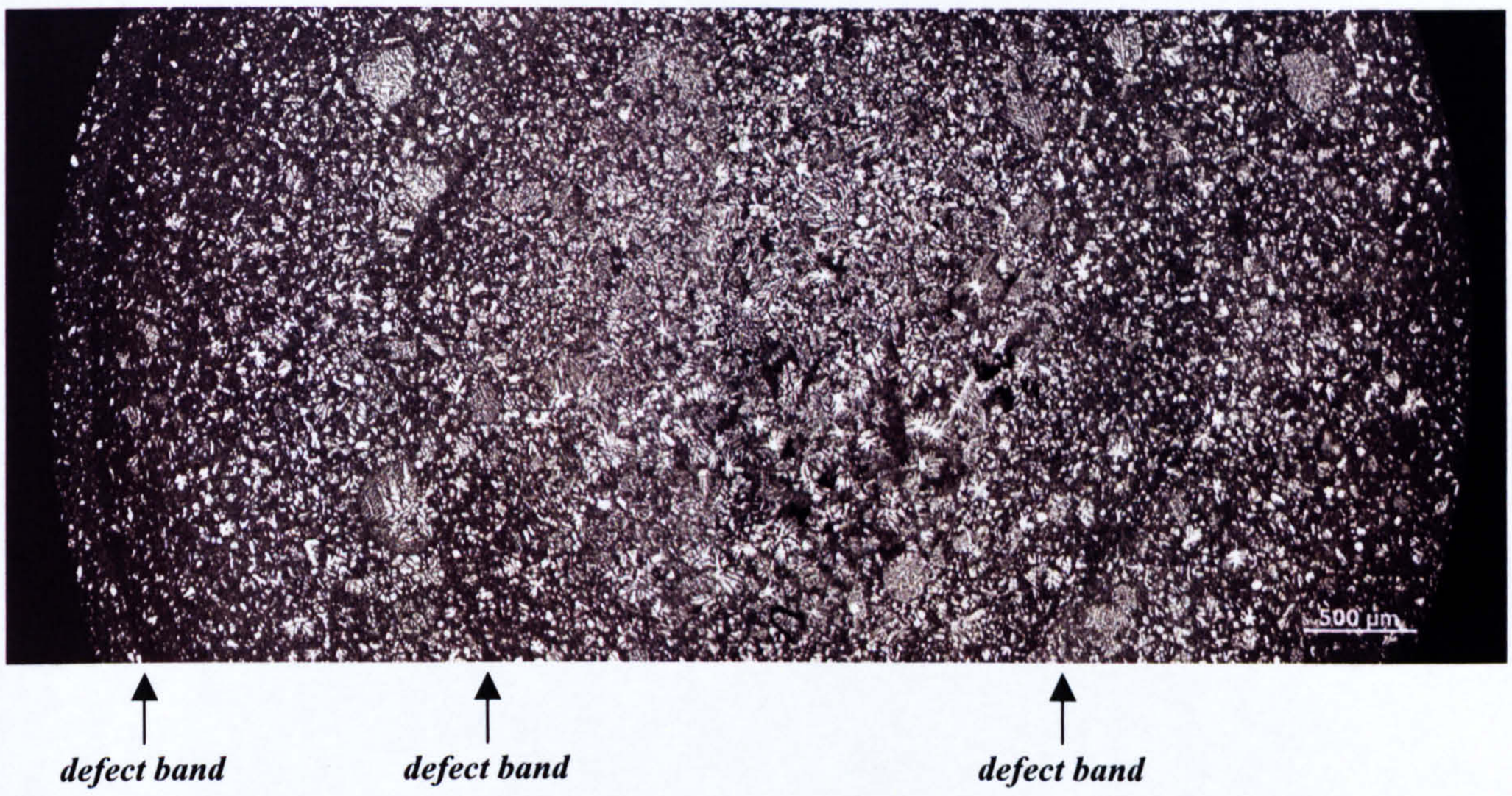

Figure 4.2.3 *Montage of optical micrographs showing the as-cast microstructure through the cross-section of a ϕ6mm AZ91D alloy bar produced by the HPDC process.*

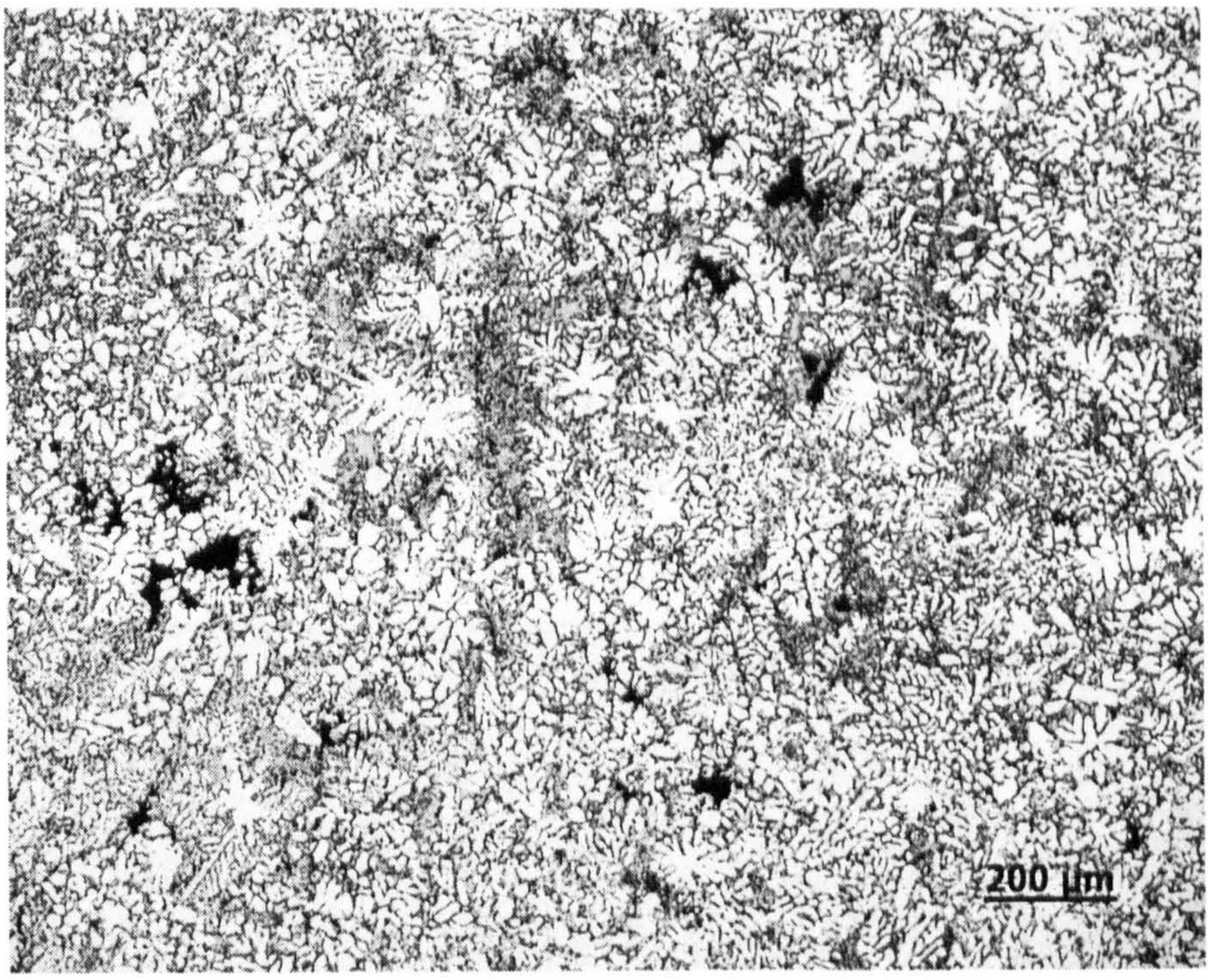

(a)

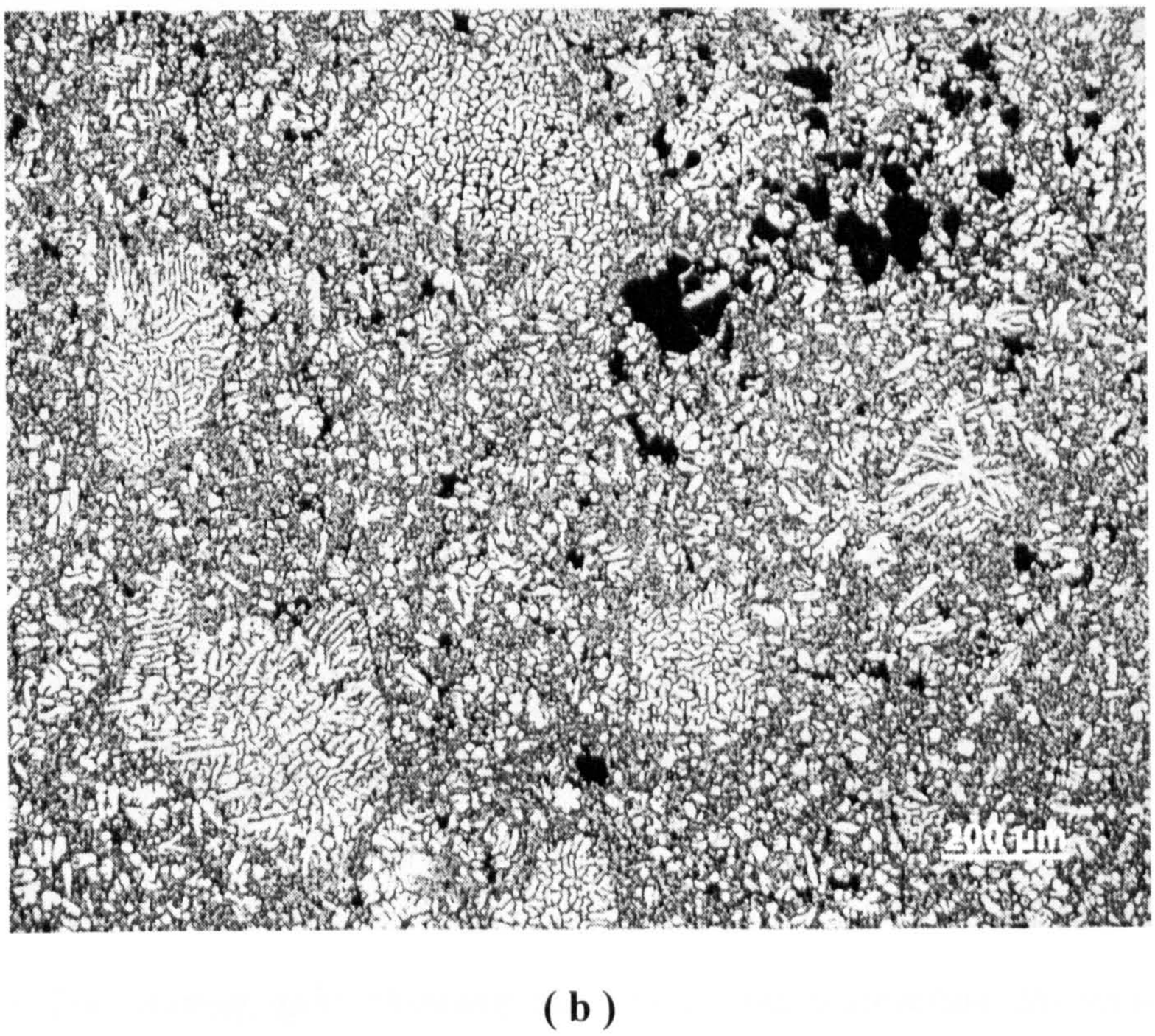

(b)

Figure 4.2.4 *Optical micrograph showing the detailed microstructure in a ϕ6mm AZ91D alloy bar produced by the HPDC process. (a) Densely populated dendrites with porosity and (b) large primary dendrites are presented in the HPDC sample.*

Figure 4.2.5 presents the micrographs showing the as-cast microstructure through the entire cross-section of a ϕ6mm AZ91D alloy bar produced by the optimised RDC process. **Figure 4.2.5a** shows a lower solid fraction of 19.1% (produced at a shearing temperature of 593°C), and **Figure 4.2.5b,** a higher solid fraction of 31.5% (produced at a shearing temperature of 585°C).

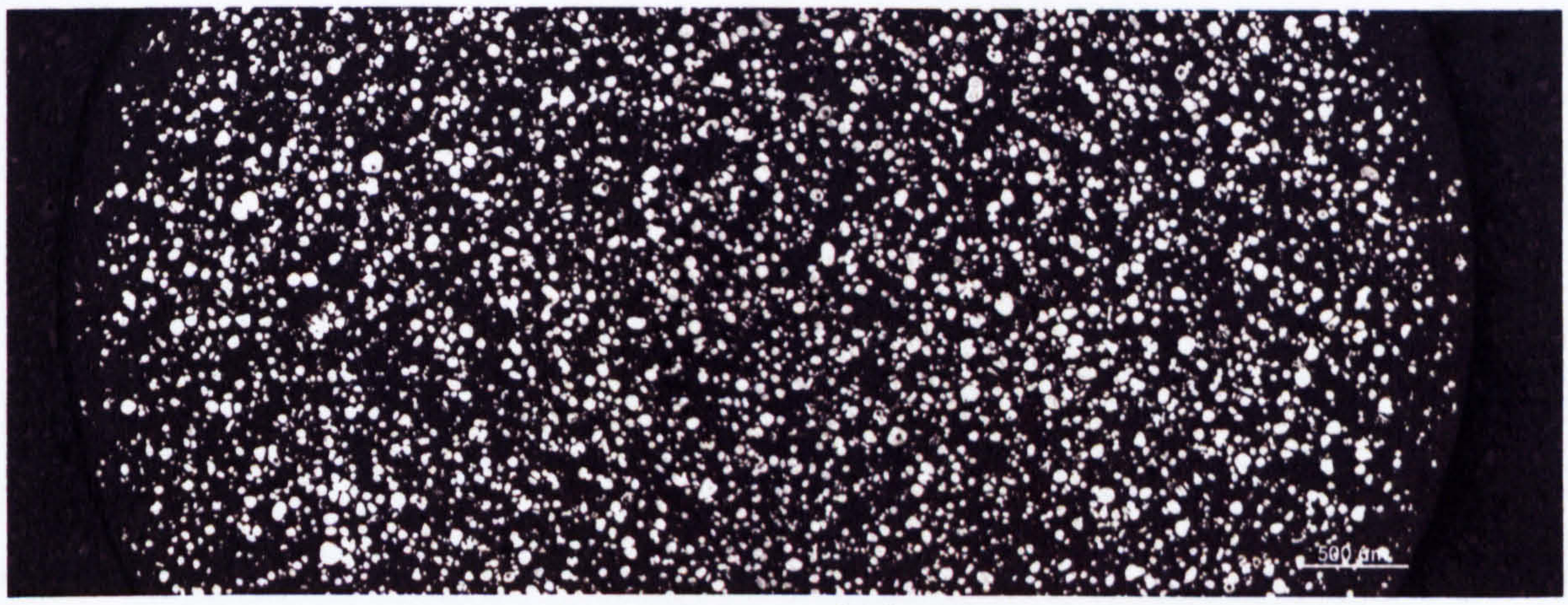

(a)

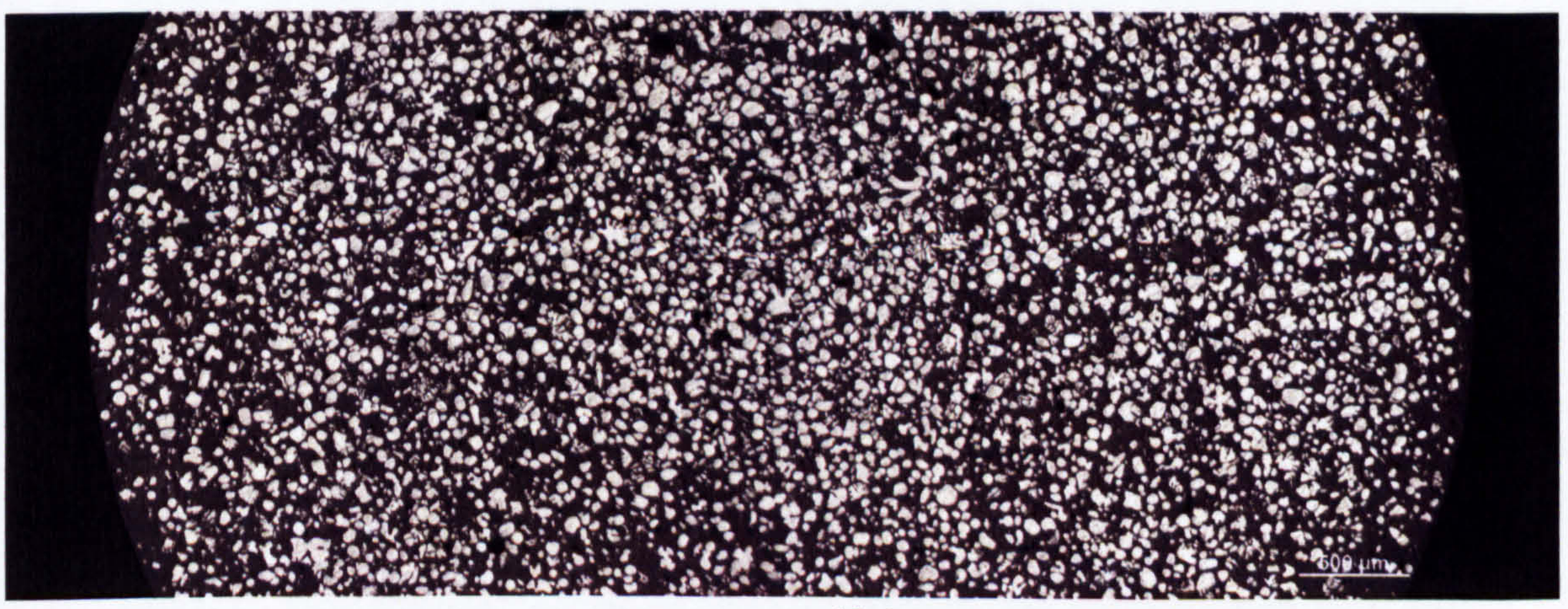

(b)

Figure 4.2.5 *The micrographs showing the as-cast microstructure through the entire cross-section of a ϕ6mm AZ91D Mg-alloy bar produced by the RDC process. (a) Lower solid fraction, 19.1% (produced at the shearing temperature of 593 ℃), and (b) higher solid fraction, 31.5% (produced at the shearing temperature of 585 ℃)*

In contrast to Figure 4.2.3 (microstructure of HPDC samples), the structure of RDC AZ91D is unique and essentially different from that generated by conventional die-casting technologies. The primary particles in the RDC samples are very fine and spherical. There is no entrapped gas porosity, only very fine micro-shrinkage (a few micron in size) could be observed occasionally, the micro-shrinkage defects as shown in **Figure 4.2.6**. The total porosity measured was much less between 0.3% and 0.5% in comparison to the ≥2% of conventional HPDC.

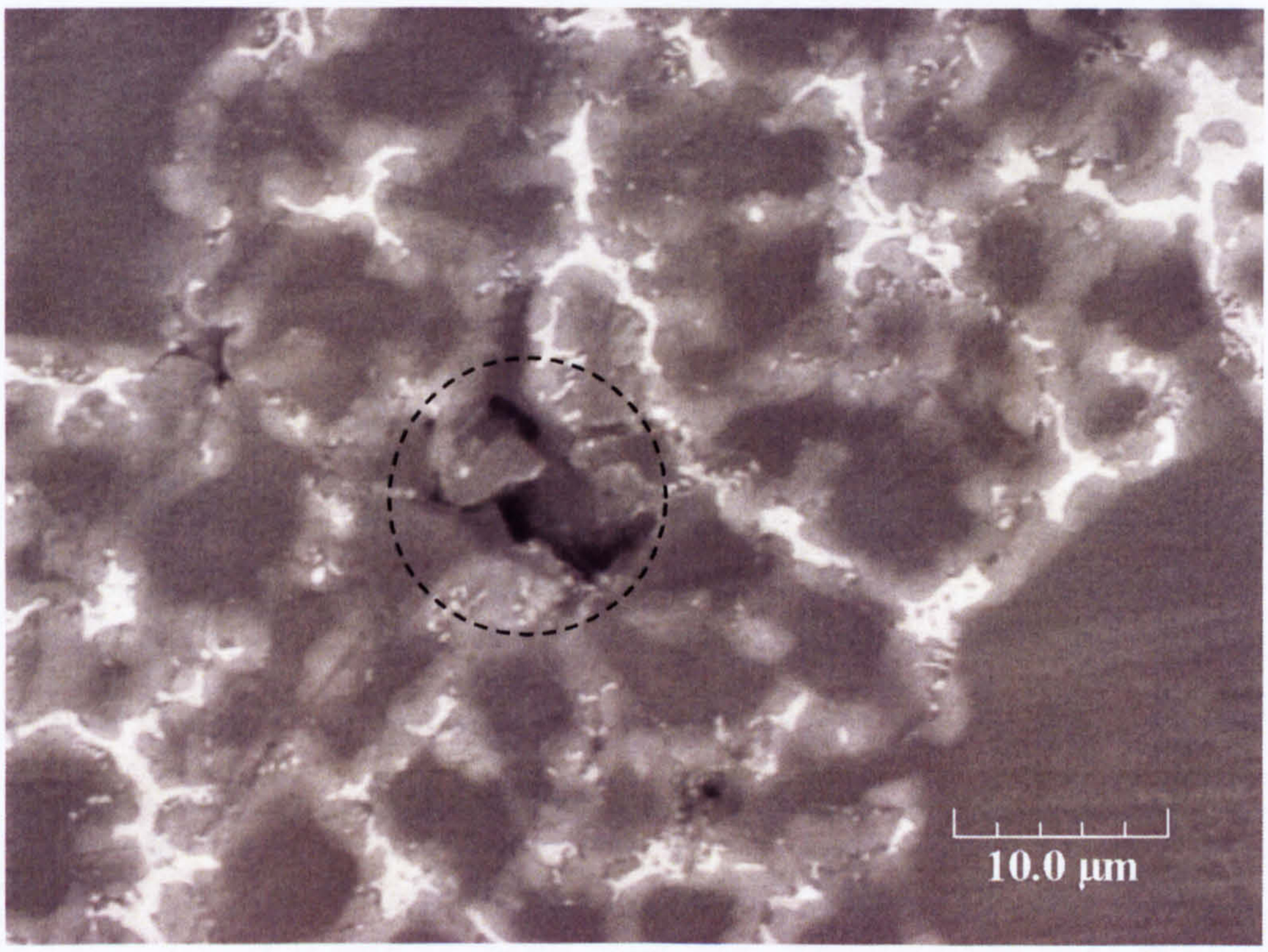

Figure 4.2.6 *Detailed micrographs showing the very fine* micro-shrinkage *(circled) found in the RDC AZ91D Mg-alloy samples.*

Quantitative metallography was used to quantify the distribution of the primary particles in the samples with different solid fractions; the results are presented in **Figure 4.2.7**. Figure 4.2.7 indicates that the primary solid phase had a uniform distribution throughout the entire cross section of the RDC samples. Only a slightly lower solid fraction was observed at the sample surface, which coincides with a slight enrichment of Al at the surface region. The uniformity of RDC microstructures was also demonstrated by microstructure examinations at different cross sections, as show in **Figure 4.2.8**.

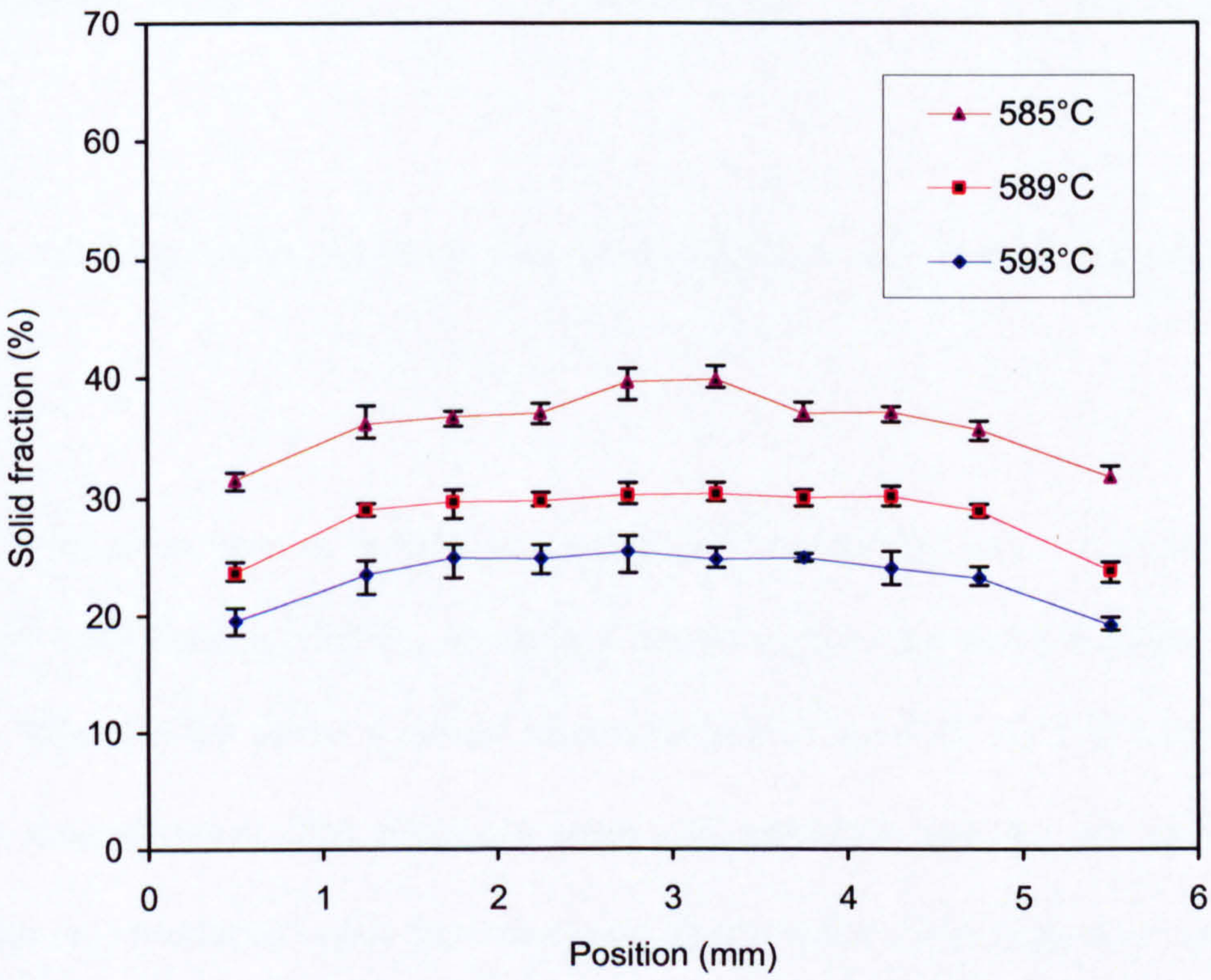

Figure 4.2.7 *Variation of volume fraction of the primary α-Mg particles in the cross section of ϕ6mm RDC AZ91D Mg-alloy bars processed at different shearing temperatures (585℃, 589℃ and 593℃). The three relatively flat lines show that the distributions of the primary α-Mg particles through the cross sections are very uniform.*

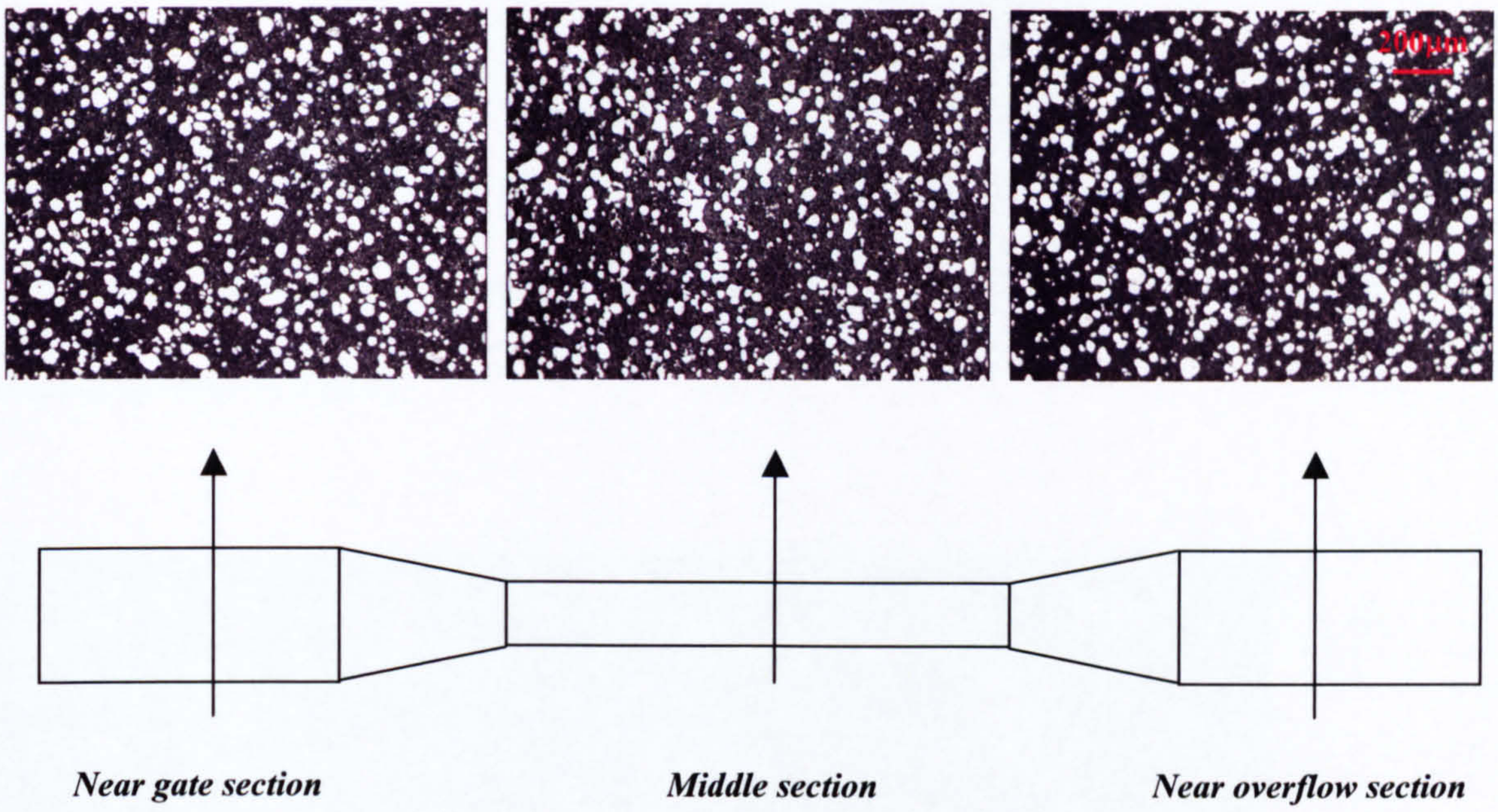

Figure 4.2.8 *The microstructures observed at different cross sections of a RDC sample.*

The solidification process in RDC process is clearly identified as two distinct stages, the primary solidification and the secondary solidification (see the discussion in section 5.2.1). **Figure 4.2.9** shows a typical microstructure of the RDC AZ91D Mg-alloy under higher magnification. The relatively large and spherical particles are primary α-Mg particles (α_1) produced inside the twin-screw slurry maker under high shear rate and high intensity of turbulence. Secondary solidification began when the semisolid slurry was transferred to the shot sleeve. A partial volume fraction of the primary α-Mg phase was produced in the remaining liquid. Such particles usually have a dendritic morphology. The semisolid slurry is then delivered to the die cavity with a controlled shot speed and pressure. The dendrites formed in the shot sleeve are fragmented when they pass through the narrow gate, resulting in the dendrite fragments observed in the final microstructure,

it is denoted here as α_2. The remaining liquid in the semisolid slurry then solidified in the die cavity under high cooling rate, and the resulting microstructure is fine α-Mg particles (α_3) mixed with the $Mg_{17}Al_{12}$ β-phase. It should be pointed out here that no entrapped liquid was observed inside α-Mg solid particles, which is evident in thixomoulding microstructures [CZE01].

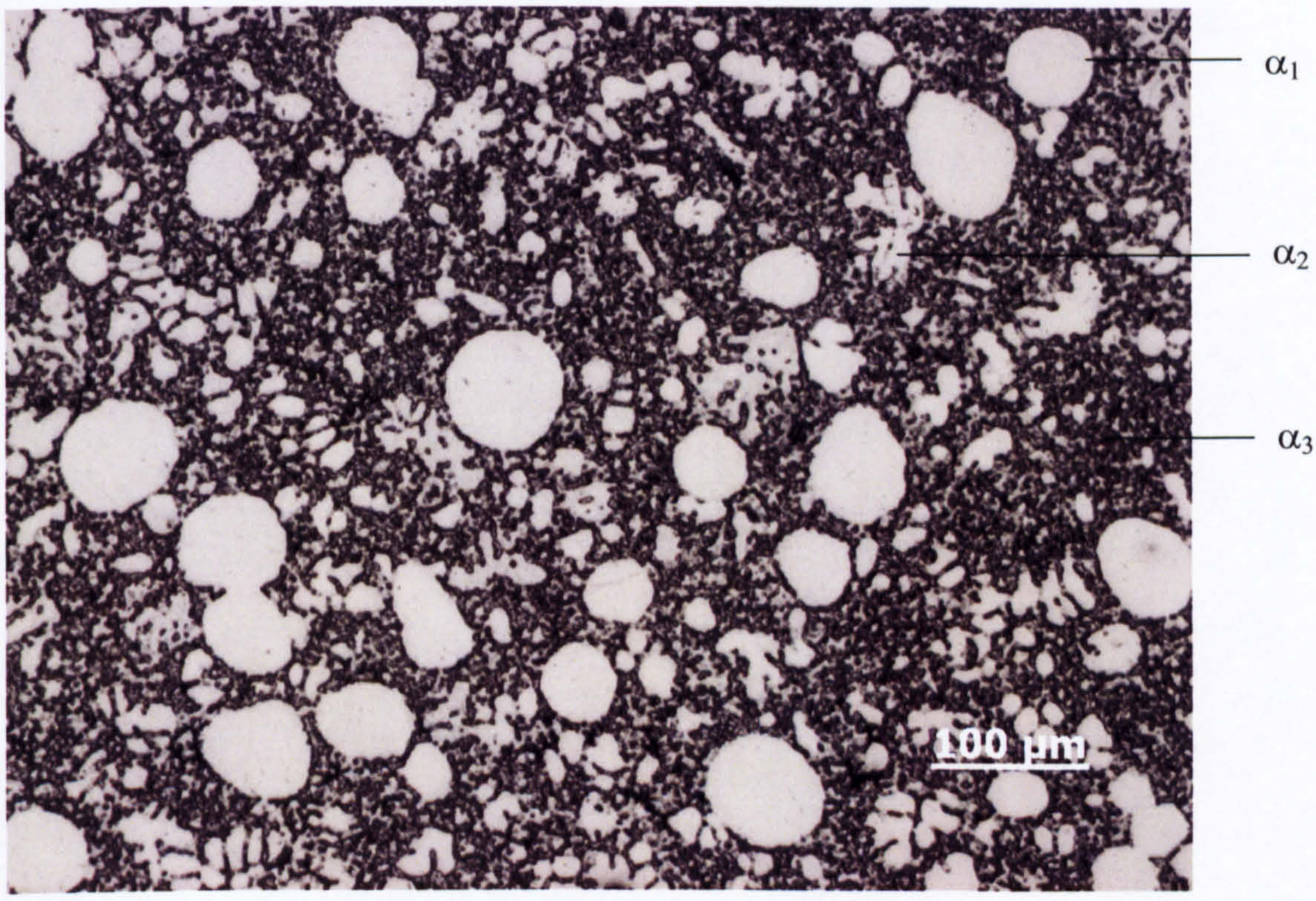

Figure 4.2.9 *A typical microstructure of the RDC AZ91D Mg-alloy in a higher magnification showing the primary phases of α_1 , α_2 and α_3 generated in different solidification stages in RDC process.*

The X-ray diffraction traces of AZ91D alloy produced by both RDC and HPDC processes are presented in **Figure 4.2.10**. The results indicate that only the α-Mg solid solution and the intermetallic compound β-$Mg_{17}Al_{12}$ phase were present in both samples.

No evidence for the presence of any other phases was detected by the X-ray analysis. For the β phase, it is reported that some of the Al atoms are substituted by Zn, resulting in the possibility of forming $Mg_{17}(Al, Zn)_{12}$ [CZE01]. In this study, we simplify the form as just $Mg_{17}Al_{12}$.

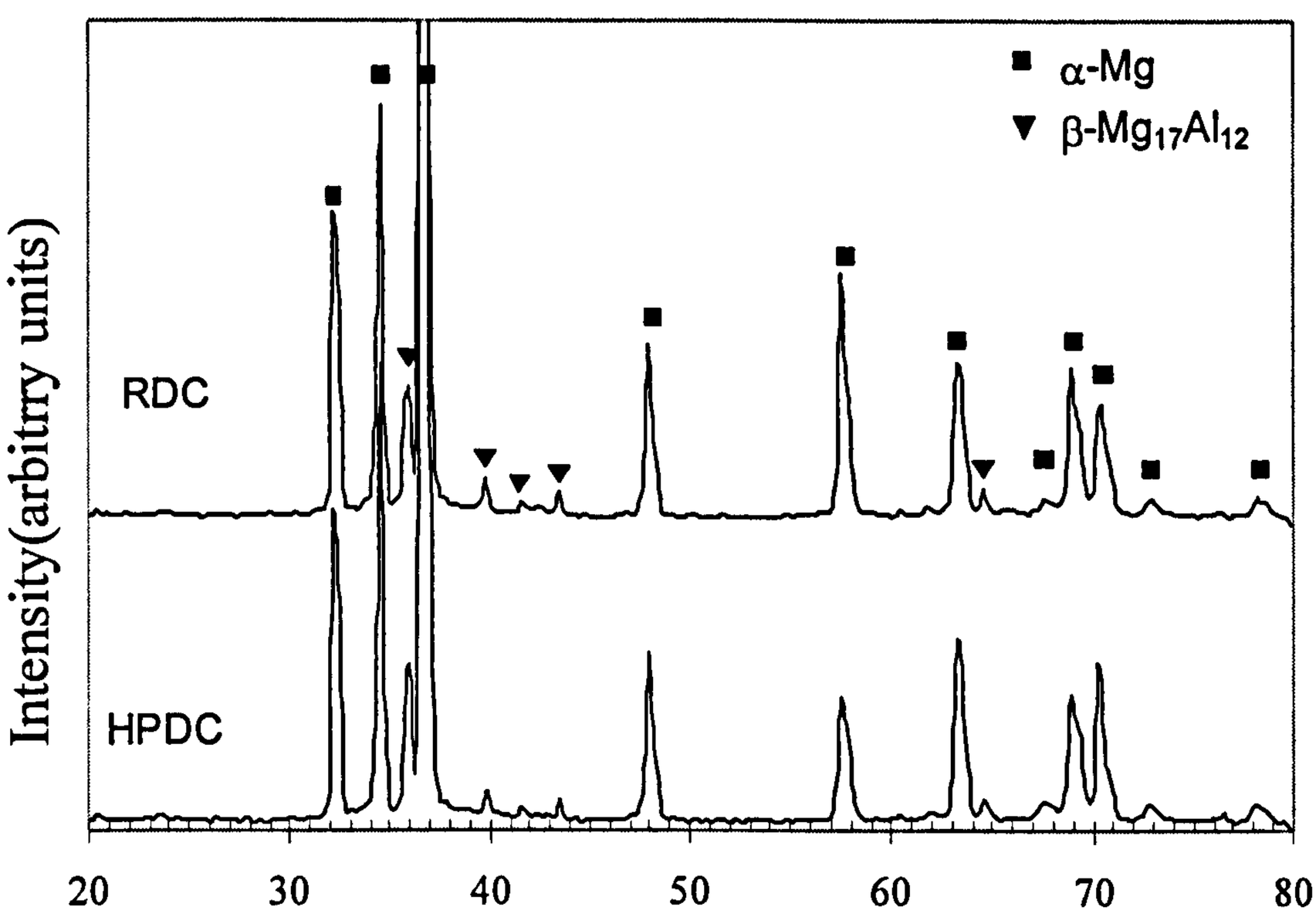

***Figure 4.2.10** X-ray diffraction traces showing the phases present in the AZ91D Mg-alloy processed by both HPDC and RDC processes.*

In order to check the effects of melting and Rheo-Diecasting on the chemical composition of the AZ91D Mg-alloy, chemical analysis was carried out on samples taken from the melting furnace and the RDC sample. The results are presented in **Table 4.2.1** in comparison with the chemical compositions of the AZ91D ingot. There was very little change in the composition of the alloying elements. Perhaps more importantly, there was

little change in Fe contents after both melting and Rheo-Diecasting, with the Fe content in the RDC sample being well within the specification of AZ91D Mg-alloy.

Table 4.2.1 *The chemical compositions of AZ91D Mg-alloy at different processing stages (in wt%).*

AZ91D	Zn	Al	Si	Cu	Mn	Fe	Ni	Be	Others Each
Ingot	0.67	8.76	0.047	0.014	0.25	0.0038	0.0015	0.0011	< 0.01
After Melting	0.66	8.55	0.046	0.012	0.21	0.0039	0.0011	0.0008	< 0.01
After RDC	0.63	8.52	0.048	0.014	0.18	0.0040	0.0011	0.0007	< 0.01

Detailed microstructures of RDC AZ91D Mg-alloy

The solidification of the remaining liquid in the semisolid slurry inside the die cavity without shearing is referred to as a secondary solidification. It is important to point out that the remaining liquid has previously been intensively sheared inside the slurry maker. **Figure 4.2.11** presents the SEM micrographs showing the detailed microstructures produced by secondary solidification. The solidification of the remaining liquid produces further volume fraction of primary α-Mg particles (**Figure 4.2.11a,** the dark area), with a fine size and a nearly spherical morphology, followed by the formation of a discontinuous eutectic network (the bright area). The nominal particle size of the α_3-phase from the secondary solidification was quantified and found to be around 5-10μm. The detailed microstructure of the eutectic network is shown in **Figure 4.2.11b**. It is interesting to see that the eutectic is completely divorced. The β-phase formed its own network and it is difficult to distinguish the eutectic α-phase and the primary α-phase produced by the secondary solidification.

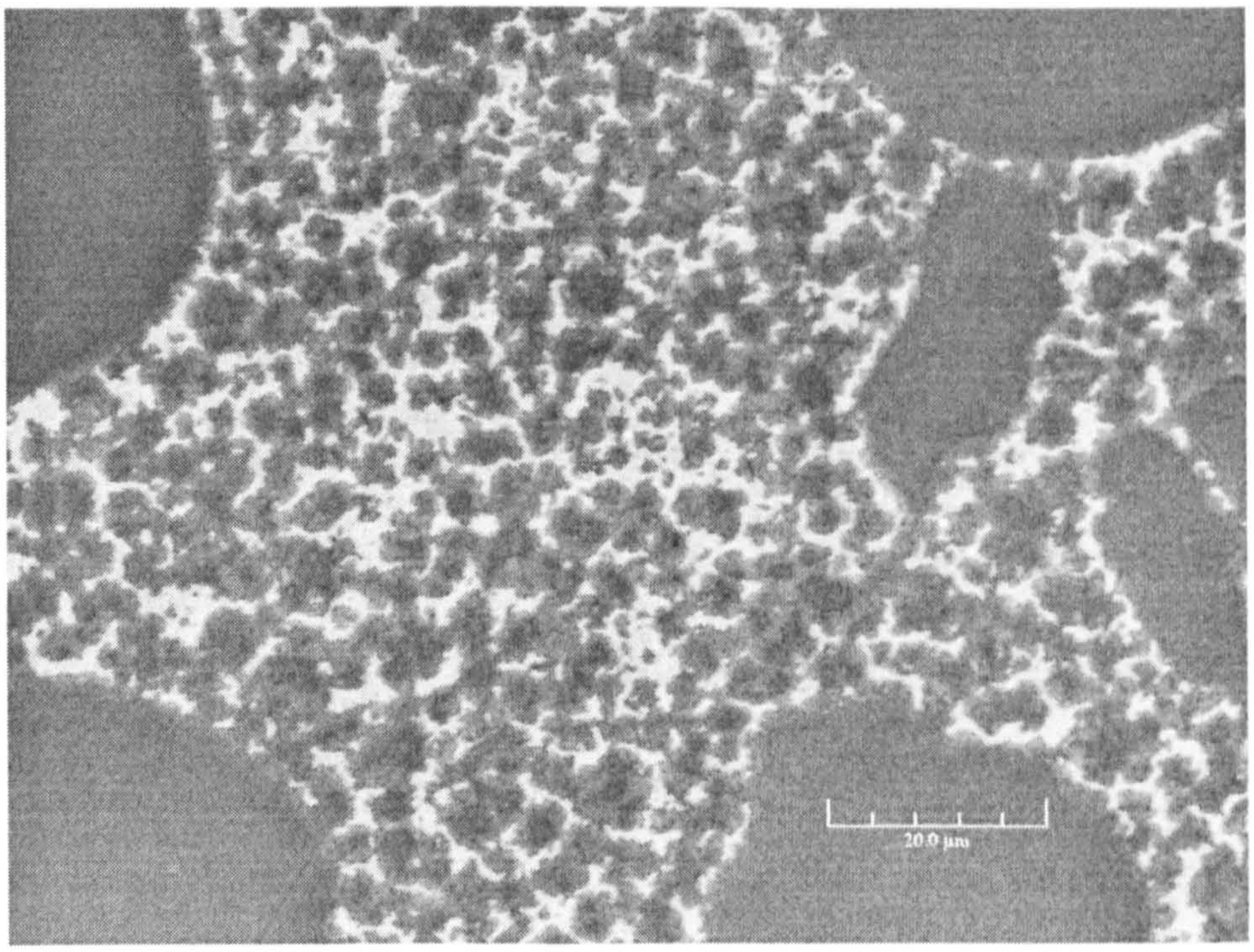

(a)

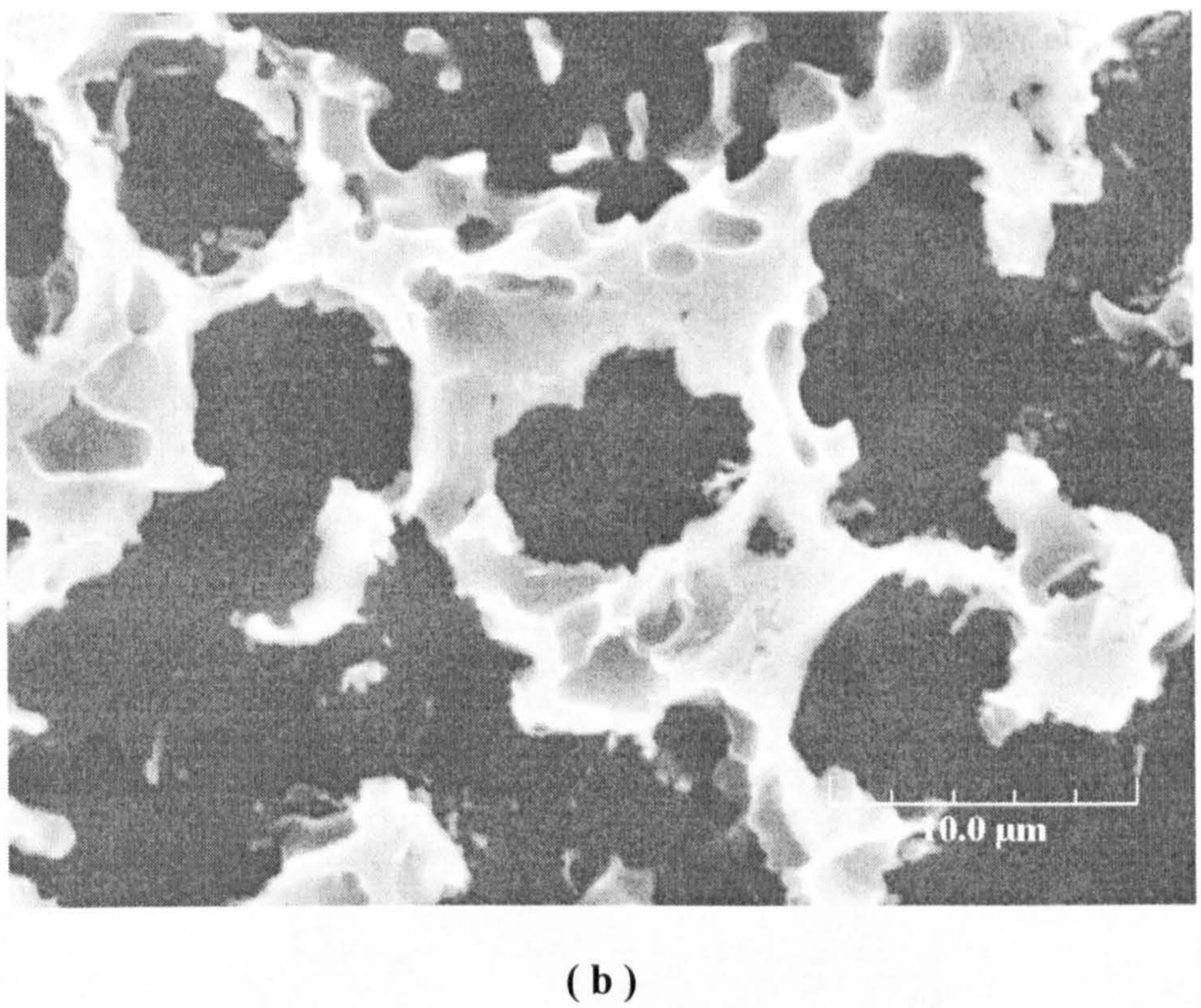

(b)

Figure 4.2.11 *SEM micrographs showing (a) the detailed microstructure of α_3 and (b) the eutectic network produced by secondary solidification in RDC process.*

Figure 4.2.12 is a typical TEM bight field image of the RDC AZ91D Mg-alloy, showing more details of the β-$Mg_{17}Al_{12}$ phase and the fine α-Mg grains, from the secondary solidification region. The β-$Mg_{17}Al_{12}$ phase was found to be located along the α-Mg grain boundaries and virtually free of dislocations. A relatively high dislocation density was observed inside some of the α-Mg grains close to grain boundaries and the β-phase particles. EDS analysis performed on the β-phase showed that it contains 66.43at%Mg, 32.22at%Al and 1.35at%Zn. The measured Mg/Al ratio, 2.06, is higher than the stoichiometric ratio, 1.42 (17/12), attributed to the contribution from the excessive Mg in the α-Mg solid solution matrix. In addition, the high zinc content appears to be concentrated in the secondary solidification stage, with more solution into the β-$Mg_{17}Al_{12}$ phases.

Figure 4.2.12 *TEM bright field images showing morphology of the β-$Mg_{17}Al_{12}$ phase in secondary solidification region. The insert is the [001] selected area electron diffraction pattern taken from the labelled β-$Mg_{17}Al_{12}$ phase.*

Figure 4.2.13 presents a SEM micrograph and the EDS line scanning of Mg and Al elements, showing the compositional variation across a primary α-Mg particle. It can be seen that concentrations of Mg and Al inside the primary α-Mg particle were constant, and that a sharp increase in Al content was found when the line was crossing the eutectic β-$Mg_{17}Al_{12}$ phase. This is in contrast to the usual observation of micro-segregation in conventional casting, due to the coring effect, which leads to a lower Al concentration in the middle of the particle and increased concentration towards the outer region of the particle. Similar to the Thixomoulding process, Czerwinstki et al [CZE01] also detected an obvious increase in Al concentration when the electron beam moved from the centre towards the primary α-Mg particle boundary, indicating the coring effects. Further EDS analysis of the chemical composition of the primary particles, and the regions produced by secondary solidification, offered the composition of the solid and liquid phases at the semisolid temperature (593°C), which are summarised in **Table 4.2.2**.

***Table 4.2.2** Comparison between chemical compositions of the liquid and solid phases at the semisolid temperature (593°C) obtained by EDS analysis and thermodynamic predictions (in wt%).*

Alloying element		Mg	Al	Zn
Liquid Phase	EDS Analysis	89.25±0.22	9.66±0.19	1.09±0.03
	Thermo-Calc	89.82	9.35	0.83
Solid Phase	EDS Analysis	97.17±0.21	2.74±0.20	0.09±0.01
	Thermo-Calc	96.95	2.98	0.07

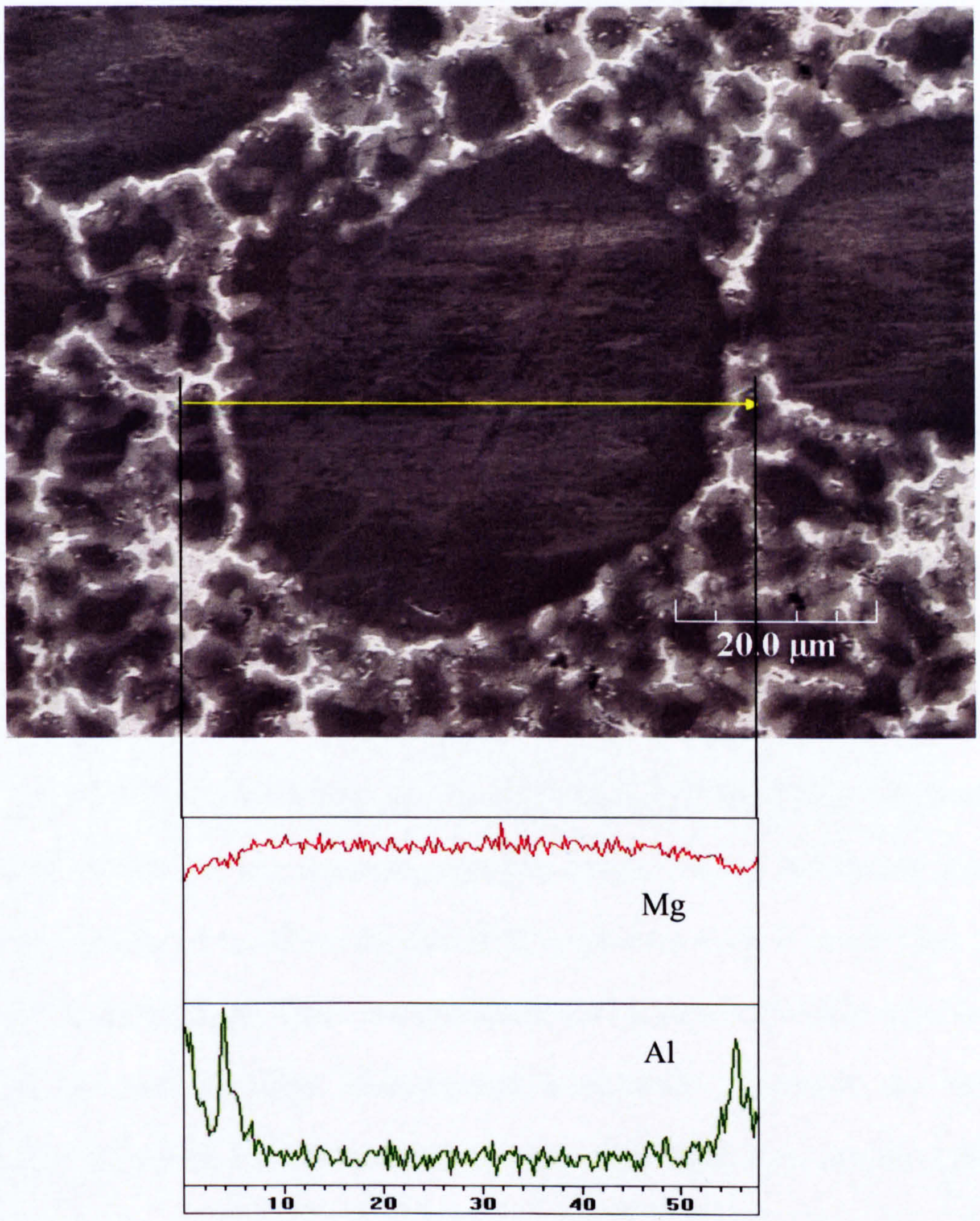

Figure 4.2.13 *EDS line scan results showing the compositional variation across a primary α-Mg particle.*

The comparison between EDS analysis and thermodynamic prediction in Table 4.2.2 indicates that the solidification process inside the twin-screw slurry maker was very close to equilibrium. However, the presence of the eutectic structure in Figure 4.2.11 shows that the secondary solidification was highly non-equilibrium. According to the equilibrium phase diagram in Figure 4.2.1, the equilibrium solidification structure of AZ91D alloy should be a single α-phase. Therefore, it can be concluded that in the RDC process the primary solidification, under intensive forced convection, is fairly close to equilibrium, while the secondary solidification, inside the die without shearing, is highly non-equilibrium.

Oxide inclusions, due to mixing with the dross and the inclusion of oxide skin of the ingots, are always detrimental to the quality of castings produced by any casting process [WAN03]. This detrimental effect is particularly severe for Mg castings. Mg has a high affinity to oxygen and any improper protection during melting and casting can cause excessive oxidation. In addition, the density of magnesium oxide is nearly twice as high as that of liquid Mg alloy. There is a continuous sedimentation of oxides from the dross layer to the melt. Detailed microstructure examination confirmed that with the appropriate protection, the RDC process does not increase the oxide content in the RDC samples. In order to examine the behaviour of oxide in the RDC samples, dross from the melting furnace was deliberately added to the Mg melt. **Figure 4.2.14(a)** is a backscattered SEM micrograph showing the morphology of oxide particles in the RDC sample with the added dross. The oxide particles, as identified by EDS analysis in **Figure 4.2.14(b)**, are fine in size (less than 3μm), spherical in morphology and uniform in distribution. No clusters of oxide particles and no evidence of any oxide skin were found in the RDC samples even with the extra dross. This is attributed to the high dispersive

mixing power of the twin-screw slurry maker. Agglomerates of oxide particles and oxide skin film, if any, would be pulverised, spheroidised and dispersed by the intensive forced convection in the slurry maker.

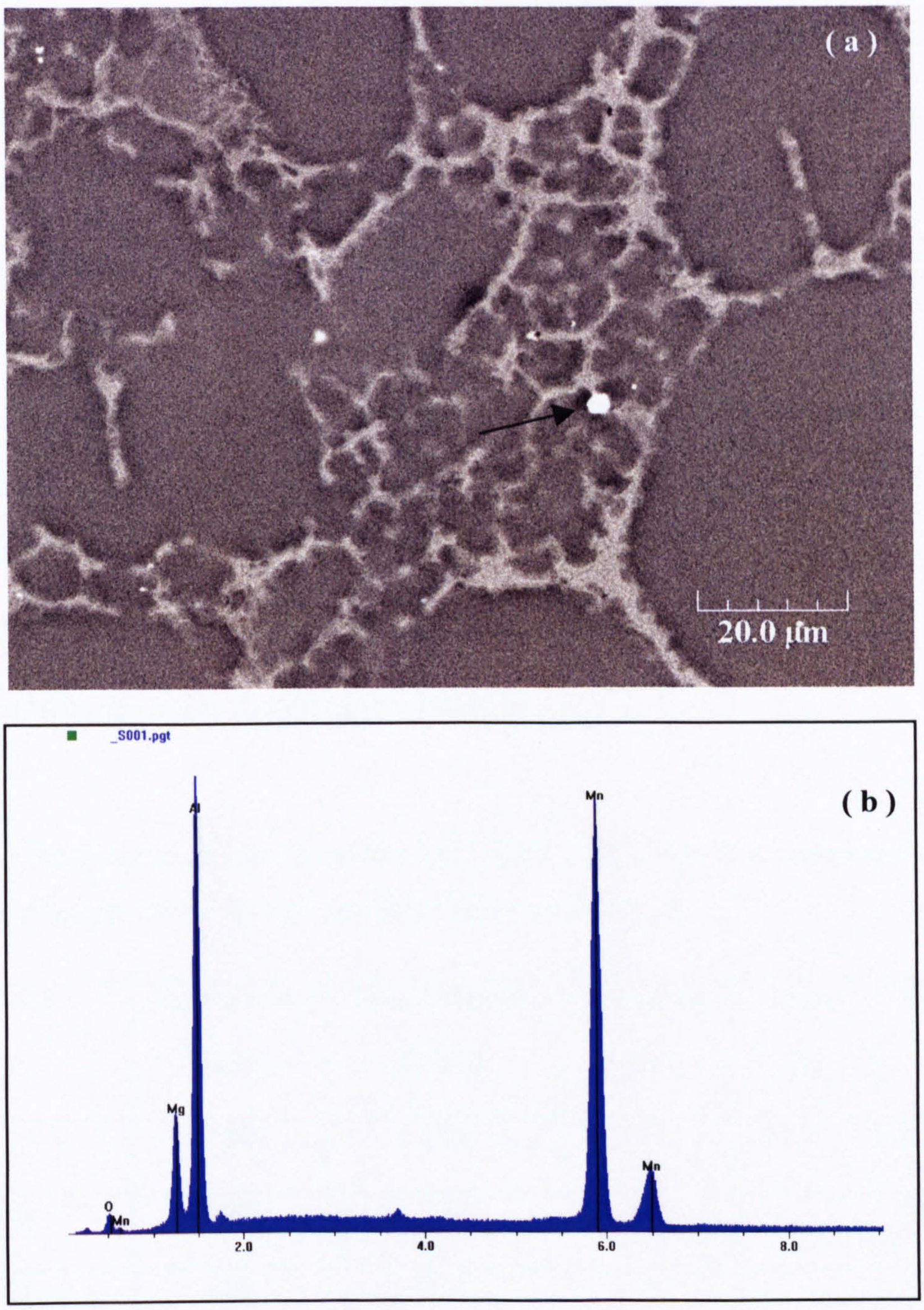

Figure 4.2.14 *(a) SEM back-scattered electron image and (b) correspondent EDS spectrum, showing the morphology of the dispersed oxide particles (arrowed) in the as-cast RDC sample with extra dross.*

4.2.3 Mechanical properties of RDC AZ91D Mg-alloy

The mechanical properties of RDC AZ91D Mg-alloy in the as-cast condition are presented in **Table 4.2.3**, and compared to those of the same alloy produced by other processes in the literature [AVE99][AGU04][MID04][KAU00]. The RDC samples show improved ultimate tensile strength (UTS) and a moderate increase of yield strength in comparison to those obtained from both HPDC process and any other semisolid processing techniques. More importantly, the RDC process offers a substantial increase in tensile elongation (7.2 %). This is a significant progress. Mg-alloys, particularly AZ91D Mg-alloy, usually suffer from low ductility in the as-cast condition. The substantially improved ductility provided by the RDC process can promote wider applications of Mg-alloys. In this work, the significant improvement in mechanical properties of RDC AZ91D Mg-alloy is contributed to the fine and uniform microstructures and much reduced casting defects.

***Table 4.2.3** Mechanical properties of the RDC AZ91D Mg-alloy in comparison with those of the same alloy produced by different processing technologies.*

Processes	Yield strength (MPa)	Tensile Strength (MPa)	Elongation (%)	Impact (J)	Reference
HPDC	150	230	3	3	[AVE99]
Thixocasting	140	240	3.6		[AGU04]
Thixomoulding	160	230	6		[MID04]
New Rheocasting	--	230	5.5		[KAU00]
Rheo-Diecasting (RDC)	146±2	246±4	7.2±0.4	4.6±0.7	This work

Porosity is a well-known problem in any casting process, especially for the Mg-Al system in this study, as it is deemed to be prone to micro shrinkage and orientated porosity [POL95]. Semisolid processing is capable of eliminating it, for instance, Thixomoulding process assures a 50% reduction of porosity [CZE01]. In this work, the RDC samples produced during process optimisation were selected to investigate the relationships between mechanical properties and defect levels; the results are plotted in **Figure 4.2.16**. From Figure 4.2.16, it is evident that the mechanical properties appear to be dependent on the porosity level, increased number of defects, results in lower UTS and elongation. After a primary optimisation, the defects were significantly reduced to a level of 0.3% - 0.5% in RDC AZ91D Mg-alloy samples.

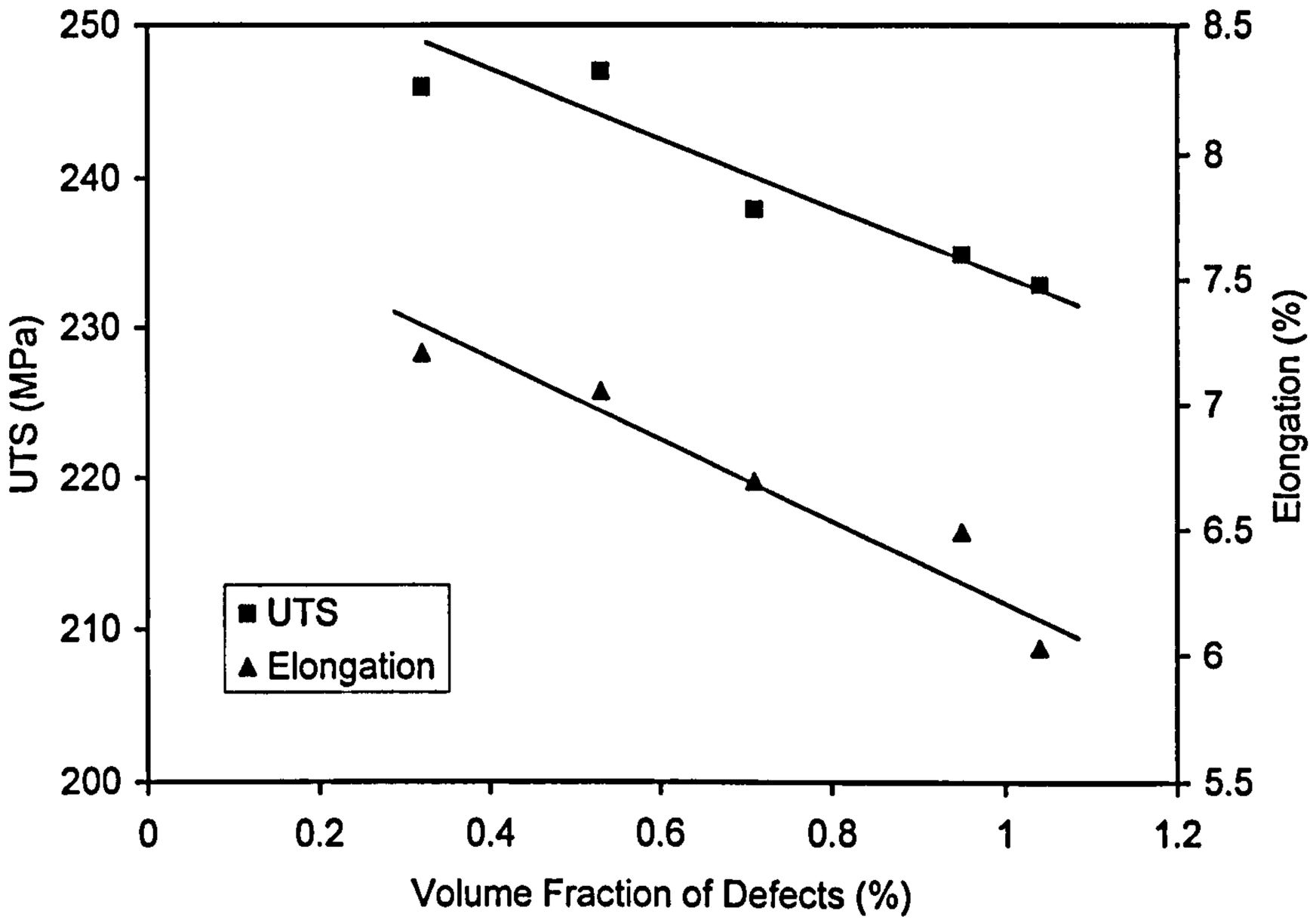

Figure 4.2.15 *The tensile properties versus volume percentage of defects in RDC AZ91D Mg-alloy samples.*

4.3 Effects of the Twin-Screw shearing parameters on the microstructure of RDC AZ91D Mg-alloy

4.3.1 Effects of shearing time

To investigate the effects of shearing time on the microstructure of RDC AZ91D alloy, the shearing time was varied between 3 seconds to 200 seconds with a constant shearing temperature of 593°C. **Figure 4.3.1** and **Figure 4.3.2** present the microstructures produced at different shearing times under the shearing speed of 300rpm and 800rpm, respectively. **Table 4.3.1** summarises the average values, for microstructural characteristics of different shearing times, obtained by quantitative analysis.

***Table 4.3.1** Summary of the quantitative metallography results for RDC AZ91D samples produced at different shearing times under the shearing speed of 300 and 800 rpm.*

Items \ Shearing Time(s)		3	10	13	16	20	35	70	150	200
300 rpm	Vol. Fraction of α_1 (%)	7.90	13.75	15.33	20.27	20.70	20.45	21.25	22.79	
	Vol. Fraction of α_2 (%)	17.43	13.62	14.09	8.78	7.78	7.56	8.00	7.73	
	Vol. Fraction of $\alpha_1+\alpha_2$ (%)	25.33	27.38	29.42	29.05	28.47	28.01	29.25	30.52	
	Density of α_1 (mm^{-2})	87	107	111.6	129.7	127.2	109.3	103	85.5	
	Particle Size of α_1 (μm)	33.68	39.23	40.22	41.87	42.21	47.30	48.89	54.30	
	Shape Factor of α_1	0.79	0.79	0.795	0.806	0.827	0.817	0.83	0.838	
800 rpm	Vol. Fraction of α_1 (%)	8.43	12.93	17.19	17.72	17.39	17.57	17.23	18.85	18.01
	Vol. Fraction of α_2 (%)	18.96	16.50	11.88	11.80	15.20	15.03	16.31	10.25	15.23
	Vol. Fraction of $\alpha_1+\alpha_2$ (%)	27.39	29.43	29.06	29.52	32.59	32.60	33.55	29.10	33.25
	Density of α_1 (mm^{-2})	98	112	125	121.5	117.3	111.8	83.5	83.2	82.0
	Particle Size of α_1 (μm)	37.38	39.60	39.81	41.50	41.60	42.38	47.85	51.26	49.29
	Shape Factor of α_1	0.793	0.785	0.813	0.807	0.803	0.80	0.80	0.836	0.805

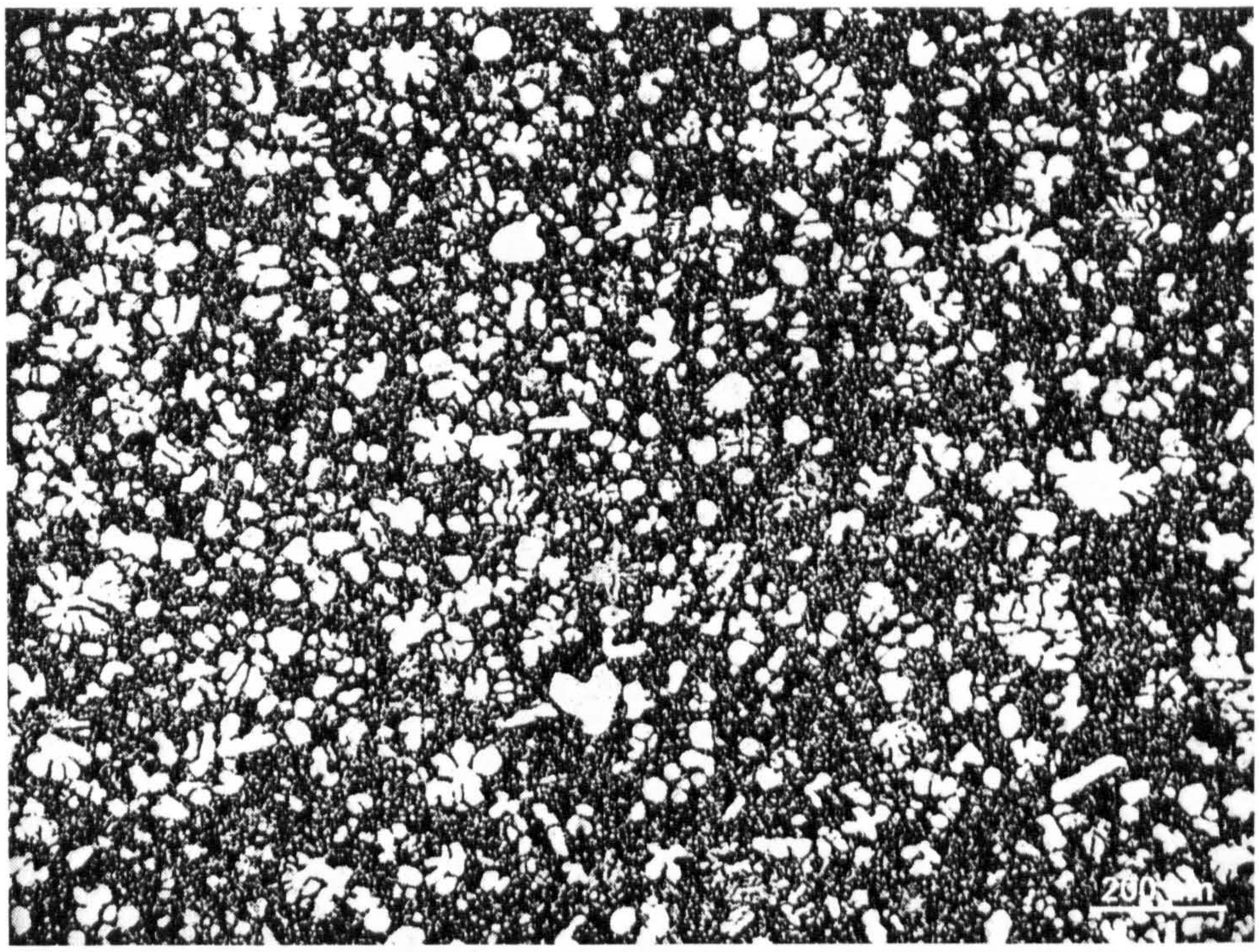

(a)

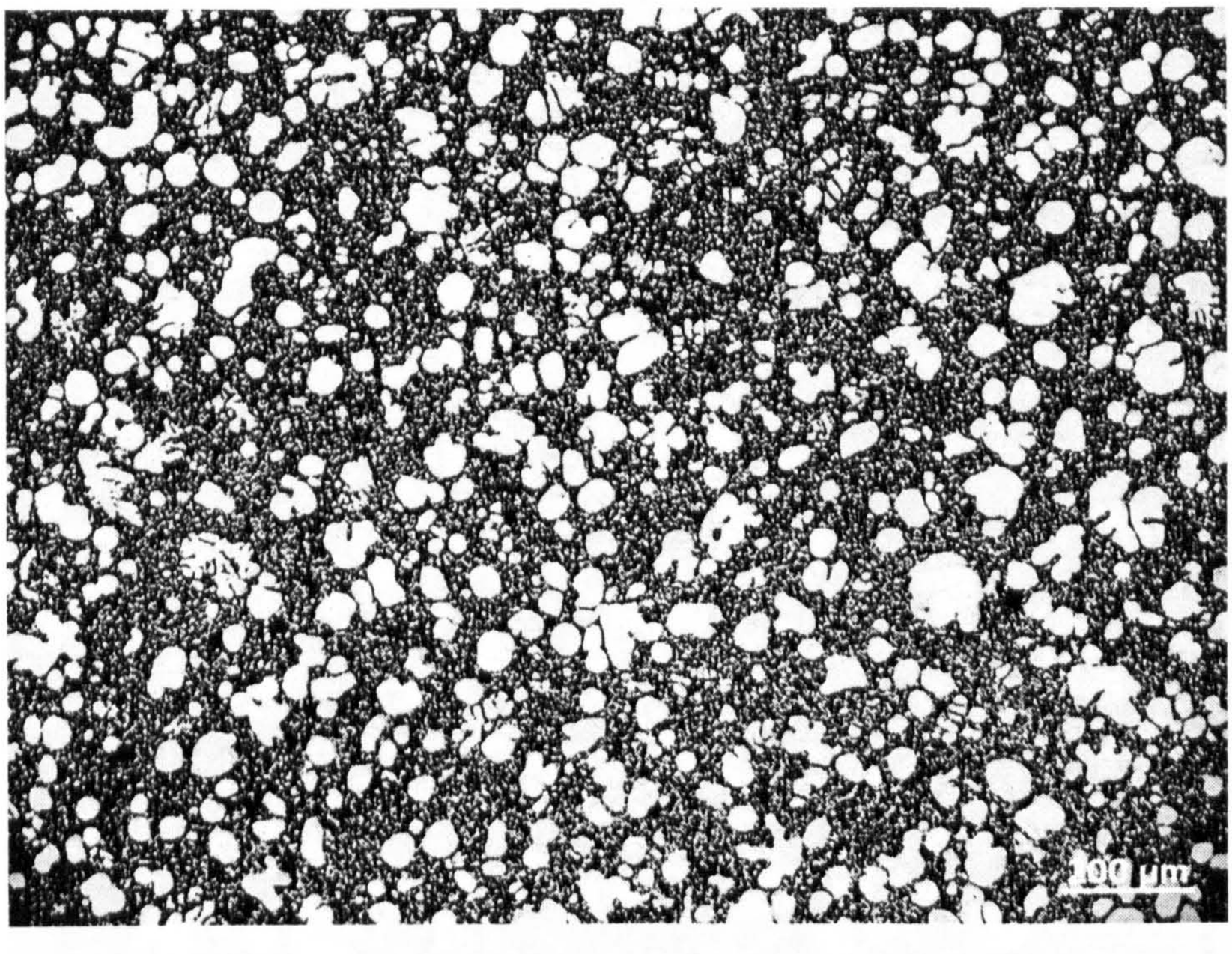

(b)

Figure 4.3.1 *Microstructures produced with the shearing speed of 300rpm at shearing times (a) 3s, (b) 20s, (c) 35s, (d) 150s*

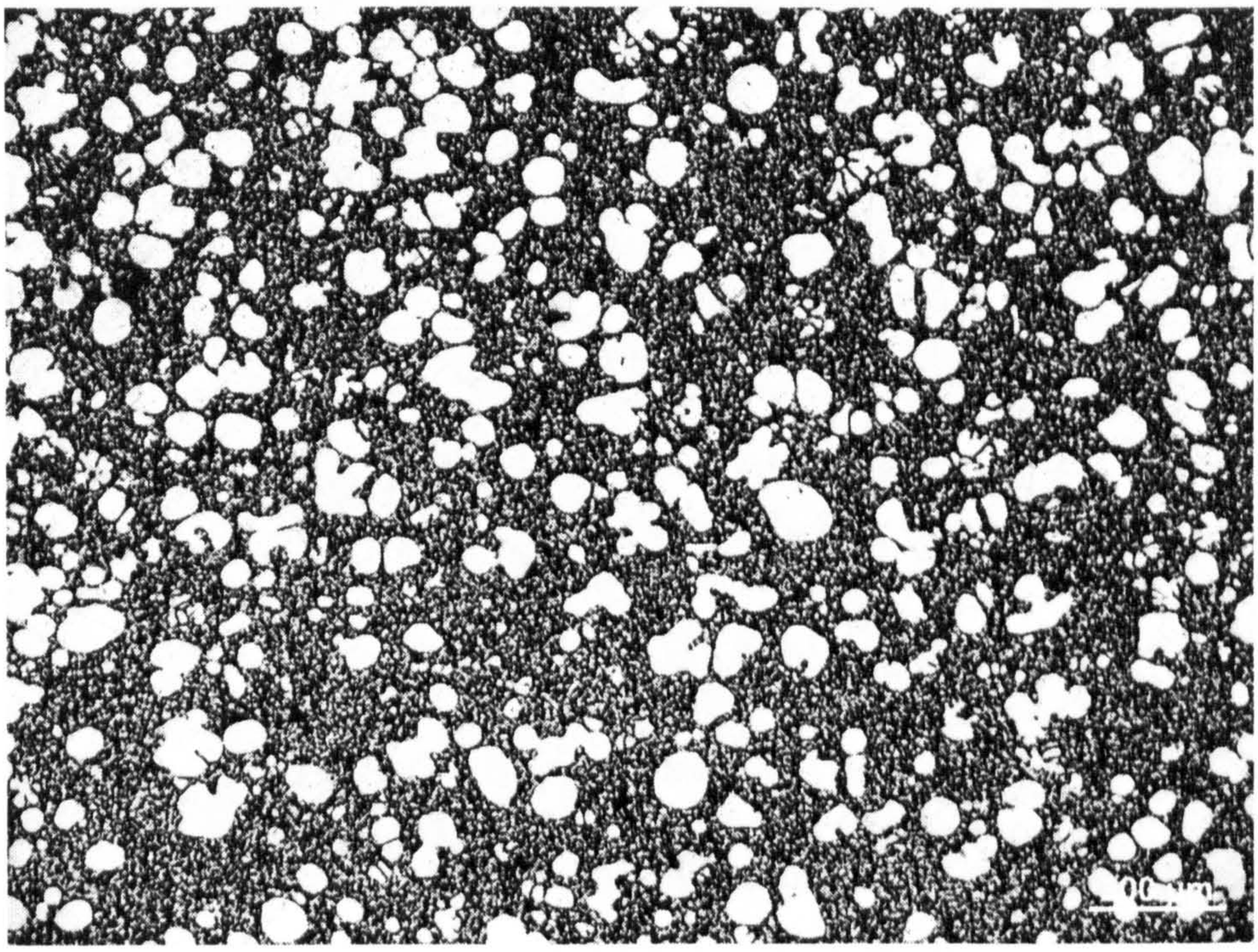

(c)

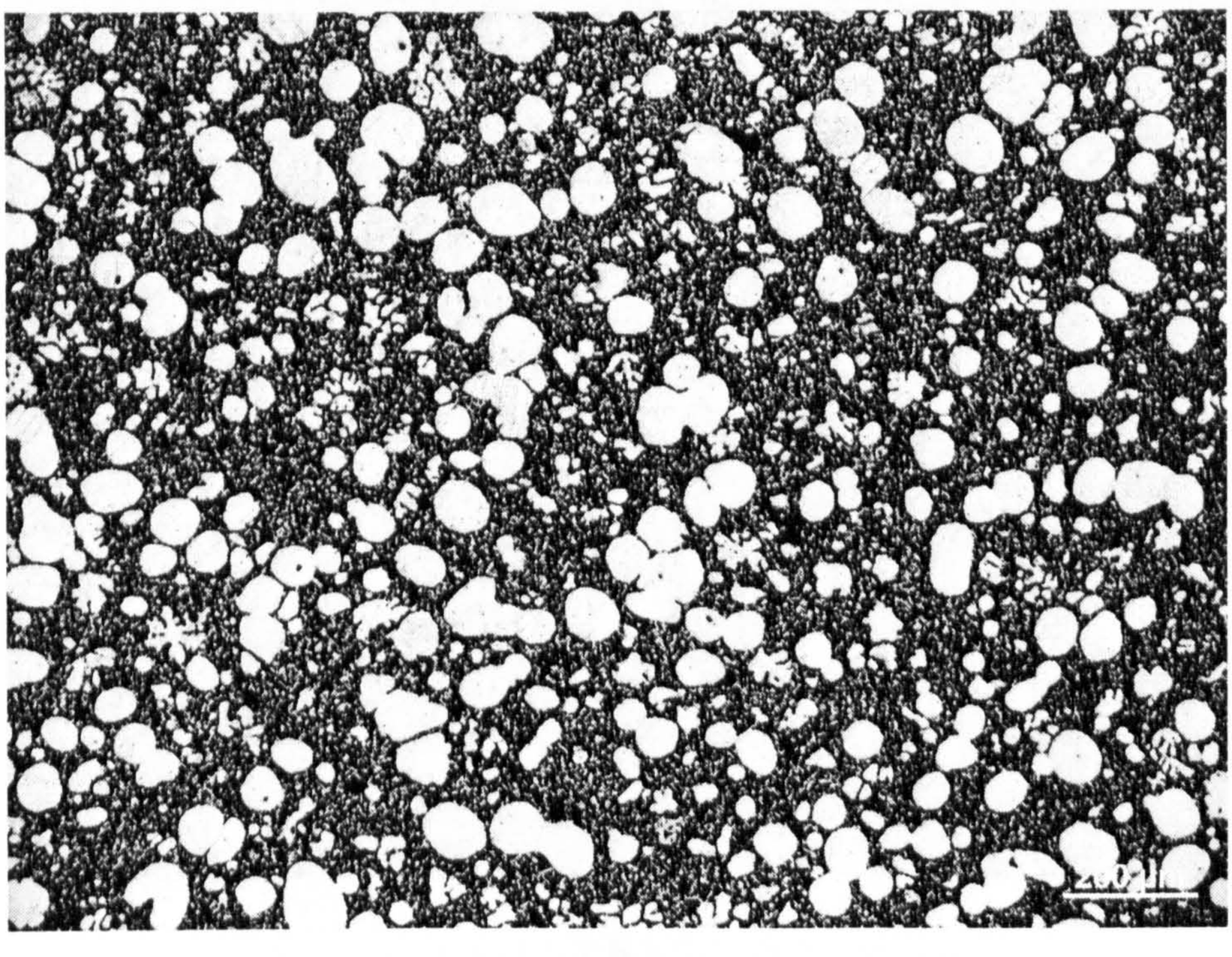

(d)

Figure 4.3.1 *(continued) Microstructures produced with the shearing speed of 300rpm at shearing times (a) 3s, (b) 20s, (c) 35s, (d) 150s*

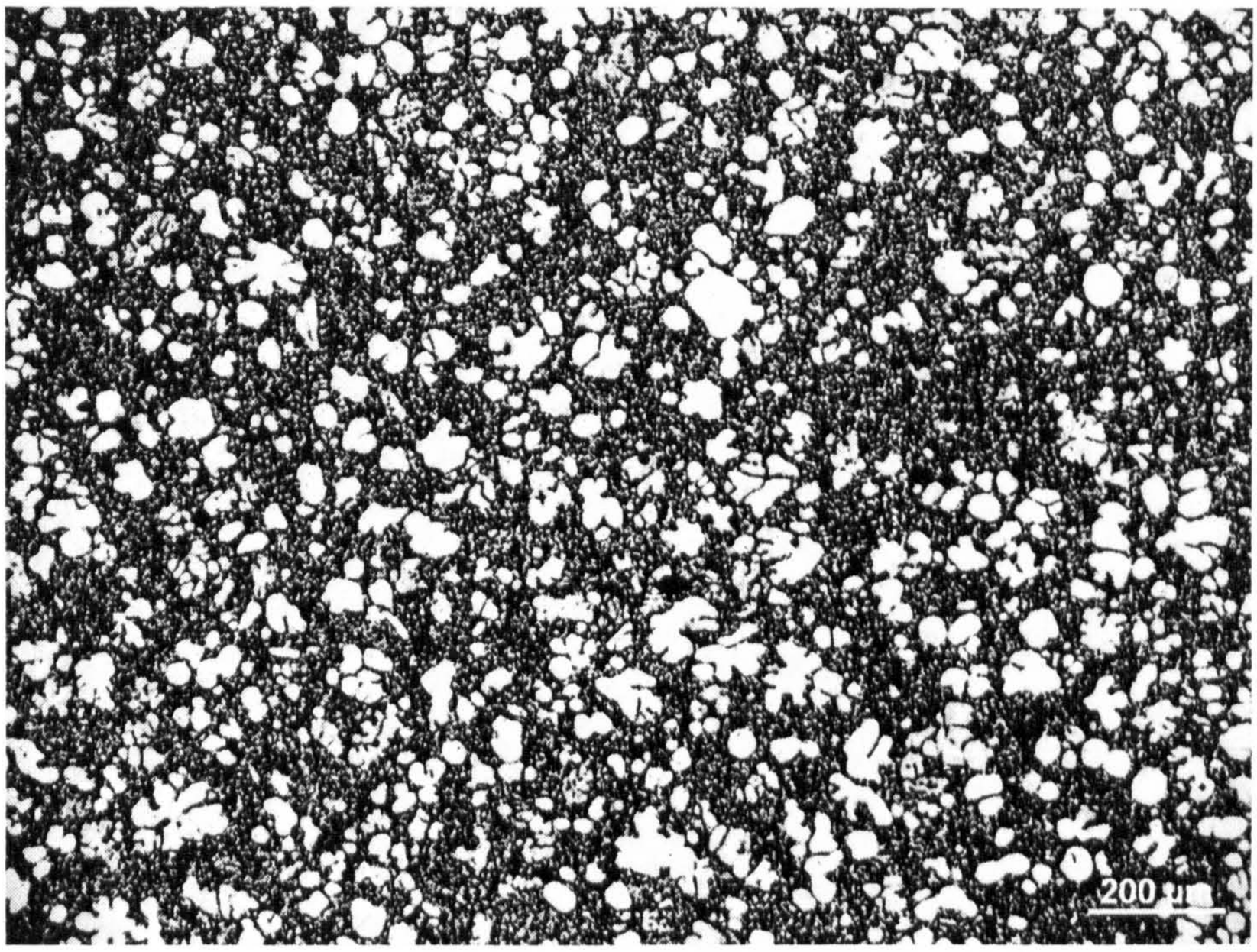

(a)

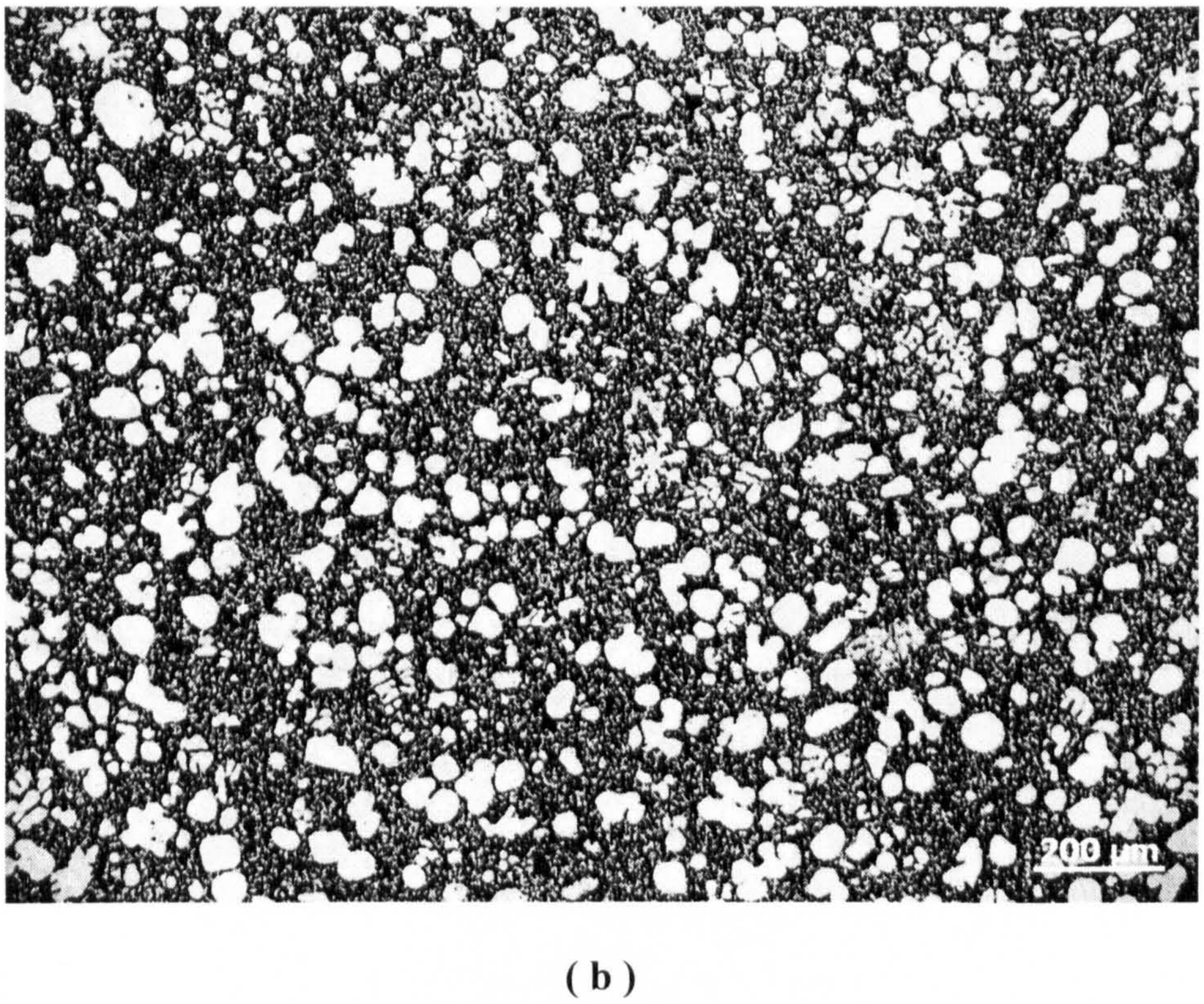

(b)

Figure 4.3.2 *Microstructures produced with a shearing speed of 800rpm at shearing times (a) 3s, (b) 16s, (c) 35s, (d) 200s*

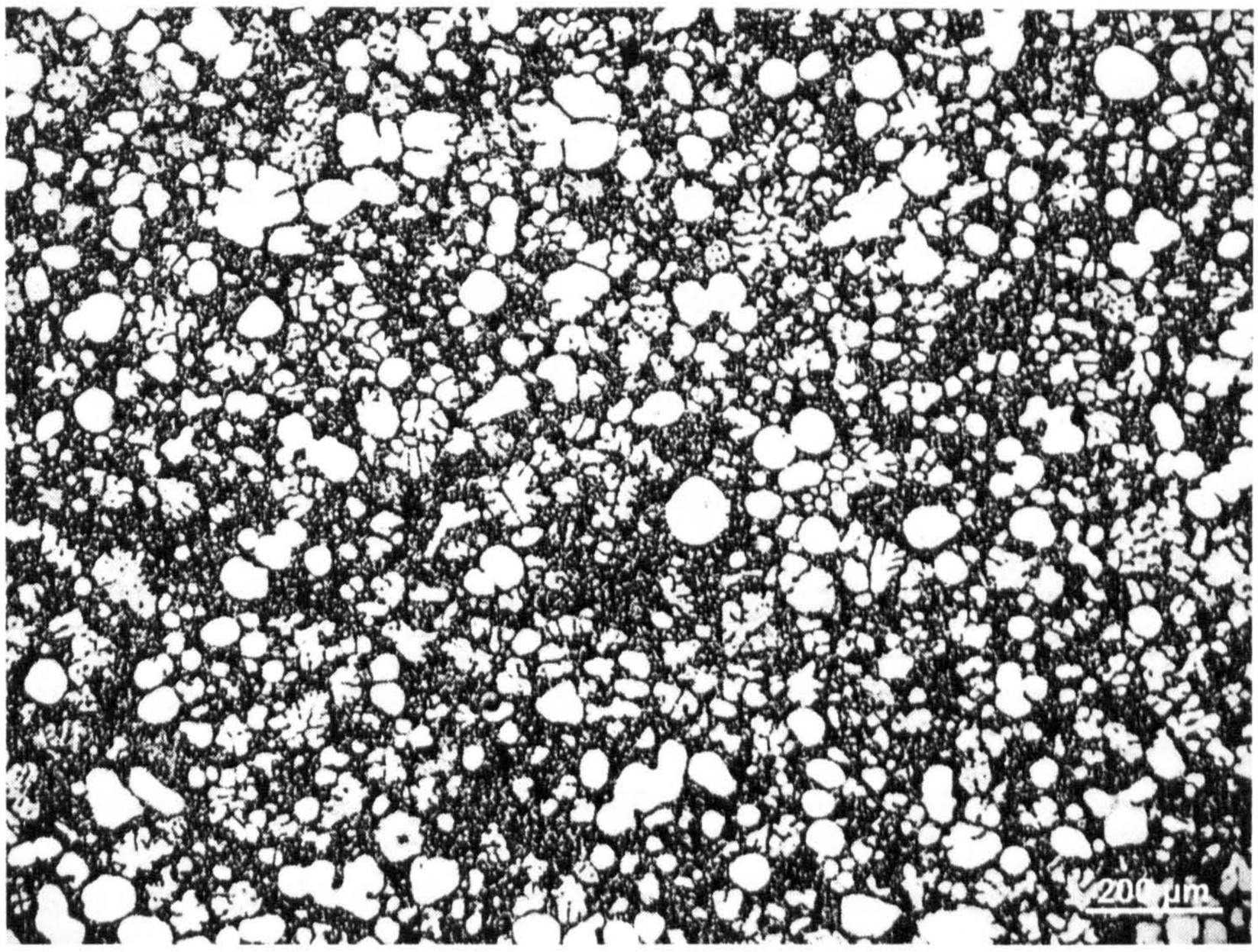

(c)

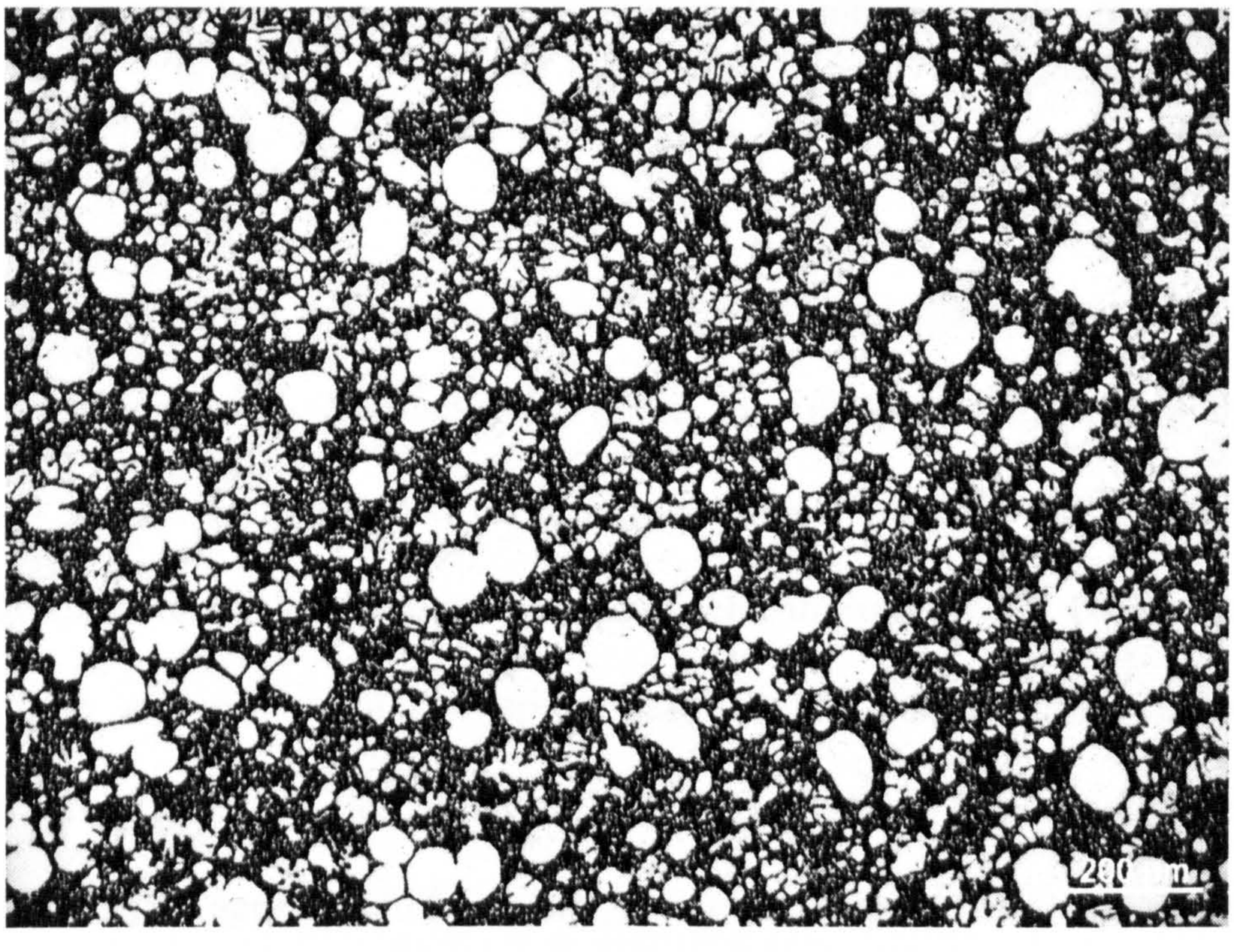

(d)

Figure 4.3.2 *(continued) Microstructures produced with a shearing speed of 800rpm at shearing times (a) 3s, (b) 16s, (c) 35s, (d) 200s*

The measured volume fraction of the primary α-phase is plotted in **Figure 4.3.3,** as a function of shearing time and screw rotation speed. Figure 4.3.3 indicates that solidification inside the twin-screw slurry maker occurred in two stages. The first stage is a continuous cooling process, where the initially superheated melt was cooled continuously to the semisolid processing temperature, producing the desired volume fraction of the solid particles. This stage lasted about 15 seconds, and solid volume fraction increased with the increase of shearing time. Once the melt reached the semisolid temperature, it experienced an isothermal shearing process, where solid volume fraction was fairly constant. At the continuous cooling stage, screw rotation speed had little effect on the solid volume fraction, but it did affect the final solid fraction before the isothermal shearing started. Higher screw rotation speed led to a smaller solid fraction, suggesting that intensive shearing partially suppresses the formation of the primary phase.

Figure 4.3.4 and **Figure 4.3.5** present the particle size and shape factor of the primary phase as a function of shearing time, under two different screw rotation speeds, respectively. At the early stages of shearing, less than 3 seconds, the primary particles were fairly spherical, as indicated by the shape factor in Figure 4.3.5. Further increase in shearing time and screw rotation speed only slightly improved the shape factor. However, the primary particle size increases with the increase in shearing time, and the particle growth rate appeared to be higher at a lower screw rotation speed (see Figure 4.3.4). The solid lines in Figure 4.3.4 represent the power law fit to the experimental data.

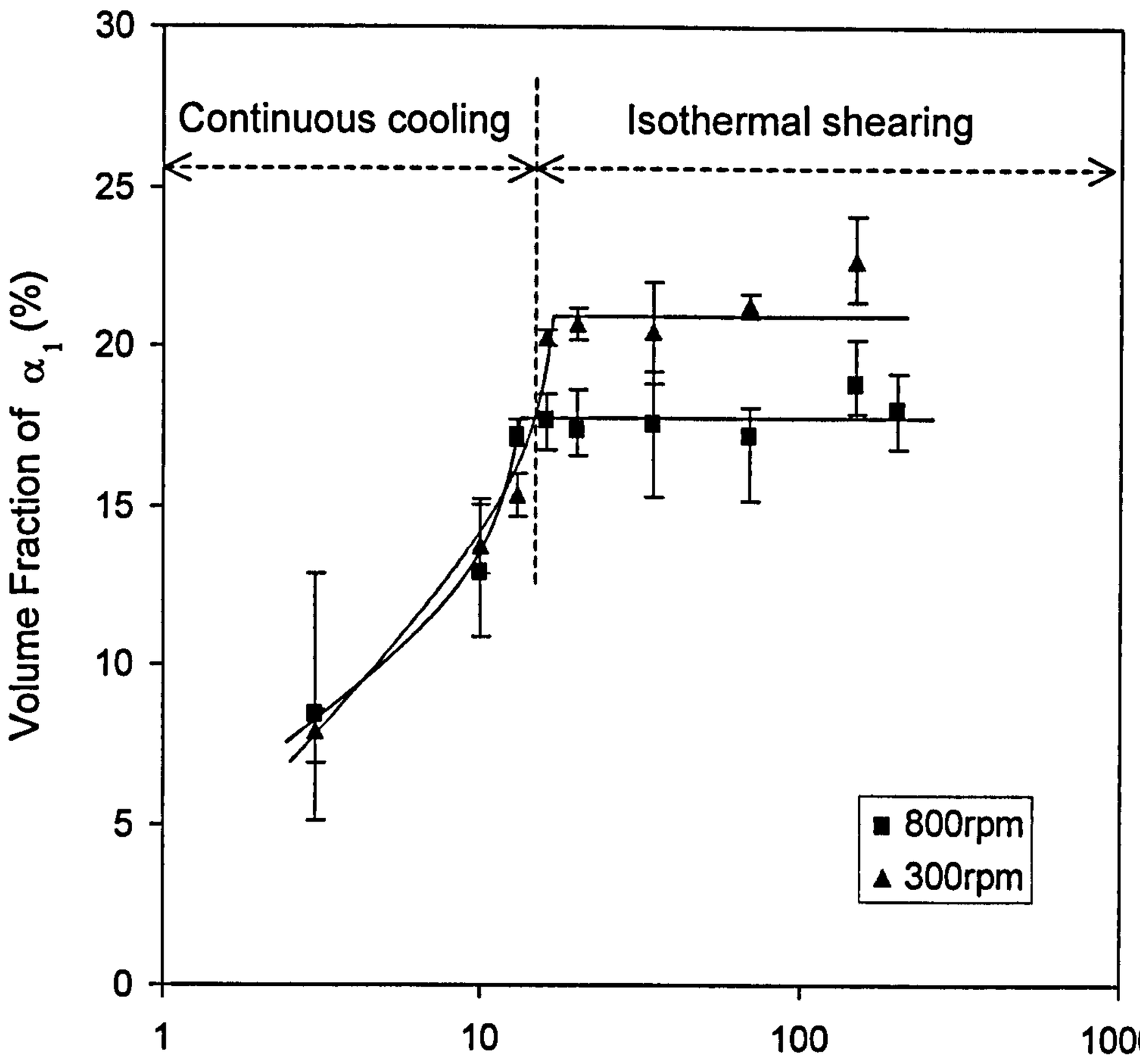

Figure 4.3.3 *Volume fraction of the primary particles (α_1) formed in the twin-screw slurry maker as a function of shearing time and screw rotation speed. The shearing temperature was 593°C. The solid lines represent the best fit to the experimental data. Also marked in the figure is the boundary between continuous cooling and isothermal shearing during the primary solidification.*

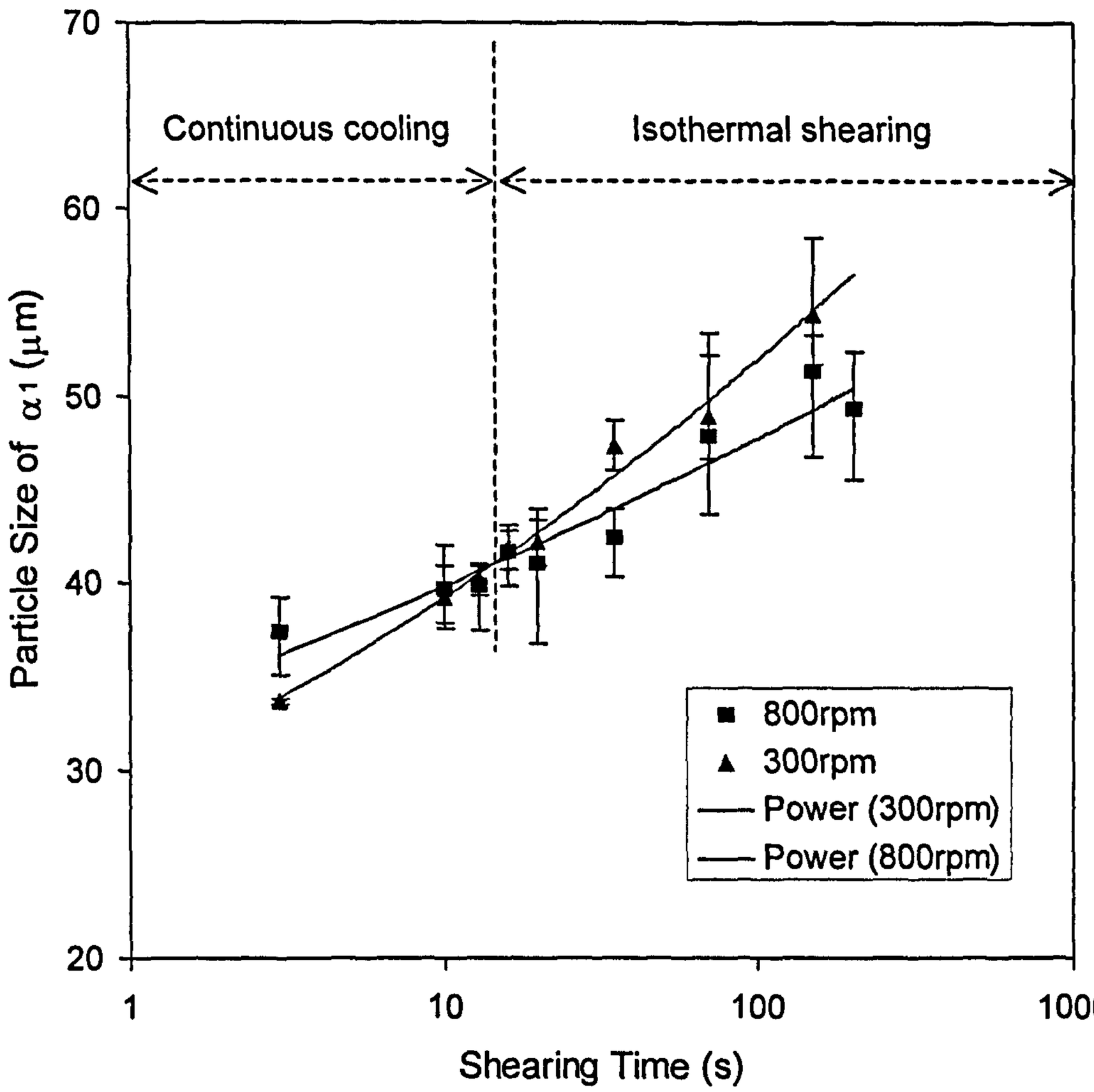

Figure 4.3.4 *Size of the primary particles (α_1) formed in the twin-screw slurry maker as a function of shearing time and screw rotation speed. The shearing temperature was 593°C. The solid lines represent the best fit to the experimental data.*

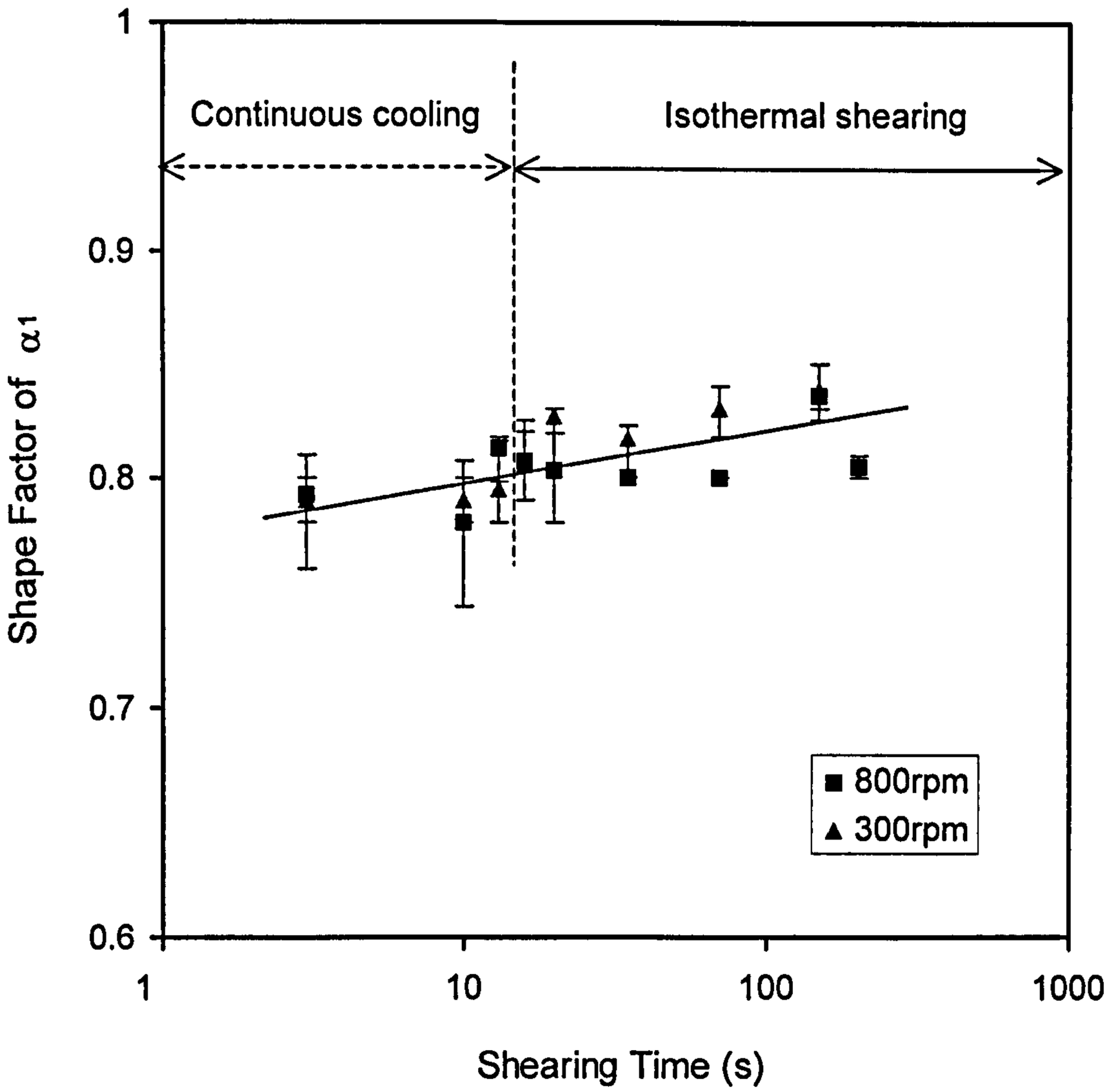

Figure 4.3.5 *Shape factor of the primary particles (α_1) formed in the twin-screw slurry maker as a function of shearing time and screw rotation speed. The shearing temperature was 593°C. The solid lines represent the best fit to the experimental data.*

The measured density of the primary particles formed in the twin-screw slurry maker is plotted in **Figure 4.3.6**, as a function of shearing time and screw rotation speed. At the continuous cooling stage, particle density increased with the increase of shearing time, while at the isothermal shearing stage it decreased with further increase in shearing time. There is a maximum in the density-time curve, which coincides with the transition between the continuous cooling and isothermal shearing. The increase in particle density implied that there was a continuous nucleation during the continuous cooling stage, while the decrease in particle density suggested that Ostwald ripening took place, through dissolution of smaller particles, during the isothermal shearing stage.

Shearing in the twin-screw slurry maker also had an effect on the formation of the primary phase in the shot sleeve. The measured volume fraction of the dendrite fragments formed during the secondary solidification is given in **Figure 4.3.7**, as a function of shearing time and screw rotation speed. Generally, at the continuous cooling stage, volume fraction of α_2 decreased with the increase of shearing time, while it is almost constant with prolonged shearing time at the isothermal shearing stage. Figure 4.3.7 also revealed that high screw rotation speed promoted the formation of the α_2 particles, suggesting that increasing the intensity of forced convection enhances secondary solidification in the shot sleeve.

Figure 4.3.8 shows the measured total volume fraction of α_1 and α_2 as a function of shearing time and the screw rotation speed. The total volume fraction of α_1 and α_2 increased with the increase in shearing time at the continuous cooling stage, while it became almost constant at the isothermal shearing stage. A comparison between Figure 4.3.7 and Figure 4.3.8 indicated that the formation of the primary phase in the shot sleeve

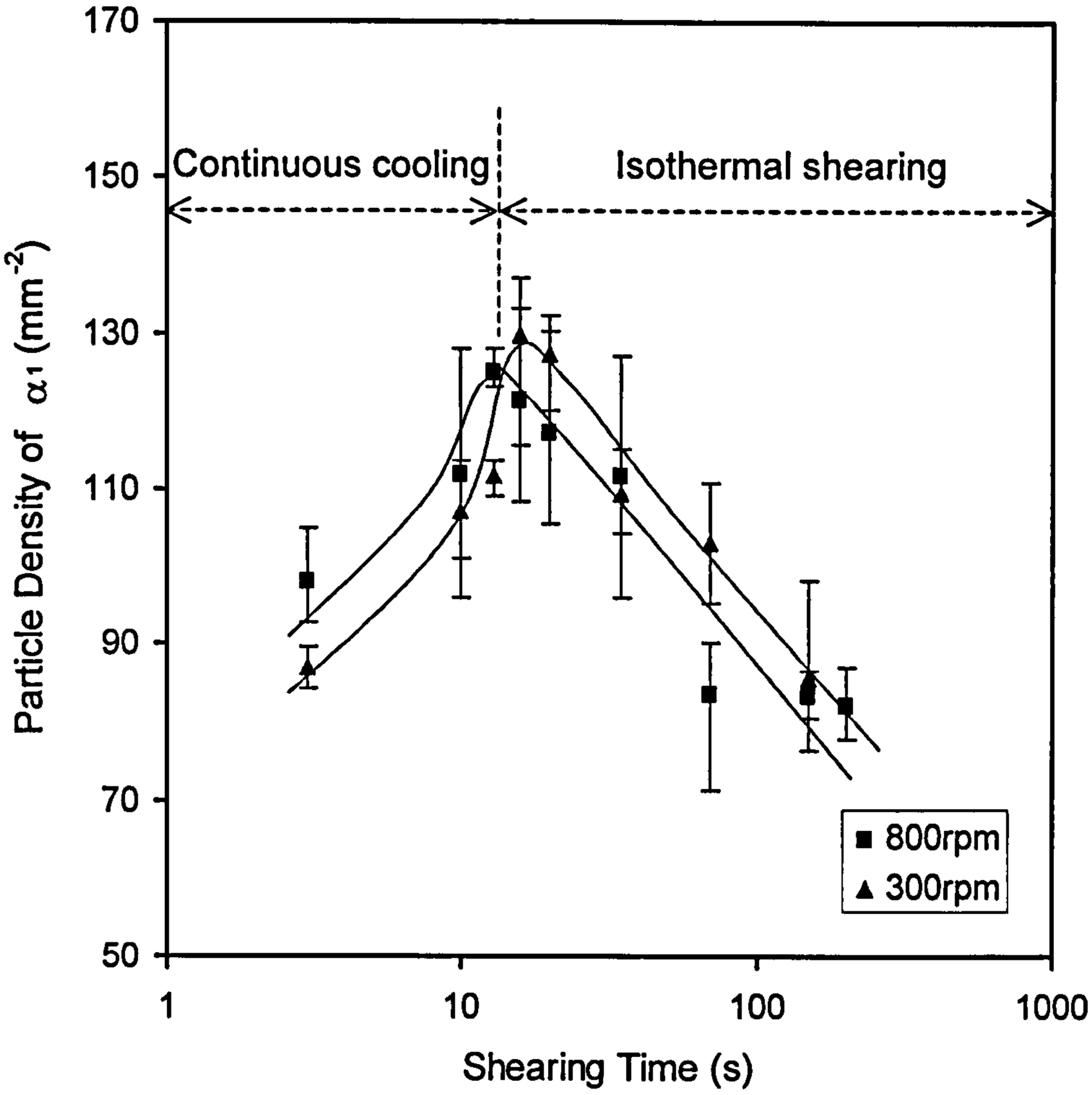

Figure 4.3.6 *Density of the primary particles (α_1) formed in the twin-screw slurry maker as a function of shearing time and screw rotation speed. The shearing temperature was 593°C. The solid lines represent the best fit to the experimental data.*

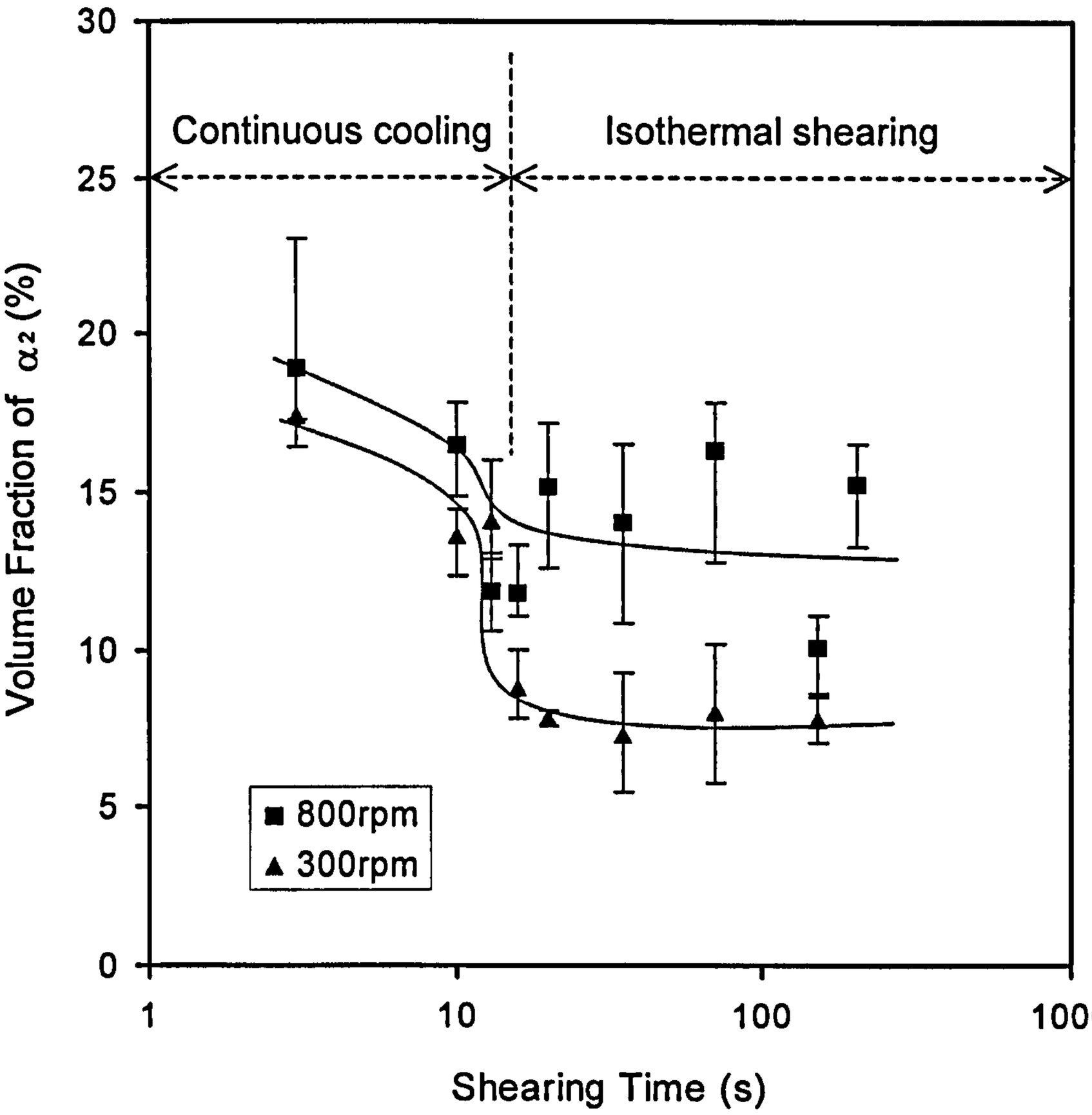

Figure 4.3.7 *Volume fraction of the primary phase (α_2) formed in the shot sleeve as a function of shearing time and screw rotation speed. The shearing temperature was 593°C. The solid lines represent the best fit to the experimental data.*

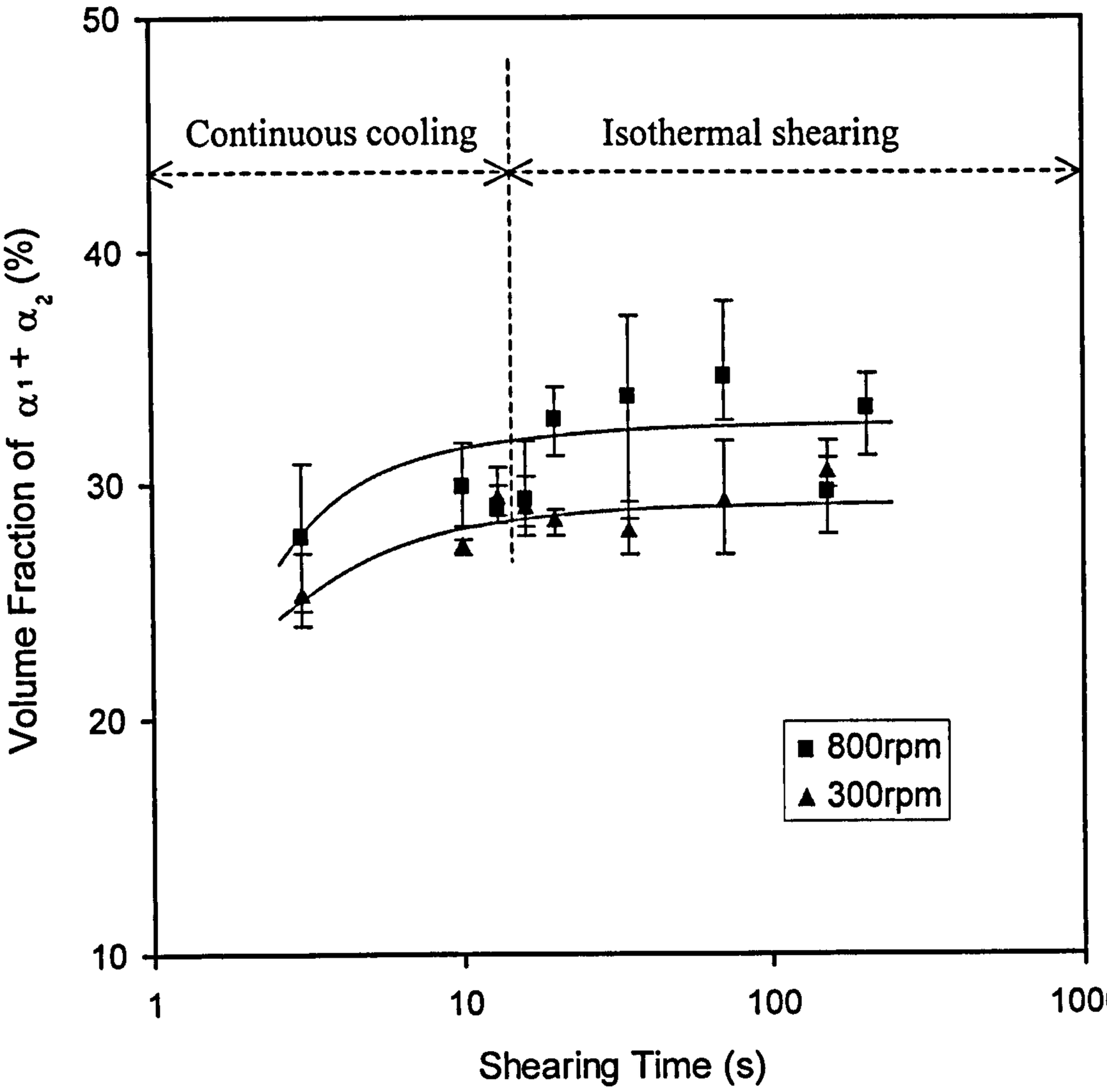

Figure 4.3.8 *Total volume fraction of the primary particles ($\alpha_1 + \alpha_2$) as a function of shearing time and screw rotation speed. The shearing temperature was 593°C. The solid lines represent the best fit to the experimental data.*

is a temperature-controlled process. At a given shearing temperature, if the shearing in the twin-screw slurry maker produced less solid phase (smaller volume fraction of α_1), the volume fraction of α_2 would increase to keep the total solid fraction fairly constant. Therefore, it can be concluded that both increase in the shearing intensity and prolonged shearing time, promote the formation of the primary phase in the shot sleeve.

Higher magnification investigations (**Figure 4.3.9**) indicate that the shearing time and shearing speed produce no distinct changes to the detailed microstructure of α_3.

		Shearing Speed (rpm)	
		300	*800*
Shearing Time (S)	*3*	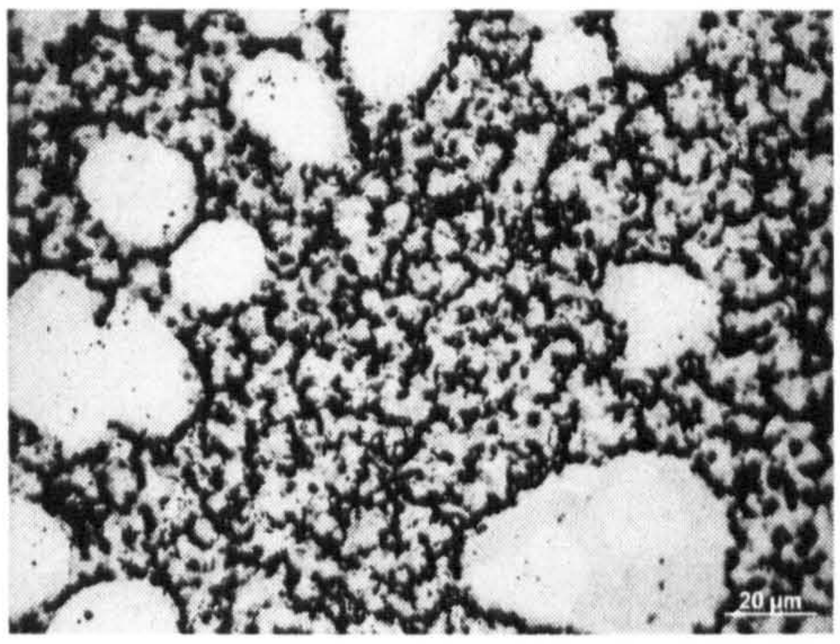	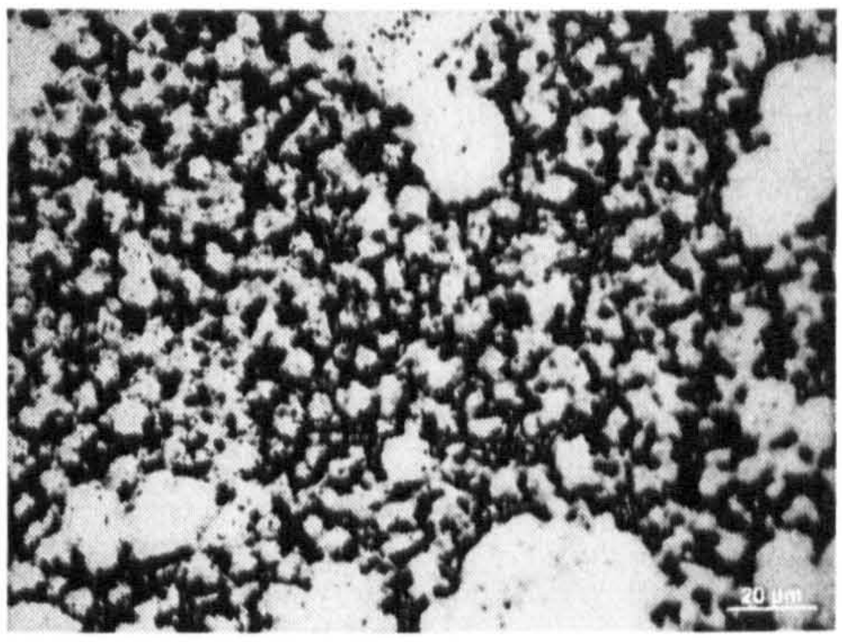
	35	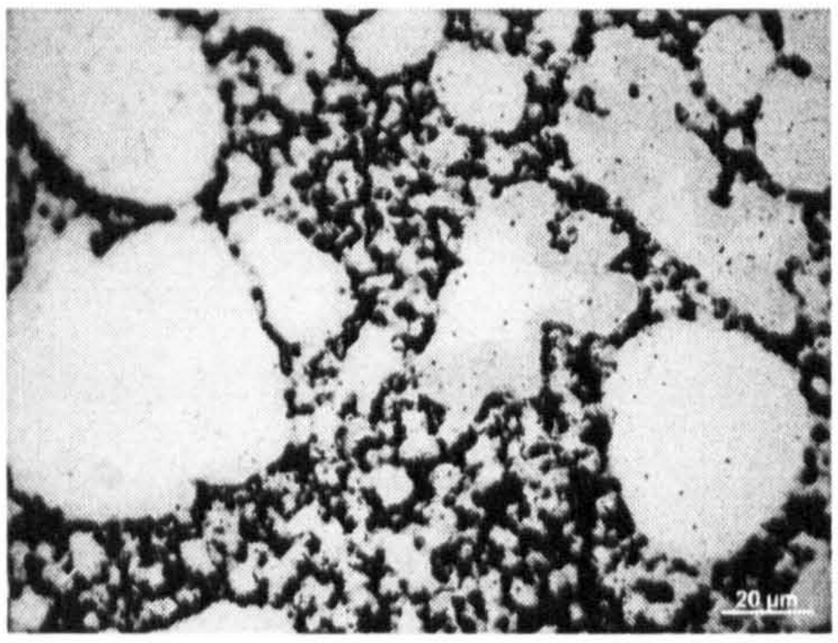	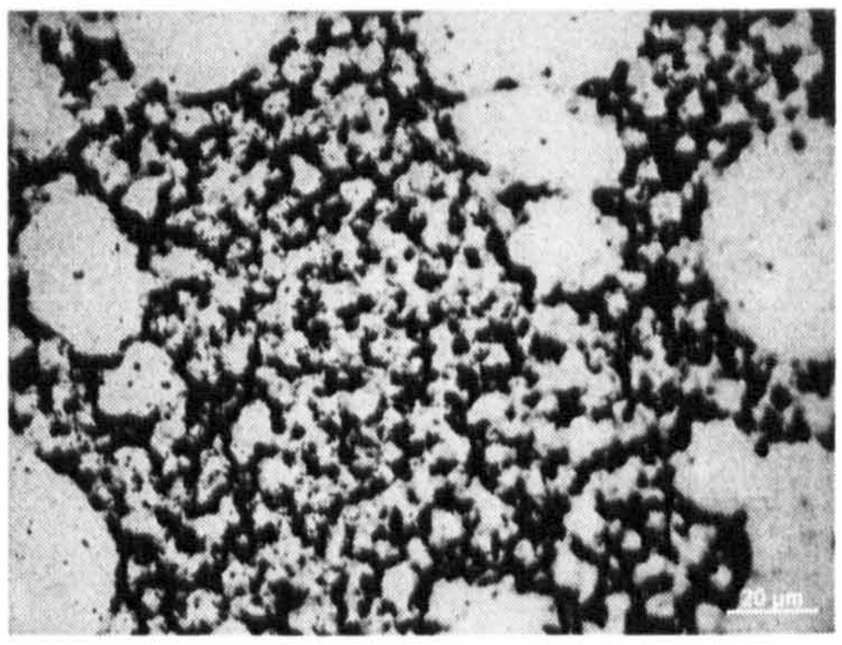
	150	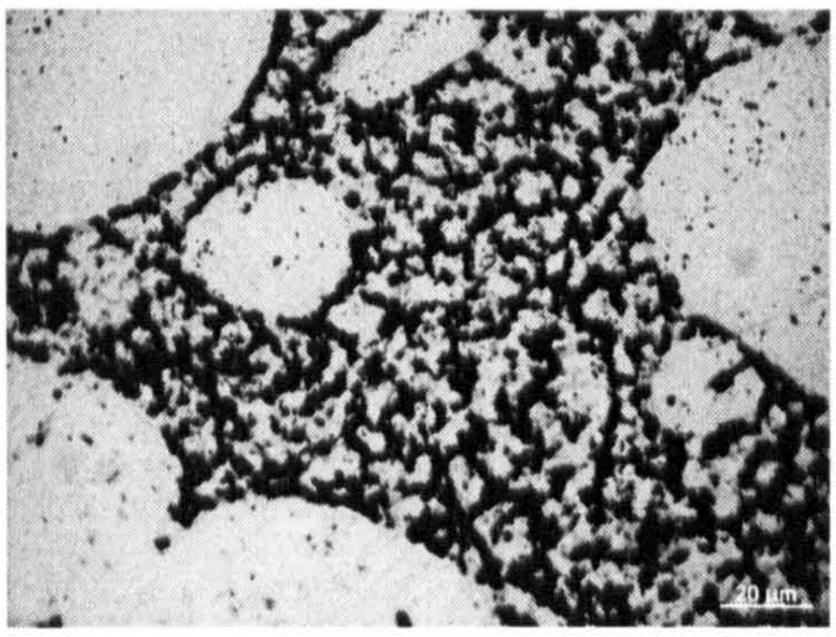	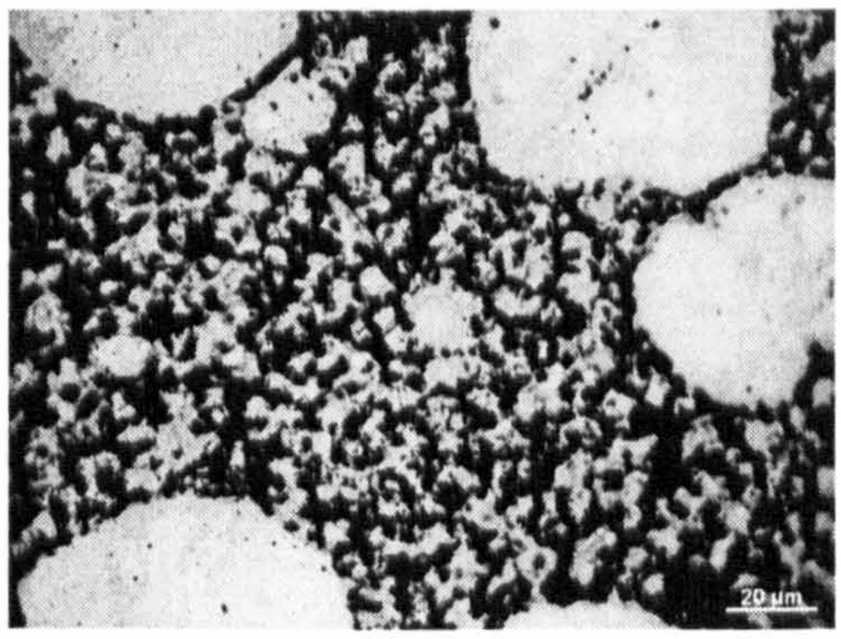

Figure 4.3.9 *The detailed optical microstructure of α_3 shows no distinct changes caused by effects of the shearing time and shearing speed.*

4.3.2 Effects of shearing intensity

Experiments were conducted at a shearing temperature of 593°C and a shearing time of 35 seconds to investigate the shearing speed effects. The shearing intensity was varied between 100rpm to 900rpm. **Figure 4.3.10** shows the effect of shearing intensity on the microstructure of RDC AZ91D alloy. **Table 4.3.2** summarises the average values, for microstructural characteristics of different shearing intensity, obtained by quantitative analysis.

***Table 4.3.2** Summary of the quantitative metallography results for RDC AZ91D samples produced at different shearing speed.*

Shr.Rate (rpm) / Items	100	300	500	800	900
Vol. Fraction of α_1 (%)	18.92	20.45	17.30	17.57	13.70
Vol. Fraction of α_2 (%)	11.58	7.56	15.30	15.03	15.70
Vol. Fraction of $\alpha_1+\alpha_2$ (%)	30.49	28.01	32.63	32.60	29.40
Density of α_1 (mm^{-2})	95	109.3	97.5	111.8	77.0
Density of α_2 (mm^{-2})	206.6	165.7	362.5	320.2	450.7
Density of $\alpha_1+\alpha_2$ (mm^{-2})	301.6	275.1	460	432	527.6
Particle Size of α_1 (μm)	47.31	47.3	43.89	42.38	43.9
Shape Factor of α_1	0.798	0.817	0.821	0.80	0.827

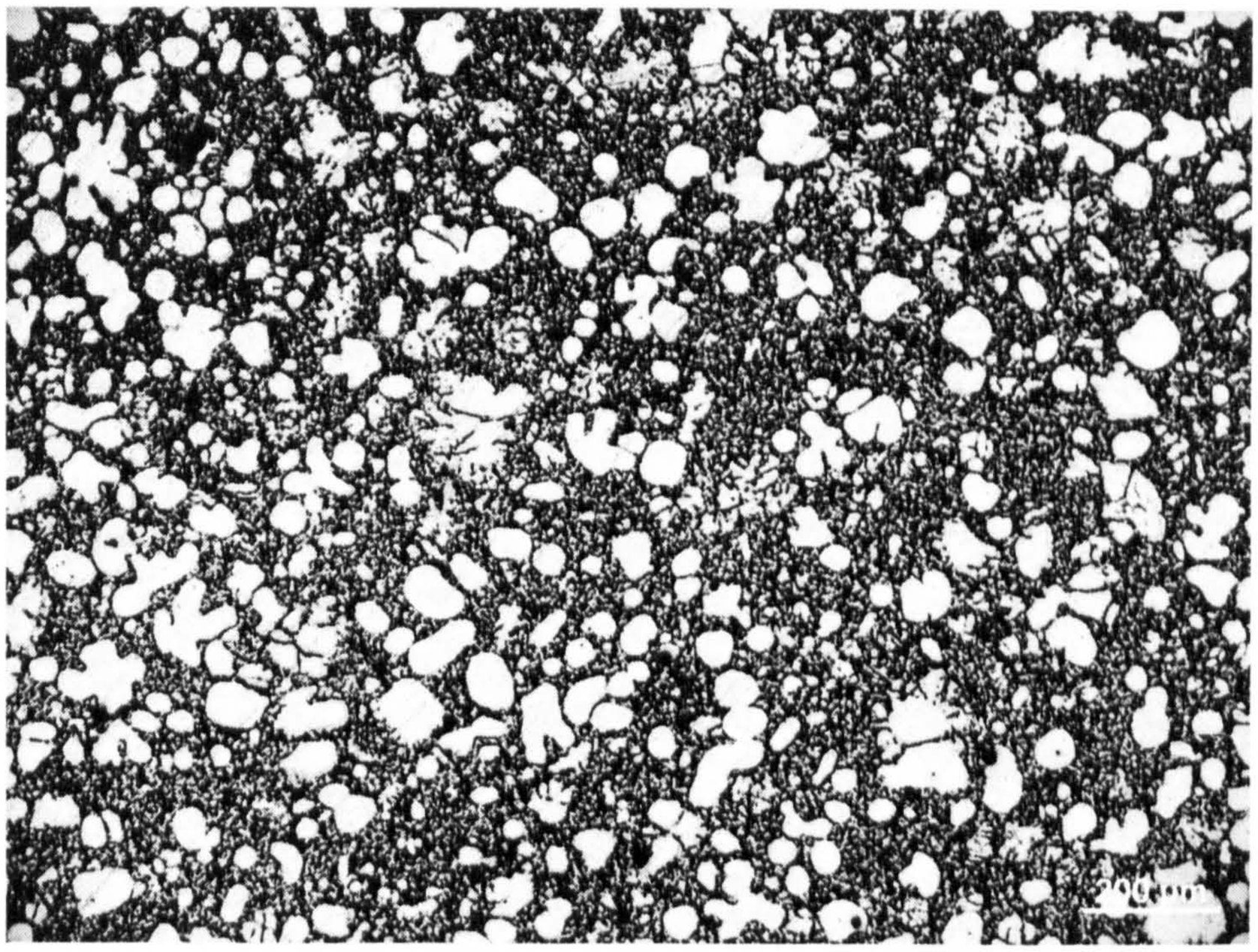

(a)

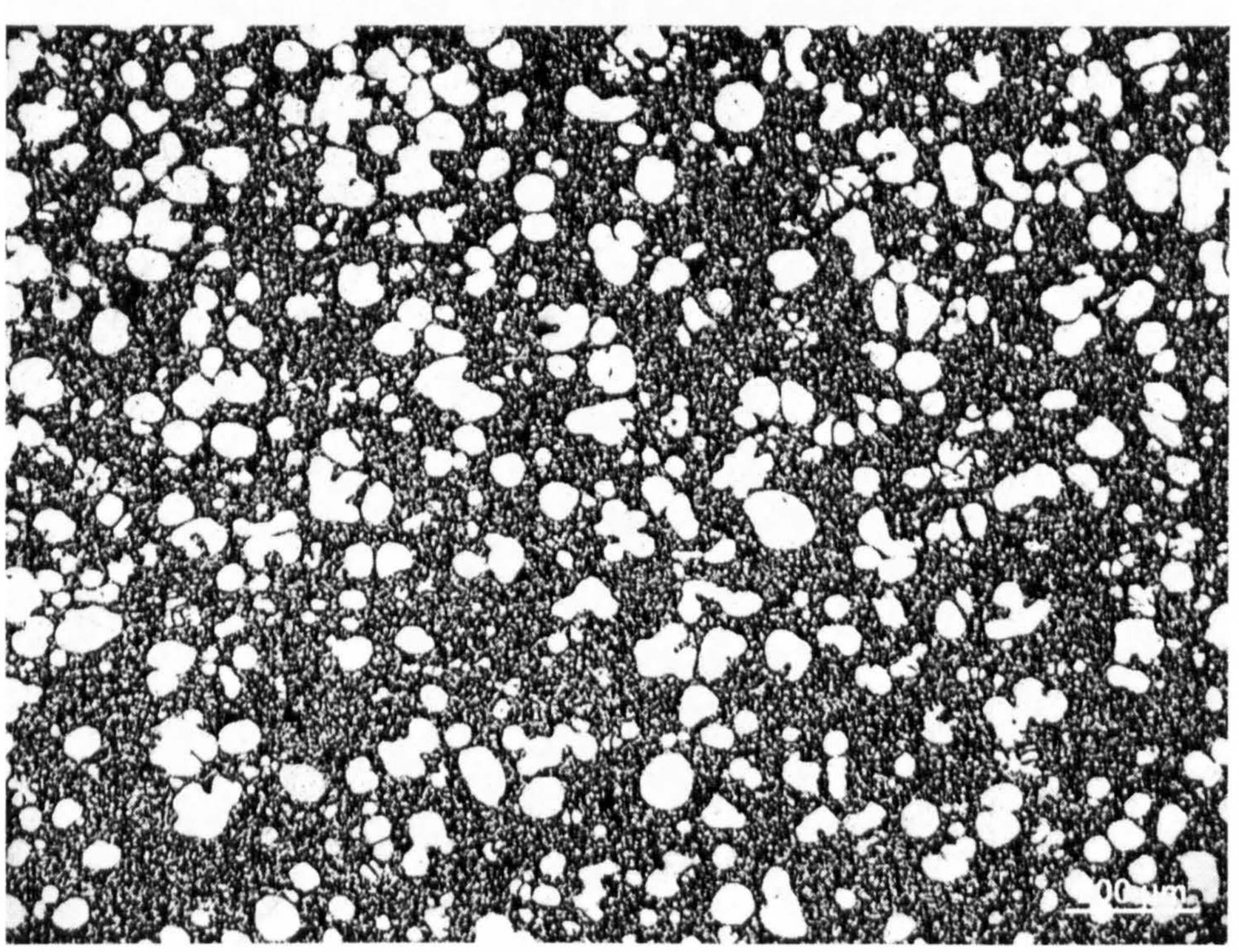

(b)

Figure 4.3.10 *The effect of shearing speed on the microstructure of RDC AZ91D alloy, at (a) 100 rpm, (b) 300 rpm, (c) 500 rpm, (d) 900 rpm.*

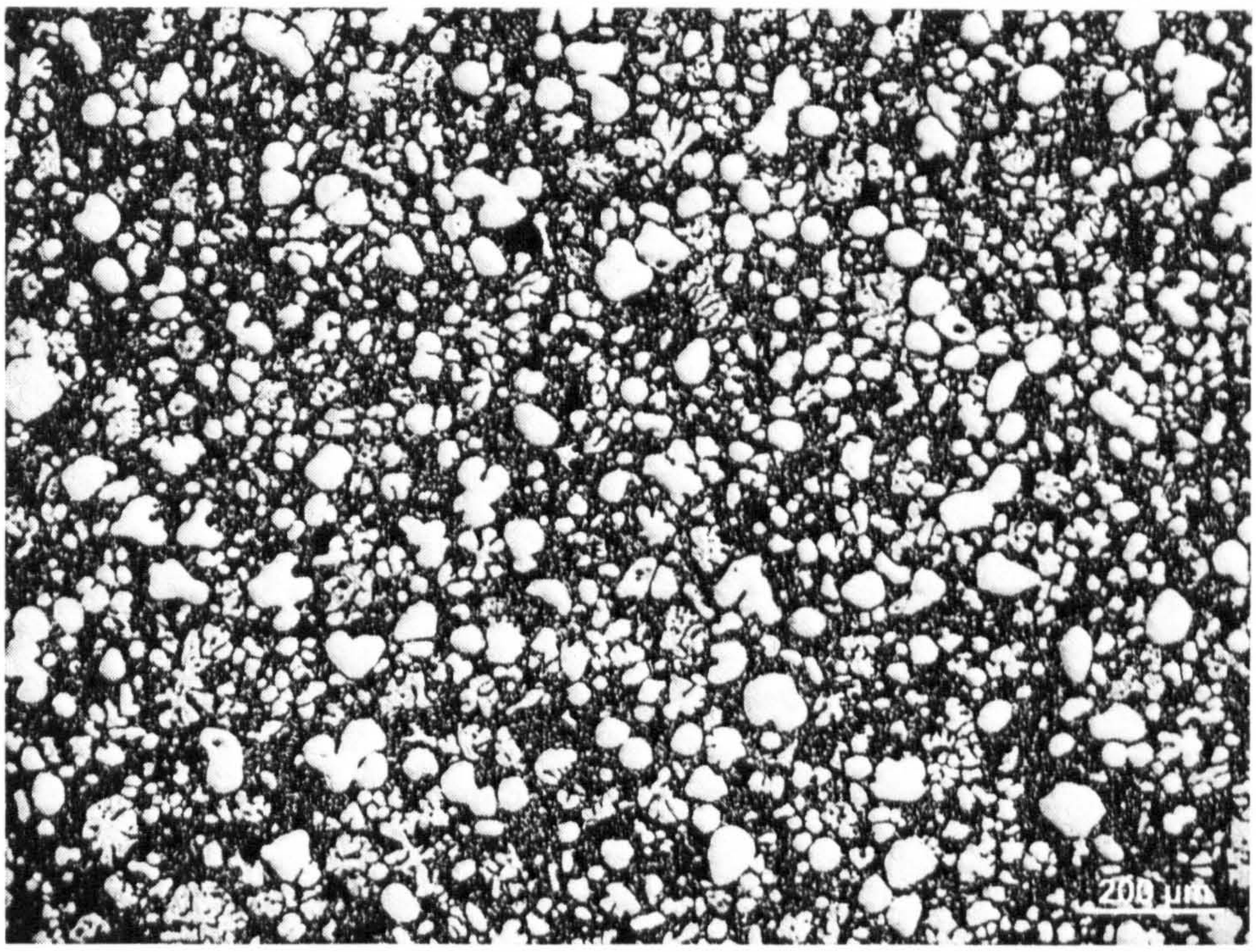

(c)

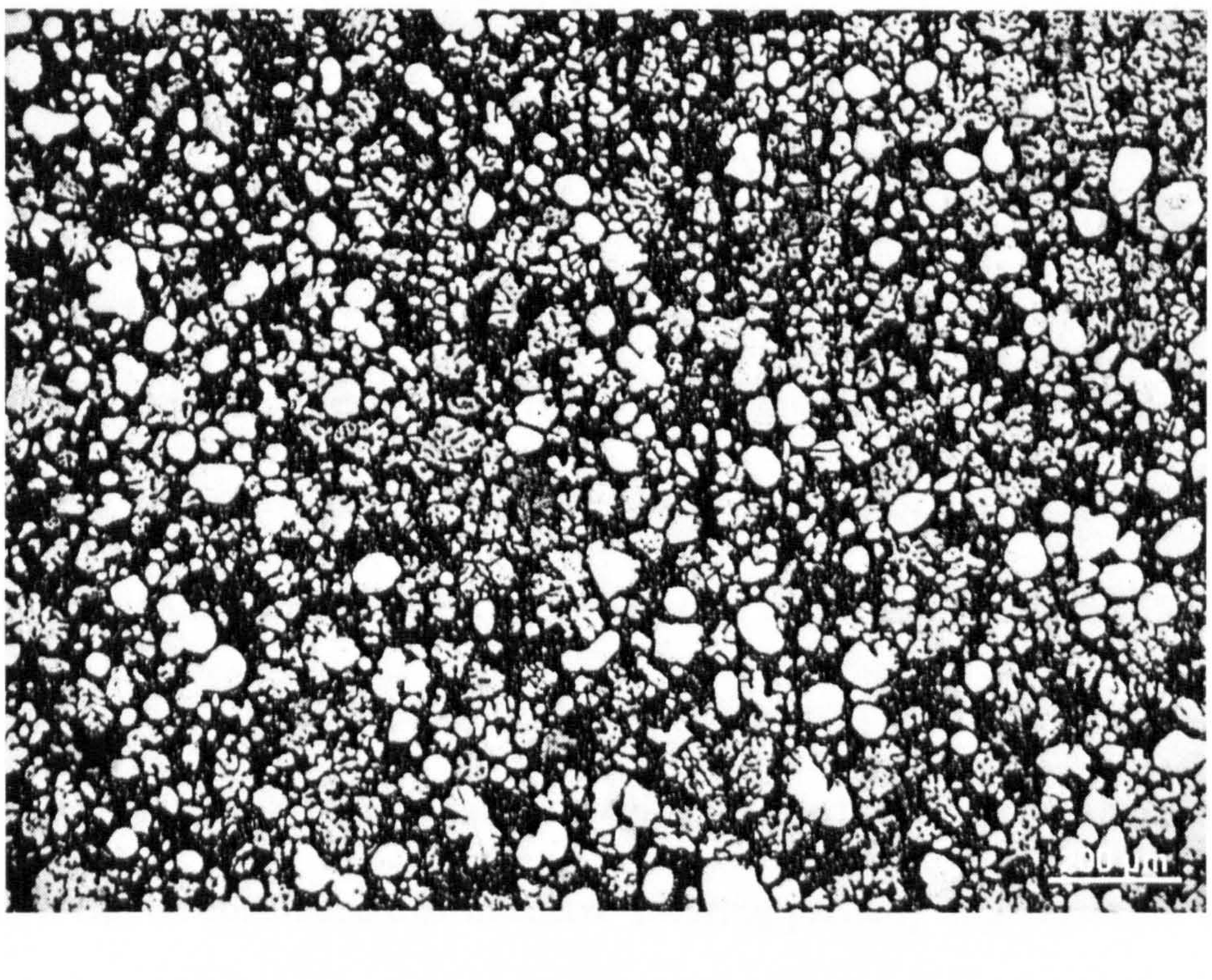

(d)

Figure 4.3.10 *(continued) The effect of shearing speed on the microstructure of RDC AZ91D alloy, at (a) 100 rpm, (b) 300 rpm, (c) 500 rpm, (d) 900 rpm.*

The measured particle size and shape factor of the primary particles formed during the primary solidification are presented in **Figure 4.3.11**. The primary particle size decreased slightly with an increase in the screw rotation speed, while the shape factor of the primary particles increased only slightly with the increase in screw rotation speed.

The measured volume fraction and particle density of the primary phase formed in the twin-screw slurry maker are plotted in **Figure 4.3.12**, as a function of the screw rotation speed. Figure 4.3.12 revealed that solid fraction decreased with the increase in screw rotation speed, indicating that intensive shearing suppressed, to some degree, the formation of the primary phase in the twin-screw slurry maker. However, intensive shearing did not promote nucleation in the twin-screw slurry maker, as indicated by the constant particle density in Figure 4.3.12. It is necessary to point out that all the samples have been sheared for 35 seconds; some particles are already dissolved, due to Ostwald ripening, during this time.

In contrast to the results presented in Figure 4.3.11 and Figure 4.3.12 for the primary solidification, intensive shearing promoted the formation of α_2, as indicated by the increase in α_2 volume fraction with screw rotation speed in **Figure 4.3.13**. However, intensive shearing did not change the total volume fraction of the primary phase ($\alpha_1+\alpha_2$). This is consistent with the experimental results presented in the previous section 4.3.1. Therefore, it can be concluded that intensive shearing partially suppresses the formation of primary phase during primary solidification, promotes the formation of primary phase in the shot sleeve, but does not affect the total volume fraction of the primary phase.

The effects of shearing intensity on the formation of α_2 are presented in **Figure 4.3.14**, in which the density of α_2 and total density of α_1 and α_2, are plotted against the screw rotation speed. It is interesting to note that the particle density of α_2 and the total density of α_1 and α_2 increased with the increase in screw rotation speed. It is necessary to point out that particles of α_2 refer to the fragments formed during the mould filling, from the original dendrites formed in the shot sleeve, and therefore the density of α_2 is considerably higher than the density of dendrites. However, since the die casting conditions have been kept constant for all the experiments, the increase in density of dendrite fragments corresponds to the increase in the density of dendrites. Hence, we can conclude that intensive shearing promotes nucleation of the primary particles in the shot sleeve at the secondary solidification stage. The increase in the total particle density in Figure 4.3.14 is mostly due to the increase of α_2 density, since intensive shearing had very little effect on the density of α_1 (see Figure 4.3.12).

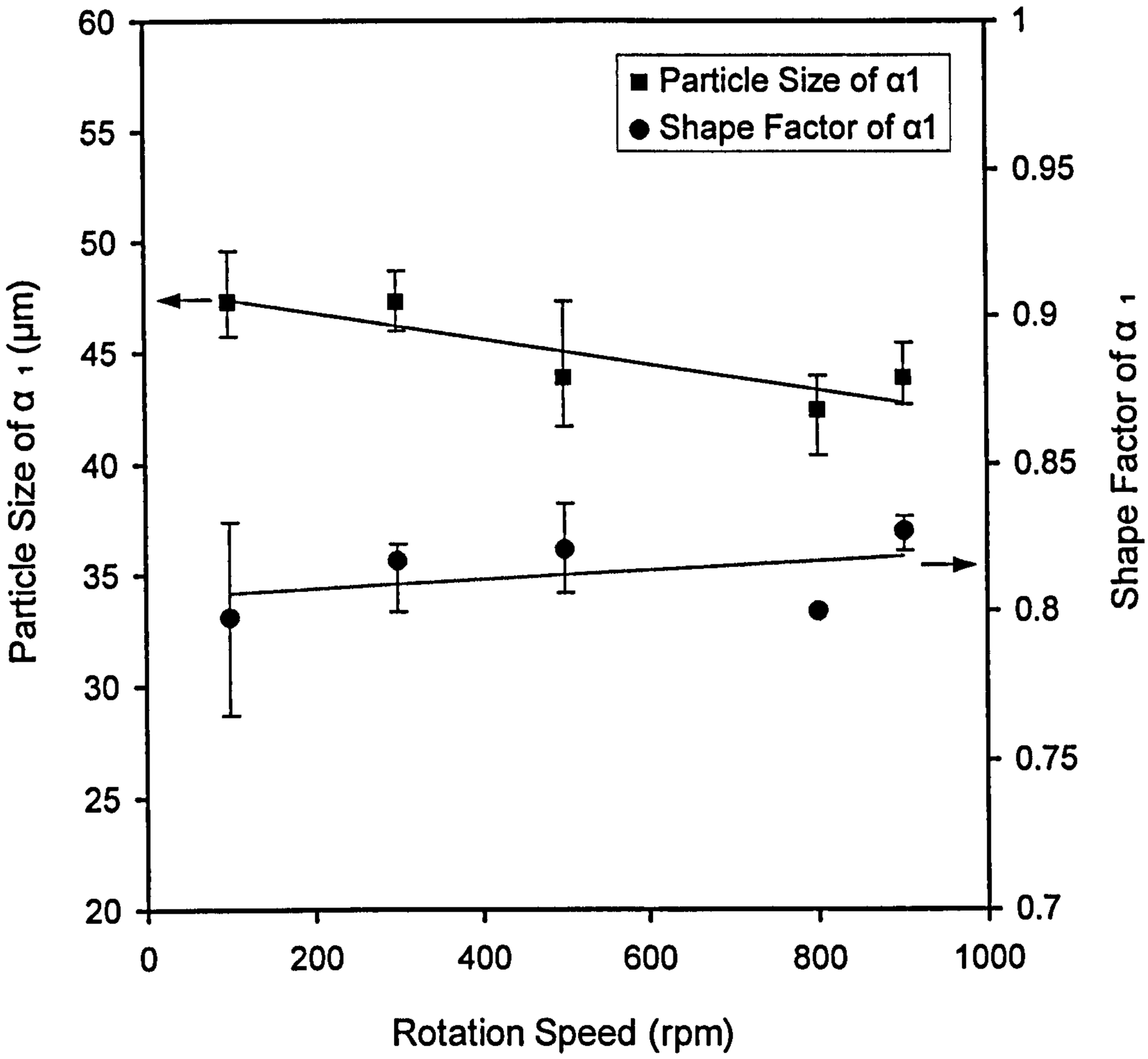

Figure 4.3.11 *Size and shape factor of the primary particles (α_1) formed in the twin-screw slurry maker, as a function of screw rotation speed. The shearing temperature was 593°C and shearing time was 35 seconds. The solid lines represent the best fit to the experimental data.*

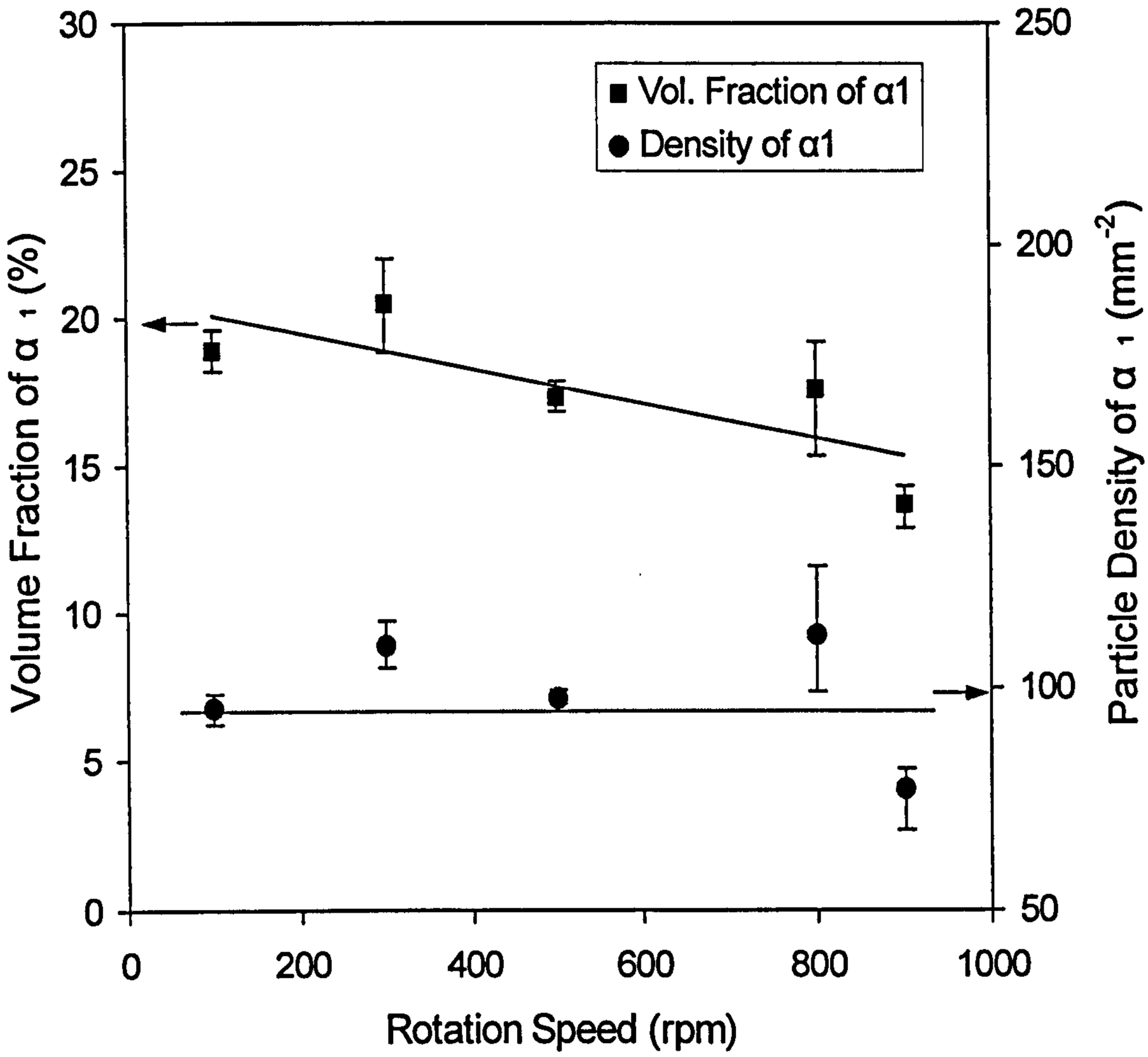

Figure 4.3.12 *Volume fraction and particle density of the primary particles (α_1) formed in the twin-screw slurry maker, as a function of screw rotation speed. The shearing temperature was 593°C and shearing time was 35 seconds. The solid lines represent the best fit to the experimental data.*

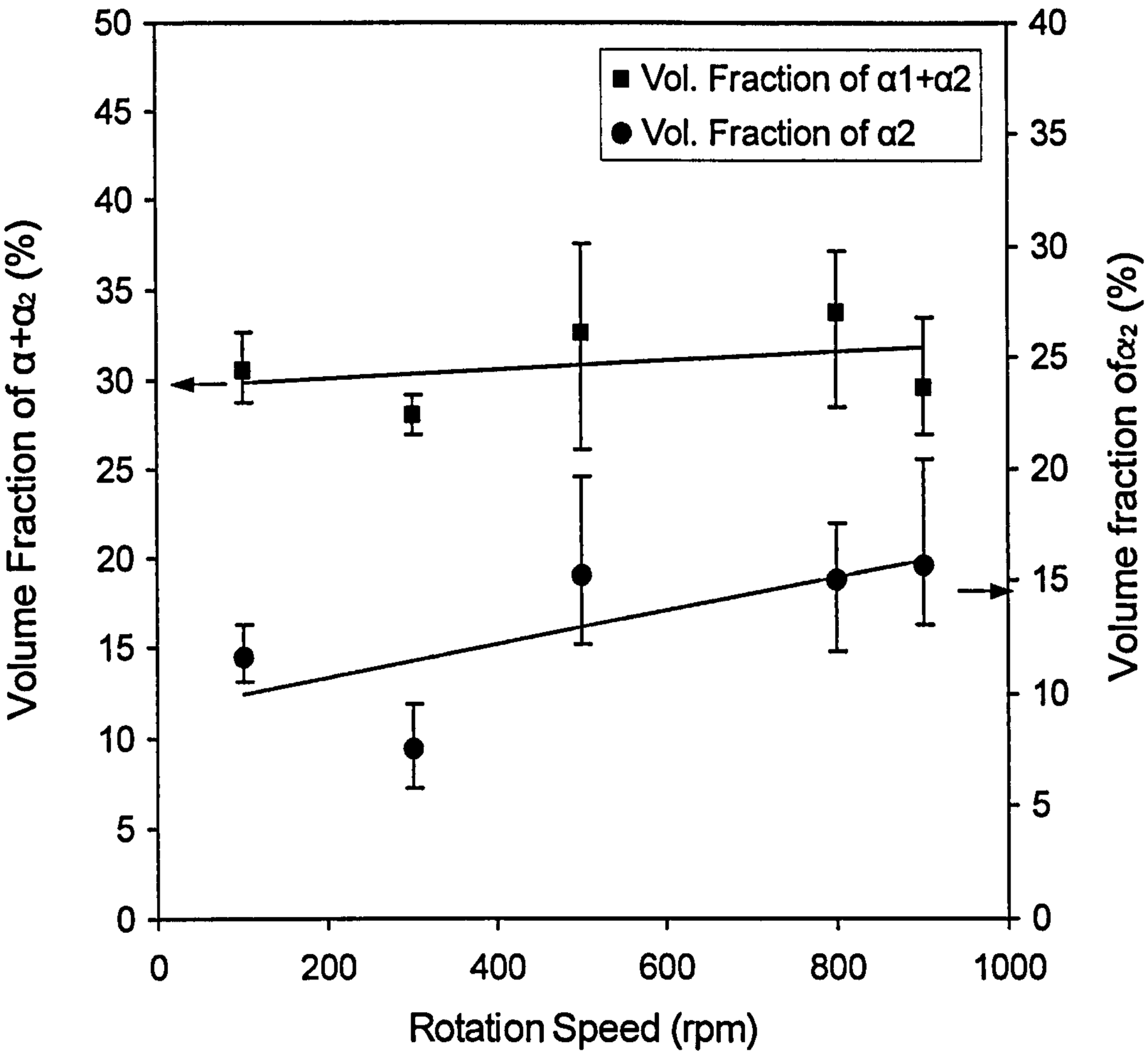

Figure 4.3.13 *Volume fraction of the primary particles formed in the shot sleeve (α_2) and the total volume fraction of $\alpha_1 + \alpha_2$, as a function of screw rotation speed. The shearing temperature was 593°C and shearing time was 35 seconds. The solid lines represent the best fit to the experimental data.*

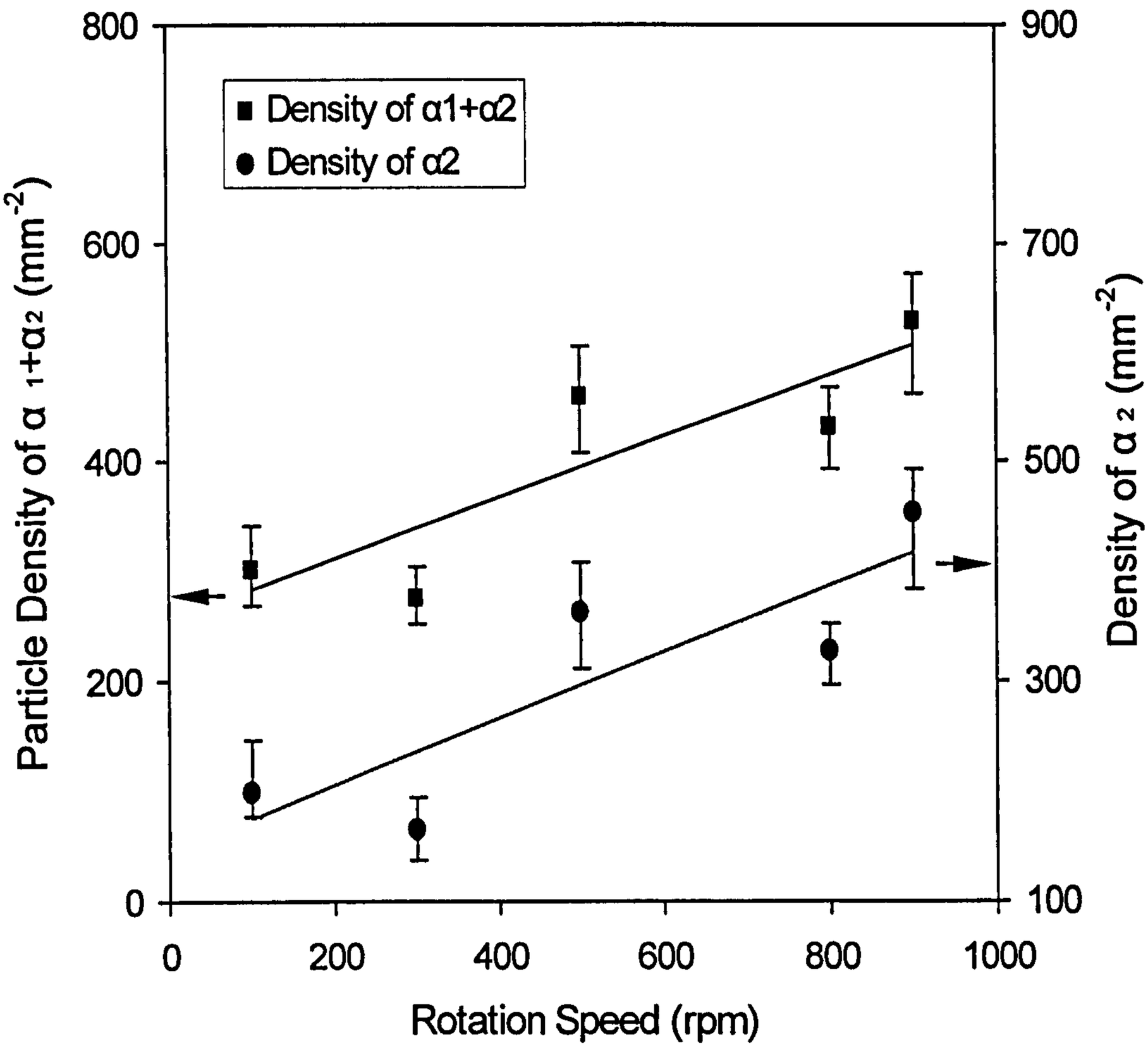

Figure 4.3.14 *Density of primary particles formed in the shot sleeve (α_2) and the total particle density as a function of screw rotation speed. The shearing temperature was 593°C and shearing time was 35 seconds. The solid lines represent the best fit to the experimental data.*

4.3.3 Effects of shearing temperature

All the experiments in this section were conducted with a screw rotation speed of 300rpm and shearing time of 35 seconds; the Twin-Screw shearing temperature was varied between 585°C and 600°C. **Figure 4.3.15** shows the microstructure of RDC AZ91D alloy processed at different temperatures. **Table 4.3.3** summarises the average values, for microstructural characteristics of different shearing temperatures, obtained by quantitative analysis.

***Table 4.3.3** Summary of the quantitative metallography results for RDC AZ91D samples produced at different shearing temperatures.*

Shearing temperature (°C)	Volume fraction of α_1 (%)	Particle size of α_1 (μm)	Shape factor of α_1
585	31.4	42.6	0.79
589	25.1	40.9	0.78
593	19.1	40.1	0.80
597	9.1	39.2	0.79

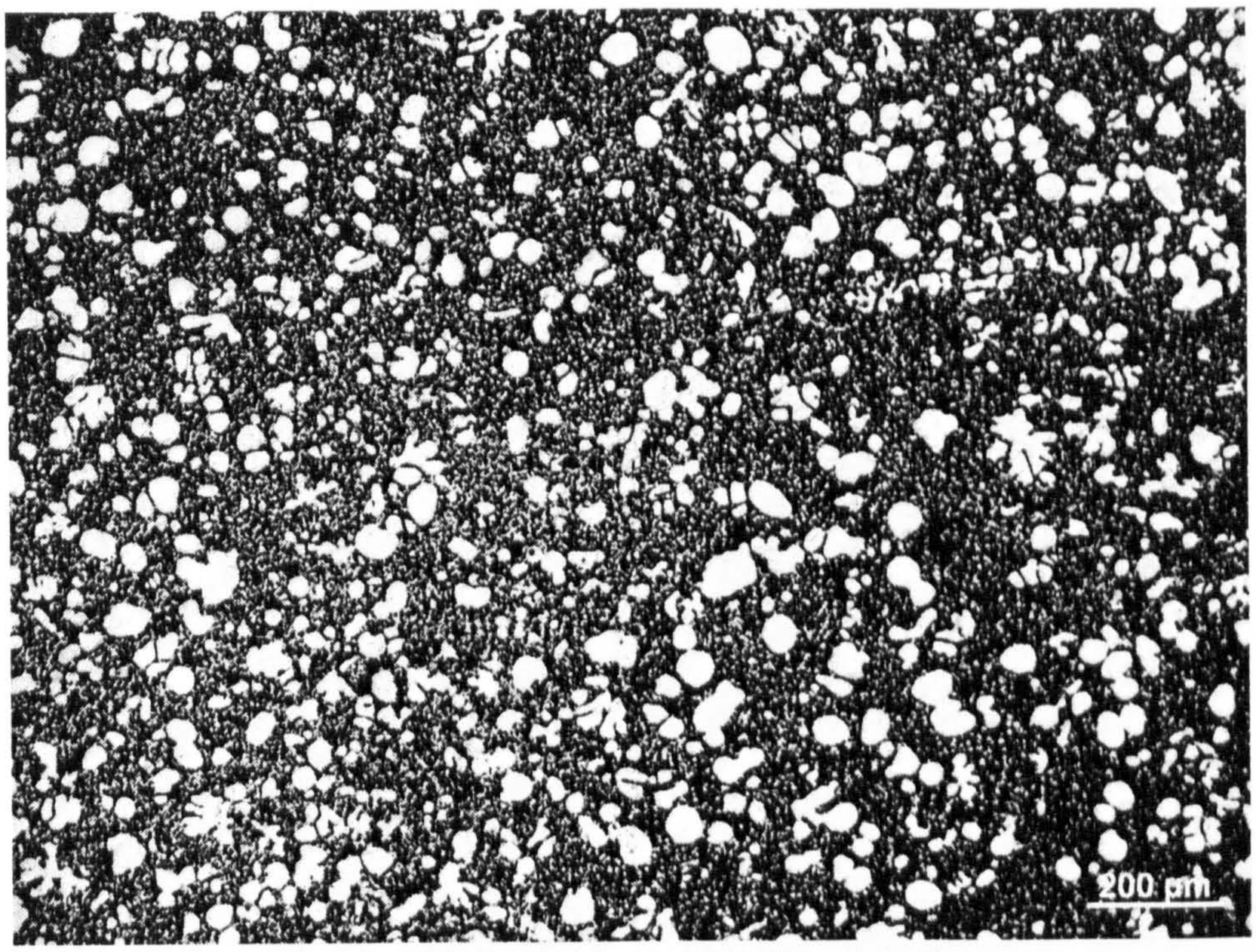

(a)

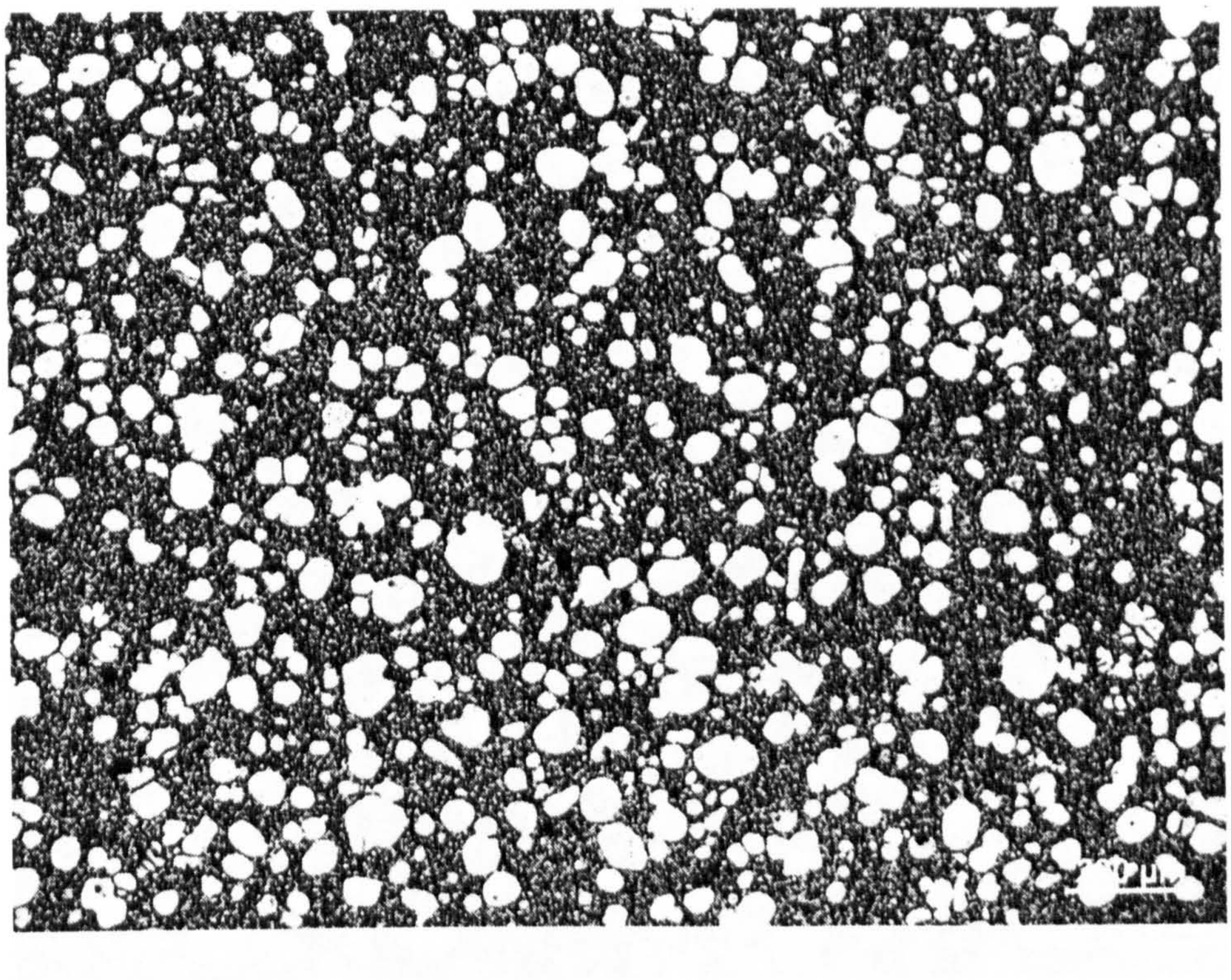

(b)

Figure 4.3.15 *Optical micrographs showing the microstructures produced at different temperatures in the RDC process (a) 597 °C, (b) 593 °C, (c) 589 °C, (d) 585 °C.*

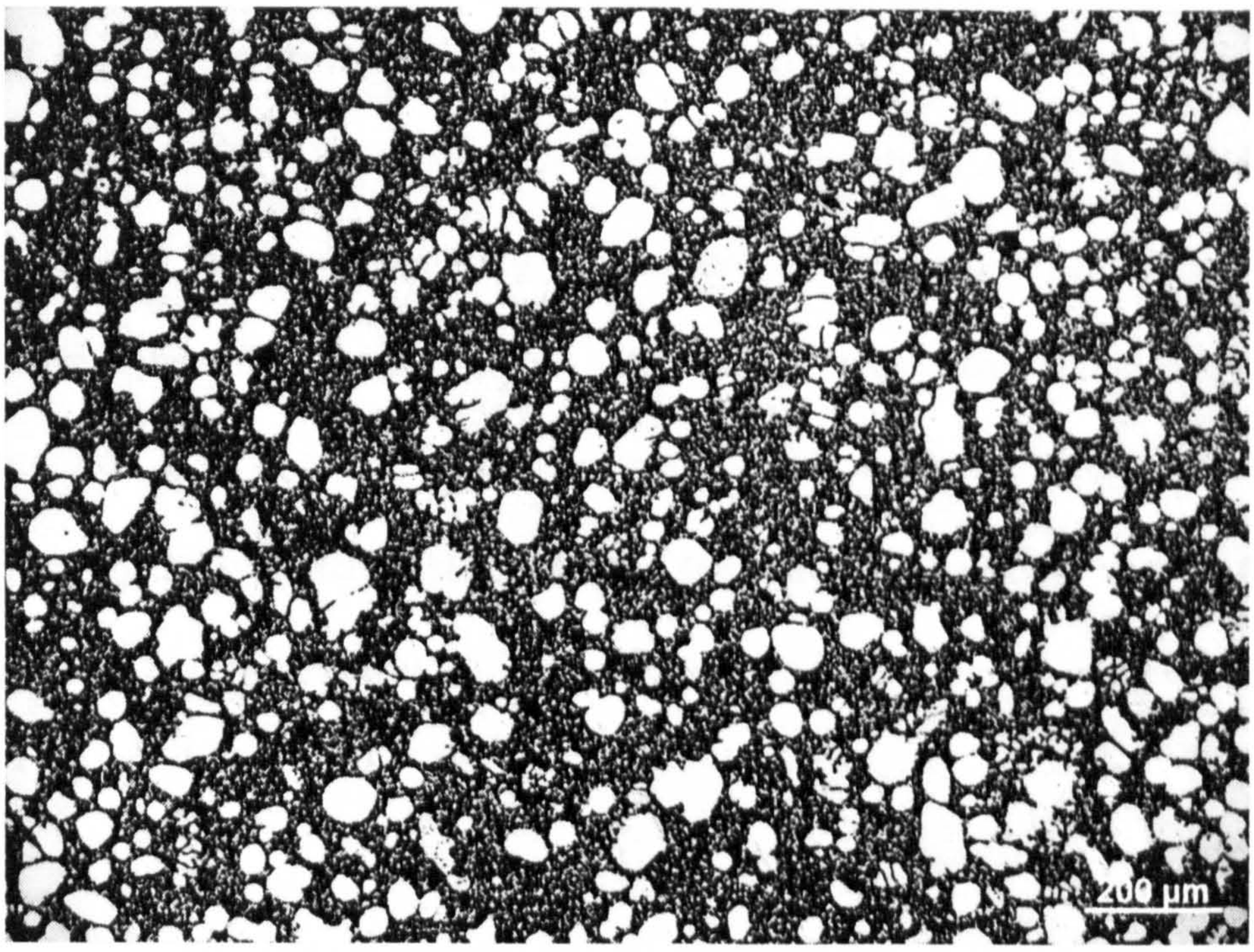

(c)

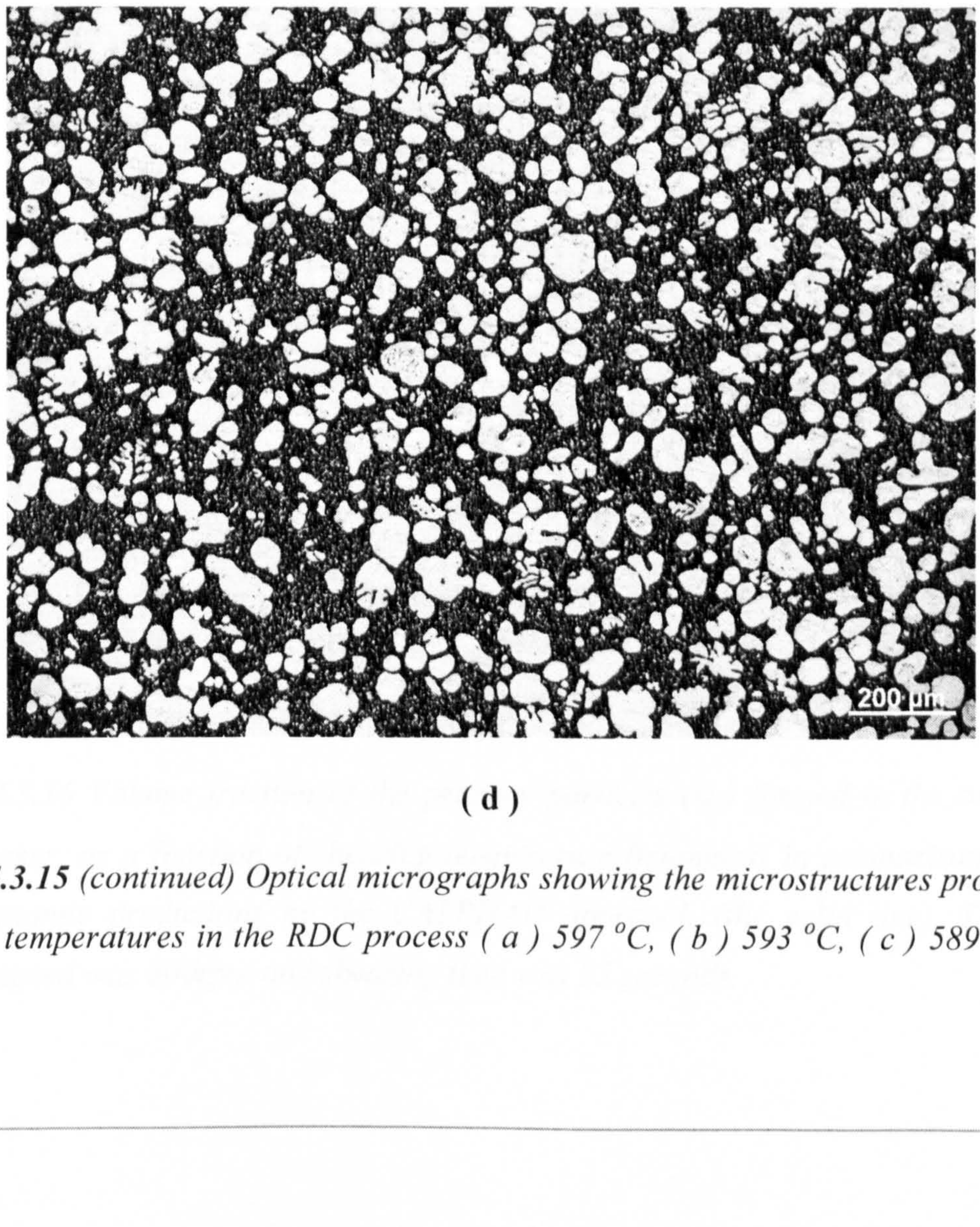

(d)

Figure 4.3.15 *(continued) Optical micrographs showing the microstructures produced at different temperatures in the RDC process (a) 597 °C, (b) 593 °C, (c) 589 °C, (d) 585 °C.*

The measured volume fraction of the primary phase is presented in **Figure 4.3.16**, as a function of shearing temperature, in comparison with the equilibrium solid fraction for the same alloy predicted by the CALPHAD approach [FAN05b]. Solid fraction decreased with the increase in shearing temperature, and the experimental data was close to the thermodynamic predictions. In addition, it was also found that shearing temperature did not have a strong effect on particle size and morphology of the primary phase formed in the twin-screw slurry maker, the particle size being around 40μm and the shape factor being around 0.79, as shown by the experimental results presented in **Figure 4.3.17.**

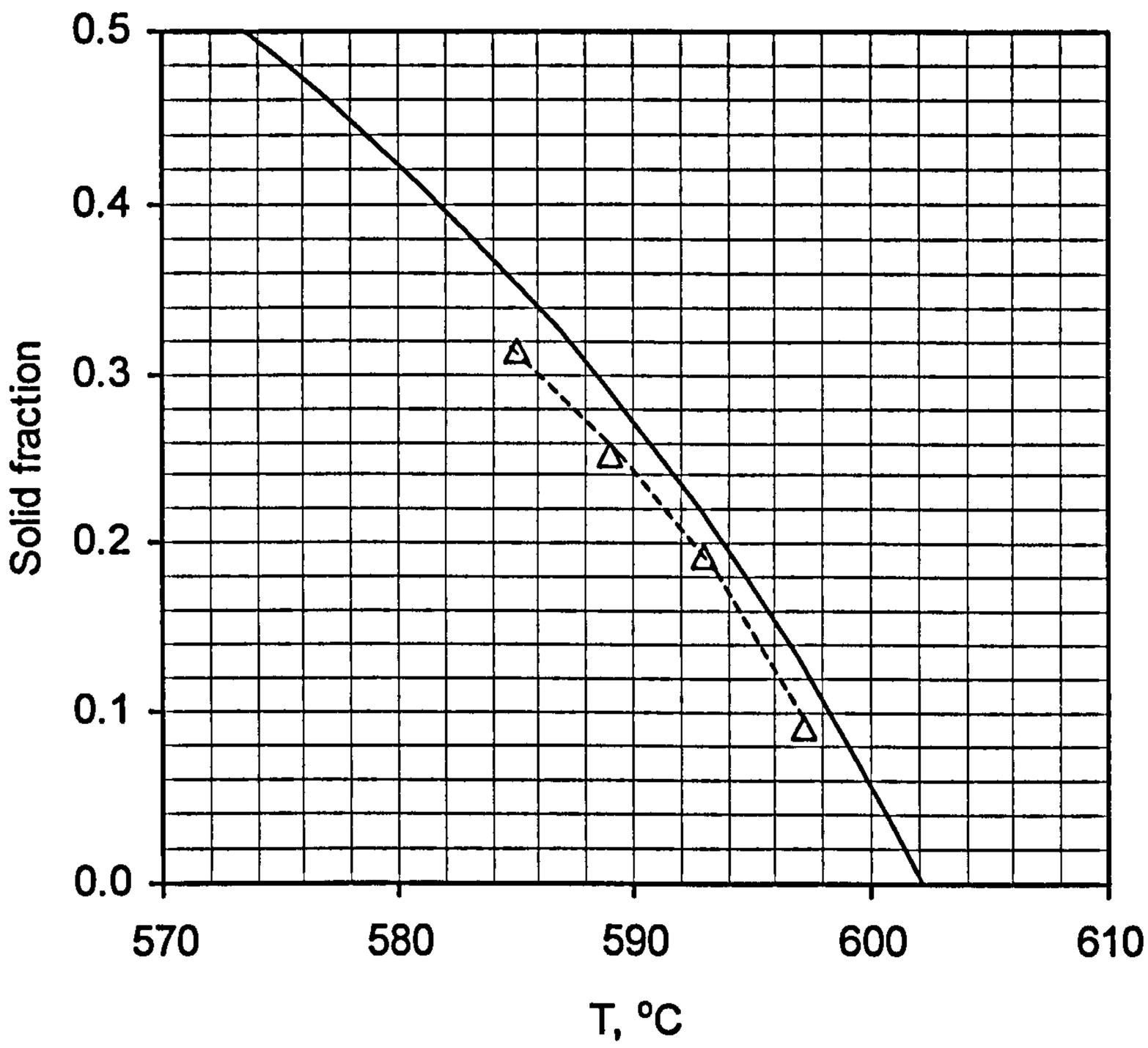

Figure 4.3.16 *Volume fraction of the primary particles (α_l) formed in the twin-screw slurry maker, as a function of shearing temperature (triangles) in comparison with the thermodynamic predictions by the CALPHAD approach (the solid line). The screw rotation speed was 300rpm and shearing time was 35 seconds.*

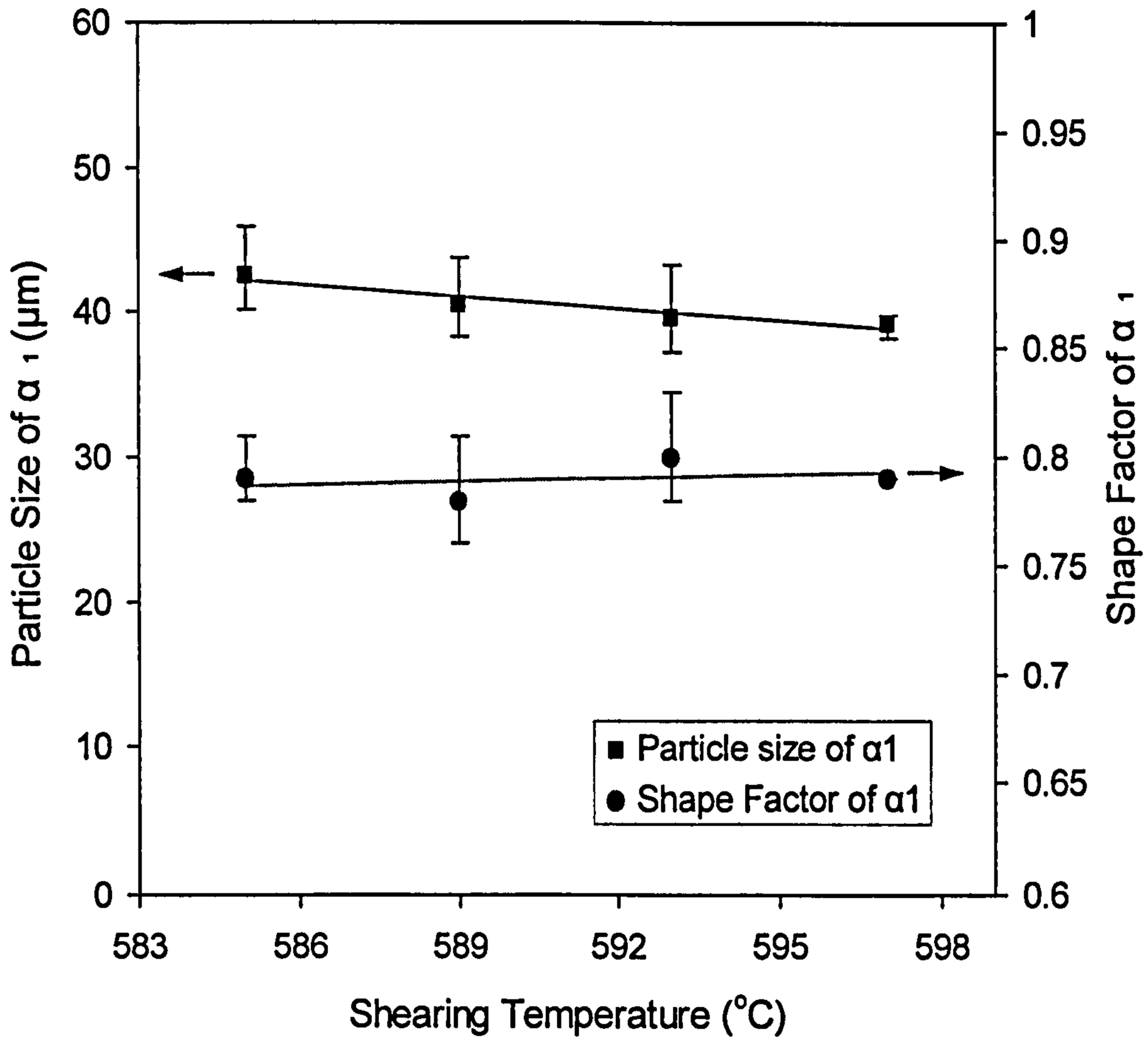

Figure 4.3.17 *Size and shape factor of the primary particles (α_1) formed in the twin-screw slurry maker, as a function of shearing temperature. The screw rotation speed was 300rpm and shearing time was 35 seconds. The solid lines represent the best fit to the experimental data.*

In the RDC process the variation of solid fraction is achieved by changing the barrel temperature. **Figure 4.3.18** shows the microstructure of RDC AZ91D alloy processed at 600°C, which more or less coincides with its liquidus. The primary particles are fine in size and less spherical in morphology. It is likely that such primary particles were formed in the shot sleeve, and fragmented by the intensive shear flow at the gate. However, different from the non-uniform microstructure produced by HPDC process (Figure 4.2.3), the microstructure here is extremely uniform throughout the entire sample. This is referred to as liquidus rheocasting [FAN02a]. By reducing the processing temperature below the liquidus, semisolid slurries with different solid fractions can be produced.

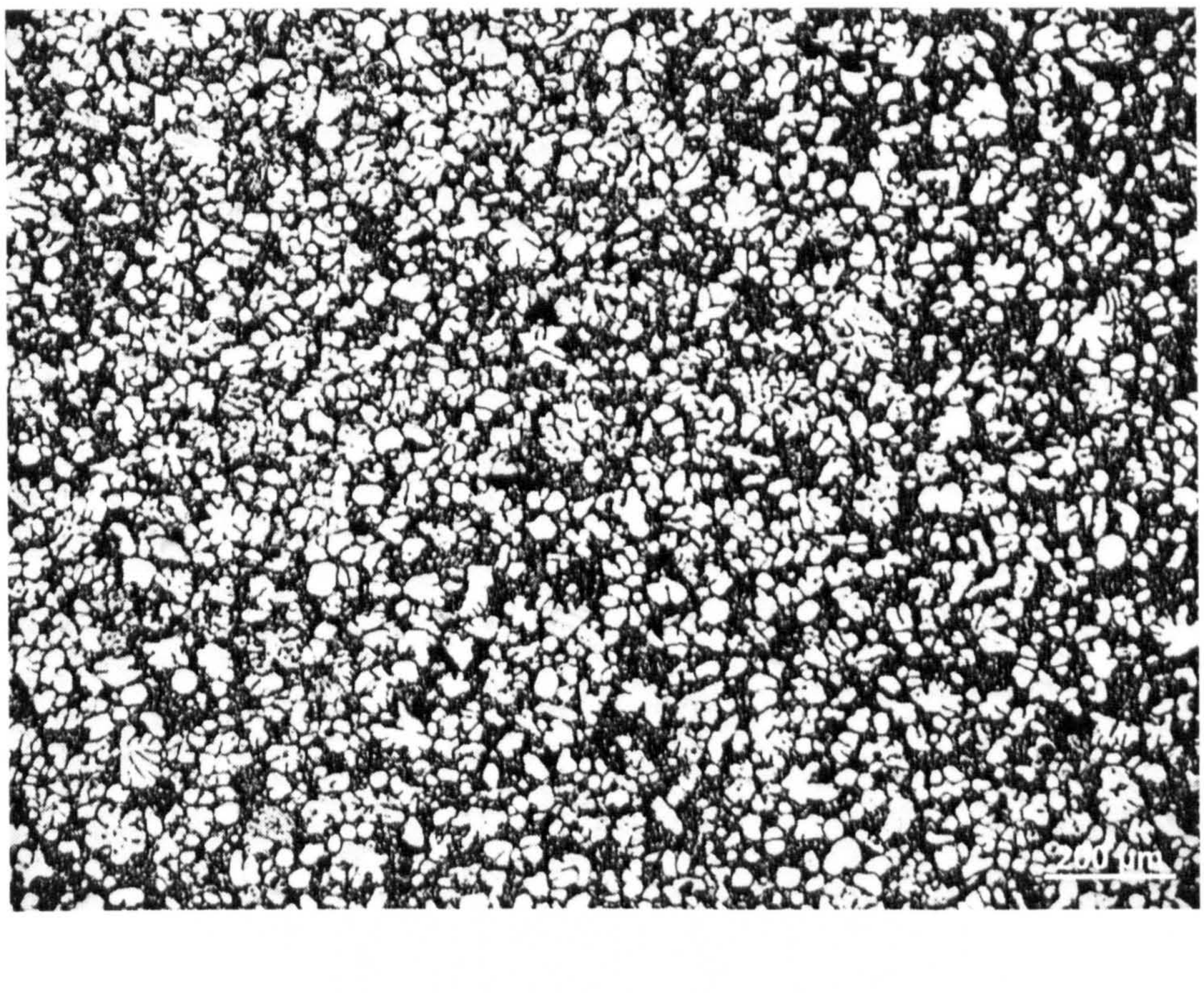

Figure 4.3.18 *Micrograph shows the microstructure of RDC AZ91D alloy processed at a near liquidus temperature of 600°C.*

Detailed microstructural examination (**Figure 4.3.19**) indicates that there are no significant effects of shearing temperature on the size and morphology of α_3 produced by secondary solidification. It was found that the effects of shearing intensity and shearing time on the formation of α_3, presented in Figure 4.3.9, were very limited. The particle size of α_3 is fine in size (around 5-10μm) and uniform in distribution. However, it should be pointed out that the fine and uniform microstructure of α_3 is a result of the intensive forced convection in the RDC process, once the intensity of turbulence reaches a substantial level, further increase of the intensity of forced convection (the investigation range of shearing speed is below 900rpm in this study) does not improve the microstructure.

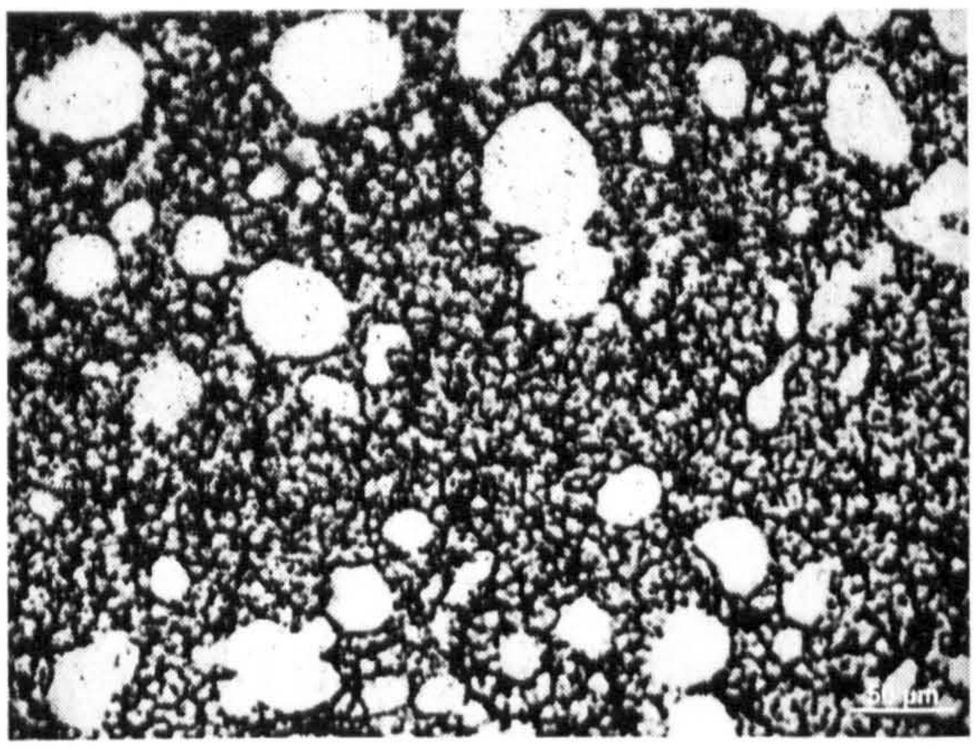

(a) 597 °C

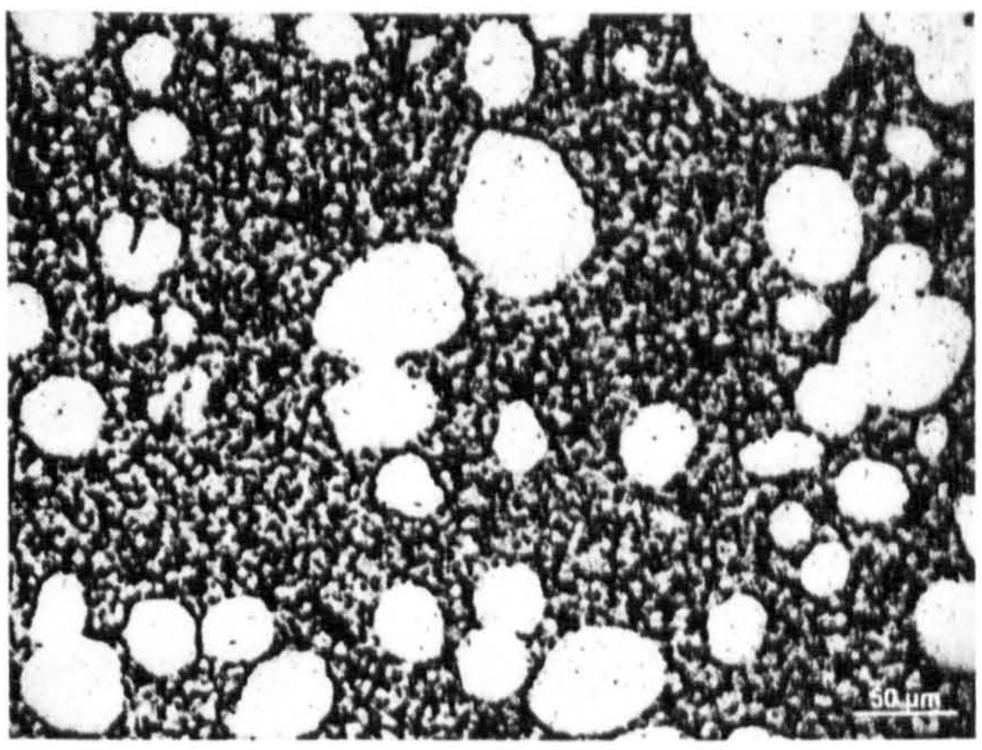

(b) 593 °C

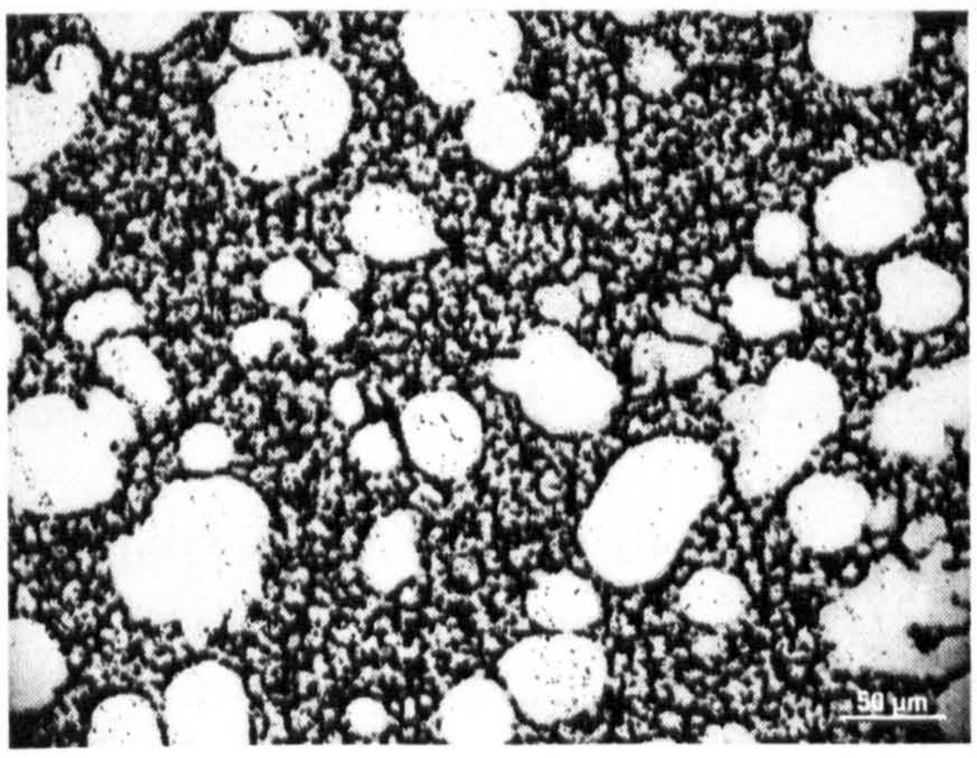

(c) 589 °C

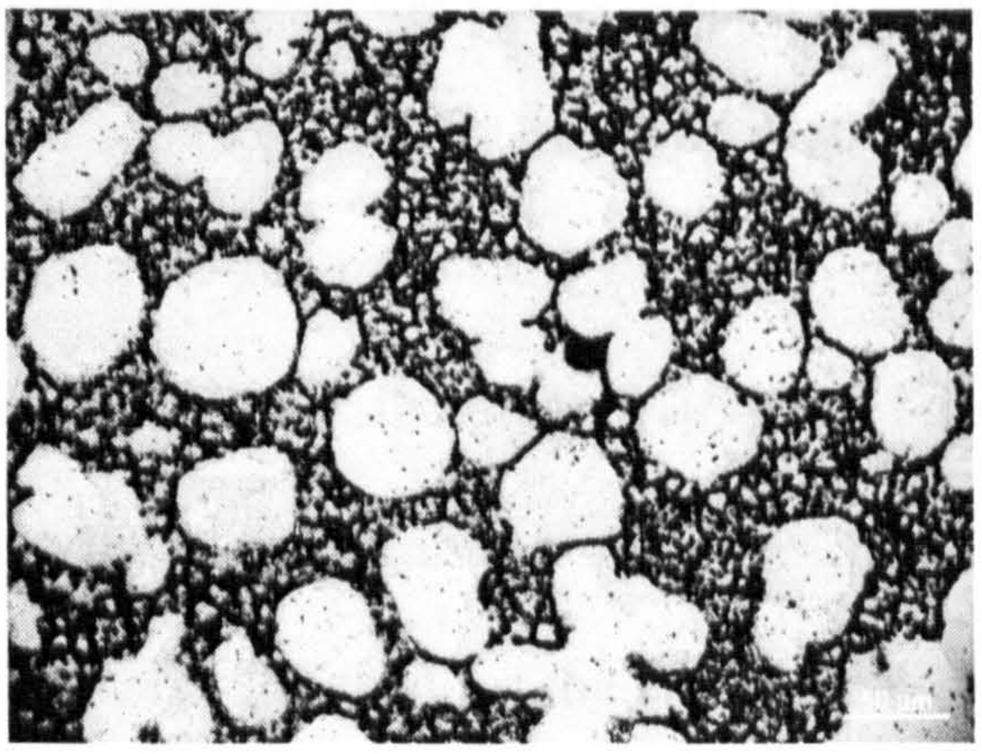

(d) 585 °C

Figure 4.3.19 *Detailed microstructures of α_3 obtained under different shearing temperatures of (a) 597 °C, (b) 593 °C, (c) 589 °C and (d) 585 °C.*

4.4 Microstructure and mechanical properties of heat treated Rheo-Diecast AZ91D Mg-alloy

4.4.1 Solution treatment of RDC AZ91D Mg-alloy

Figure 4.4.1 shows the variation of Vickers hardness for AZ91D Mg-alloy, produced by both the RDC and HPDC processes, against time at solution treatment temperature 413°C. The first point on each of the curves corresponds to the as-cast state (no solution treatment) and it is always higher than those samples that are solution treated. It is interesting to note that the hardness value decreases faster for the RDC alloy than that produced by HPDC, indicating an accelerated dissolution of the β-$Mg_{17}Al_{12}$ phase for the RDC alloy. As shown in Figure 4.4.1, the RDC alloy reached its minimum hardness value at 5 hours (18ks), compared to nearly 16 hours (57.6ks) for the HPDC alloy. The hardness value of the RDC AZ91D Mg-alloy reached a steady state with increasing solution time after 5 hours (18ks) exposure to the temperature. The alloys produced by both of the casting processes exhibited essentially the same hardness level after solution treatment for 16 hours (57.6 ks) or longer. **Table 4.4.1** lists the important features during the solution treatment for the AZ91D alloy produced by both RDC and HPDC processes.

***Table 4.4.1** Important features of solution behaviour obtained for the AZ91D Mg-alloy*

Process	Initial Vickers hardness	Vickers hardness at Steady Level	Time to minimum hardness (hour)	Average grain size after solution (μm)
RDC	66.8	54.9	5	34.1
HPDC	64.3	54.8	16	47.6

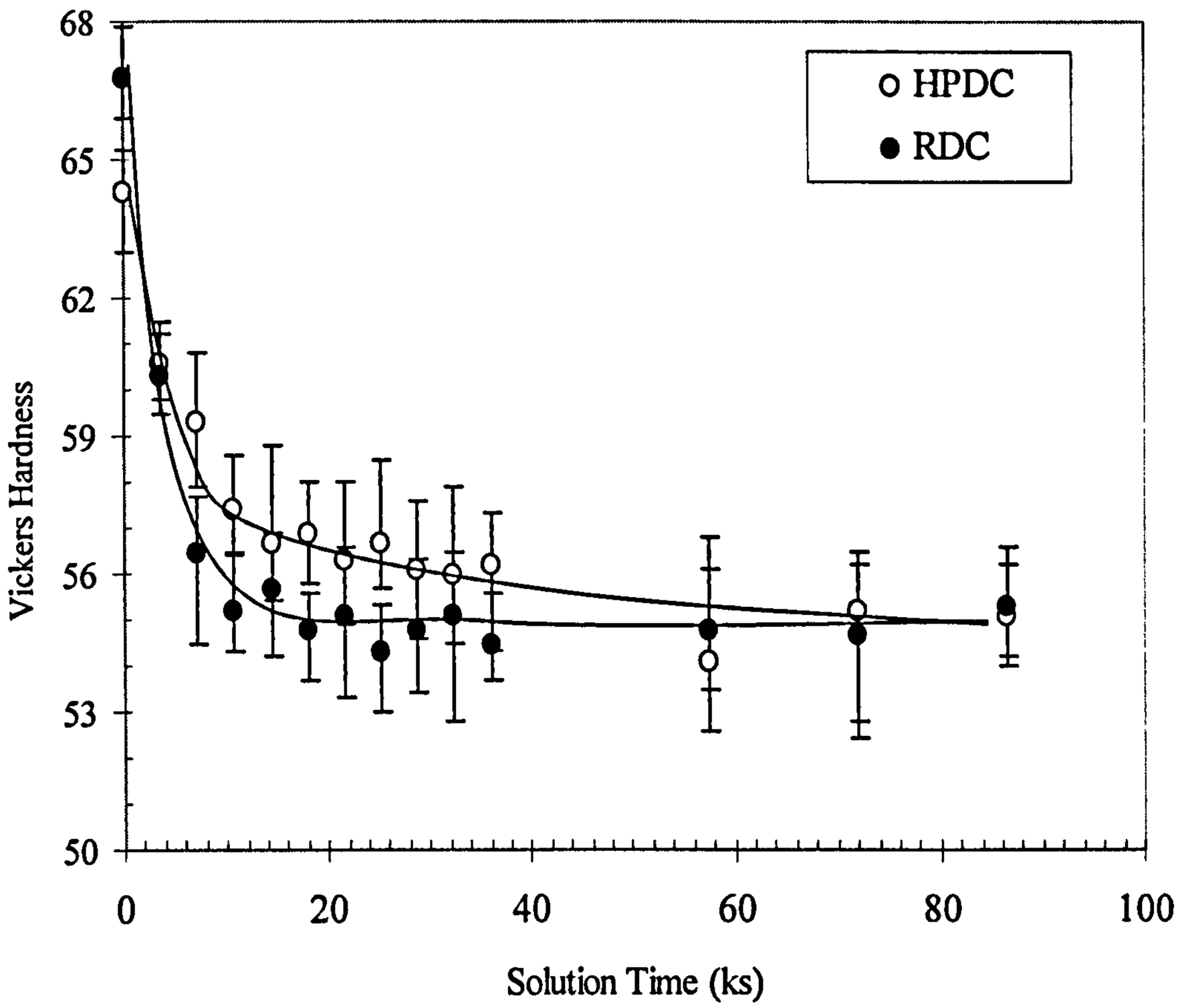

Figure 4.4.1 *Variation of Vickers hardness for AZ91D Mg-alloy produced by the RDC and HPDC process, against time at solution treatment (T4) temperature, 413℃, indicating a faster reduction of the hardness for the RDC AZ91D alloy, compared with the HPDC alloy.*

Figure 4.4.2, the XRD analysis revealed that, in the alloy samples from both the HPDC and RDC processes, the β-$Mg_{17}Al_{12}$ phase has been completely dissolved into the α-Mg solid solution after 24 hours at 413°C and a single solid solution phase remains. **Figure 4.4.3** is an optical micrograph showing the typical microstructure of the RDC AZ91D Mg-alloy after solution treatment for 24 hours.

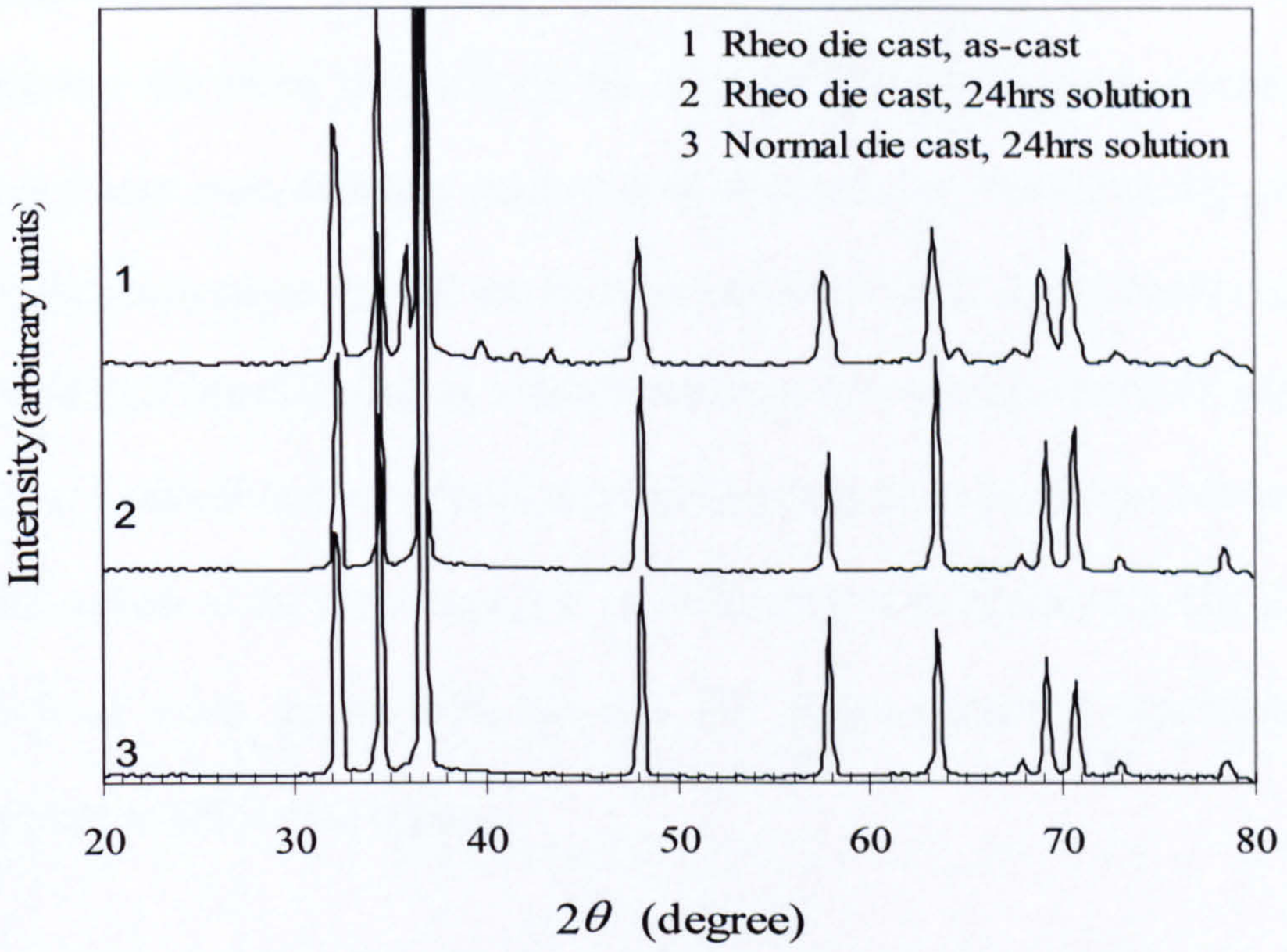

Figure 4.4.2 *XRD spectra obtained from the AZ91D alloy before and after solution treatment (T4) at 413℃ for 24 hours. This indicates that the eutectic β-$Mg_{17}Al_{12}$ phase has been dissolved completely and a single α-Mg solid solution phase is present for the alloy produced by both RDC and HPDC process.*

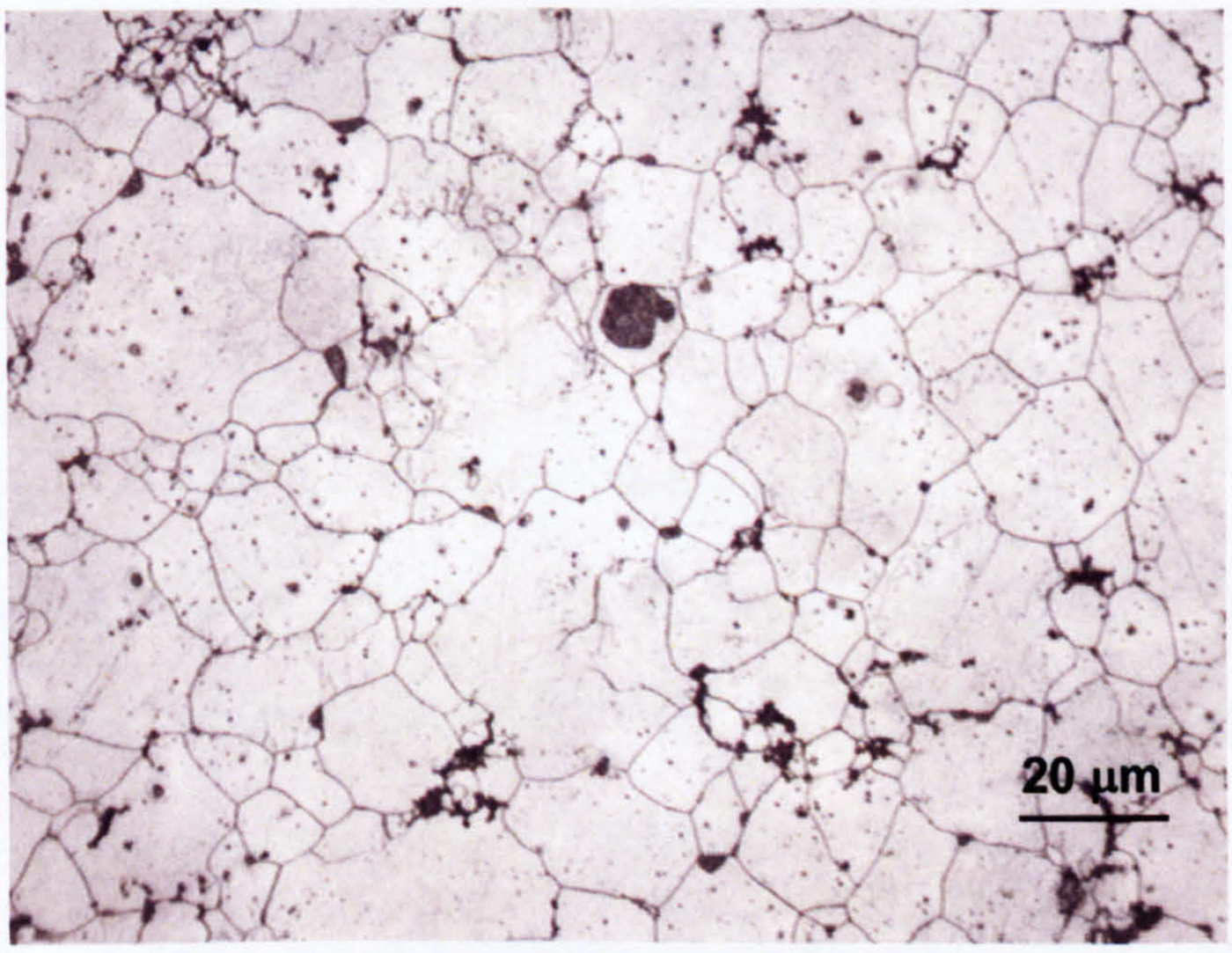

Figure 4.4.3 *Optical micrograph showing the typical microstructure of the RDC AZ91D Mg-alloy after solution treatment at 413℃ for 24 hours.*

In magnesium alloys that contain high levels of aluminium, e.g. > 3wt% Al, the grain boundaries are often obscured by the eutectic phase. The grain boundaries can be revealed very well during a solution heat treatment by dissolving the eutectic phase. Detailed observations by OM and SEM revealed that the microstructural evolution of the RDC AZ91D Mg-alloy during solution treatment (T4) can be described in terms of three stages, (i) dissolution of eutectic non-equilibrium β-$Mg_{17}Al_{12}$ phase into the α-Mg solid solution phase at the early stage, (ii) modification of the primary α-Mg globules, (iii) growth of α-Mg grains, with the first two stages occurring simultaneously in the secondary solidification region.

The structure of the secondary solidification region was eventually replaced by new, fine α-Mg grains, which were well defined by the sharp grain boundaries, resulting from the dissolution of the β-phase. **Figure 4.4.4** shows the microstructure of the RDC AZ91D Mg-alloy treated at 413°C for 0.5 hours, revealing the partial dissolution of the β-phase and those newly formed grains with sharp grain boundaries.

During the dissolution process, the quantitative metallography revealed that the β-phase dissolves quite quickly at this solution temperature. **Table 4.4.2** summarizes the quantitative analysis results of dissolving of β-phase during solution treatment for both RDC and HPDC process. It can be seen that the β-$Mg_{17}Al_{12}$ phase needs one hour (3.6ks) or so to dissolve completely in the RDC alloy, compared to around 2 hours (6.3ks) in the HPDC alloy. The maximum difference in the dissolution kinetics of the β-phase between the RDC and HPDC alloys was evident early in the solution treatment. For instance, in the first 15 minutes (0.9ks), the volume fraction of the β-phase reduced from 14.8 vol % to 7.3 vol % at a dissolution rate of 8.33 vol%/ks for the RDC alloy, compared to a rate

Table 4.4.2 *Quantitative analysis results of dissolving of β-phase (in Vol%) during solution treatment for both RDC and HPDC process.*

Solution time (ks) / Process	0	0.9	1.8	2.7	3.6	4.5	5.4	6.3
RDC	14.8	7.3	3.2	1.4	0.17	0.09	0	
HPDC	15.2	9.6	6.2	3.5	1.5	0.7	0.4	0

of 6.2 vol%/ks from 15.2 vol % to 9.6 vol % for the HPDC alloy. The difference in the dissolution rate of the β-phase decreased with increasing solution time. This accelerated dissolution kinetics of the β-phase verifies the faster hardness reduction shown in Figure 4.4.1 for the RDC AZ91D Mg-alloy.

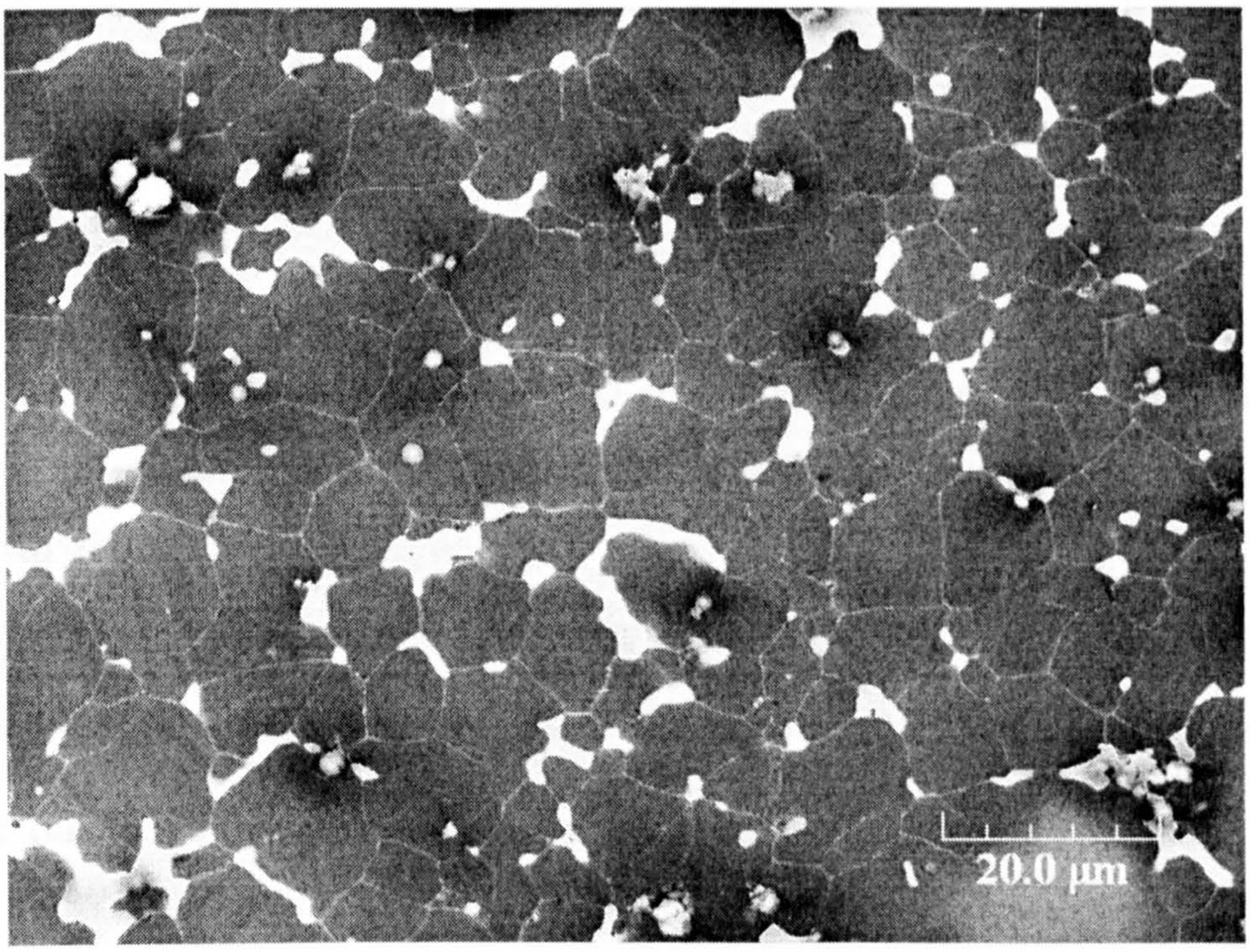

Figure 4.4.4 *SEM micrograph of the RDC AZ91D Mg-alloy after solution treatment at 413℃ for 0.5 hours. The partial dissolution of the β-$Mg_{17}Al_{12}$ phase (white area) and the formation of the new α-Mg fine grains well defined by the sharp boundaries can be observed.*

During solution treatment of RDC AZ91D Mg-alloy, the grain growth was experimentally measured from a starting solution time of 0.5 hours (1.8ks). At the solution time of 0.5 hours, the average size of the new α-Mg grains formed in the secondary solidification region was measured to be about 7.3 μm, growing to 34.1μm with an increase in time to 24 hours (86.4ks), as shown in **Figure 4.4.5**.

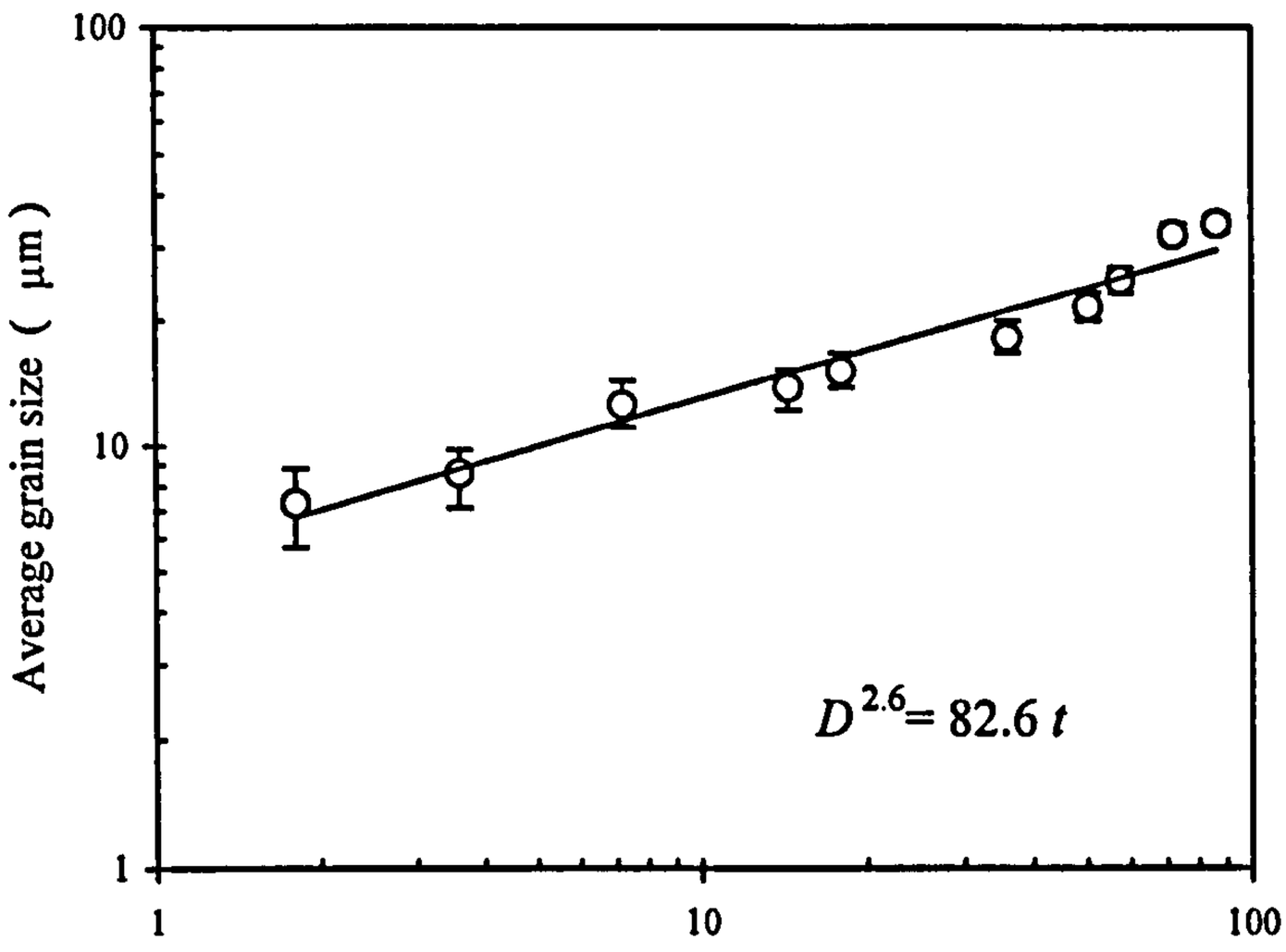

Figure 4.4.5 *Plot of average grain size D (μm) against solution treatment time t (ks), showing grain growth kinetics for the RDC AZ91D Mg-alloy during solution treatment at 413℃ up to 24h hours (86.4ks).*

In Figure 4.4.5, power law was used to fit the experimental date to extract the growth constants. It is found that grain growth kinetics satisfies the following relationship:

$$D^{2.6} = 82.6\,t \qquad \textbf{Equation 4.4.1}$$

Where *D* is average grain size and *t* is solution time. In the present study, the coarsening exponent '*n*' was experimentally determined to be 2.6.

4.4.2 Aging of RDC AZ91D Mg-alloy

Figure 4.4.6 is the age-hardening curve of the AZ91D Mg-alloy samples aged at 216°C for different lengths of time, after being subject to the solution treatment. A log scale has been used in the curves so that the early stage of precipitation can be seen more clearly. It is a characteristic hardness curve for an aging process. In Figure 4.4.6, the hardness of the alloy increases linearly as a function of aging time, before reaching the peak hardness and then decreases slowly. The alloy produced by the RDC process reaches its peak hardness in 5.5 hours (19.8ks), compared to 11 hours (39.6ks) when produced by HPDC. This indicates an accelerated age-hardening response at this aging temperature for the RDC AZ91D Mg-alloy. **Table 4.4.3** lists the important features of the age-hardening curves obtained for the AZ91D Mg-alloy, produced by RDC and HPDC processes.

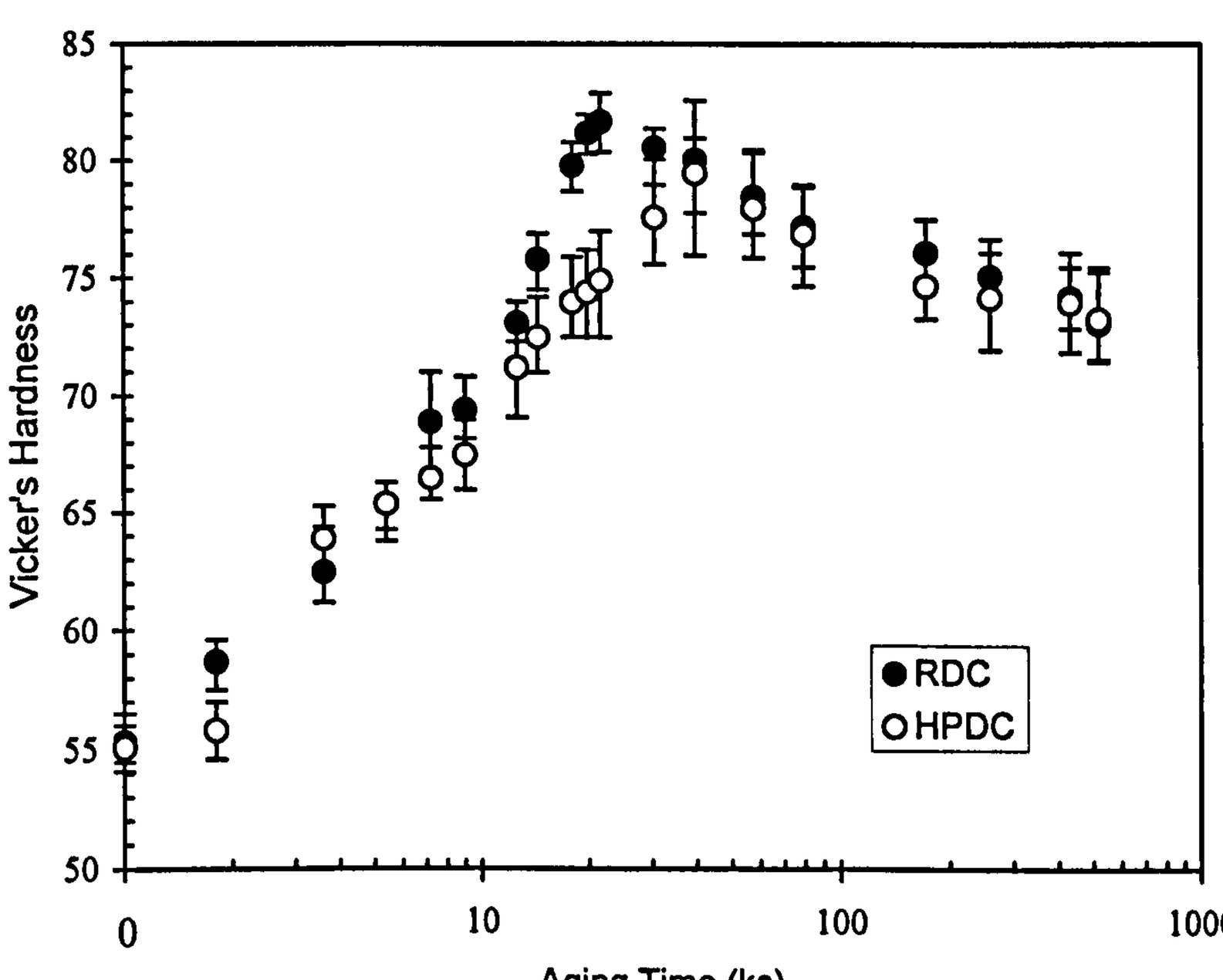

Figure 4.4.6 Age-hardening curves for the AZ91D Mg-alloy produced by the RDC and HPDC processes, aged at 216℃ after solution treatment for 24 hours at 413℃.

*Table 4.4.3 Important features of aging behaviour obtained for the AZ91D Mg-alloy**

Process	Vickers hardness after T4	Peak Vickers hardness	Incubation Time (hour)	Time to Peak Hardness (hour)
RDC	55.3	81.7	<0.5	5.5
HPDC	55.1	79.5	~1.0	11

** Solution treated (T4) at 413℃ for 24 hours followed by aging at 216℃ for up to 144 hours*

During ageing at 216 ℃ for different length of time, the precipitation of the β-phase from the super-saturated α-Mg solid solution occurs. **Figure 4.4.7** shows SEM micrographs of the RDC AZ91D Mg-alloy microstructure under different ageing states: under-aged (Figure 4.4.7.a), peak-aged (Figure 4.4.7.b) and over-aged (Figure 4.4.7 c), as defined by the age hardening curve in Figure 4.4.6.

Figure 4.4.7a shows the initial precipitation in the RDC AZ91D alloy, which had been solution treated at 413℃ for 24 hours with subsequent aging at 216℃ for 0.5 hours (1.8ks). The detailed observation of the early stage of precipitation by SEM indicated a lamellar growth of the precipitates from the grain boundaries into the grain interior, which is a typical morphology for the discontinuous precipitates of the β-$Mg_{17}Al_{12}$ phase. From Figure 4.4.7a, it is obvious that the discontinuous precipitation of the β–$Mg_{17}Al_{12}$ phase in the RDC AZ91D Mg-alloy begins at an aging time as short as 0.5 hours, and that the precipitation preferentially initiated at some of the grain boundaries. In contrast, further microstructure examination has observed no precipitates for the same alloy produced by HPDC in the same aging period. In fact, an obvious increase in hardness has been observed at an aging time of 0.5 hours (1.8 ks) for the RDC alloy, compared to 1

hour (3.6 ks) for the HPDC alloy, as shown in Figure 4.4.6. This reduction in incubation period clearly demonstrates accelerated aging kinetics for the RDC AZ91D Mg-alloy.

With the increase of aging time, the discontinuous precipitation ceases and continuous precipitates of the β-$Mg_{17}Al_{12}$ were found to form in the remaining regions of the grains that have not been occupied by discontinuous precipitates. At the peak aging time (5.5 hours), all of the grains contain the lamellar discontinuous precipitates along the grain boundaries and the platelet-shaped continuous precipitates inside the grains, as shown in **Figure 4.4.7b**.

TEM micrographs of the RDC AZ91D alloy aged at 216°C for 5.5 hours (peak-aged) are shown in **Figure 4.4.8**. Two types of precipitates are clearly seen, with the coarse discontinuous lamellar precipitate growing initially from grain boundaries into the grain, **Figure 4.4.8a**, and the fine laths forming inside the α-Mg grains, **Figure 4.4.8b**.

Figure 4.4.7c is a SEM micrograph showing the microstructure of the over-aged (solution for 24 hours at 413 °C followed by ageing at 216 °C for 120 hours) RDC AZ91D alloy. The microstructure of the over-aged condition was found to be essentially the same as the peak aged state, containing both types of precipitates of the β-$Mg_{17}Al_{12}$ phase. In **Figure 4.4.7c**, however, it reveals the precipitates of the β-phase getting coarser.

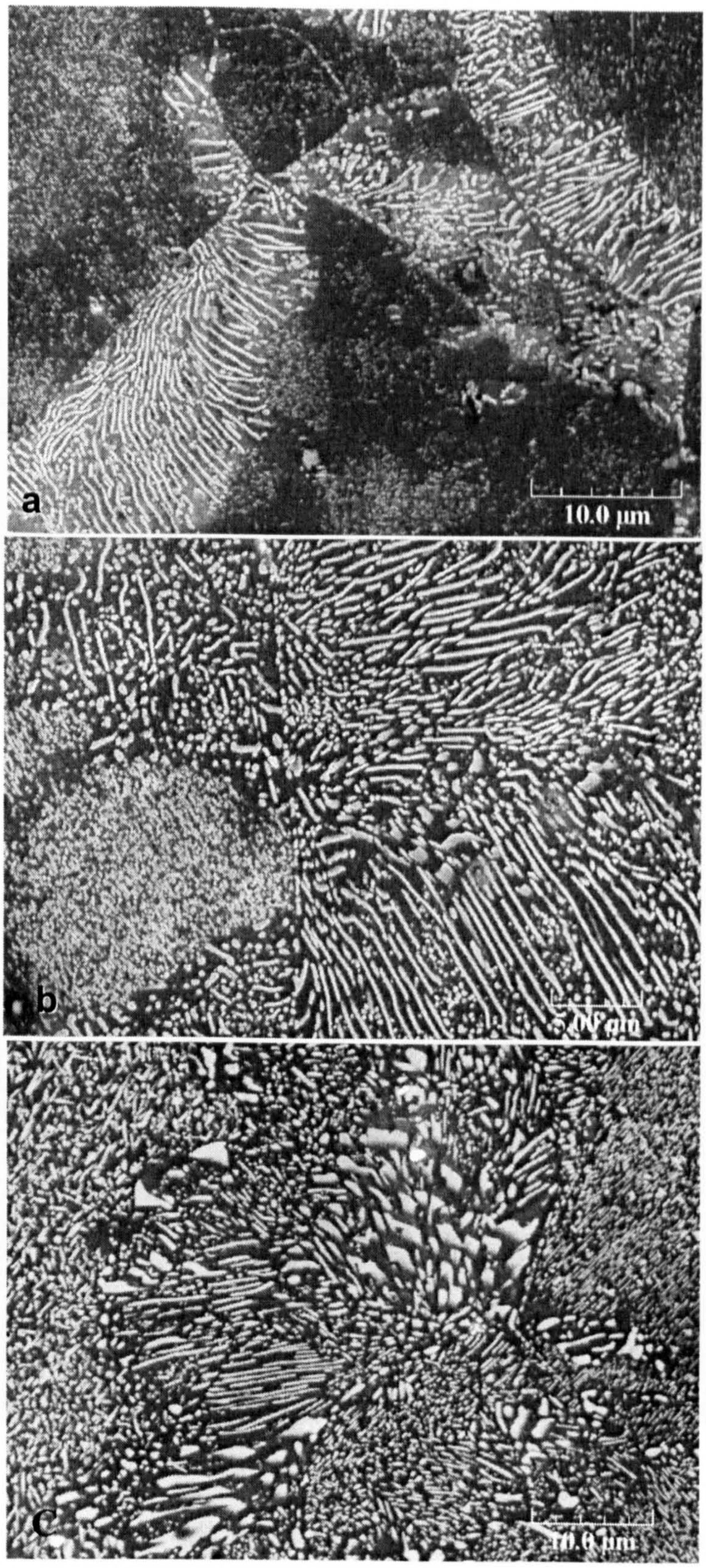

Figure 4.4.7 *SEM micrographs showing the microstructure of the RDC AZ91D Mg-alloy solution treated at 413 ℃ for 24 hours followed by aging at 216 ℃ for (a) 30 min (1.8ks, under aged); (b) 5.5 hours (19.8ks, peak aged) and (c) 120 hours (432ks, over aged).*

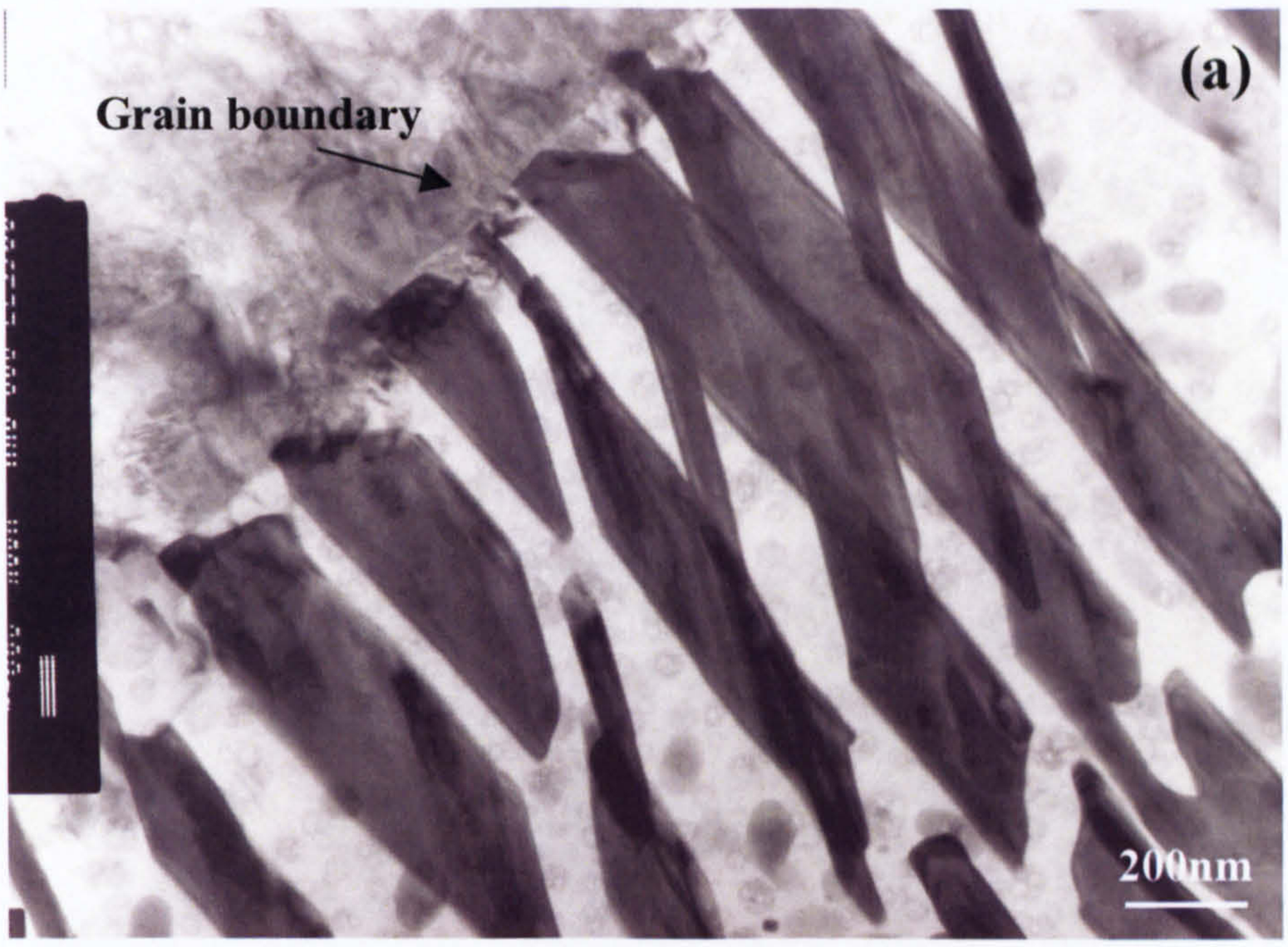

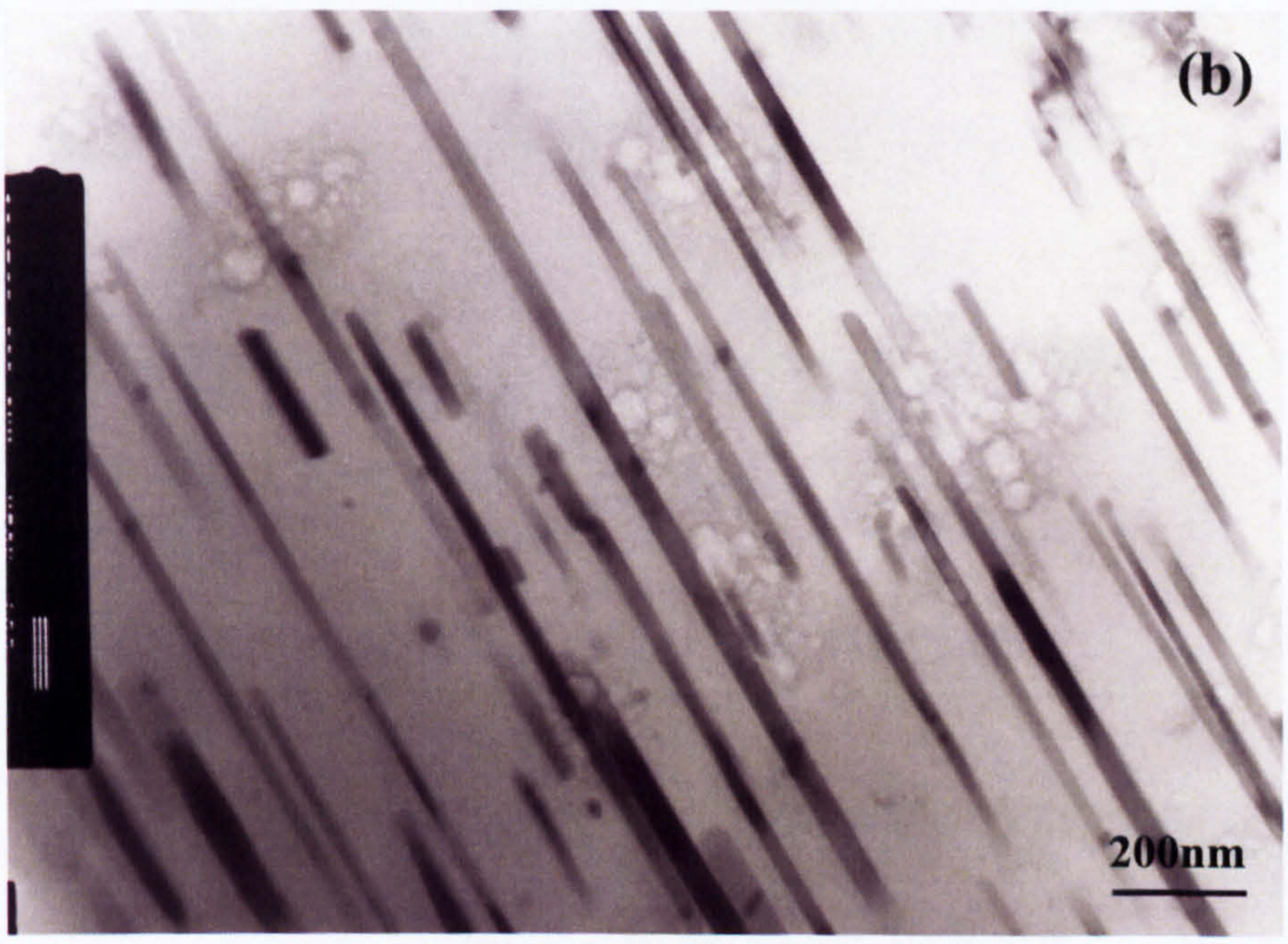

Figure 4.4.8 *TEM bright field images showing the typical (a) discontinuous precipitation along the grain boundary, with a lamellar morphology and (b) continuous precipitation inside the grain, with a needle shaped morphology. The sample is processed by RDC, solution treated at 413℃ for 24 hours and followed by aging at 216℃ for 5.5 hours.*

4.4.3 Mechanical properties of heat-treated RDC AZ91D Mg-alloy

In section 4.2.3, the Rheo-Diecasting process has been shown to improve the mechanical properties of as-cast RDC AZ91D Mg-alloy. A significant increase in elongation, up to 7.4 % for the RDC AZ91D Mg-alloy in the as-cast condition, has been demonstrated and compared with conventional HPDC and other semisolid processes. Due to the low or even eliminated porosity in RDC AZ91D Mg-alloy samples, further improvement to mechanical properties with heat treatment is possible.

The mechanical properties of RDC AZ91D Mg-alloy samples under different heat treatment conditions are tabulated in **Table 4.4.4**. Compared with the RDC as-cast condition, T4 (solution) heat treatment improves ductility substantially (the elongation is 11.2 %), but decreases strength. In contrast, T6 (solution plus aging) heat treatment improves ultimate tensile strength (the UTS is increased up to 255 MPa), with a moderate elongation. T5 (artificial aging) heat treatment slightly reduces strength and ductility of the as-cast RDC alloy in the present study.

***Table 4.4.4** Mechanical properties of RDC AZ91D Mg-alloy heat-treated under different conditions.*

Samples	Conditions	YS (MPa)	UTS (MPa)	Elongation (%)
RDC	As-cast	146±2	246±4	7.2±0.4
RDC+T4	413°C, 5 hrs	95±7	230±9	11.2±1.0
RDC+T5	216°C, 5 hrs	133±9	236±12	6.5±1.1
RDC+T6	413°C, 5 hrs + 216°C, 5.5hrs	134±9	255±9	6.7±1.1
RDC+Tx	365°C, 2hrs	132±8	249±11	9.1±1.0

In Table 4.4.4, a newly developed heat treatment for RDC AZ91D alloy, denoted as the T_x heat treatment, however, gives the as-cast RDC AZ91D Mg-alloy a further substantial improvement in tensile strength (with a UTS of 249 MPa) and ductility (the elongation is 9.1 %). Due to the low heat treatment temperature and short treatment time, a promising advantage of the T_x treatment is the economical in heat treatment cost.

4.5 Component production trials

Component production trials have been conducted to confirm the reliability of the slurry maker and consistency of the RDC process. An automotive component die, with two cavities and four sliding cores with complex geometry, was selected. The component die was originally designed for Al-alloys, and was used here for Rheo-Diecasting Mg component without any modification. The section thickness of the component varied between 2-6 mm, the runner had a thickness of 10mm and the biscuit was 60mm in diameter.

Figure 4.5.1a is a Twin-Screw Rheo-Diecast AZ91D magnesium alloy component; photographs (**Figure 4.5.1b** and **Figure 4.5.1c**) are showing the details of the thin wall and complex component produced by RDC AZ91D alloy. It shows the outstanding filling capacity and surface finish.

The structural examinations were performed by cutting 6 samples from different positions of the RDC AZ91D components, corresponding to the farthest position, the thickest section and thinnest section, as shown in **Figure 4.5.2**. Figure 4.5.2 presents a photograph of the casting, with micrographs showing the microstructures at different positions in the RDC AZ91D Mg-alloy component. Even though the magnesium alloy is more difficult to die cast, due to its low thermal capacity compared with aluminium alloy component, these successful trials indicate that the RDC AZ91D components have a very good surface finish, close to zero porosity and very fine and uniform microstructure throughout the entire casting, including the runners and biscuit.

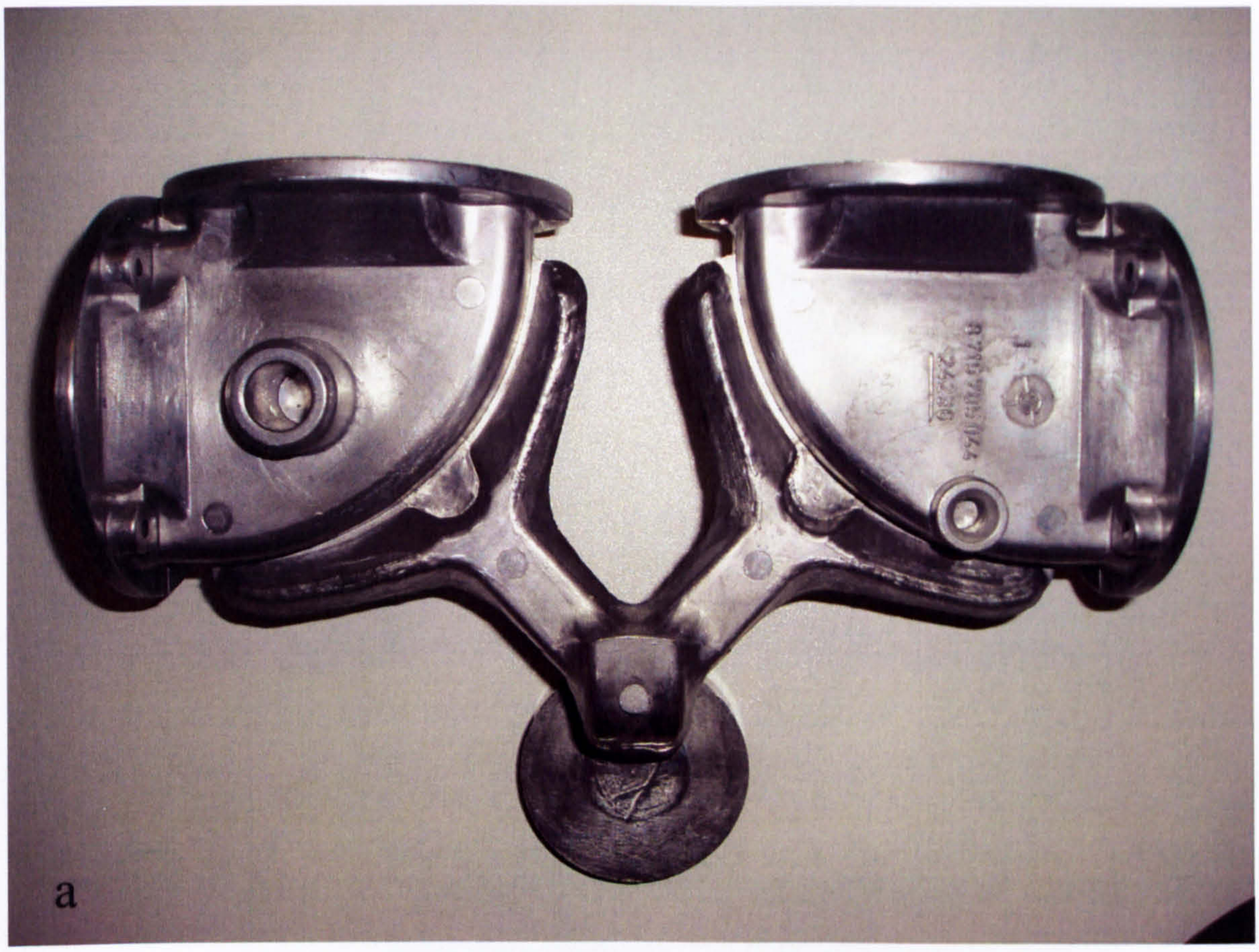

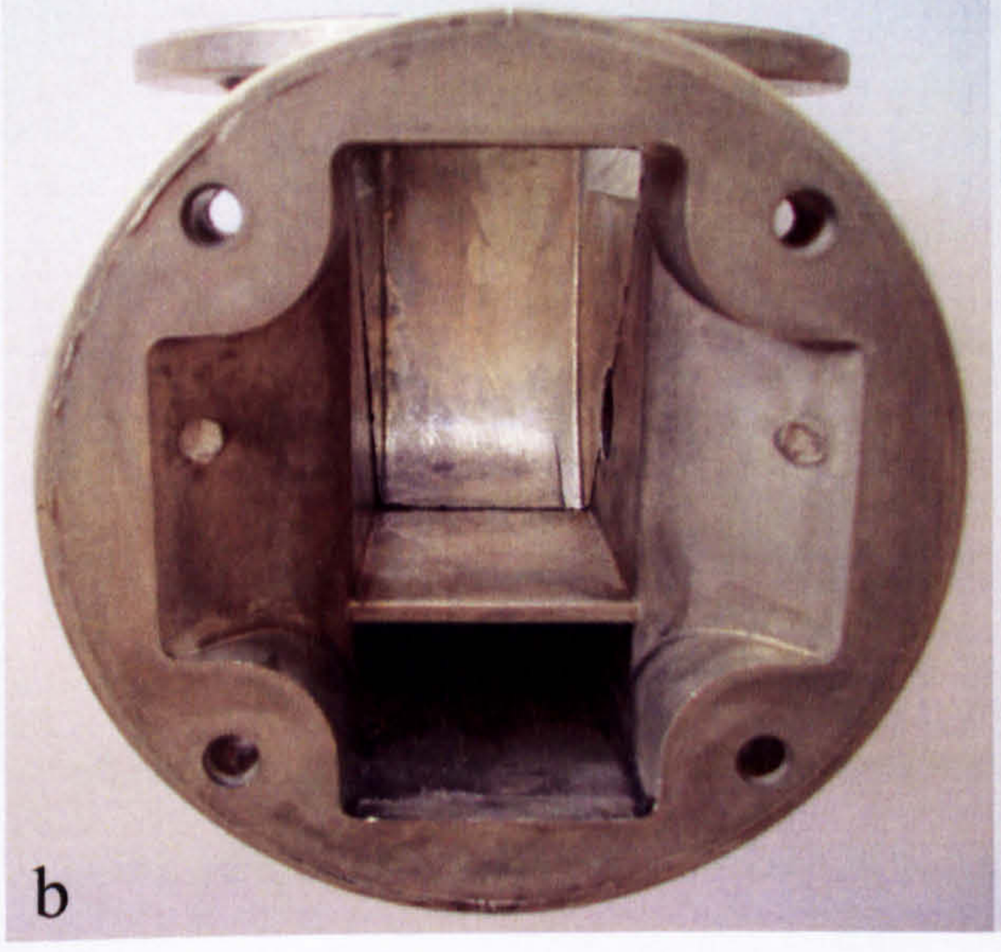

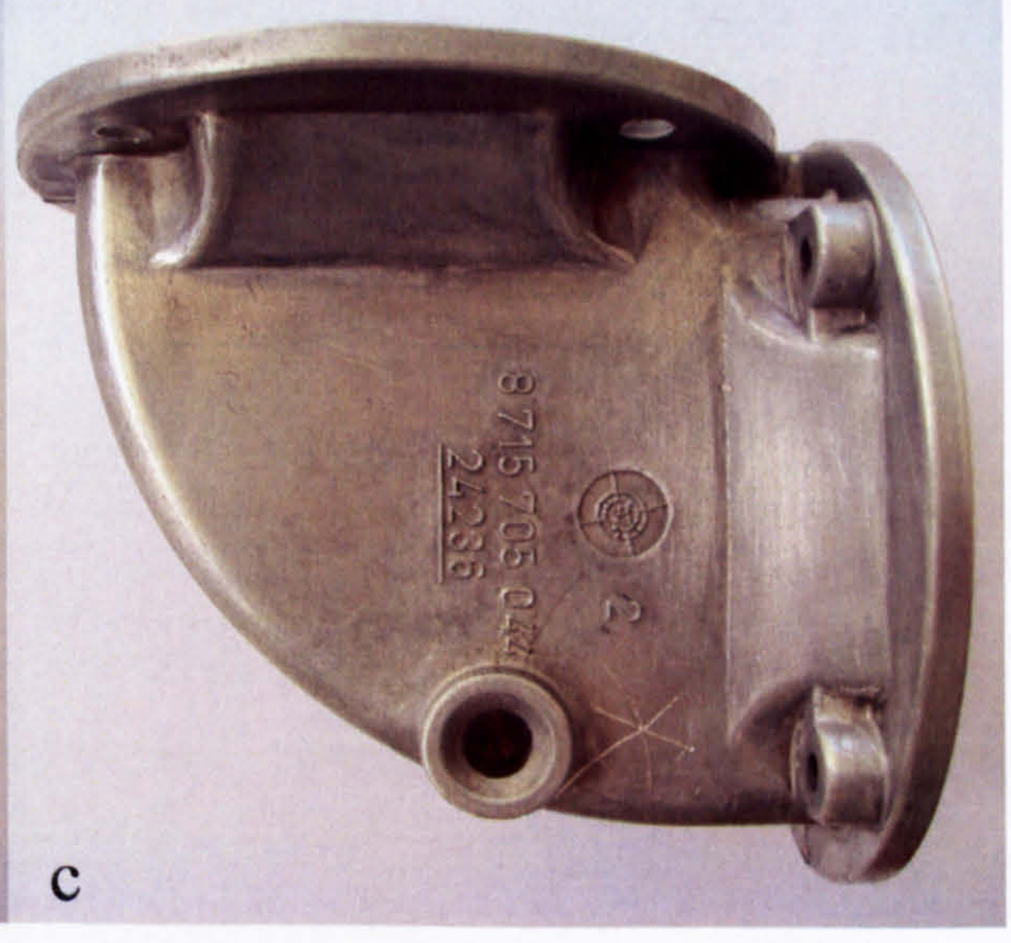

Figure 4.5.1 *(a) Photograph of a RDC AZ91D Mg-alloy component. (b) and (c) Photographs showing that RDC produced a complex and thin-wall component, exhibiting excellent filling capacity and surface finish.*

Figure 4.5.2 *Optical micrographs showing the microstructures of the RDC AZ91D Mg-alloy component at different locations.*

Figure 4.5.3b and Figure 4.5.3c show the chemical compositions (Alwt% and Znwt%, respectively) of the RDC AZ91D Mg-alloy component, as a function of test positions (shown in **Figure 4.5.3a**). Position 1 is the biscuit, 2-3 are the runner and positions 4-6 are located at various parts of the component. In Figure 4.5.3, Series A and Series B refer to two different cavities of component in one casting. Figure 4.5.3 indicates that the Al and Zn content in the RDC AZ91D sample were consistent throughout the entire casting including the runner and biscuit. The Al content varied between 8.8-9.2wt%, and Zn content was between 0.6-0.7wt%. The uniform characteristics of RDC Mg-component suggest that the Rheo-Diecasting process is particularly suitable for production of high-integrity, airtight or highly stressed components in the automotive industry.

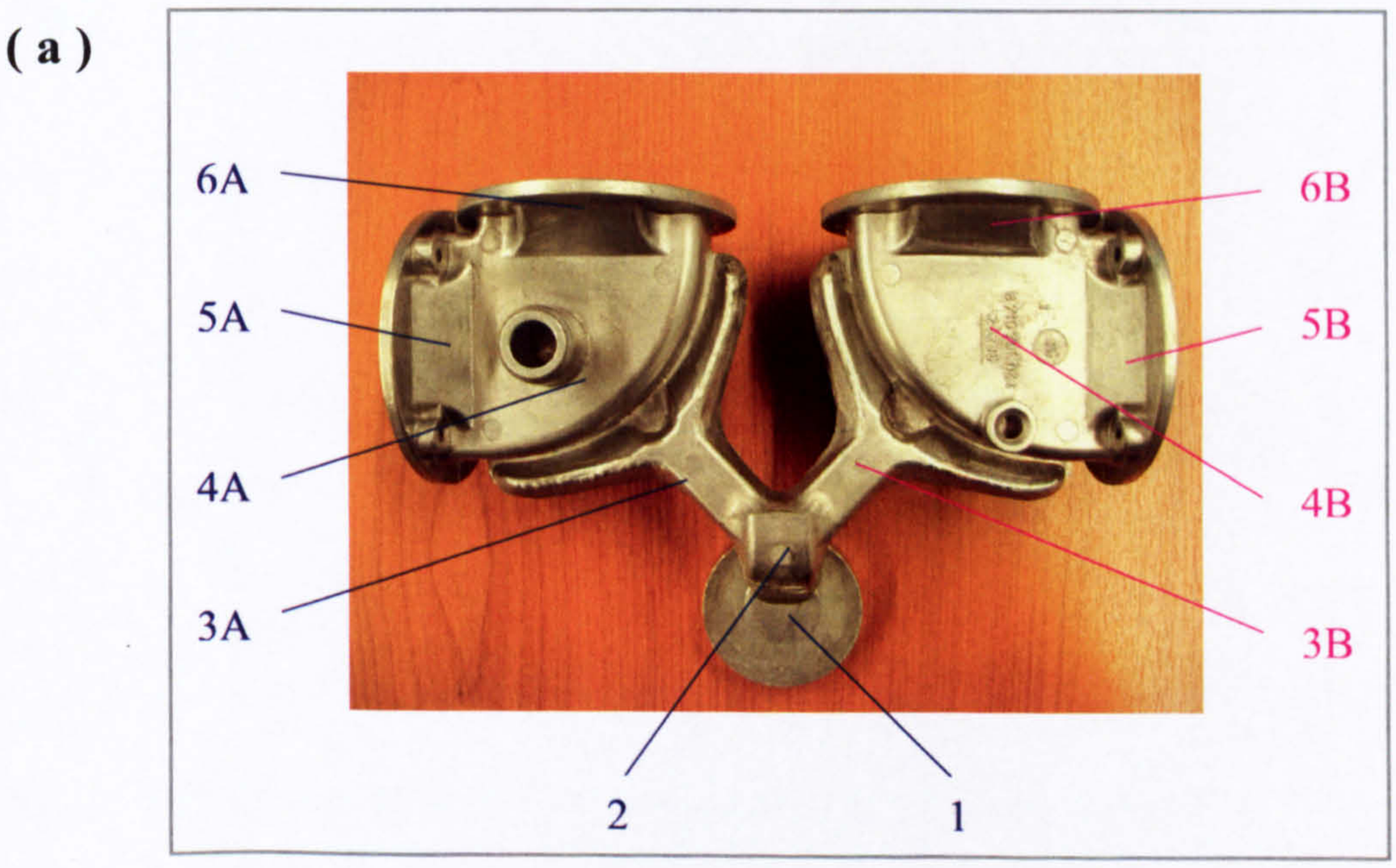

Figure 4.5.3 *The chemical compositions of the RDC AZ91D Mg-alloy component at different locations. (a) Photograph illustration the test positions. (b) and (c) are showing the composition uniformity of element Al (wt%) and Zn (wt%) in the RDC AZ91D Mg-alloy component.*

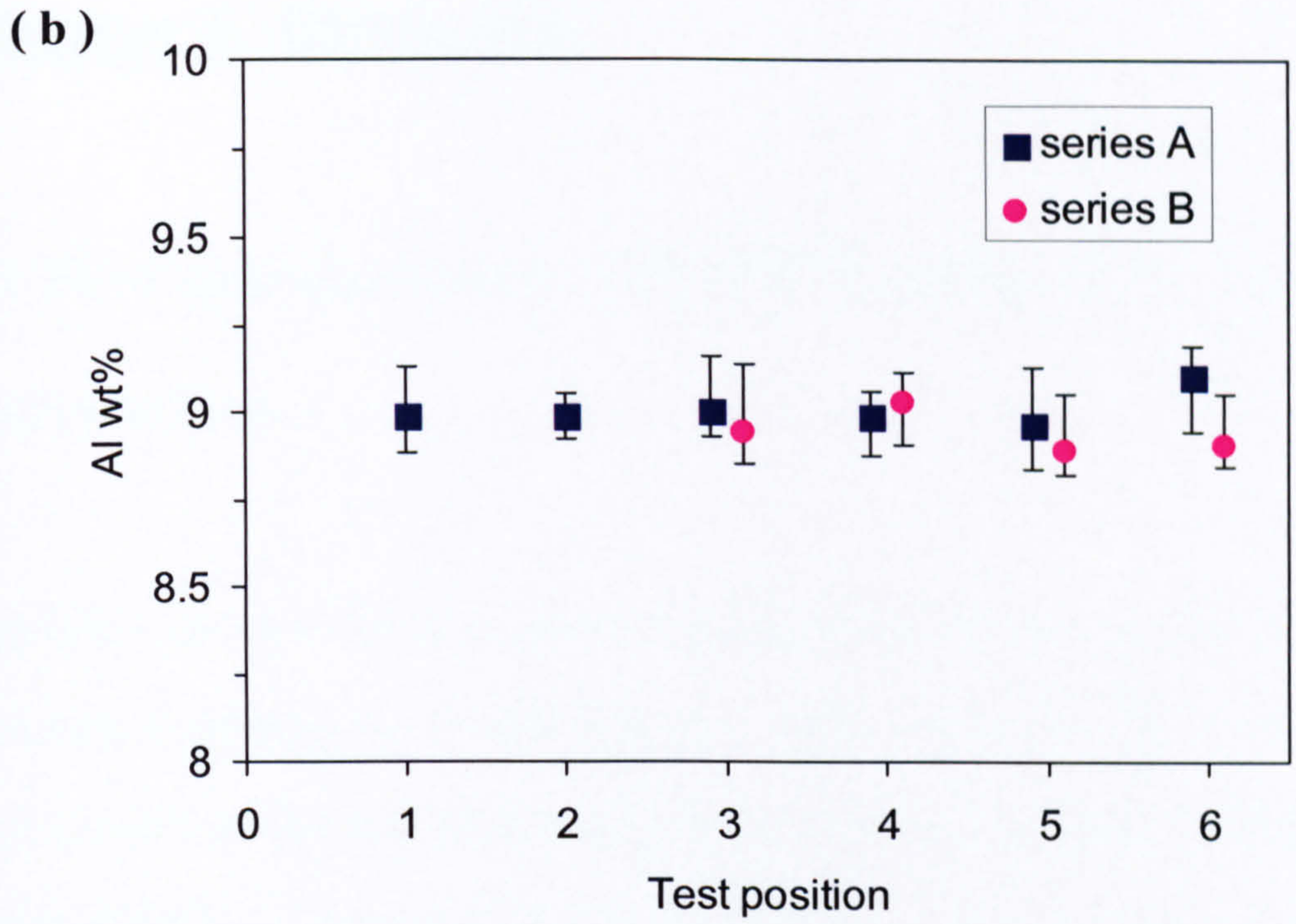

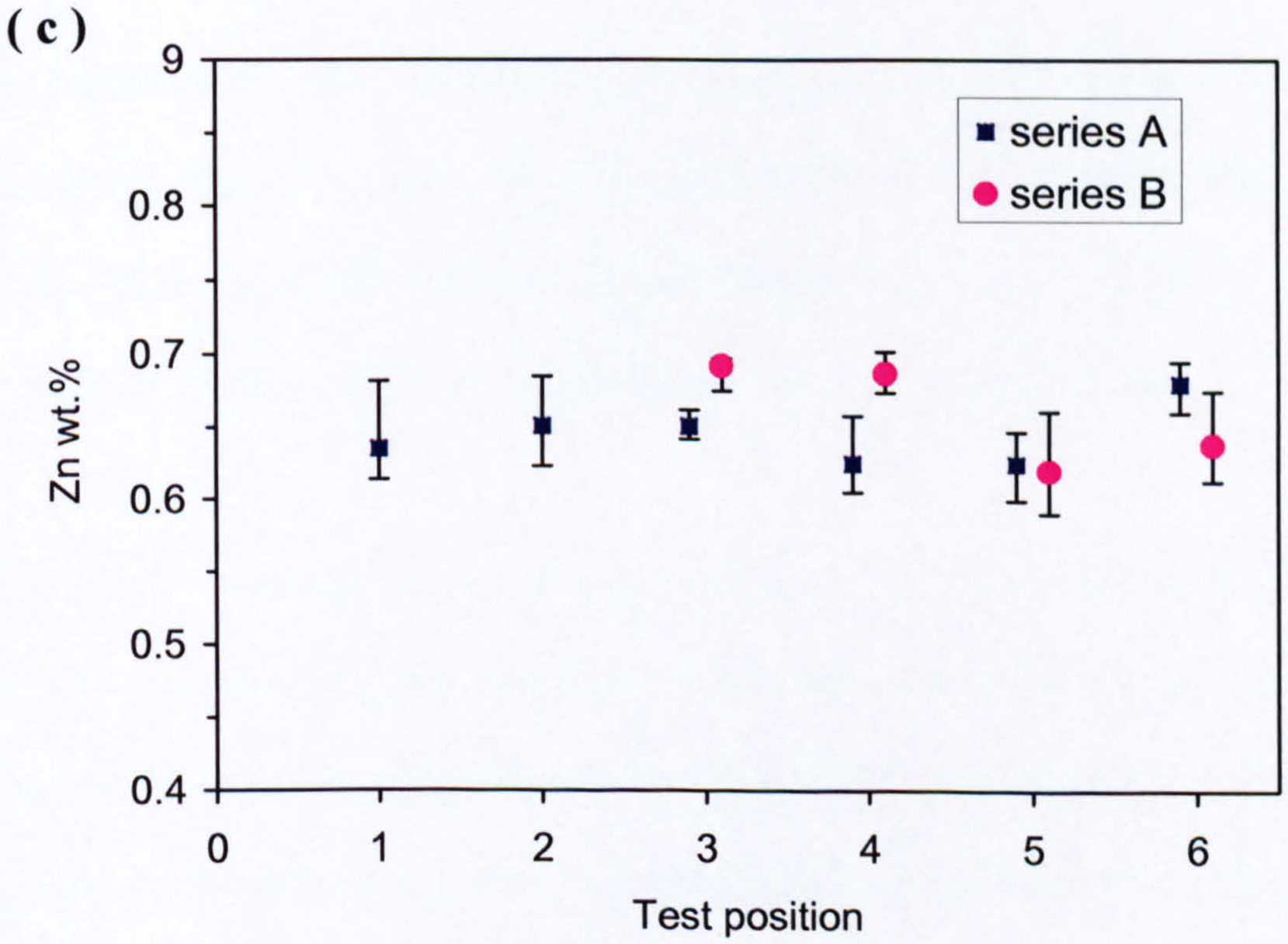

Figure 4.5.3 *(continued) The chemical compositions of the RDC AZ91D Mg-alloy component at different locations. (a) Photograph illustration the test positions. (b) and (c) are showing the composition uniformity of element Al (wt%) and Zn (wt%) in the RDC AZ91D Mg-alloy component.*

Chapter 5. Discussion

5.1 Flow characteristics of AZ91D Mg-alloy in the Twin-Screw slurry maker

Research on the rheology of semisolid slurries suggests that an ideal semisolid slurry, for semisolid processing, can be described as a suitable volume fraction of solid particles, with fine particle size and spherical morphology, dispersed uniformly throughout a liquid matrix [FAN02a]. Enhancing the effective nucleation and promoting spherical growth can obtain semisolid slurry, with these characteristics. Such conditions can be created with uniform temperature and chemistry throughout the whole volume of liquid alloy, as produced by high shear rate and high intensity of turbulence during the solidification process. These conditions can be effectively achieved by the application of the Twin-Screw Slurry Maker, which is the key technology of the RDC process.

The Twin-Screw Slurry Maker has a pair of screws rotating inside a barrel (see ***Figure 3.1***). The specially designed screws are co-rotating, fully intermeshing and self-wiping. During the slurry making process, the metal fluid flows in 'figure of 8' motions around the profile of the screws, and the 'figure of 8' moves from one pitch to the next, forming a 'figure of 8' shaped helix and pushing the fluid along the axial direction of the screws, as schematically illustrated in **Figure 5.1.1a** [FAN01]. In this continuous flow field, the fluid undergoes cyclic stretching and folding processes. This is shown schematically in **Figure 5.1.1b**. Figure 5.1.1b also indicates that the elemental volume of alloy melt will experience a cyclic variation of shear rate due to the continuous change of the gap

between the screw and the barrel. The lowest shear rate is found at the gap between the screw root and the inner barrel surface, the highest is at the intermeshing regions. Therefore, all the material in the Twin-Screw Slurry Maker will undergo a shear deformation with cyclic variation of the shear rate. In consideration of the viscosity of liquid metals, or even semisolid slurries, the intensity of turbulence inside the barrel is expected to be very high.

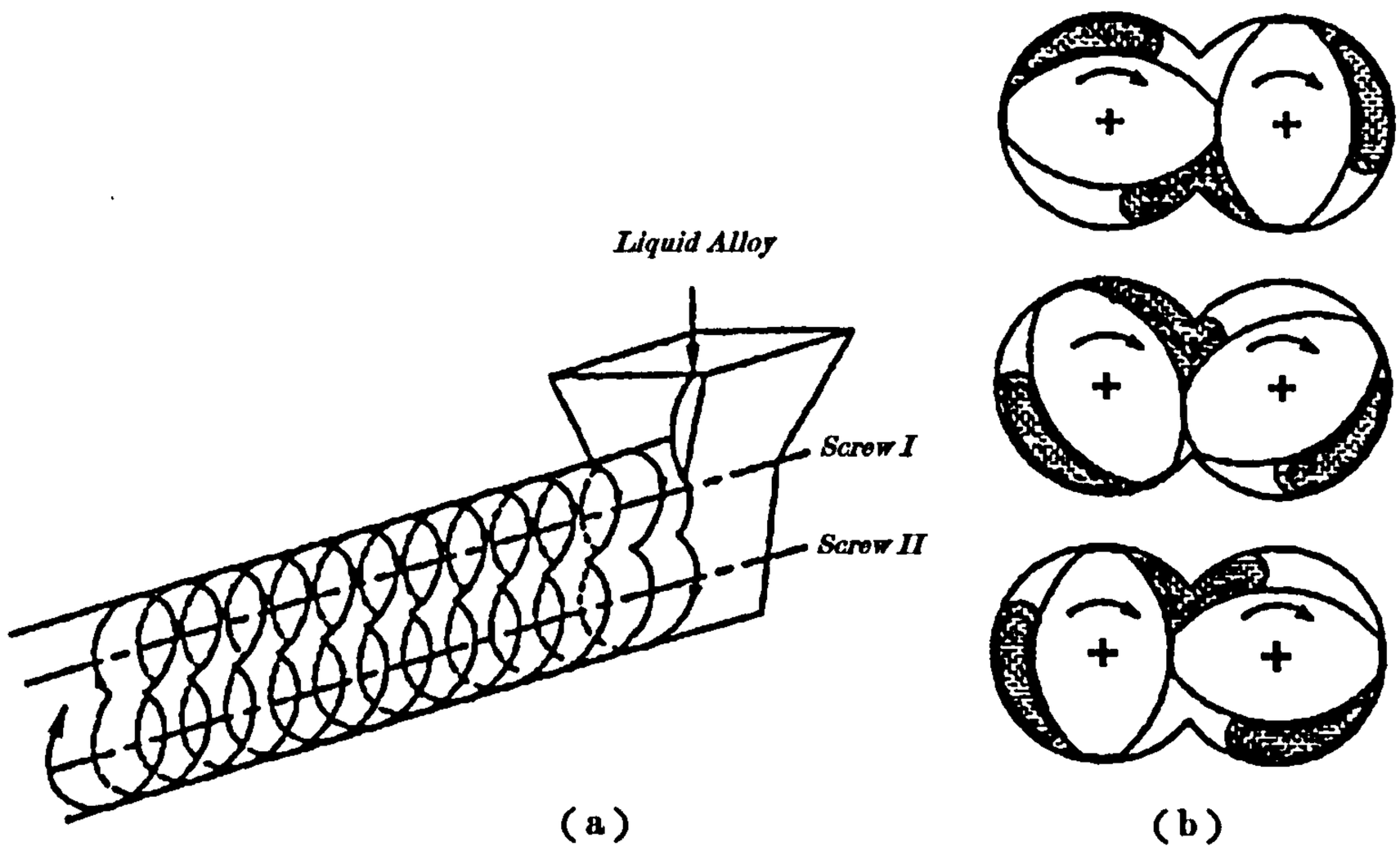

Figure 5.1.1 *Schematic illustration of the flow pattern in the Twin-Screw slurry maker. (a) The figure of 8 pattern in twin-screw channels; (b) Stretching and folding processes during the movement of the slurry from one screw to the other.*

Although the exact shear rate cannot be calculated because of the complexity of the screw geometry, the intermediate shear rate can however be evaluated by a simple equation [FAN01]:

$$\gamma = \omega\pi \left(\frac{D}{\delta} - 2 \right) \qquad \textbf{Equation 5.1.1}$$

Where D is the screw diameter, ω is the screw rotation speed and δ is the gap between the tip of a screw flight and the barrel surface. In this study, the specially designed Twin-Screw slurry maker has a maximum rotation speed of 1000 rev min^{-1}, which corresponds to a shear rate of 3663 s^{-1} in the gap between the tip of the screw flight and the barrel.

Therefore, the fluid flow in the Twin-Screw slurry maker is characterised by high shear rate, high intensity of turbulence and cyclic variation of shear rate. The characteristic of fluid flow in twin-screw maker is essential for promoting non-dendritic solidification behaviour and, furthermore, to achieve the ideal semisolid slurry.

5.2 Solidification behaviour of AZ91D Mg-alloy in the Rheo-Diecasting process

5.2.1 The progression of solidification in the RDC process

The progression of solidification in the RDC process can be mainly described in two stages, as illustrated schematically in **Figure 5.2.1** [FAN05d]. Solidification inside the twin-screw slurry maker, under intensive forced convection to produce semisolid slurry, is referred to as *primary solidification;* while the solidification of the remaining liquid, during transfer to the shot sleeve and inside the die cavity without shearing, is referred to as *secondary solidification.* The primary solidification can also be divided into two sub-stages, namely, continuous cooling, from the pouring temperature to the SSM processing temperature, and isothermal shearing, at the SSM processing temperature. The secondary solidification begins when the semisolid slurry is transferred to the shot sleeve. Due to the relatively low temperature of the shot sleeve (usually below 400°C), further volume fraction of the primary α-Mg phase is produced in the remaining liquid. However, the solidification process is continuing until all the remaining liquid finally solidifies in the die cavity, under a high pressure and high cooling rate.

5.2.2 Discussion on nucleation

The experimental results presented in section 4.3 explained the nucleation behaviour of AZ91D Mg-alloy in the RDC process. During the continuous cooling stage of the primary solidification, volume fraction of α_1 increases with shearing time (***Figure 4.3.3***),

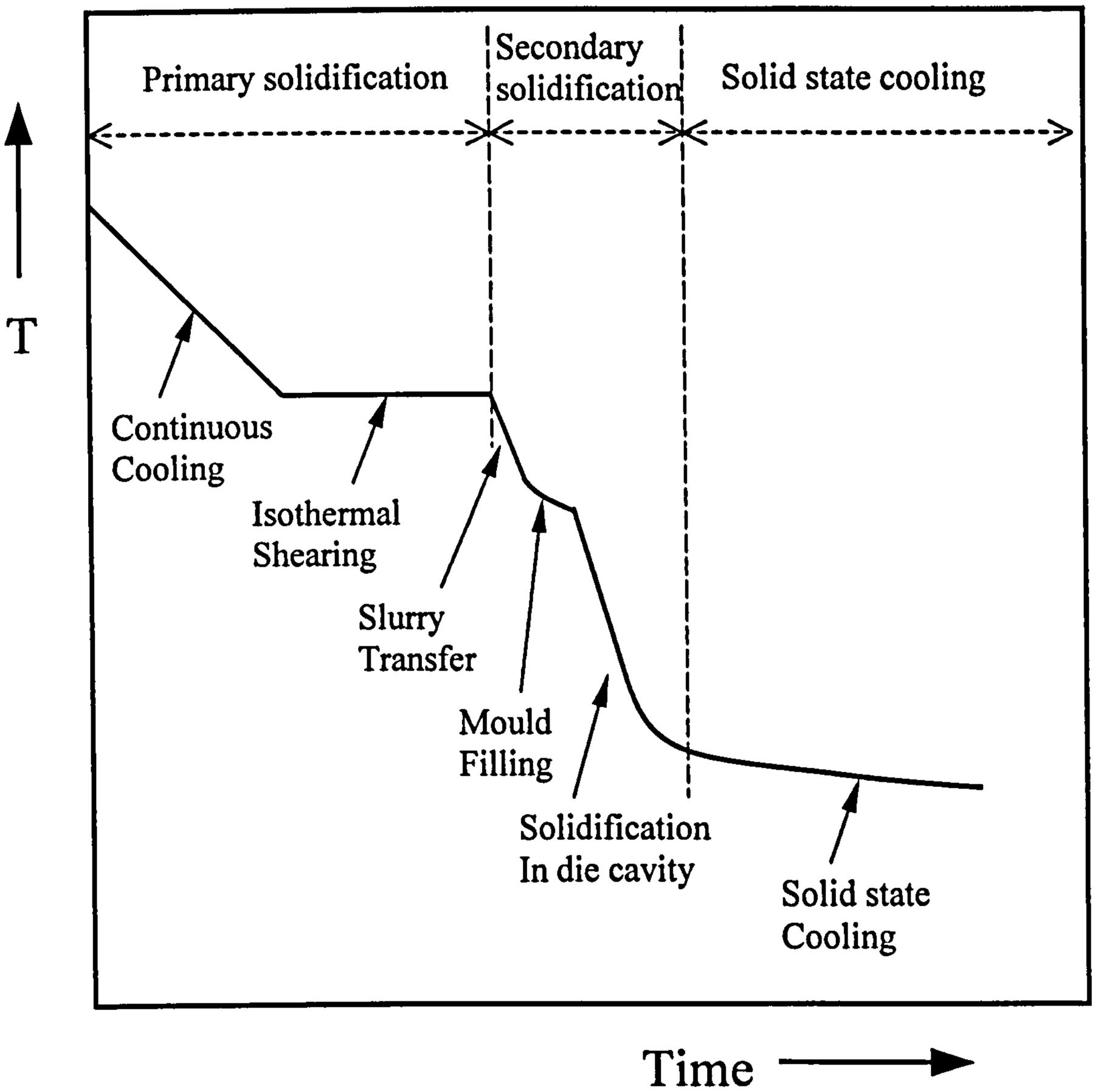

Figure 5.2.1 *Schematic illustration for the progression of solidification during the RDC process.*

as expected according to the thermodynamic prediction. However, at the same time the particle density of α_1 also increases continuously (***Figure 4.3.6***). The increased particle density during the continuous cooling stage can be explained by a continuous nucleation mechanism [FAN05d].

The continuous nucleation can be understood in terms of the competition between nucleation and growth under small undercooling. The average cooling rate during the

continuous cooling stage for AZ91D Mg-alloy in the Twin-Screw Slurry Maker is about 4K/s, which is small compared with those achieved by most of the die casting processes. Low cooling rate, in combination with intensive melt stirring, makes a small undercooling more likely during the primary solidification, leading to a relatively small nucleation rate. However, under the intensive forced convection generated by the Twin-Screw the nuclei grow spherically with an extremely fast growth rate, as will be discussed in the following section. Nevertheless, once the spherical particles reach a critical size corresponding to the solid fraction for the melt temperature, the driving force for fast growth will diminish because spherical particles are energetically stable [WAN90]. In competition with the growth of the existing primary particles, further cooling favours the nucleation of new ones. Therefore, when the temperature of the melt is reduced below the liquidus of the alloy, heterogeneous nucleation takes place, and all the nuclei will grow very rapidly to a volume fraction corresponding to the melt temperature. Further cooling of the melt under intensive forced convection will repeat the above cooling-nucleation-growth-cooling process, until the melt reaches the semisolid processing temperature.

A large nucleation rate is normally a necessary requirement for grain refinement, but not a sufficient one on it's own. The final effect of grain refinement is also dependant on the survival rate of the nuclei. In the conventional casting processes, overheated liquid metal is poured into the relatively cold mould. Heterogeneous nucleation takes place immediately in the undercooled liquid close to the mould wall. The majority of the nuclei are transferred, by the convection caused by mould filling, to the overheated liquid region and dissolved; only a small proportion of the nuclei survive and contribute to the final microstructure, resulting in a coarse and non-uniform microstructure. It is, therefore,

clear that an important step towards microstructural refinement is to make sure that every single nucleus formed during nucleation can survive and contribute to the final microstructure.

A 100% nucleus survival rate can be achieved by creating the following conditions [FAN05d]: (1) uniform temperature and chemical composition throughout the entire volume of the liquid alloy; (2) well-dispersed heterogeneous nucleation agents; (3) rapid extraction of latent heat to prevent re-coalescence. Under such conditions, nucleation will occur throughout the entire volume of the liquid and each nucleus will survive and contribute to the final solidified microstructure, producing a fine and uniform microstructure. The nucleation under such conditions has been termed by Fan [FAN05c] as effective nucleation.

As has been discussed previously in section 5.1, the melt flow inside the twin-screw slurry maker is characterised by high shear rate, high degree of turbulence and cyclic variation of shear rate. Such characteristics make the twin-screw mechanism very powerful for dispersive mixing. Consequently, the temperature and composition fields inside the slurry maker are extremely uniform throughout the entire alloy melt, during both the continuous cooling stage and the isothermal shearing stage. It is also likely that the dispersive mixing power of the twin-screw mechanism can disperse any potential agglomerates of nucleation agents, and hence increases their patency for heterogeneous nucleation. Therefore, the twin-screw mechanism is an important approach for achieving effective nucleation. This conclusion is well supported by the experimental results presented in the previous section (e.g., ***Figure 4.2.5*** and ***Figure 4.3.4***).

Based on the experimental results and discussion above, it can be concluded that nucleation under intensive forced convection in the Twin-Screw Slurry Maker is a continuous and an effective process.

5.2.3 Discussion on nuclei growth

The experimental results in ***Figure 4.3.4*** imply that growth of the primary particles after the nucleation inside the twin-screw slurry maker is very fast. This is evident by the measured particle size at the early stages of solidification, which is already around 35μm after only 3 seconds of shearing. In addition, particle growth shows the same kinetics during both the continuous cooling and isothermal shearing stages. This is contrary to the normal case, where growth occurs until the solid fraction reaches an equilibrium value and then coarsening commences. This would show a distinct change in kinetics from growth stage to coarsening stage.

The other fact established by the present experimental results is that solidification under intensive forced convection in Twin Screw Slurry Maker produces spherical particles during the primary solidification process (***Figure4.2.5, Figure 4.2.9***). This suggests that particle growth inside the twin-screw slurry maker is spherical growth, rather than dendrite fragmentation as suggested by the dendrite fragmentation theory [FLE91]. Therefore, it can be concluded that particle growth under high shear rate and high degree of turbulence is spherical and with a very fast growth rate. This conclusion is also well supported by the theoretical predictions by various techniques. Vogel et al [VOG79] theoretically investigated the effect of laminar flow on the stability of the solid-liquid interface based on the stagnant boundary layer approach, and concluded that laminar

flow enhances growth rate. More recent theoretical work has introduced turbulent flow into the solidification process. These include stability analysis using a boundary element method by Qin and Fan [QIN00], and Monte Carlo simulation by Das and Fan [DAS02]. All these studies conclude that intensive forced convection, in particular turbulent flow, during solidification promotes spherical growth with enhanced growth rate. A general agreement is that laminar flow reduces the stagnant boundary layer and causes particle rotation, resulting in a rosette type of morphology, while turbulent flow can penetrate the inter-dendritic arm space, and therefore suppress dendritic growth and promote spherical growth.

In addition, the experimental results in ***Figure 4.3.3*** and ***Figure 4.3.12*** show that increasing the intensity of forced convection decreases the solid fraction produced by primary solidification. There are two possible mechanisms responsible for such results. One of the mechanism is friction heating caused by intensive forced convection in the semisolid slurry, resulting in an increased slurry temperature and therefore a decreased solid fraction. The other possibility is that intensive shearing in the semisolid state, particularly with a high degree of turbulence, may change the energy level or even change the arrangement of atomic clusters in the remaining liquid, in such a way that the liquidus of the alloy is displaced to a lower temperature, leading to a decreased solid fraction at the primary solidification stage.

5.2.4 Discussion on particle coarsening

The experimental results in ***Figure 4.3.4*** reveal that solidification inside the twin-screw slurry maker is mainly characterised by particle coarsening, since the growth rate is

extremely fast. In addition, the solid particles have a fairly spherical morphology (with the shape factor being 0.8) in the very early stages of solidification, and prolonged shearing only slightly increases the shape factor (see ***Figure 4.3.5***). A major change occurs at the isothermal shearing stage with a decrease in particle density observed (see ***Figure 4.3.6***). Particle coarsening, under intensive forced convection, is mainly achieved by Ostwald ripening through the dissolution of the smaller particles, rather than through the diffusion of solid matters from areas with high curvature to areas with low curvature.

Ostwald ripening is described by the classical LSM theory [WAG68], which predicts that particle size (d) increases with time (t) according to the following equation:

$$d^n - (d_o)^n = k\,t \qquad \textbf{Equation 5.2.1}$$

Where d_o is the initial particle size, k is the coarsening rate constant, and n is the coarsening exponent.

Power law was used in ***Figure 4.3.4*** to extract the exponent n and the coefficient k, for different screw rotation speeds, from the experimental data. The results are presented in **Table 5.2.1**. It is interesting to note that the coarsening exponent n is much larger under intensive forced convection than that under static condition. The values for n are 8.2 and 12.7 for screw rotation speeds of 300rpm and 800rpm, respectively. The values of n are much larger than the 7/3 predicted theoretically by Wan and Sahm [WAN90] for the case of laminar melt flow. In addition, the results in Table 5.2.1 suggest that both n and k are strongly dependent on the intensity of forced convection, and that they increase with the increase in the intensity of forced convection. Therefore, the coarsening process under

intensive forced convection in the twin-screw slurry maker can be described by the following equations:

$$d^{8.2} = 1.18 \times 10^{12} t \quad \text{(at 300rpm)} \qquad \textbf{Equation 5.2.2}$$

$$d^{12.7} = 2.28 \times 10^{19} t \quad \text{(at 800rpm)} \qquad \textbf{Equation 5.2.3}$$

Equations 5.2.2 and Equation 5.2.3 suggest that Ostwald ripening is extremely slow under intensive forced convection in comparison with coarsening under static conditions. This slow coarsening rate can be attributed to the unique solidification behaviour under intensive forced convection. As discussed previously, under intensive forced convection, crystals grow in a spherical manner with an extremely fast rate. Consequently, when the primary phase reaches the predetermined solid fraction, the solid particles have a morphology close to spherical (see ***Figure 4.3.5***) and a particle size with a narrow distribution around the mean diameter. Under such conditions, the driving force for Ostwald ripening is substantially reduced, resulting in a much lower coarsening rate.

Table 5.2.1 *Summary of coarsening exponent (n) and coarsening coefficient (k) as a function of screw rotation speed.*

Screw rotation speed (rpm)	*n*	*k*
300	8.2	1.18×10^{12}
800	12.7	2.28×10^{19}

5.2.5 Solidification behavior of AZ91D Mg-alloy in the RDC process

As illustrated in ***Figure 5.2.1***, there are a total of 5 detailed solidification stages in the RDC process: continuous cooling, isothermal shearing, slurry transfer, mould filling, and in the die cavity.

During continuous cooling, which lasts about 15 seconds, heterogeneous nucleation occurs continuously and effectively throughout the entire volume of the melt, with a small undercooling. Due to the extremely uniform temperature and composition in the melt, every single nucleus survives, achieving maximum nuclei survival rate, and growth rate at this stage is extremely fast.

During the solidification, the interface morphology of the growing α_1-phase, as well as the final grain structure of the castings, are decided by the thermal conditions [SMA99] and the solute diffusion conditions [DAS02], at the solid/liquid interface. Under intensive shearing generated by the twin-screw slurry maker, the fluid flow characteristic inside the machine can mainly be described by high intensity of turbulence. Generally, the growth of the initial solid is controlled by the nature of the diffusion field existing around the liquid/solid interface. Under a turbulent flow, mass transportation in the whole of the liquid takes place by convection and liquid penetration of the interdendritic regions of the growing solid is promoted, meanwhile the rejected solute is quickly transported away from the liquid/sold interface regions. The result is a relatively uniform solute concentration at the growing solid-liquid interface, the stable diffusion fields being destabilised or even eliminated, i.e., both the temperature and composition gradient, in the solid/liquid interface, is significantly evened. Therefore, the conditions in the Twin-

Screw slurry maker promote symmetrical growth of the initial solid, resulting in the growth of the nuclei in a spherical manner. The fast and spherical growth of the continuous cooling solidification stage leads to the formation of a fine and spherical microstructure.

The isothermal shearing stage is basically a coarsening process. This is achieved through dissolution of the smaller particles. The large shape factor, achieved by spherical growth at the continuous cooling stage, limits the coarsening through mass transportation from high curvature region to the low curvature region in the same particle.

The secondary solidification starts when the semisolid slurry is delivered to the shot sleeve. Due to the low heat capacity and relatively low temperature of the shot sleeve, heterogeneous nucleation occurs in the intensively sheared liquid, and nearly all the nuclei survive. However, the surviving nuclei grow dendritically in the shot sleeve due to the absence of shearing. Such dendrites can be further fragmented when they pass through the narrow gate during the mould filling.

Inside the die cavity, the remaining liquid still has largely uniform temperature and composition fields, due to the previous intensive shearing in the slurry maker and later through the gate. Under the large cooling rate (about 10^3K/s) provided by the metallic die block, nucleation is expected to take place throughout the entire remaining liquid with a much higher nucleation rate, producing the very fine α_3 particles. It is clear from the above discussion that, the uniformity of temperature and composition in the remaining liquid is crucial to the formation of a fine and uniform solidification microstructure.

5.3 Microstructural evolution during the heat treatment of RDC AZ91D Mg-alloy

5.3.1 Traditional heat treatment of AZ91 Mg-alloy

Conventionally, AZ91 alloy cast under traditional gravity and low-pressure conditions is usually subjected to a subsequent T6 heat treatment. T6 treatment involves two steps, solution treatment at ~413°C for 16~24 hours and subsequent aging at ~168°C for 16 hours or alternatively 216°C for 6 hours [AVE99]. Solution treatment causes the β phase to dissolve, and it might be expected that subsequent quenching and aging would induce precipitation hardening. However, aging results in transformation of the super-saturated solid solution directly to a coarsely dispersed equilibrium precipitate, β phase, without the appearance of G.P zones or intermediate precipitates [CLA68]. Moreover, the β phase usually forms by discontinuous precipitation, in which even coarser cells spread out from grain boundaries. Therefore the strengthening response to aging is relatively poor.

5.3.2 Dissolution in RDC AZ91D Mg-alloy

As shown in ***Figure 4.4.1***, the faster reduction in hardness for the RDC AZ91D Mg-alloy during solution treatment can be attributed to a faster dissolution of the β-$Mg_{17}Al_{12}$, which has been verified by the microstructural observation and quantitative metallography (***Table 4.4.2***). The difference in dissolution rate of the β-phase between RDC and HPDC AZ91D alloy samples, can be explained in terms of the homogeneity of

size and morphology of the β-$Mg_{17}Al_{12}$ phase. In fact, microstructural examination of the HPDC samples revealed some coarse lumps of the β-$Mg_{17}Al_{12}$, for which it obviously takes much longer time to diffuse in order to dissolve completely. In other words, due to the presence of the coarse β-phase and large primary dendrites (***Figure 4.2.4***), the interfacial area for the diffusion of Al from β to α-phase decreases, resulting in a slow β dissolution rate for the HPDC sample. A homogenous distribution and a much finer eutectic structure throughout the entire RDC sample (***Figure 4.2.5***, ***Figure 4.2.7*** and ***Figure 4.2.11***), reduce the diffusion distance and increase the diffusion area, so that the dissolution process for the RDC AZ91D sample is relatively faster. After solution treatment for 5 hours (18ks) at 413°C, the hardness of the RDC samples almost reached its minimum value and then the hardness was essentially constant with the solution time increasing up to 24 hours (see ***Figure 4.4.1***).

During the solution treatment, dissolution of the eutectic β phase is accompanied with the redistribution of Al solute in the secondary α-Mg grains (5-10 μm in size) to the primary α-Mg globules (average 40μm in size, ***Table 4.3.3***). This process is driven by the push towards the equilibrium structure. The dissolution of the β-$Mg_{17}Al_{12}$ phase corresponds to the reduction of the hardness. It was evident that the solution treatment significantly changed the microstructure of the alloys through the dissolution of the β-$Mg_{17}Al_{12}$ phase and redistribution of solute elements, as revealed by SEM shown in ***Figures 4.4.4***. With the dissolution of the β-$Mg_{17}Al_{12}$ phase, the secondary α-Mg phase transformed its morphology and took the shape of classic grains, bounded by the sharp grain boundaries. The final grain size is dependent upon the solution temperature and the time at temperature for subsequent grain growth [CEL00].

The relation for normal grain growth in pure metals and solid-solution alloys is generally accepted as described in ***Equation 5.2.1***. Based on the experimental observations and models for grain coarsening, the coarsening exponent n can be varied within wide limits, depending on material and temperature [HU70]. Usually the value of n is larger than 2 and only approaches 2 in very pure metals or at very high temperatures. The grain growth during solution treatment of the RDC AZ91D Mg-alloy in the present study is continuous and obeys the grain growth law with the n value being found to be 2.6 (see ***Figure 4.4.5***), in between 2 and 3.

5.3.3 Precipitation in RDC AZ91D Mg-alloy

During subsequent aging of the RDC AZ91D alloy, ***Figure 4.4.8*** clearly shows that, the β-phase precipitates out from the super-saturated α-Mg solid solution in forms of both discontinuous and continuous precipitation.

In section 5.3.2, we have discussed a faster dissolution response of the RDC AZ91D Mg-alloy to solution treatment, that is, an accelerated dissolution of the β-$Mg_{17}Al_{12}$ during solution treatment at 413°C. According to the age-hardening curves, ***Figure 4.4.6***, the alloy produced by the RDC process also exhibited accelerated age-hardening kinetics compared to the HPDC alloy. Similar accelerated aging kinetics have been observed by Cerri *et al* [CER02] in their thixocast AZ91D alloy, which was subjected to 2 hours solution heat treatment at 415°C and subsequently aged at 220°C. They suggested that the faster ageing kinetics compared to HPDC alloy was probably attributed to the higher degree of super-saturation for the semisolid processed alloy. In the present study, however, such accelerated aging kinetics are not attributed to the higher degree of the

super-saturation, due to much longer solution treatment time (24 hours) at a similar temperature. Instead, the accelerated aging kinetics would be attributed to the finer and more uniform grain structure for the RDC AZ91D Mg-alloy, compared to the HPDC alloy. Despite the grain growth after solution treatment at 413°C for 24 hours, the RDC AZ91D Mg-alloy exhibited average grain size of 34.1μm in diameter, which is finer than that of HPDC alloy after the same solution treatment, being measured to be 47.6μm (see ***Table 4.4.1***). The finer grain structure provides more grain boundaries along which the discontinuous precipitation of the β-phase takes place (see ***Figure 4.4.7***), and gives more opportunities for the continuous precipitation to occur under faster age-hardening kinetics. Nevertheless, there are some very coarse α-Mg grains found in the solution treated HPDC AZ91D alloy, a result of the inhomogeneity in its as-cast microstructure. It apparently needs a longer time for the precipitation reaction of the β-$Mg_{17}Al_{12}$, either discontinuous or continuous.

Furthermore, the microstructural observation in the present study confirmed the previous investigations [CEL00][NIE02] for AZ91 alloy and revealed both the discontinuous and continuous precipitation reactions taking place during aging. The morphologies for discontinuous and continuous β-$Mg_{17}Al_{12}$ precipitates, along grain boundaries and inside grains, respectively, are coarse platelets and fine laths as revealed in ***Figure 4.4.7b,c*** and ***Figure 4.4.8***. However, the most important aspect for the study of heat treatment is the revelation of the accelerated solution and ageing kinetics for the RDC AZ91D Mg-alloy. In fact, both the solution and aging period for the RDC AZ91D Mg-alloy can be much reduced compared to the conventional HPDC process, which is an essential potential in reducing heat treatment cost and promoting efficiency.

5.4 Improved mechanical properties of Rheo-Diecast AZ91D Mg-alloy

Table 4.2.3 summarises a comparison of mechanical properties between RDC and other processes, for AZ91D Mg-alloy. From Table 4.2.3 it can be concluded that the mechanical properties of castings depend strongly on the varied fabricating route. The tensile properties of the investigated RDC AZ91D Mg-alloy are evidently higher than those of the same alloy produced by typical HPDC methods or other SSM casting processes.

It is well known that the mechanical properties of cast alloys are strongly influenced by a variety of casting defects. A larger amount of defects produce a lower UTS and elongation. Conventional die-castings are especially prone to high levels of porosity due to the high velocity splash of molten metal during the die filling. Contrarily, due to the stable laminar flow of the semisolid slurry as it enters the die, the Rheo-Diecasting process results in low levels of porosity (reduced to 0.3%-0.5%), with a fine and uniform microstructure. This in turn will lead to higher strength and elongation compared with samples obtained by other processing techniques, as shown by the comparison in ***Table 4.2.3.*** The UTS is 248 MPa and elongation is up to 7.4%, in the present study for RDC AZ91D Mg-alloy. In addition, the yield strength and other tensile properties of the Mg-alloys have a strong dependence on grain size [AND03]. For the RDC samples the microstructure is fairly constant in terms of grain structure (see ***Figure 4.2.5***). It is reasonable to expect a fairly constant yield strength as measured around 146 MPa.

In the RDC microstructure, the divorced eutectic β-phase forms a discontinuous network and fine distribution. The β-phase in the RDC samples is a harder intermetallic compound, and in the form of a divorced eutectic with fine distribution, is expected to be beneficial mechanical properties.

Under T4 heat treatment condition, the RDC AZ91D structure transforms into a single α-phase structure through solid solutioning, eliminating the relatively brittle β-phase network (see ***Figure 4.4.3*** and ***Figure 4.4.4***). Consequently a much-improved elongation is expected (11.2 %), as confirmed by the experimental results presented in ***Table 4.4.4***. Ageing of the RDC samples produces coarse laminar $Mg_{17}Al_{12}$ precipitates, through initially discontinuous precipitation at grain boundaries and then continuous precipitation in the grain interior, as shown in ***Figure 4.4.7***. Due to the incoherent nature of the β-precipitates in the α-Mg phase, the precipitation strengthening effect is relatively weak. This explains why only a moderate increase in strength of the RDC samples can be achieved by heat treatment under both T5 and T6 conditions, see Table 4.4.4. The investigations on heat treatment of RDC AZ91D Mg-alloy, indicate that the T4 is an effective heat treatment for improving the ductility of the as-cast RDC samples, and that both T5 and T6 slightly improve the tensile mechanical properties under the present experimental conditions. However, a newly developed, energy efficient heat treatment (denoted as T_x) has exhibited a superior combination of tensile properties for RDC AZ91D Mg-alloy, as summarised in Table 4.4.4. The substantially improved ductility, together with the high level of strength, provided by the RDC process and the subsequent specially developed T_x heat treatment, will provide the opportunities to promote wider applications of Mg-alloys.

5.5 Advantages of Rheo-Diecasting of magnesium alloy

In summary to our comprehensive experiments and studies, a number of advantages for the Rheo-diecasting of Mg-alloy have been clearly revealed.

(A) Fine and uniform microstructure

The microstructure is extremely fine and uniform, resulting from enhanced nucleation and spherical growth during solidification, under high shear rate and high intensity of turbulence in the Twin-Screw slurry maker, as demonstrated in ***Figure 4.2.5***, ***Figure 4.2.7*** and ***Figure 4.2.8***. This uniformity gives rise to less chemical segregation or micro-segregation (see ***Figure 4.2.13*** and ***Figure 4.5.3***), superior structure integrity and isotropy (***Figure 4.5.2***). Additionally, magnesium oxides are also found to be fine, spherical and well-dispersed, reducing or eliminating any detrimental effects (***Figure 4.2.14***). These characteristics of the RDC microstructure all contribute to further enhanced mechanical properties.

(B) Much reduced cast defects

In the RDC process, tendencies to form solidification shrinkage and porosity are much reduced, as the feeding magnesium alloy has up to 40% free flowing solid at the time of injection, as demonstrated in ***Figure 4.1.9***.

In castings, volumetric shrinkage is a result of the much lower density of the liquid state compared to the solid state. The reported density of liquid magnesium is 1.59g/cm^3, at its melting point [AVE99], in contrast to 1.74g/cm^3 for the density of solid magnesium.

Clearly, the presence of solids during the Rheo-Diecasting process will reduce the volume shrinkage proportionally to the amount of solid fraction in the feeding slurry.

In addition, a distinct feature of the semisolid slurry is the viscous flow. The vigorously agitated metals at 40%-50% solid have viscosities typically in the range of 0.1Pa.s to 10 Pa.s, this is two to four orders of magnitude higher than the viscosities of fully liquid metals [CAH96]. Therefore, the presence of a volume fraction of solid particles, which are fine and spherical as controlled by the RDC process, not only results in reduced solidification shrinkage, but also ensures a viscous flow to achieve the subsequent stable laminar mould filling (see ***Figure 4.1.9***), eliminating the tendency of air entrapment. The much lower porosity level has been introduced in this study, which is in the range of 0.3%-0.5% for RDC AZ91D Mg-alloy.

(C) Improvement to mechanical properties

As discussed in section 5.4, the unique microstructure and much lower level of casting defects produced in the RDC AZ91D alloy samples, leads to higher strength and superior elongation compared with samples obtained by other processing techniques, see ***Table 4.2.3***.

(D) Cost saving and high productivity

RDC is an economic process, with production rates similar to high-pressure die-casting process. In the RDC process, the component shaping system and the slurry making system are parallel. Once the SSM slurry is transferred to the HPDC machine, the slurry supply system starts to prepare slurry for the next shot. The slurry making process is more efficient (around 30 seconds) than component shaping process, therefore, the cycle

time of the RDC process is determined by the component shaping process. Consequently, the RDC process has an equivalent or even shorter cycle time than the conventional HPDC process, since a SSM Mg-slurry feed has less heat to be removed than a fully liquid feed. The result of the low processing temperature and low heat capacity of magnesium, is a shortened production cycle time and hence a high productivity.

In addition, the RDC process is suitable for use with conventional Mg-alloys, which are freely available in the market, eliminating the need for specially preparing of feedstock materials. Compared to Thixo-route, the associated cost saving from material preparation alone in the Rheo-route is considered up to 40% [HAL00].

(E) Tight dimensional control

The RDC process has demonstrated that it is suitable for producing high quality magnesium components with varying section thickness, see ***Figure 4.5.1***. The RDC process utilises semisolid metal slurries, which have close-to-ideal microstructure and outstanding flow behaviour, resulting in forming stresses much lower than for solid metals and comparable with liquid metals. This enables near-net forming of intricate and thin-walled Mg-alloy parts with less constriction and higher dimension precision.

(F) Longer die life

Another distinct feature for RDC process is the much-reduced casting temperature. Comparing the casting temperature of the melt in Mg die-casting and in the RDC process, the casting temperature is 50-100°C lower than that used in conventional die-casting, as tabulated in **Table 5.5.1** (data is collected from references

[AVE99][MEL][DAS06]). It is clear that the semisolid magnesium slurry filling the die at a much lower temperature results in a lower thermal shock to the die and lower sticking tendency, compared with normal die-casting. Therefore, die life can be extended several times.

***Table 5.5.1** Typical casting temperatures of Mg alloys in RDC and HPDC process (data collected from references [AVE99][MEL][DAS06]).*

Alloy	Solidus and Liquidus °C	Casting Temperature °C	RDC Temperature °C
AZ91	468-598	640-675	580-598
Electron21	545-640	>680	620-640
AM60	565-615	650-680	600-615
AM20	543-630	670-705	610-630
ZA105	450-585	650-680	550-585
ZK60	450-636	>676	615-636

(G) Other advantages

Furthermore, the following advantages of RDC process have been identified in our studies:

- The RDC process can be achieved by simply attaching the slurry maker to a standard cold chamber HPDC machine, without any modification.
- RDC components can be subjected to full heat treatment for enhancing mechanical performance without compromising the surface quality and dimensional control.
- Well-dispersed oxide particles, with fine size and spherical morphology are achieved by the dispersive mixing power of the Twin-Screw mechanism.
- Lower scrap rate of the RDC Mg-alloy, which is recyclable.

Chapter 6. Conclusions

1. The primary particles in the RDC samples are very fine and spherical (mean size around 40μm); with the primary solid phase uniformly distributed throughout the entire cross section of the RDC samples. Concentrations of Mg and Al inside the primary α-Mg particle are fairly constant.

2. The secondary solidification in the shot sleeve is usually of a dendritic morphology, and resulting microstructure from solidification in the die cavity is extremely fine α-Mg granules (nominal size of 5-10μm) mixed with the non-equilibrium eutectic network. The eutectic structure in RDC AZ91D alloy is completely divorced.

3. Solidification inside the TSSM occurs in two stages: continuous cooling and isothermal shearing. The particle density increased with the increase of shearing time during continuous cooling stage, while at the isothermal shearing stage it decreased with further increase in shearing time. The increase in particle density implies that continuous nucleation occurs during the continuous cooling stage, while the decrease in particle density suggested that Ostwald ripening takes place with an extremely slow coarsening rate.

4. Intensive shearing partially suppresses the formation of primary phase during primary solidification, promotes the formation of primary phase in the shot sleeve, but does not affect the total volume fraction of the primary phase.

5. The solution treated RDC AZ91D alloy demonstrates an important characteristics of accelerated dissolution of the β-$Mg_{17}Al_{12}$ phase compared to the HPDC sample. In subsequent ageing treatments, the RDC AZ91D alloy also exhibits an important attribute of accelerated age-hardening behaviour.

6. The as-cast state of RDC AZ91D alloy has improved ultimate tensile strength and yield strength. More importantly, the RDC process offers a substantial increase in tensile elongation compared to that obtained from both HPDC process and other semisolid processing techniques.

7. Due to the fine microstructure and improved mechanical properties, the RDC process has proved to be particularly suitable for production of Mg-alloy components of higher integrity and superior performance.

Chapter 7. Suggestions for further work

This study has been focused on the optimisation of the RDC process for improved microstructure and mechanical properties of AZ91D Mg-alloy under the laboratory conditions. It has identified a number of advantages of the RDC process over the conventional HPDC process and other SSM processing technologies. The scientific understanding has been concentrated on solidification behaviour of AZ91D alloy under intensive forced convection provided by a twin-screw mechanism. However, this study can only be treated as a starting point for further detailed studies on both technological development and scientific understanding. It has opened many new directions for future research. In this chapter, some of the major research directions identified as a direct consequence of the work presented in this thesis are presented as follows:

- **Process development:** To realise the full potential of the RDC process as a viable industrial technology, further technological development is required to test the technology in an industrial production environment. The research along this direction should be on the robustness of the twin-screw slurry maker, the reliability of the temperature control system and the interface between the slurry maker and the HPDC machine.

- **Rheo-Diecasting of other Mg-alloys:** So far, the RDC process has only been applied to Mg-based cast alloys, such as AZ91 and AM50. The indication from this work is that the advantages of the RDC process identified for AZ91D alloy should be equally valid for other Mg-based alloys. To realise the full potential of

the RDC process, further processing research should be focused on wrought Mg-alloys (e.g., AZ31), creep resistance alloys (e.g., AJ62).

- **Mg-alloys specially designed for the RDC process:** The current commercially available Mg-alloys were developed about 50 years ago for either HPDC process or other casting techniques. They are usually not suitable for heat treatment. Special alloys should be developed to exploit the full advantages of the RDC process, such as heat treatability, tolerance to freezing range, divorced eutectic structure and more compacted morphology of the intermetallic compounds.

- **Processing of metal matrix composites (MMCs):** The dispersive mixing power of the twin-screw slurry maker can be utilised to produce MMCs under the semisolid conditions. Ceramic powders with a fine particle size can be introduced into a Mg-based semisolid slurry, and dispersed uniformly by the twin-screw mechanism. This will be followed by component shaping using the HPDC process. It is anticipated that the RDC MMC components should have much improved ductility and toughness compared with those produced through the conventional route.

- **Fatigue properties of the RDC Mg-alloys:** The RDC Mg-alloys exhibit fine and uniform microstructure throughout the entire casting, much reduced (or even eliminated) casting defects. All these are expected to be beneficial to improved fatigue properties due to the elimination of the stress concentration points for fatigue crack initiation. Further research should be focused on testing of the RDC sample to establish such advantages.

- **Corrosion resistance of the RDC Mg-alloys:** The RDC process produces Mg-alloy components with extremely uniform chemical compositions through solidification under intensive forced convection. Therefore, the corrosion resistance of the RDC Mg-alloys is expected to be much better than those processed by the conventional casting routes. Research along this direction should be focused on establishing the corrosion behaviour of the RDC samples and understanding the mechanisms for improved corrosion resistance.

- **Increased in-house recycling of Mg-scrap through the RDC process:** It is demonstrated in this study that the oxide particles and intermetallic compounds in the RDC samples have a compact (usually spherical) morphology, find particle size and uniform distribution throughout the entire component. The implication of this result is that more scraps can be recycled in-house without sacrificing the mechanical and corrosion performance of the RDC components. Further research work is required to establish the advantages of the RDC process on direct recycling of scraps.

References

[AGH04] E.Aghion, D.Eliezer: Magnesium Alloys, S.Neaman Inst., Israel, 2004, p176, p191, p217, p293.

[AGU04] J.Aguilar, M.Fehlbier, T.Grimmig, and A.B.Polaczek: in Proceedings of the 8th International conference on Semisolid processing of Alloys and Composites, Limassol, Cyprus, 2004, 11-3.

[AND03] P.Andersson, C.H.Caseres, and J.Joike: Materials science forum 419-422(2003) 123.

[ANT96] F.S.Antonin, M.Suery, P.Meneses, and F.Moret: Journal of Nuclear Materials, 233-237B (1996) 935.

[AST81a] ASTM Standards, American Society for Testing and Materials, part7, 1981, B199-72, E8.

[AST81b] ASTM Standards, American Society for Testing and Materials, part10, 1981, E23.

[AVE99] M.M.Avedesian, H.Baker: Magnesium and Magnesium Alloys, ASM International, Materials Park, OH, USA, 1999, p73, P90, p230.

[BAK92] H.Baker et al.: Metals Hand book, ASM International, tenth edition, 1992, p456.

[BAL01] A.Balasundaram, and A.M.Gokhale: in Magnesium Technology 2001, TMS, 2001, p155.

[BAR95] J.P.Barnak, A.F.Sprecher, and H.Conrad: Scripta Metallurgica et Materialia, 32 (1995) 879.

[BAU00] J.Baur: in Proceedings of the 6th International conference on Semisolid processing of Alloys and Composites, Turin, Italy, 2000, p289.

[BIL68] H.Biloni, and B.Chalmers: Journal of Materials Science, 3 (1968) 139.

[BLA96] S.Blais, W.Loue, and C.Plucnon: in Proceedings of the 4th International conference on Semisolid processing of Alloys and Composites, Sheffield, UK, 1996, p187.

[BOE00] W.J.Boettinger, S.R.Coriell, A.L.Greer, A.Karma, M.Rappaz, and R.Trivedi: Acta Materialia, 48 (2000) 43.

[BOW01] A.L.Bowles, J.R.Griffiths, and C.J.Davidson: in Magnesium Technology 2001, TMS, 2001, p161.

[BRA02] H.Bramann, A.B.Polaczek, and P.R.Sahm: in Proceedings of the 7th International conference on Semisolid processing of Alloys and Composites, Tsukuba, Japan, 2002, p329.

[BRO90] S.B.Brown: in Proceeding of 5th International Conference on the Modeling of Casting, Welding, and Solidification Processes, TMS, Warrendale, PA, 1990, p168.

[BRO99] E.L.Brown, and K.P.Young: Die Casting Engineering, 12 (1999) 70.

[BRU00] S.Brusethaug, and J.Voje: in Proceedings of the 6th International conference on Semisolid processing of Alloys and Composites, Turin, Italy, 2000, p451.

[BUC04] F.V.Buch, A.G.Volkswagen, and Wolfsburg: in Proceedings of the 6th International Conference on Magnesium Alloys and their applications, Wiley-VCH Verlag GmbH, Weinheim, 2004, p55.

[BUH04] A.Buhrig, and J.Aguilar: in Proceedings of the 8th International conference on Semisolid processing of Alloys and Composites, Limassol, Cyprus, 2004, 1-v.

[CAH96] R.W.Cahn, P.Haasen, and E.J.Kramer: Material Science and Technology, VCH Verlagsgesellschaft mbH, Weinheim, v8 (1996) p132-136; v15,p50.

[CEL00] S.Celotto, Acta Materialia, 48 (2000) 1775.

[CER02] E.Cerri, S.Barbagallo, M.Cabibbo, and E.Evangelista: in Magnesium technology 2002, The Minerals,Metals and Materials society, Warrendale, USA, 2002, p221.

[CHE02] J.Y.Chen, and Z.Fan: Materials Science and Technology, 18 (2002) 237, 243, 250, 258.

[CHI00] G.Chiarmetta: in Proceedings of the 6th International conference on Semisolid processing of Alloys and Composites, Turin, Italy, 2000, p15.

[CLA68] J.B.Clark,: Acta Metallurgica, 16 (1968) 141.

[COL03] G.S.Cole: in Proceedings of the second international conference on platform science and technology for advanced magnesium alloys 2003, Trans tech publications Ltd 2003, Swizerland, p43.

[CZE01] F.Czerwinski, A.Zielinska-Lipiec, P.J.Pinet and J.Overbeeke: Acta Materialia, 49 (2001) 1225-1235.

[DAS02] A.Das, S.Ji, and Z.Fan: Acta Materialia, 50 (2002) 4571.

[DAS06] A.Das, G.Liu, and Z.Fan: Materials Science and Engineering A, 419(2006)349.

[DOH84] R.D.Doherty, H.I.Lee, and E.A.Feest: Materials Science and Engineering A, 65 (1984) 181.

[EML66] E.F.Emley: Principles of Magnesium Technology, Pergamon press, 1966, p420, p437, p788.

[ESK02] G.I.Eskin, B.I.Semenov, and Y.P.Kirdeeb: in Proceedings of the 7th International conference on Semisolid processing of Alloys and Composites, Tsukuba, Japan, 2002, p397.

[FAN99] Z.Fan, S.J.Bevis, and S.Ji: PCT Patent, WO 01/21343 A1, 1999.

[FAN00] Z.Fan, S.Ji, and M.J.Bevis: in Proceedings of the 6th International conference on Semisolid processing of Alloys and Composites, Turin, Italy, 2000, p61.

[FAN01] Z.Fan, S.Ji, and J.Zhang: Materials Science and Technology, 17 (2001) 837.

[FAN02a] Z.Fan: International Materials Reviews, 47 (2002) 49.

[FAN02b] Z.Fan: in Proceedings of the 7th International conference on Semisolid processing of Alloys and Composites, Tsukuba, Japan, 2002, p671.

[FAN05a] Z.Fan, S.Ji, and G.Liu: Materials Science Forum, 488-489 (2005) 405.

[FAN05b] Z.Fan, G.Liu, and Y.Wang: Journal of Materials Science, January 29, 2006.

[FAN05c] Z.Fan: Materials Science and Engineering A, 413/4 (2005) 72.

[FAN05d] Z.Fan, G.Liu: Acta Materialia, 53 (2005) 4345-4537.

[FIN02] M.Findon, A.M.Figueredo, and M.M.Makhlouf: in Proceedings of the 7th International conference on Semisolid processing of Alloys and Composites, Tsukuba, Japan, 2002, p557.

[FLE74] M.C.Flemings, Solidification processing, McGraw-Hill (1974), New York, p33.

[FLE91] M.C.Flemings: Metallurgical Transactions A, 22A (1991) 957.

[FLE92] M.C.Flemings, S.F.Chen, I.Dienwanit, and J.A.Cornei: in Proceedings of the 2nd International conference on Semisolid processing of Alloys and Composites, Cambridge, MA, 1992, p202.

[FLE00] M.C.Flemings: in Proceedings of the 6th International conference on Semisolid processing of Alloys and Composites, Turin, Italy, 2000, p11.

[FRI00] H.Friedrich, and S.Schumann: in Proceedings of 2nd Israeli international conference on Mg Science and Technology, Dead Sea, Israel, 2000, p9.

[FRI01] H.Friedrich, and S.Schumann: in Proceedings of IMA 2001 Magnesium Conference, Brussels, Belgium, 2001, p8.

[GAL03] U.Galovsky, K.Renger: in: A.Dahle, proceedings of the 1st international light metals technology conference 2003, CAST Center Pty Ltd, 2003, p269.

[GEB00] J.C.Gebelin, C.Geindreau, L.Orgeas, P.Poyer, D.Favier, and J.L.Auriault: in Proceedings of the 6th International conference on Semisolid processing of Alloys and Composites, Turin, Italy, 2000, p155.

[GHO94] D.Ghosh, C.V.Schilt: in Proceedings of the 3rd International conference on Semisolid processing of Alloys and Composites, University of Tokyo, Japan, 1994, p85.

[GIO00] P.Giordno, F.Boero, and G.Chiarmetta, in Proceedings of the 6th International conference on Semisolid processing of Alloys and Composites, Turin, Italy, 2000, p29.

[GIO02] P.Giordano, and G.L.Chiarmetta: in Proceedings of the 7th International conference on Semisolid processing of Alloys and Composites, Tsukuba, Japan, 2002, p665.

[GRE72] P.Greenfield: Magnesium, Mills and Boon Limited, London, 1972, p11.

[HAG00] T.Haga, and S.Suzuki: in Proceedings of the 6th International conference on Semisolid processing of Alloys and Composites, Turin, Italy, 2000, p221.

[HAG04] T.Haga, M.Ikawa, P.Kapranos: in Proceedings of the 8th International conference on Semisolid processing of Alloys and Composites, Limassol, Cyprus, 2004, 15-3.

[HAL00] K.Hall, H.Kaufmann and A.Mundl: in Proceedings of the 6th International conference on Semisolid processing of Alloys and Composites, Turin, Italy, 2000, p23.

[HEL96] A.Helawell, in Proceedings of the 4th International conference on Semisolid processing of Alloys and Composites, Sheffield, UK, 1996, p60.

[HIR98] G.Hirt, K.Sommer, R.Cremer, and A.Winkelmann: in Proceedings of the 5th International conference on Semisolid processing of Alloys and Composites, Golden, CO, 1998, p157.

[HU70] H.Hu, B.B.Rath: Metallurgical Transactions, 1 (1970) 3181.

[IVA04] L.Ivanchev, and G.Govender: in Proceedings of the 8th International conference on Semisolid processing of Alloys and Composites, Limassol, Cyprus, 2004, 14-4.

[JI 00] S.Ji and Z.Fan: in Proceedings of the 6th International conference on Semisolid processing of Alloys and Composites, Turin, Italy, 2000, p723.

[JI 02a] S.Ji, and Z.Fan: Metallurgical and Materials Transactions A, 33 (2002) 3511.

[JI 02b] S.Ji, Z.Fan, G.Liu, and X.Fang: in Proceedings of the 7th International conference on Semisolid processing of Alloys and Composites, Tsukuba, Japan, 2002, p683.

[JI 05] S.Ji, Z.Zhen, and Z.Fan: Materials science and technology, submitted 2005.

[JOL76] P.A.Joly, and R.Mehrabian: Journal of Materials Science, 11 (1976) 1393.

[JUN01] B.I.Jung, C.H.Jung, T.K.Han, and Y.H.Kim: Journal of Materials processing Technology, 111 (2001) 69.

[KAT91] T.Z.Kattamis, and T.J.Piccone: Materials Science and Engineering A, 131 (1991) 265.

[KAU00] H.Kaufmann, and P.J.Uggowitzer: in Magnesium alloys and their applications, Wiley-VCH, Weinheim, 2000, p533.

[KE 04] W.Ke, E.H.Han, Y.F.Han, K.Kainer, and A.A.Luo: Magnesium science, technology and applications, ttp Trans Tech publications, Switzerland, 2004, P1.

[KEN88] M.P.Kenney, J.A.Courtois, R.D.Evans, G.M.Farrior, C.P. Kyonka, A.A.Koch, and K.P.Young: in 'Metals Handbook', Metals Park, OH, ASM International, 9 edn, 15 (1988) 327-338.

[KIM98] K.B.kim, H.I.Lee, and H.K.Moon: in Proceedings of the 5th International conference on Semisolid processing of Alloys and Composites, Golden, CO, 1998, p415.

[KIR94] D.H.Kirkwood: International Materials Reviews, 39 (1994) 173.

[KIU92] M.Kiuchi, and S.Sugiyama: in Proceedings of the 2nd International conference on Semisolid processing of Alloys and Composites, Cambridge, MA, 1992, p47.

[KOP98] R.Kopp, D.Neudenberger, M.Wimmer, and G.Winning: in Proceedings of the 5th International conference on Semisolid processing of Alloys and Composites, Golden, CO, 1998, p165.

[KOR02] Z.Koren, H.Rosenson, E.M.Gutman, Y.Unigovski, and A.Eliezer: Journal of light metals, 2 (2002) 81.

[KUR86] W.Kurz, DJ.Fisher, Fundamentals of solidification, 1986 Trans Tech publications Ltd, Switzerland, p11-12.

[LAN00] B.Landkof: in: Israeli International Conference on Mg science and technology, Dead Sea, Israel, 2000, p50.

[LAN04] J.Langlais, in Proceedings of the 8th International conference on Semisolid processing of Alloys and Composites, Limassol, Cyprus, 2004, 10-2.

[LEH85] H.Lehuy, J.Masounave, J.Blain: Journal of Materials Science, 20 (1985) 105.

[LIU98] C.Liu, Y.Pan, and S.Aoyama: in Proceedings of the 5th International conference on Semisolid processing of Alloys and Composites, Golden, CO, 1998, p439.

[LIU02] Y.Liu, Z.Fan: in Proceedings of the 7th International conference on Semisolid processing of Alloys and Composites, Tsukuba, Japan, 2002, p587.

[LIU04] Y.Liu, A.Das, and Z.Fan: Materials Science and Technology, 20 (2004) 35.

[LYO96] R.Lyon, J.F.King, and Nuttall: in Proceedings of the Third Magnesium Conference, G.W.Lorimer ed., Manchester, 1996, p99-108.

[MAD96] M.Mada, and F.Ajersch: Materials Science and Engineering A, 212 (1996) 171.

[MAT02] S.Mathieu, C.Rapin, J.Hazan, and P.Steinmetz: Corrosion science, 44 (2002) 2737.

[MEL] MEL, Electron 21 preliminary date, Magnesium Electron, Manchester.

[MID04] S.P.Midson, R.K.Kilbert, S.E.LeBeau, and R.F.Decker: in Proceedings of the 8th International conference on Semisolid processing of Alloys and Composites, Limassol, Cyprus, 2004, 10-1.

[MOD00] M.Modigell, J.Koke, R.Kopp, D.Neudenberger, P.R.Sahm, and O.Klaassen: in Proceedings of the 6th International conference on Semisolid processing of Alloys and Composites, Turin, Italy, 2000, p605.

[MOL86] J.M.Molenaar, L.Katgerman, W.H.Kool, and R.J.Smeulders: Journal of Materials Science, 21 (1986) 389.

[NAD98] NADCA: Magnesium die casting, North American Die casting Association, USA, 1998, p1, p19, p43.

[NAN90] W.S.Nan, S.Guangji, and Y.Hanguo: Materials Transactions, JIM, 31 (1990) 715.

[NIE98] F.Niedermaier, J.Langgartner, G.Hirt, and I.Niedick: in Proceedings of the 5th International conference on Semisolid processing of Alloys and Composites, Golden, CO, 1998, p407.

[NIE02] J.F.Nie: in Magnesium technology 2002, The Minerals,Metals and Materials society, Warrendale, USA, 2002, p103.

[NIS00] N.Nishino, H.Kawahara, Y.Shimizu and H.Zwahori: in Magnesium Alloys and their Applications, Wiley-VCH Verlag GmbH, Weinheim, 2000, p59.

[PAS92] L.Pasternak, R.D.Carnaha, R.Decker, and R.Kilbert: in Proceedings of the 2nd International conference on Semisolid processing of Alloys and Composites, Cambridge, MA, 1992, p159.

[PIT98] H.E.Pitts, and H.V.Atkinson: in Proceedings of the 5th International conference on Semisolid processing of Alloys and Composites, Golden, CO, 1998, p97.

[POL94] I.J.Polmear: Materials Science and Technology, 10 (1994) 1.

[POL95] I.J.Polmear: Light alloys, Butterworth Heinemann, Oxford, third edition1995, p3, 197-225.

[POR92] D.A.Porter and K.E.Easterling, Phase transformations in metals and alloys, second edition 1992, Chapman and Hall, London, p139,p185.

[POT00] R.Potzinger, H.Kaufmann, and P.J.Uggowitzer: in Proceedings of the 6th International conference on Semisolid processing of Alloys and Composites, Turin, Italy, 2000, p85.

[POW04] B.R.Powell, L.J.Oniment, J.E.Allison and P.P.Ried: in:A.A.Luo, Magnesium Technology 2004, TMS, Pennsylvania, 2004, p3.

[QIN00] R.S.Qin, and Z.Fan: in Proceedings of the 6th International conference on Semisolid processing of Alloys and Composites, Turin, Italy, 2000, p819.

[RIC03] N.Richetts, S.Cashion and R.Bailey: in: A.Dahle, proceedings of the 1st international light metals technology conference 2003, CAST Center Pty Ltd, 2003, p275.

[ROB92] B.R.Robert: Metallic Materials Specification Handbook, Chapman and Hall, London, 4th edition 1992, p1, 95, 181.

[ROV99] M.M.Rovira, B.C.Lancccini, and M.H.Robert: Journal of materials Processing Technology, 92-93 (1999) 42.

[RYO94] Y.H.Ryoo, and D.H.Kim: in Proceedings of the 3rd International conference on Semisolid processing of Alloys and Composites, University of Tokyo, Japan, 1994, p95.

[SAH98] P.R.Sahm: in Proceedings of the 5th International conference on Semisolid processing of Alloys and Composites, Golden, CO, 1998, xli.

[SAN94] S.Sannes, H.Gjestland, L.Arnberg, and J.K.Solberg: in Proceedings of the 3rd International conference on Semisolid processing of Alloys and Composites, University of Tokyo, Japan, 1994, p271.

[SCH03] S.Schumann and H.Friedrich: in Proceedings of the second international conference on platform science and technology for advanced magnesium alloys 2003, Trans tech publications Ltd 2003, Swizerland, p51.

[SCH04] S.Schumann: in Proceedings of the International Conference on Magnesium Science Technology and Applications, Beijing, China, 2004, p3.

[SCH05] S.Schumann, in: W.Ke, E.H.Han, K.Kainer and A.A.Luo, Magnesium Science,Technology and Applications. 2005 Trans Tech Publications Ltd, Switzerland, p1.

[SEQ96] W.P.Sequeira, G.L.Dunlop, and M.T.Murray: in Proceedings of the 3rd international Mg conference, Institute of Materials, London, 1996, p63.

[SHE02] M.T.Shehata, E.Essadiqi, and V.Kao: in Proceedings of the 7th International conference on Semisolid processing of Alloys and Composites, Tsukuba, Japan, 2002, A-33.

[SMA99] R.E.Smallman and R.J.Bishop: Modern physical metallurgy and materials engineering, Butterworth-Heinemann, Oxford, sixth edition 1999, p43.

[SMI91] D.M.Smith, J.A.Eadyl, M.Hogan, and D.W.Irwin: Metallurgical Transactions A, 22A (1991) 575.

[SOH02] K.Y.Sohn, B.M.Kang, C.J.Kim, and S.Y.Lee: in Proceedings of the 7th International conference on Semisolid processing of Alloys and Composites, Tsukuba, Japan, 2002, p89.

[SPE72] D.B.Spencer, R.Mehrabian and M.C.Flemings: Metallurgical Transactions A, 3 (1972) 1925.

[SUN04] S.Y.Sung, S.K.Kim, and Y.J.Kim: in Proceedings of the 8th International conference on Semisolid processing of Alloys and Composites, Limassol, Cyprus, 2004, 2-2-07.

[TAU98] G.Tausig, K.Xia: in Proceedings of the 5th International conference on Semisolid processing of Alloys and Composites, Golden, CO, 1998, p473.

[TUR91] L.S.Turng, and K.K.Wang: Journal of Materials Science, 26 (1991) 2173.

[VIV93] C.Vives, J.Bas, G.Beltran, and G.Fontaine: Materials Science and Engineering A, 173 (1993) 239.

[VOG79] A.Vogel, R.D.Doherty, and B.Cantor: in Solidification and casting of metals, The Metals Society, London, 1979, p518-525.

[WAG68] C.Z.Wagner: Electrochem. 65 (1968) 581.

[WAN90] G.Wan, P.R.Sahm: in Proceedings of the 2nd International conference on Semisolid processing of Alloys and Composites, Cambridge, MA, 1992, p328.

[WAN03] G.G.Wang, B.Froese, and P.Bakke: in Magnesium technology 2003, TMS,2003, p65.

[WAN05a] Y.Wang, G.Liu, Z.Fan: Scripta Maerialia, 54/5(2005) 903-908.

[WAN05b] Y.Wang, G.Liu, Z.Fan: Acta Materialia, 54/3(2005) 689-699.

[YOU83] K.P.Young, C.P.Kyonka, and J.A.Courtois: Fine Grained Metal Composition, US Patent 4415374, 1983.

[YUR02] J.A.Yurko, R.A.Martinez, and M.C.Flemings: in Proceedings of the 7th International conference on Semisolid processing of Alloys and Composites, Tsukuba, Japan, 2002, p659.

[ZHA03] Y.Zhang, K.Zhang, G.Liu, J.Xu, and L.Shi: Journal of Materials processing Technology, 137 (2003) 195.

Appendix

Table A-1 Volume fraction measurement for the primary α-Mg particles in the cross section of ϕ6mm RDC AZ91D alloy bars processed at different shearing temperatures. The measurements ate conducted on 3 different crossing lines, 10 equidistant areas were performed on each measured line under a magnification of 100, as sketch illustrated in Figure A-1.

Position (mm) / Vol. Fraction(%)		0-1	1-1.5	1.5-2	2-2.5	2.5-3	3-3.5	3.5-4	4-4.5	4.5-5	5-6
593°C	Line1	19.71	24.73	23.22	25.01	26.79	24.53	25.29	23.92	22.88	18.72
	Line2	20.68	23.98	26.09	23.58	25.85	22.88	24.63	25.46	22.58	19.86
	Line3	18.26	21.88	25.53	26.03	23.65	26.95	24.87	22.66	24.18	18.99
	Average	19.55	23.53	24.95	24.87	25.43	24.79	24.93	24.01	23.21	19.19
589°C	Line1	24.22	28.53	28.25	29.66	31.00	30.17	30.08	29.53	28.35	22.83
	Line2	23.82	29.16	30.67	29.31	30.07	31.03	29.29	30.02	28.95	23.98
	Line3	23.03	29.38	30.13	30.26	29.55	29.73	30.63	30.61	29.21	24.57
	Average	23.69	29.02	29.68	29.75	30.21	30.31	30.00	30.05	28.85	23.80
585°C	Line1	30.79	35.81	36.82	36.25	39.29	40.15	36.75	36.46	35.75	30.80
	Line2	32.13	35.01	37.2	36.99	40.75	41.01	37.91	37.5	36.28	31.63
	Line3	31.73	37.68	36.19	37.82	38.68	38.31	36.28	37.23	34.79	32.55
	Average	31.55	36.16	36.73	37.02	39.57	39.82	36.98	37.06	35.61	31.66

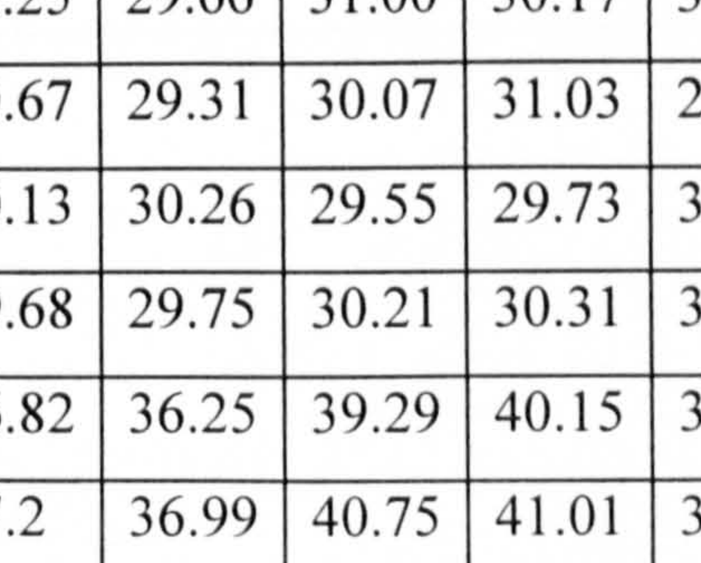

Figure A-1 Sketch illustration of the measure lines on the ϕ6mm RDC AZ91D alloy bars.

Table A-2 Defect measurement results for RDC AZ91D alloy samples with different tensile properties. The samples were selected randomly from processing optimisation according to the relative tensile properties.

	Tensile Properties		Volume fraction of defects (Vol%)					
	UTS (MPa)	Elongation (%)	1	2	3	4	5	Average
Sample1	246	7.20	0.27	0.30	0.44	0.23	0.36	0.32
Sample2	247	7.05	0.58	0.49	0.65	0.62	0.31	0.53
Sample3	238	6.69	0.78	0.81	0.52	0.85	0.59	0.71
Sample4	235	6.49	0.88	1.08	0.70	1.10	0.99	0.95
Sample5	233	6.03	1.21	0.96	0.67	1.12	1.25	1.04

Table A-3 Microstructure analysis results for RDC AZ91D alloy at different shearing time, under the shearing speed of 300rpm and shearing temperature of 593°C (Part I). All the metallographic samples were cut through the middle sections from bars labelled 'E' (see Figure 3.2), produced in different batches, at least 5 areas were performed on each sample. In these Tables (from Table A-3 to Table A-9), Fsa_1 is volume fraction of primary α_1-phase, Fsa_2 is volume fraction of primary α_2-phase, $Dena_1$ is density of primary α_1-phase, $Dena_2$ is density of primary α_2-phase, d_1 is mean diameter of primary α_1-phase. The minimum (Min.), maximum (Max.) and average (Ave.) value were tabulated.

Vol. Fraction (%) \ Time (s)		3	10	13	16	20	35	70	150
$Fsa_1 + Fsa_2$	Min.	23.95	26.95	28.66	27.79	27.73	26.95	26.98	29.82
	Max.	27.04	27.63	30.69	30.30	28.87	29.19	31.80	31.08
	Ave.	25.33	27.38	29.42	29.05	28.47	28.01	29.25	30.52
Fsa_1	Min.	6.89	12.88	14.66	19.99	20.18	18.81	20.89	21.35
	Max.	8.58	15.22	16.02	20.52	21.15	21.96	21.63	24.09
	Ave.	7.9	13.75	15.33	20.27	20.70	20.45	21.25	22.79
Fsa_2	Min.	16.43	12.33	12.89	7.80	7.55	5.45	5.76	6.99
	Max.	18.81	14.47	16.03	10.0	8.06	9.68	10.17	8.46
	Ave.	17.43	13.62	14.09	8.78	7.78	7.56	8.0	7.73

Table A-4 Microstructure analysis results for RDC AZ91D alloy at different shearing time, under the shearing speed of 300rpm and shearing temperature of 593°C (Part II).

Items \ Time (s)		3	10	13	16	20	35	70	150
$Dena_1+Dena_2$ (mm^{-2})	Min.	416.5	286.3	332.8	320.9	278.8	251.7	301.5	304.3
	Max.	501.7	357.5	365.3	369	293.3	304	335	311.5
	Ave.	464.3	314.3	349.7	343.2	285	275.1	318	307
$Dena_1$ (mm^{-2})	Min.	84.3	95.9	109	115.7	120	106.7	95.1	76.2
	Max.	89.5	113.7	113.7	137	132	115	110.8	98
	Ave.	87	107	111.6	129.7	127.2	109.3	103	85.5
$Dena_2$ (mm^{-2})	Min.	327.5	188	223.6	183.7	146.6	136.7	190.7	213
	Max.	414	243.8	253.3	233.1	173	192.3	239.7	228.6
	Ave.	377.6	207.5	238	213.5	157.8	165.7	215	221.5
d_1 (μm)	Min.	33.56	37.83	39.3	40.73	40.93	46.05	46.65	51.7
	Max.	33.83	40.88	41.0	42.75	43.37	48.7	53.3	58.3
	Ave.	33.68	39.23	40.22	41.87	42.21	47.3	48.89	54.3
Shape factor of a1	Min.	0.78	0.78	0.78	0.79	0.82	0.80	0.818	0.82
	Max.	0.80	0.80	0.816	0.825	0.83	0.823	0.84	0.85
	Ave.	0.79	0.79	0.795	0.806	0.827	0.817	0.83	0.838

Table A-5 Microstructure analysis results for RDC AZ91D alloy at different shearing time, under the shearing speed of 800rpm and shearing temperature of 593°C (Part I).

Vol. Fraction (%) \ Time (s)		3	10	13	16	20	35	70	150	200
Fsa_1+ Fsa_2	Min.	23.87	27.27	28.31	28.13	31.20	28.50	31.42	27.26	31.17
	Max.	30.17	30.76	29.93	31.82	34.13	36.22	37.83	31.25	34.71
	Ave.	27.39	29.43	29.06	29.52	32.59	32.6	33.55	29.10	33.25
Fsa_1	Min.	5.10	10.88	16.69	16.78	16.55	15.31	16.18	17.87	16.80
	Max.	12.86	15.02	17.72	18.53	18.61	19.18	18.03	20.16	19.10
	Ave.	8.43	12.93	17.19	17.72	17.39	17.57	17.23	18.85	18.01
Fsa_2	Min.	16.72	13.95	10.60	10.99	12.59	10.8	13.39	9.49	13.26
	Max.	23.05	18.23	13.04	13.29	17.16	17.08	20.27	11.09	16.53
	Ave.	18.96	16.50	11.88	11.80	15.20	15.03	16.31	10.25	15.23

Table A-6 Microstructure analysis results for RDC AZ91D alloy at different shearing time, under the shearing speed of 800rpm and shearing temperature of 593°C (Part II).

Items \ Time (s)		3	10	13	16	20	35	70	150	200
$Dena_1+ Dena_2$ (mm^{-2})	Min.	343.9	292	325.8	314.3	445.6	395	449.3	358.3	455.5
	Max.	409	448.2	360.4	355	479	460.1	556.3	368.2	496.7
	Ave.	381.8	395	340.1	330.9	467.7	432	487.3	361.6	471.6
$Dena_1$ (mm^{-2})	Min.	92.7	101	123	108.3	105.5	99.3	73.3	80.3	77.8
	Max.	105	127.7	127.7	133.1	130.2	135.5	99.7	86.6	86.9
	Ave.	98	112	125	121.5	117.3	111.8	83.5	83.2	82
$Dena_2$ (mm^{-2})	Min.	238.9	186	198	198.1	315.5	295.7	363.7	276	373.9
	Max.	315.5	334	233.8	221.5	373.2	335	465	282	419
	Ave.	283.8	283	215	209.3	350.3	320.2	403.8	278.5	389.6
d_1 (μm)	Min.	35.11	37.59	37.5	39.85	38.8	40.35	43.7	47.15	45.55
	Max.	39.25	41.95	40.91	43.17	43.96	45.2	52.16	53.6	52.32
	Ave.	37.38	39.6	39.81	41.50	41.6	42.38	47.85	51.26	49.29
Shape factor of a1	Min.	0.76	0.77	0.80	0.79	0.78	0.80	0.80	0.82	0.80
	Max.	0.81	0.81	0.82	0.82	0.83	0.80	0.80	0.85	0.81
	Ave.	0.793	0.785	0.813	0.807	0.803	0.80	0.80	0.836	0.805

Table A-7 Microstructure analysis results for RDC AZ91D alloy at different shearing speed, under the shearing time of 35s and shearing temperature of 593°C (Part I).

Vol. Fraction (%) \ Shr.Rate (rpm)		100	300	500	800	900
$Fsa_1 + Fsa_2$	Min.	28.75	26.95	29.27	28.50	26.99
	Max.	32.61	29.19	37.58	36.22	33.39
	Ave.	30.49	28.01	32.63	32.6	29.40
Fsa_1	Min.	18.20	18.81	16.87	15.31	12.91
	Max.	19.59	21.96	17.90	19.18	14.29
	Ave.	18.92	20.45	17.30	17.57	13.70
Fsa_2	Min.	10.55	5.45	12.17	10.8	13.09
	Max.	13.02	9.68	19.68	17.08	20.46
	Ave.	11.58	7.56	15.30	15.03	15.70

Table A-8 Microstructure analysis results for RDC AZ91D alloy at different shearing speed, under the shearing time of 35s and shearing temperature of 593°C (Part II).

Items \ Shr.Rate (rpm)		100	300	500	800	900
$Dena_1$+ $Dena_2$ (mm^{-2})	Min.	267.3	251.7	407	395	461
	Max.	340.5	304	505	460.1	571
	Ave.	301.6	275.1	460	432	527.6
$Dena_1$ (mm^{-2})	Min.	91.5	104.2	95.9	99.3	68.0
	Max.	98.5	115	99.3	135.5	81.6
	Ave.	95	109.3	97.5	111.8	77.0
$Dena_2$ (mm^{-2})	Min.	176	136.7	311	295.7	380.2
	Max.	246	192.3	406.5	335	490.6
	Ave.	206.6	165.7	362.5	320.2	450.7
d_1 (μm)	Min.	45.73	46.05	41.7	40.35	42.69
	Max.	49.65	48.7	47.3	45.2	45.46
	Ave.	47.31	47.3	43.89	42.38	43.9
Shape factor of a1	Min.	0.77	0.80	0.805	0.80	0.81
	Max.	0.83	0.823	0.836	0.80	0.832
	Ave.	0.80	0.817	0.82	0.80	0.827

Table A-9 Microstructure analysis results for RDC AZ91D alloy at different shearing temperature, under shearing time of 35s and shearing speed of 300rpm. Measurements were under the optical magnification of 40.

Items \ Shearing Temp. (°C)		585	589	593	597	600*
Fsa_1 (Vol%)	Min.	29.8	24.5	18.8	7.10	29.0
	Max.	32.3	26.3	20.5	12.51	35.3
	Ave.	31.4	25.1	19.1	9.07	31.8
d_1 (μm)	Min.	40.2	39.2	37.9	38.1	22.8
	Max.	45.8	43.7	43.2	39.8	36.0
	Ave.	42.6	40.9	40.1	39.2	29.3
Shape factor of a1	Min.	0.78	0.77	0.78	0.78	0.52
	Max.	0.81	0.81	0.83	0.80	0.61
	Ave.	0.79	0.78	0.80	0.79	0.56

* Quantitative analysis were intended on the primary particle of α_1 , except those samples obtained at the shearing temperature of 600°C were the primary phase of α_2.

Table A-10 Vichers hardness measurement results for solution treated AZ91D alloy (T4, at 413 °C) on both HPDC and RDC samples at different solution time.

Time (h) \ HV (ks)		HPDC			RDC		
		Min.	Max.	Ave.	Min.	Max.	Ave.
0	0	63.0	65.2	64.3	65.9	67.9	66.8
1	3.6	59.8	61.5	60.6	59.4	62.2	60.3
2	7.2	57.9	60.8	59.3	54.5	57.7	56.5
3	10.8	56.4	58.6	57.4	54.3	56.5	55.2
4	14.4	55.4	58.8	56.7	54.2	56.9	55.7
5	18.0	55.8	58.1	56.9	53.7	55.6	54.8
6	21.6	54.9	58.0	56.3	53.3	56.6	55.1
7	25.2	55.7	58.5	56.7	53.0	55.3	54.3
8	28.2	54.5	57.6	56.1	53.4	56.3	54.8
9	32.4	54.5	57.9	56.0	52.8	56.5	55.1
10	36.0	54.3	57.3	56.2	53.7	55.6	54.5
16	57.6	52.6	56.1	54.1	53.5	56.8	54.8
20	72.0	52.8	56.5	55.2	52.4	56.2	54.7
24	86.4	54.0	56.6	55.1	54.2	56.2	55.3

Table A-11 Vichers hardness measurement results for aging treated AZ91D alloy (T6, at 216 °C) on both HPDC and RDC samples at different aging time.

Time (h) \ HV (ks)		HPDC			RDC		
		Min.	Max.	Ave.	Min.	Max.	Ave.
0	0	54.1	56.0	55.1	54.5	56.5	55.3
0.5	1.8	54.6	57.0	55.8	57.5	59.6	58.7
1.0	3.6	62.5	65.3	63.9	61.2	64.4	62.5
1.5	5.4	63.8	66.3	65.4	64.3	66.3	65.4
2.0	7.2	65.6	67.8	66.5	66.7	71.0	68.9
2.5	9.0	66.0	69.0	67.5	68.2	70.8	69.4
3.5	12.6	69.1	73.1	71.2	72.3	74.0	73.1
4.0	14.4	71.0	74.2	72.5	74.5	76.9	75.8
5.0	18.0	72.5	75.9	74.0	78.7	80.9	79.8
5.5	19.8	72.5	76.2	74.4	80.3	82.0	81.2
6.0	21.6	72.5	77.0	74.9	80.4	82.9	81.7
8.5	30.6	75.6	80.1	77.6	79.0	81.4	80.6
11.0	39.6	76.0	82.6	79.5	77.8	81.0	80.1
16.0	57.6	75.9	80.5	78.0	76.9	80.4	78.5
22.0	79.2	74.7	79.0	76.9	75.5	78.9	77.2
48.0	172.8	73.3	76.4	74.7	74.9	77.5	76.1
72.0	259.2	72.0	76.1	74.2	74.2	76.7	75.1
120	432	71.9	75.5	74.0	72.9	76.1	74.2
144	518.4	71.5	75.3	73.3	71.6	75.5	73.1

Table A-12 Chemical composition measurement for a RDC AZ91D Mg-alloy component. 5 burns were performed on 3 different areas of the sample.

Composition (wt.%) / Test Position	Al			Zn		
	Minimum Value	Maximum Value	Average	Minimum Value	Maximum Value	Average
1	8.886	9.134	8.99	0.614	0.682	0.635
2	8.921	9.057	8.994	0.604	0.685	0.651
3a	8.930	9.165	9.007	0.642	0.662	0.651
3b	8.737	9.197	8.950	0.675	0.697	0.692
4a	8.879	9.058	8.99	0.605	0.658	0.625
4b	8.911	9.113	9.03	0.674	0.702	0.687
5a	8.838	9.132	8.966	0.599	0.643	0.625
5b	8.821	9.057	8.89	0.590	0.661	0.620
6a	8.949	9.193	9.108	0.671	0.695	0.680
6b	8.843	9.053	8.911	0.613	0.675	0.638